A DAMAGE IDENTIFICATION PROCEDURE FOR BRIDGE STRUCTURES WITH ENERGY DISSIPATION DEVICES

G.Benzoni – C. Amaddeo – A. DiCesare – G.Palermo

FINAL

REPORT No SRMD-2007/08

Report submitted to Caltrans under contract No 59A0438

August 8, 2008

**Department of Structural Engineering
University of California, San Diego
La Jolla, California 92093-0085**

REPORT No SRMD-2007/08

A DAMAGE IDENTIFICATION PROCEDURE FOR BRIDGE STRUCTURES WITH ENERGY DISSIPATION DEVICES

By

Gianmario Benzoni
Research Scientist

Carmen Amaddeo
Visiting Scholar

Antonio DiCesare
Visiting Scholar

Giuseppe Palermo
Visiting Scholar

Department of Structural Engineering
University of California San Diego
La Jolla, California 92093-0085

August 8, 2008

TABLE OF CONTENTS

LIST OF FIGURES

LIST OF TABLES

1) INTRODUCTION

The importance of bridge structures in an era of natural and man-made risks is unquestionable. Bridges represent the keystone of an efficient transport infrastructure needed in full operation conditions when a disastrous event strikes. After natural events like the 1994 Northridge, USA, the 1995 Kobe, Japan, the 1999 Chi-Chi, Taiwan and the 1999 Duzce, Turkey earthquakes it became evident that the demand for bridge structures could greatly benefit from the application of isolation/energy dissipation techniques. A pilot project was initiated after the 1994 Northridge earthquake by the California Department of Transportation that identified the use of isolation devices as the only economical as well as convenient approach to retrofit particularly complicated structures as the bridges part of the Toll Bridge project (Mellon 1997). Most of these projects are now completed and the California experience greatly improved the confidence of bridge designers in the US about the use of this technology. An increasing number of new bridges are also protected, worldwide, with isolation solutions taking advantage of a continuous research effort in the technological improvement of these devices, testing programs, and code development. Despite the level of maturity achieved in the field of seismic isolation, open questions still remain on the durability of seismic response modification devices (SRMD) under working conditions. Devices are traditionally designed with emphasis on their extreme condition performance, like during a seismic event, but relative motion of the bridge components, service traffic loads, together with different environmental conditions raise concerns about the stability of their performance for the future. The use of new advanced material, like composites, for isolators and energy dissipators, underlines the importance of the assessment of the performance characteristics of anti-seismic devices during their service life.

The assessment of the general structural conditions of bridges equipped with SRMDs represents an excellent example of needed integration between global and local approaches to structural health monitoring (SHM). The SRMDs devices, in fact, tend to concentrate a significant contribution to the non-linear performance of the structure and in this sense to be a possible candidate for degradation during the service life as well as during seismic events. The "local" detection of the device performance changes is, for this reason, of paramount importance. However, this information becomes relevant only if related to the "global" structural conditions. The variability of the device performance characteristics is, in fact, not immediately reflected in a critical change of the structural performance but should be identified through changes of the structural parameters.

In order to verify device performance characteristics, the option of removal from the bridge structure of sample devices is available. However, this solution involves a significant economical effort, particularly if associated to disruption of the regular traffic. It provides also a device response verification difficult to correlate to the structural performance. Health monitoring techniques offer a valuable alternative not requiring the removal of sample bearings from the bridge and maintaining the above-mentioned correlation between global and local responses. Applications to isolated bridges are however very limited and do not include experimentally validated performance curves of isolation devices extending in the damaged range.

1.1 Background on Seismic Isolation

In conventional seismic design the ground motion is assumed to transfer to the structure a certain amount of energy. The dissipation of this amount of energy, necessary to reduce the level of accelerations, is generally achieved through inelastic deformation of the structural components. In seismic isolation the energy is largely prevented from entering the structure by decoupling the latter from the ground motion, thereby reducing both the ductility demand and the floor accelerations (base isolation) or by simply decoupling the superstructure from the supporting elements as often operated for bridge structures. Typically, isolation systems artificially increase the period of vibration and the energy dissipated by a structure. Added damping is an inherent property of most isolators but it may be also provided by supplemental energy dissipation devices installed across the isolation interface. The basic concepts of isolation and dissipation are particularly interesting in bridges because of a series of potential advantages related to their specific structural characteristics. In most cases the importance of bridges, as strategic structures that require a higher degree of protection, suggests the concentration of damage potential into few mechanical elements that may easily be checked and replaced if needed, often without the need of interruption of the structural function. Specifically, the protective systems provide a concentration of nonlinear, large deformation behavior into one group of elements (the isolation bearings and dampers). These can be designed, tested and built with great care to fulfill their purpose. Additionally, since the remainder of the structure is intended to remain elastic, prediction and monitoring of its response is more reliable and economical.

Significant advances in the field of energy dissipation for improved structural resistance have been made in recent years. Developments in research and analysis techniques have been paralleled by improvements and refinements of device hardware. The two main approaches to seismic isolation can be classified as:

- Passive protection;
- Active protection.

In passive protection the designer can count on characteristics of the utilized devices assumed as constant during the structural response. Instead in an approach based on active (or semi-active) technologies the device characteristics can be adjusted to specific modifications of the structural response. The devices of an isolating system can be classified as:

- Isolators;
- Auxiliary devices.

The isolators are devices that mainly support vertical loads, allowing for large horizontal displacements, with high vertical stiffness and relatively low horizontal stiffness and/or resistance. They can be further subdivided into elastomer-steel isolators, sliding isolators and hybrid. Usually the auxiliary devices play the function of dissipating energy and/or re-centering the system with respect to the seismic horizontal actions. They can also provide a lateral constraint under horizontal service loads. A broad classification for auxiliary

devices includes devices with non-linear behavior independent from the deformation velocity, devices with viscous behavior and devices with linear or quasi-linear behavior. Many combinations of isolators and auxiliary devices have been applied to different structures, both buildings and bridges around the World and at the present time there are several innovative devices under design and development.

In the United States, although seismic isolation has been used for close to twenty years and it is considered a mature technology, its use has been slowly increasing. In contrast in Japan and Europe, hundreds of isolated projects are completed every year. Several reasons can explain the inertia in the application of this technology. The first reason is that seismic isolation is perceived in the United States as expensive, complicated and time-consuming in both design and execution. It is however opinion of researchers involved in the development of this technological field (Kelly 2001) (Naaseh 2001) that the fault is not with the technology itself but with the degree of over-regulation that is associated with the technology. The use of seismic isolation is constrained by conservatism and complication built into the code documents. One of the main difficulties however has been traditionally related to the level of confidence that designer and code writers have in the performance of isolation and energy dissipation devices. Until recently very limited tests were completed on full-scale devices with reduced testing protocols due to the limitation of testing facilities, leaving unresolved questions that did not promote the use of isolation techniques, particularly for critical structures, like bridges, where the accurate knowledge of device full-scale performance is vital. The current scenario, however, was very recently modified, in this sense, by a unique program initiated by the California Department of Transportation-Caltrans (Mellon 1997). Exceptionally complicated structures, like the bridges part of the Caltrans Toll Bridge Program, were upgraded to a modern level of seismic protection with the use of isolation techniques. This approach appeared to be the only option to improve the seismic capacity to code regulated levels of protection with economically convenient solutions. However, the project required the design and construction of a dedicated facility able to perform prototype and proof tests of full-scale devices (Benzoni et al. 1998). The Caltrans Seismic Response Modification Devices Testing Facility completed, in three years of operation, the full series of tests for devices to be used on bridges as: Benicia-Martinez, Richmond San Rafael, Coronado, San Francisco- Oakland Bay and many others in the United States and around the World (Benzoni et al. 2000), (Benzoni et al. 2003), (Benzoni, Innamorato 2003). Many aspects of isolation device performance were researched, during the testing programs at the SRMD facility at UCSD. Fundamental performance characteristics were evaluated, and even commonly used devices were tested under first-time conditions. For instance full scale sliding bearings, up to 3.6 m in diameter, were tested under design and ultimate vertical load (peak load= 54,000kN), in a range of full displacement and with peak velocity up to 1.8 m/s. Viscous dampers with stroke capacity up to +/- 900 mm were subjected to thermal, wear and velocity variation tests (Infanti 2002) and elastomeric devices were tested under design vertical loads at different velocities for a range of shear strains up to 450%.

1.2 Background on Structural Health Monitoring (SHM)

The process of implementing a damage detection strategy, referred to as Structural Health Monitoring (SHM) involves the observation of a structure, over a period of time using continuous or periodically spaced measurements, the extraction of features from these measurements and the analysis of these features to determine the current state of health of the system. Ideally the assessment of the system health should not be limited to the purpose of identifying the damage but also its location, its severity and its performance impact (Sikorsky, 1999). This type of approach is defined as Level IV, based on the following classification of performance levels (Rytter, 1993):

Level I	Methods that only identify if damage occurred;
Level II	Methods that identify damage occurrence and determine the damage location;
Level III	Methods that identify if damage has occurred determine damage location and estimate its severity;
Level IV	Methods that add to the information provided by Level III also the impact of damage on the structure.

A significant amount of research has been conducted, during the past two decades, in the area of non-destructive damage evaluation (NDE) and Health Monitoring Systems. A summary of several approaches proposed can be found in Maia et al. (1997), Housner et al. (1997), Rytter (1993), Kim (1993) and Doebling et al (1996), but research is still very active particularly due to the major evolution in recent years of both practical analytical methods for the solution of inverse problems (Ewins, 2001) and data processing and signal analysis capabilities. Global approaches are often based on the analysis of changes in the dynamic properties, notably resonant frequencies, modes shapes and modal damping. Non-destructive damage detection algorithms consider, among others, changes in the modal parameters (Stubbs et. al, 2000), frequency response functions (Biswas et al. 1994), mechanical impedance functions (Salane et al. 1981), modal assurance criterion (Farrar et al 1994), energy transfer functions (Liang et al. 1995), modal strain energy (Kim et al 1993), mode shape curvature (Pandey et al 1991), flexibility coefficients derived from modal properties (Pandey et al. 1994) etc. Although the relative performance of several prominent Level II methods have been evaluated by Farrar et al (1996) using experimental data from a field structure, very limited studies has been completed for Level III and Level IV methods.

Uniqueness and observability problems can be associated with the presence of redundant structural members (as can be additional energy dissipators) and limited sensor locations (Agbabian et al 1991). The presence of noise in sensor recordings can reduce the accuracy and reliability of various identification algorithms. Most important, the algorithms must be significantly sensitive to small changes in the performances of parameters of interest, like, for instance, the parameters that characterize the effective behavior of SRMDs.

Presently, despite the large literature available on health monitoring techniques and their application to structures, the effort has been quite limited in relating this field to isolated structures (Lee et al. 2001). A specific application is reported in Lee et al. (Lee et al. 2003).

The authors, using an approach introduced by Huang et al (Huang et al. 1996) apply a two steps method to decompose the recorded response into a number of intrinsic mode function (IMF) components. A Hilbert transformation allows the construction of the time-frequency-amplitude spectrum utilized to investigate the characteristics of the structural response. In this example, the response mechanisms of the isolation bearings are regarded as unknown and assessed by the seismic response data. The identified performance curve of the bearings is however not referred to any preliminary experimental study and for this reason the assessment of the health conditions of the isolation elements is not taken into account. In another example (Chaudhary et al. 2000), the bridge's structure is reduced to a two DOF lumped mass model, selected to represent the dynamics of the bridge in the longitudinal direction. The superstructure is modeled, as suggested by Abe et al. (Abe et al. 1997), as an equivalent single degree of freedom system. The identified bearing stiffness was found to be higher than the experimental values, especially during the low level excitations of aftershocks. The discrepancy is attributed to the uncertainty associated with the determination of the friction coefficient. It is questionable, however, if the response discrepancy must be attributed only to the isolation system characterization or instead be the result of over-simplified structural scheme. In a recent publication Wolfe et al. (Wolfe et al. 2002) report some analytical and experimental studies to evaluate a strategy for structural health monitoring of non-linear viscous dampers. By inspecting changes in the probability density function of the identified dominant system parameters it is shown that the proposed approach is capable of detecting small changes, even in the presence of a modest amount of noise pollution. Further validation of the set of analytical tools suggests an extensive use of prototype and proof test data of energy dissipating devices.

All the available research on SHM of isolated bridges, as well as most of the general literature on application of these techniques to non-isolated structures, is based on damage detection algorithms performed in "unsupervised learning mode". The term unsupervised meaning that data from damaged systems are not available. In the present proposal the importance of preliminary acquisition of performance curves for the devices, extended to the damage range is considered paramount. The existing health monitoring techniques, applied to isolated structures, are also generally based on simplified models of the device performance. These assumptions do not allow these techniques to directly relate to the device performance under realistic loading conditions. This level of simplification, in fact, performs as a filter in the process of correlation between the indicators of possible damage, at the device level, and the effects on the overall structural performance making impossible to achieve the above mentioned performance level III and IV.

1.3 Research Plan

The main objective of this research is the definition of an effective health monitoring approach to be applied to bridges protected with the most common seismic response modification devices (SRMD). Mainly the attention is dedicated to those devices that have been recently extensively tested in the full-scale range of dimension, displacement, velocity and applied load. The devices that were considered for the goals of this project are viscous dampers (energy dissipators), even though the proposed algorithm, and particularly the general procedure is believed to be easily adaptable to the case of other type of devices. A

research phase is in progress, at University of California San Diego, to validate the above statement and is providing positive results.

Typically, the isolation devices have been treated, in identification algorithms, as any other structural component, source of stiffness and additional damping. Variation in the performance of these devices, however, can be difficult to be detected by traditional approaches that belong to the broad category of global (macro) methods. These approaches use measurements from a dispersed set of sensors to obtain global information about the condition of the entire system (Housner et al. 1997). The scope of monitoring the performance of bridges with SRMDs, due to the concentration of non-linear, large deformation behavior into one group of elements, pertains instead naturally to the category of local (micro) methods that are designed to provide information about a specific component of the all structural system. The proposed approach was specifically targeted to the need to maintain a level of integration between global and local performance.

To achieve the goal of this research the following tasks were completed:

Task 1- Parametric analysis of the effects of damper characteristics. A numerical study of the effects of changes in damper performance to the dynamic response of an isolated bridge, modeled by a Finite Element program was completed.

Task 2- Laboratory test on a full scale viscous damper to artificially introduce increasing levels of response degradation. Characterization of the damper performance and definition of a physical model able to reproduce the damaged conditions.

Task 3- Selection of an existing methodology for the assessment of the conditions of an existing bridge (level IV). Modification of the methodology in order to take into account the existence of SRMDs.

Task 4- Validation of the modified methodology using F.E. models of an existing isolated bridge, including realistic data obtained from damaged viscous dampers.

Task 5- Validation of the overall procedure with records from a bridge with energy dissipators in new and damaged conditions.

The five research phases are described in details in this report. For Task 1 and Tasks 2 separate reports are provided. Specifically Task 1 and Task 2 results are presented in (Benzoni et al. 2005) and (Benzoni et. al, 2007), respectively.

2) PARAMETRIC ANALYSIS OF THE EFFECTS OF DAMPER CHARACTERISTICS

This first Task (Task 1) of the research project was aimed at two specific goals:

- Evaluate the accuracy of the existing Finite Element model of the bridge under consideration (Vincent Thomas Bridge in Los Angeles).

- Perform a parametric analysis, with the above mentioned F.E. model, of the structural impact of different characteristics of the viscous dampers installed on the bridge structure.

- Detailed results for these two research phases are reported in (Benzoni et. al, 2005). In this paragraph only a summary of findings are presented.

The main case study of the overall research project consists of the Vincent Thomas Bridge, a cable-suspension structure retrofitted in different stages, and lately equipped with 48 viscous dampers. The study was conducted by means of nonlinear time-history analyses of a detailed three-dimensional FE model of the bridge provided by the California Department of Transportation (Caltrans). Such numerical model, including cables, suspenders, suspended structure, towers, cable bents and anchorages, reflects the state of the structure after the last retrofit phase, when dampers and fuses were installed and towers were stiffened. The static and time-history analyses of the bridge were both geometrically nonlinear (large displacement analyses) to account for the geometric stiffness of the cables and suspenders.

The Vincent Thomas Bridge is located in the Los Angeles metropolitan's area (Figure 1) on Route 47 (P.M. 0.86). The route is a critical artery for commercial traffic in and out of Los Angeles Harbor, and is a risk in the seismically active Southern California Region, particularly because it straddles the Palos Verdes fault zone. The structure is a cable-suspension bridge, 1849 m long, consisting of a main suspended span of approximately 457.5m, two suspended side spans of 154 m each, ten spans in the San Pedro Approach of approximately 560.6 m total length, and ten spans in the Terminal Island Approach of approximately 522 m total length (see Figure 2). The roadway width between curbs is typically 16 m, and accommodates four lanes of traffic. The clear height of the navigation channel is approximately 56.4 m. The design of the bridge was completed by Caltrans in 1960. The substructure contract was completed in 1962 while the superstructure contract was completed in early 1964. Stage 1 seismic upgrading in the form of cable restrainers, shear keys abutment seat extenders and girder lateral supports was completed in 1980. Modifications to the vertical cross frames, and the lateral bracings near the bents, and inclusion of a full length cat-walk were also made in 1980 as part of the seismic upgrading contract. New elevators at Bents 9 and 15 were added in 1992. In 1998 a seismic retrofit was completed consisting on the installation of dampers (Figure 3) between the stiffening trusses and the towers of the bridge, stiffening of the bridge towers, as well as installation of structural fuses in the side spans of the bridge.
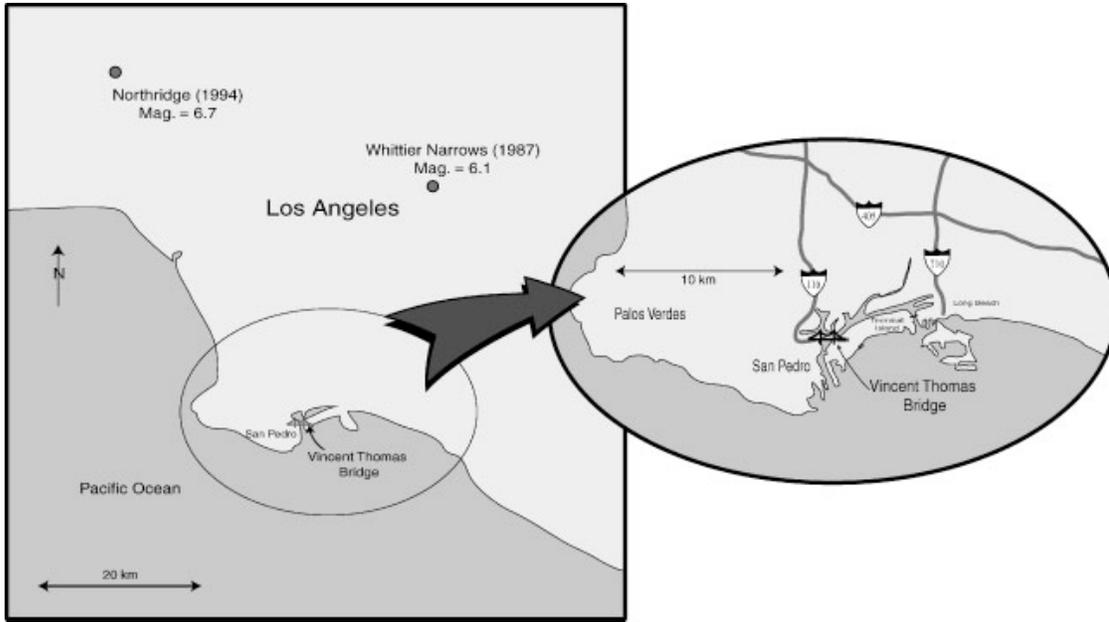
Figure 1. Location of the Vincent Thomas Bridge with respect to the 1987 Whittier Narrows earthquake and the 1994 Northridge earthquake
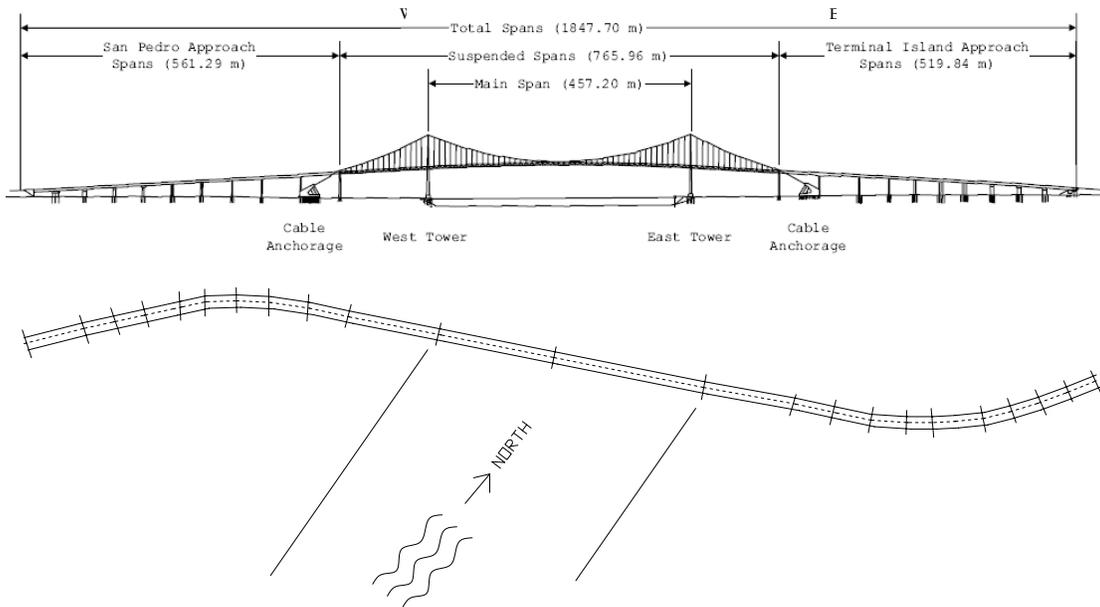
Figure 2. Vincent Thomas Bridge, front and plan views

Figure 3. Damper position

Currently, twenty-six seismic sensors are installed on the bridge to record ambient and seismic behavior. Figure 4 shows the layout of the location of all 26 sensors mounted on the bridge. A summary of the sensor numbering system and measurement directions is presented in Table 1. An enlarged view of sensor locations is presented in Figure 5.
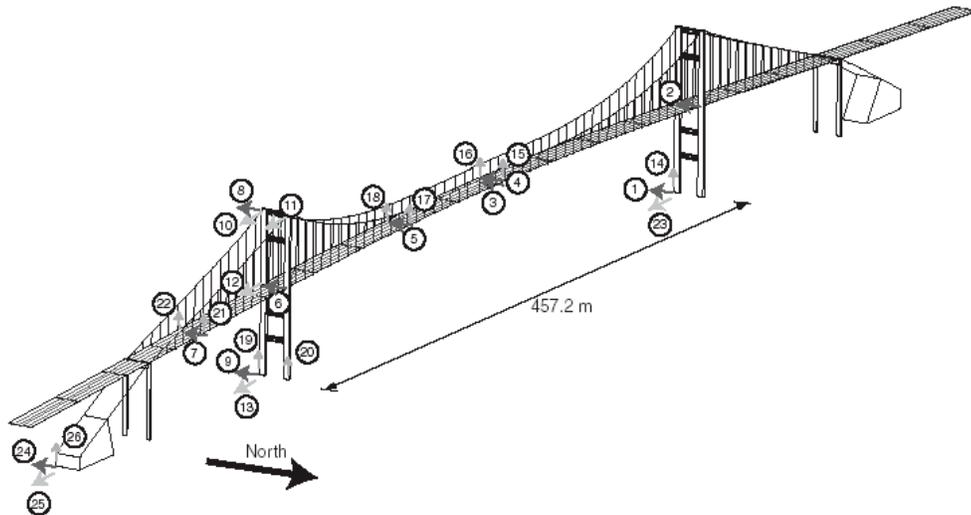
Figure 4. Accelerometer locations for the instrumental network (Smyth et al., 2003)

Location	Sensor	Sensor direction
Tower base	14, 19, 20	Vertical
	1, 9	lateral
	13, 23	longitudinal
Anchorage	26	vertical
	24	lateral
	25	longitudinal
Truss top, i.e. deck	15, 16, 17, 18, 21, 22	Vertical
	2, 4, 5, 6, 7	Lateral
	12	Longitudinal
Truss bottom	3	Lateral
Tower	8	Lateral
	10, 11	Longitudinal

Table 1. Sensor localization (Smyth et al., 2003)
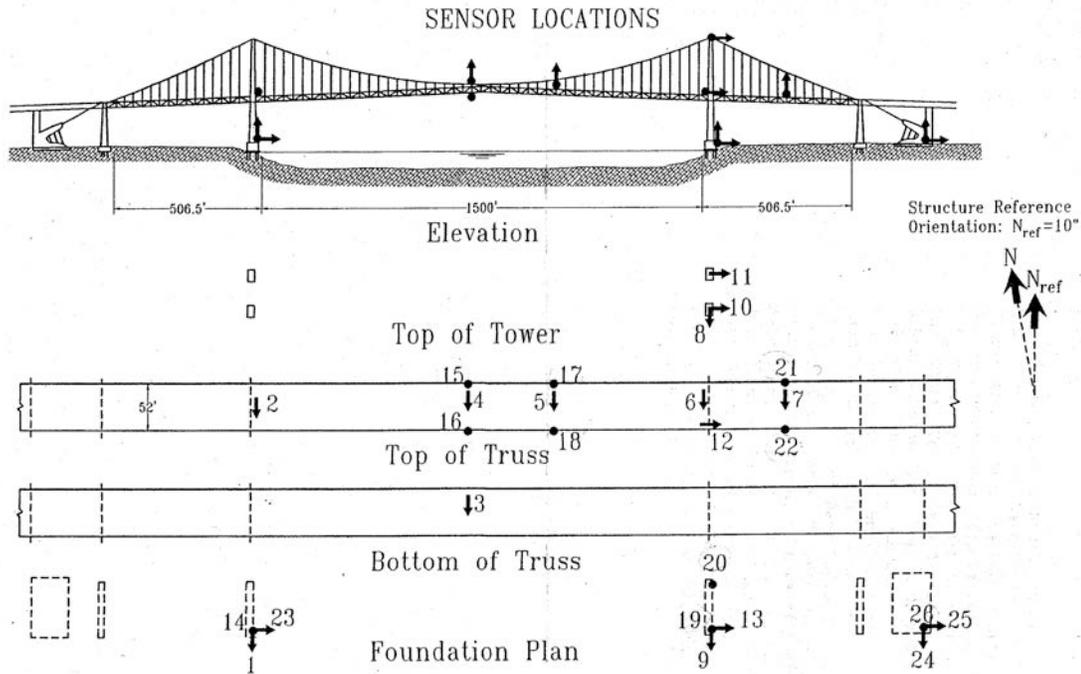
Figure 5. Sensor localization (Smyth et al., 2003)

2.1 Evaluation of the performance of the bridge F.E. model

A detailed three-dimensional finite element model of the bridge developed using the finite element analysis software Adina (2001) was provided by Caltrans.

This finite element model is composed of 3D elastic truss elements to represent the main suspension cables and suspender cables, 2D solid and shell elements to model the bridge deck, and beam elements to model the stiffening trusses and tower shafts.

As mentioned above, the first goal of Task 1 was to evaluate the accuracy of the available model in order to guarantee a reasonable dynamic response to be used in the design phase of the damage detection algorithm. A preliminary validation of the numerical model of the bridge was carried out by comparing the numerical response with recorded signals during seismic events like the 1987 Whittier-Narrow earthquake (M=6.1) and the 1994 Northridge earthquake (M=6.7). The proximity of these earthquake epicenters relative to the Vincent Thomas Bridge is shown in Figure 1. Despite the greater distance to Northridge, because of the larger magnitude of that earthquake, the observed peak input and response accelerations ranged anywhere from 1.5 to 3 times of those recorded during the Whittier–Narrows earthquake. The time history records recorded in the proximity of the bridge (see Figure 6, station 82) were selected as excitations for the F.E. model.
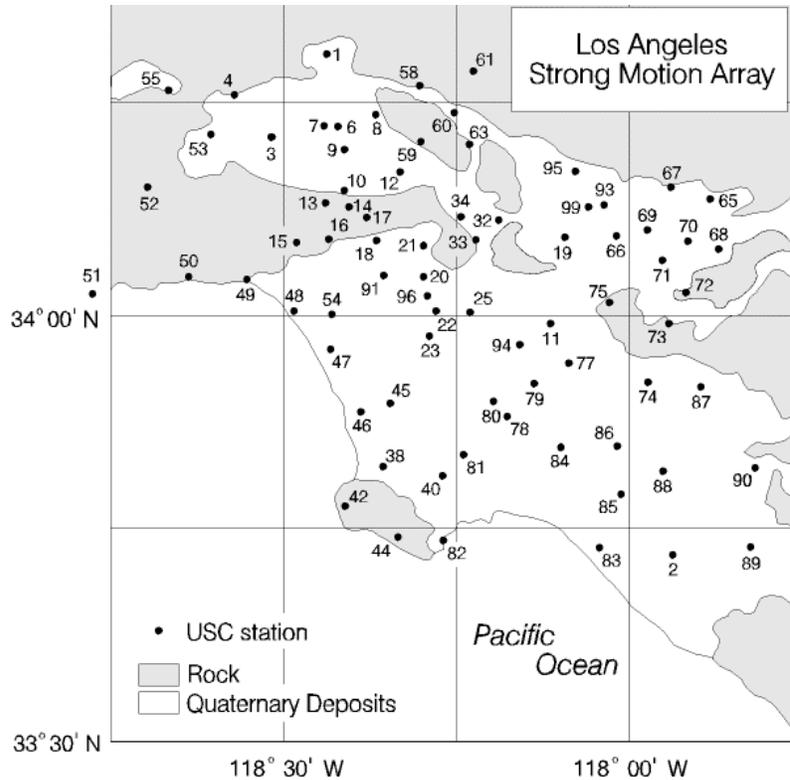
Figure 6. Strong Motion Array (USC)
The recording station nearest to the bridge is the number 82 (Terminal Island)
(www.usc.edu/dept/civil_eng/earthquake_eng/LA_array)

It must be noted that either one of the two seismic events was experienced at the bridge location after the completion of the seismic upgrade that included the installation of viscous dampers (1998). The F.E. model is instead designed consistently with the present bridge configuration. This scenario clearly invalidates the use of these recorded responses as direct reference behavior. However, the use of the records was considered appropriate for the definition of basic dynamic characteristics of the F.E. model and for a preliminary analysis of the possible effects on the structural response of the performance changes of the energy dissipators. As presented in detail in a companion report (Benzoni et. al, 2005) the recorded responses were applied at the tower base, as dynamic excitations for the model results. The numerical response time histories, in terms of displacement, velocity and accelerations are not identical to the recoded ones for the disagreement between model and physical configuration at the seismic event time. To minimize the effects of the structural modifications, the dampers elements in the model were initially de-activated. As indicated in the following figure (Figure 7) the model (red line) and recorded (black line) responses are however similar at some location, indicating a reasonable performance of the numerical model.
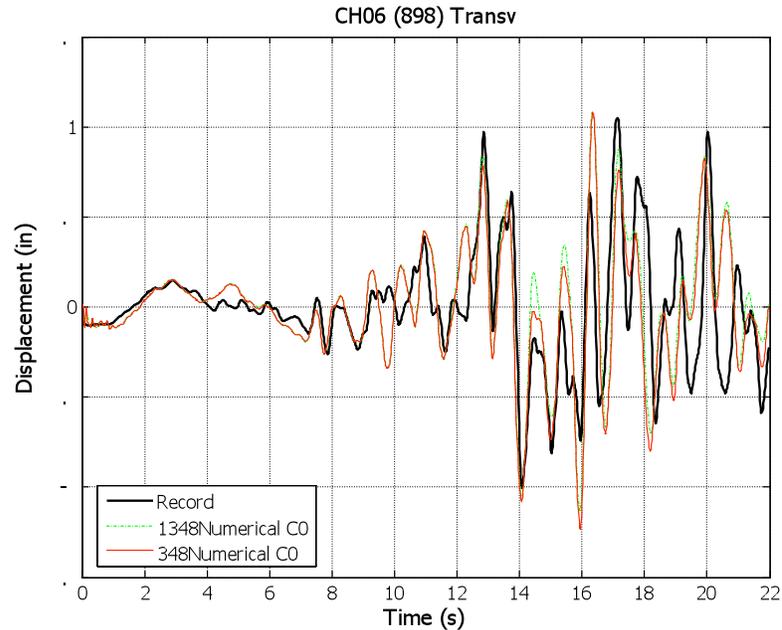
Figure 7. Northridge Earthquake. Model and Recorded transverse displacement at location of Sensor 6

Table 2 shows the main frequencies obtained from the modal analysis of the bridge and recognizable in the transfer functions, both from numerical and recorded signals. Results appear in satisfactory agreement with previous works presented in literature (Conte et al., 2003; Ingham et al., 1997). The frequencies identified in the recorded response are reasonably matched by the ones provided by the present numerical model. However more significant frequencies are indicated by the modal analysis and the transfer functions of the response obtained by the F.E. analysis. This is again attributed to the differences in the configuration of the FE model and of the actual bridge at the time of the earthquake event. Within the scope of the present project, the obtained agreement with the recorded data still indicates a general reliability of the FE model.

| Mode Shapes | Modal Frequency [Hz] | | | | | |
| | | | Conte et al. (2003) | | Ingham et al. (1997) | |
	Numerical signal	Recorded signal	Identified frequency	Computed frequency	Computed frequency	Northridge frequency
1-AS-V	-	-	0.168	0.182	0.135	0.145
1-S-V	0.130	0.210	0.224	0.226	0.229	0.220
2-S-V	-	-	0.356	0.364	0.356	0.370
1-S-T	0.570	0.570	0.483	0.511	0.471	0.551
3-V	0.910	0.902	-	-	-	-

Table 2. Comparison of system identification results (AS=Anti-Symmetric, S=Symmetric, V=Vertical, T=Torsional)

2.2 Evaluation of the structural impact of the damper degradation (Summary of results from Report SRMD 2005/12, Benzoni et Al., 2005)

The following set of analyses was aimed at the evaluation of the effects of the damper characteristics variations on the structural performance (second goal of Task 1) of the Vincent Thomas Bridge, but also to estimate the realistic range of forces and displacements associated with the devices under loading conditions. The latter information is clearly critical to relate the expected and the experimental device performance. It must be noted that, at this stage, laboratory data for such devices are available only through publications of an experimental campaign completed by HITEC (Hitech, 1999). Additional tests were completed on new devices provided by Caltrans and designated to replace some existing dampers installed on the bridge. The original dampers, removed from the bridge, will also be tested to provide information on their state of degradation. When this research phase was completed, only the theoretical characteristics of the devices were available. For this reason, variations of the dampers characteristics are simulated, numerically, starting from the theoretical parameters of damper performance.

The location and the current characteristics of the dampers are described in Table 3. It was noted that the dampers "side span to cable bent top chord dampers" are not present in the technical drawings of the bridge and are characterized by a very low C constant compared to the others. The dampers at fuses location are the only ones characterized as nonlinear dampers with an extremely high C constant.

Ref.		C	α
D5g	side span to cable bent top chord dampers	0.1	1.0
D5	side span to cable bent bottom chord dampers	5.0	1.0
D3s	side span to tower	2.5	1.0
D3m	main span to tower	4.0	1.0
D4	Side span hinge damper at fuses	100	0.5

Table 3. Location and characteristics of the dampers in the FE model

In the bridge F.E. model, damper elements are reproduced by means of nonlinear spring element with assigned stiffness and damping properties represented by a force-velocity relationship of the type $F = CV^{\alpha}$. Six different scenarios (no dampers, combo 1-5) were created by changing characteristic parameters of the dampers as indicated in Table 4. Specifically, in Table 4, the ratios of the damper constants to their nominal values are reported. Configuration 1 represents the case with damper at their nominal performance parameters (C_1, α_1). Configuration 0 (C_0) indicates the complete removal of dampers. In this case the corresponding springs, in the F.E. model, are characterized only by their linear stiffness properties.

14

		α_0 not present	α/α_1 0.25	α/α_1 0.50	α/α_1 1.00
C_0	not present	no dampers			
C/C_1	0.50				Combo 2
C/C_1	1.00		Combo 5	Combo 4	Combo 1
C/C_1	2.00				Combo 3

Table 4. Ratios of the damper constants employed in the analyses to their nominal values (Table 3)

The nonlinear time-history analysis of the structure was performed in the time domain by step-by-step integration of the equations of motion, using the Newmark method, with full Newton iteration at each time step. A basic time step of 0.02 s, suitable for such long-period structure subjected to low-frequency input motion, was used; the employed algorithm reduces the time step automatically as needed to capture any nonlinear response of the structure, like impact in the wind shoes connecting the spans and the towers.

The input records (Northridge and Whittier) were applied in the form of global ground acceleration. Analyses were performed in the longitudinal and transversal directions, separately. The results were analyzed in terms of effects on damper forces, structural displacements, member forces and global structural reactions. Detail results are presented in the SRMD Report 2005/12. (Benzoni et al., 2005). A summary of results is presented here.

Figure 8 and 9 shows the level of forces generated in the energy dissipators under the two selected seismic excitations applied in longitudinal and transverse direction, respectively. It must be noted that forces are also present in the configuration of dampers removed. In fact a linear spring is, in this case, still present in the F.E. model at the damper locations. It was noted that the dampers D5g (side span to cable bent top) attract very small forces if compared to all the other dampers, due to their very low C constant. The structural elements at fuses locations instead attract a very high force, shared with dampers, when present. The dissipators at these locations are therefore the most activated devices in both Whittier and Northridge earthquakes. Dampers D5 (side span to cable bent bottom) are the second most loaded devices, with an increase in force up to 20 and 45 times the force obtained in the configuration without dampers in the Whittier and Northridge earthquakes, respectively. The maximum and minimum force in the dampers is associated to case C/C_1=2 (Combo 3) and α/α_1=0.25 (Combo 5), respectively for the Northridge event, and to case C/C_1=2 (Combo 3) and C/C_1=0.5 (Combo 2) under Whittier excitation.
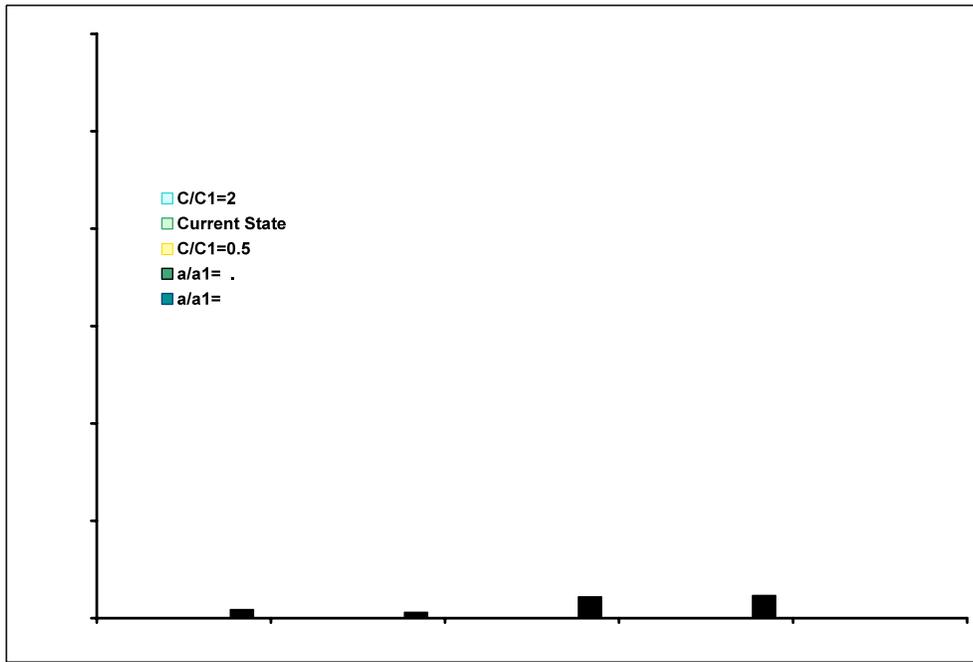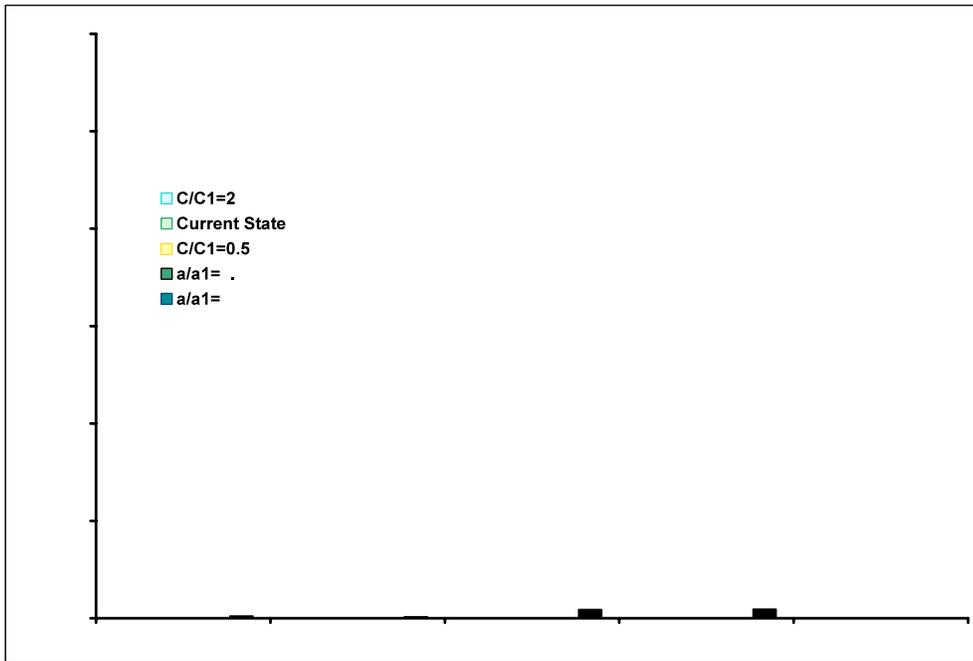
Figure 8. Axial forces in the dampers for the two earthquakes applied in longitudinal direction
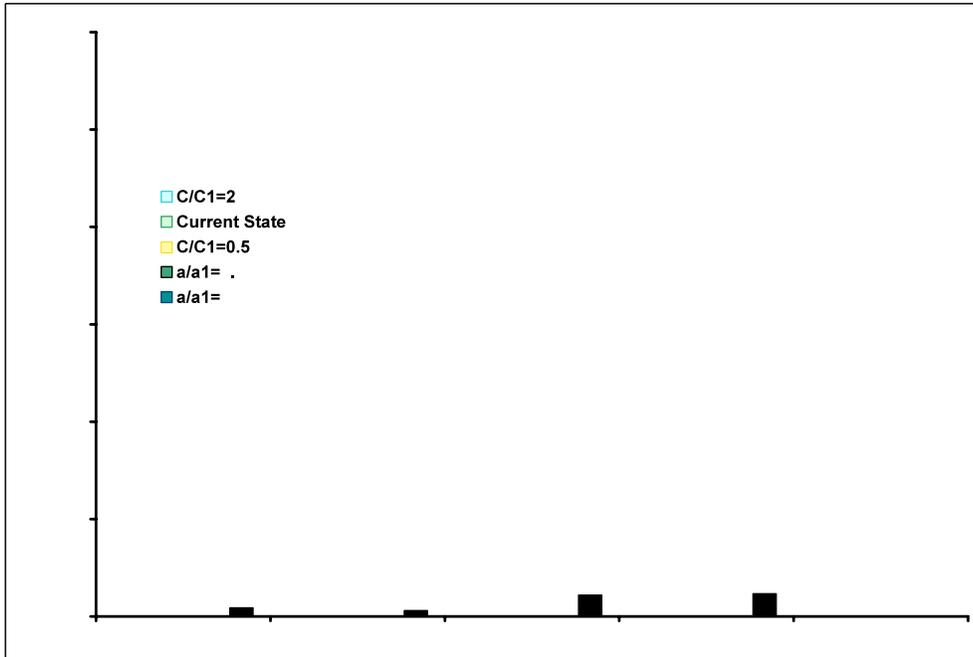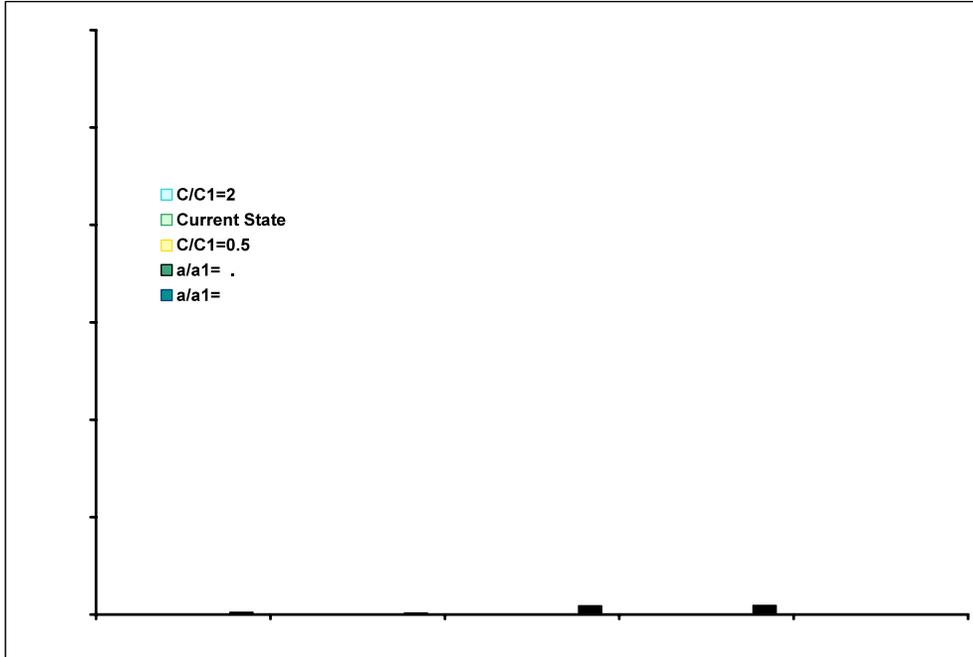
Figure 9. Axial forces in the dampers for the two earthquakes applied in transverse direction

For the Whittier earthquake applied in longitudinal direction the mid-span displacements are not significantly affected by the presence of dampers, whilst side-span displacements indicate a reduction in the order of 20% when compared with the response of the un-damped bridge. It was noted that D4 dampers (located at fuses) develop a force of the same order of magnitude for both earthquake records, while D3 dampers (at tower locations) develop a much smaller force in the Whittier record, thus being less effective for the mid-span displacements (d1). Peak displacements are reported in Figure 11 and Figure 12 for the two analyzed seismic events applied in longitudinal and transverse direction, respectively. Displacement locations d1 to d5 are down in Figure 10. The improvement in performance due to the existence of dampers is visibly non uniform along the bridge as well as function of the input characteristics. For Northridge, for instance, locations d1 to d3 experience a peak displacement significantly reduced when compared with the un-damped configuration. The same effect is not reproduced for Whittier input at the same locations.

For the Northridge input transverse displacements are high at mid-span (Figure 12), but they are not significantly affected by the presence of dampers, as well as at the side-span locations. For the Whittier earthquake a significant deformation is experienced, in lateral direction, at mid-span and also at fuses location. All the displacement values along the deck are slightly reduced by the use of dampers, specifically in the order of 5% to10% when compared to the un-damped scenario.
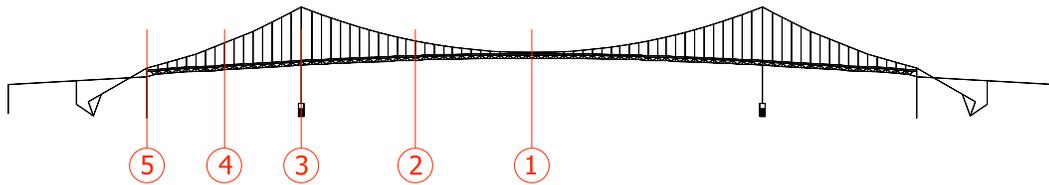
Figure 10. Reference locations for model readouts

The damper's influence in the peak forces experienced by other structural elements appears limited. The peak reduction of shear forces due to the presence of dampers is 10% and 45% for Northridge and Whittier earthquake, respectively. Elements in which peak actions occurs are in most cases in the same locations even after the introduction of dampers. In terms of global base reactions, it was observed that for both seismic inputs the total base shear is not significantly modified by the presence of dampers. The use of dampers implies a total base moment reduction of 20% and 35% for Northridge and Whittier events, respectively. Even if global forces are not significantly reduced, it appears however that the use of dampers can generate an overall re-distribution of forces on the structure. The impact of this effect need to be evaluated and it is under study with the use of the available F.E. model of the bridge.
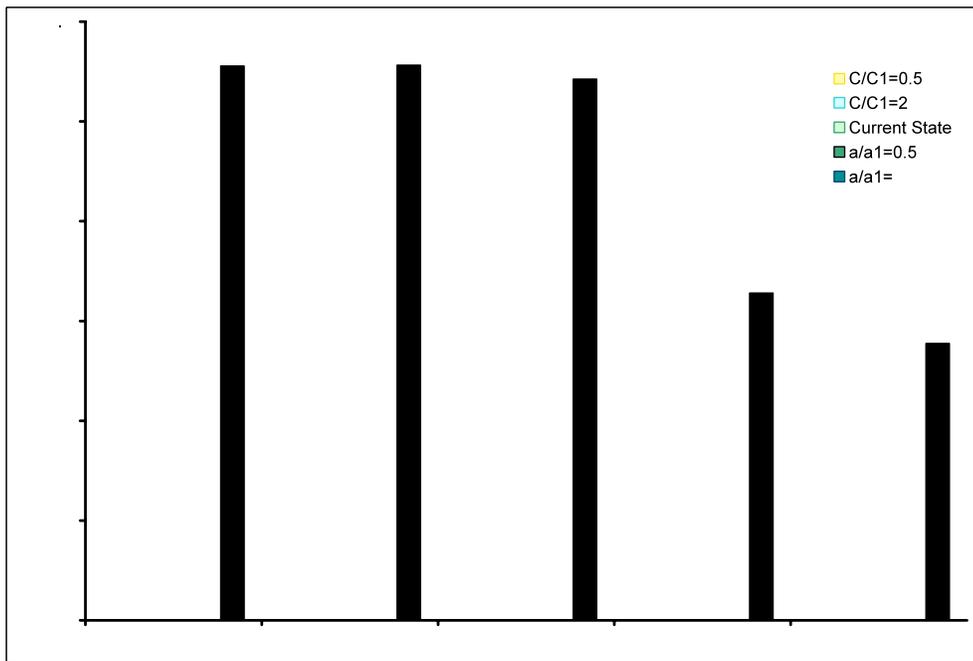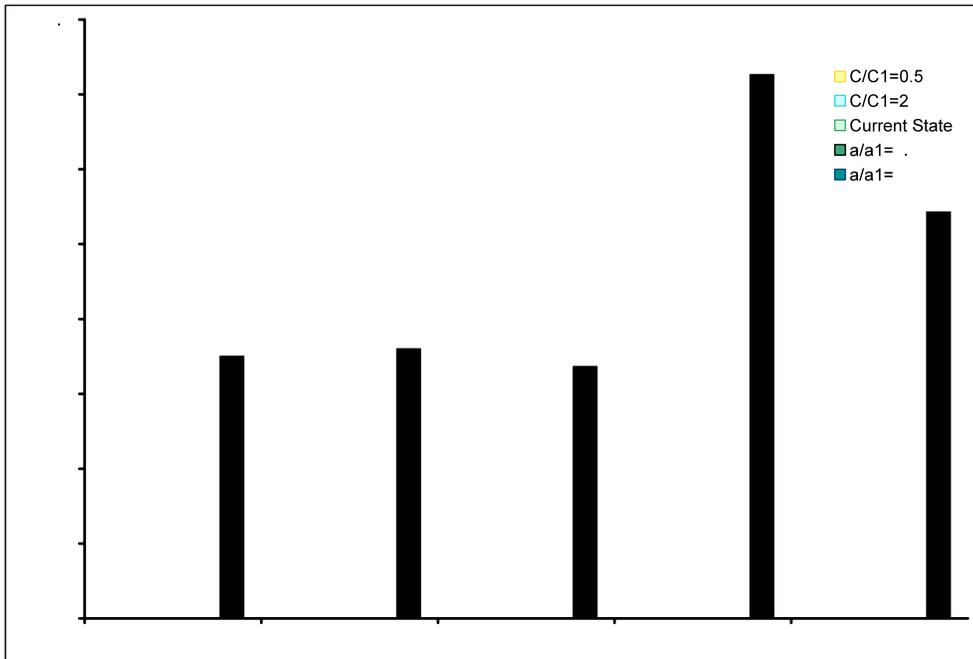
Figure 11. Peak longitudinal deck displacements for the two earthquakes
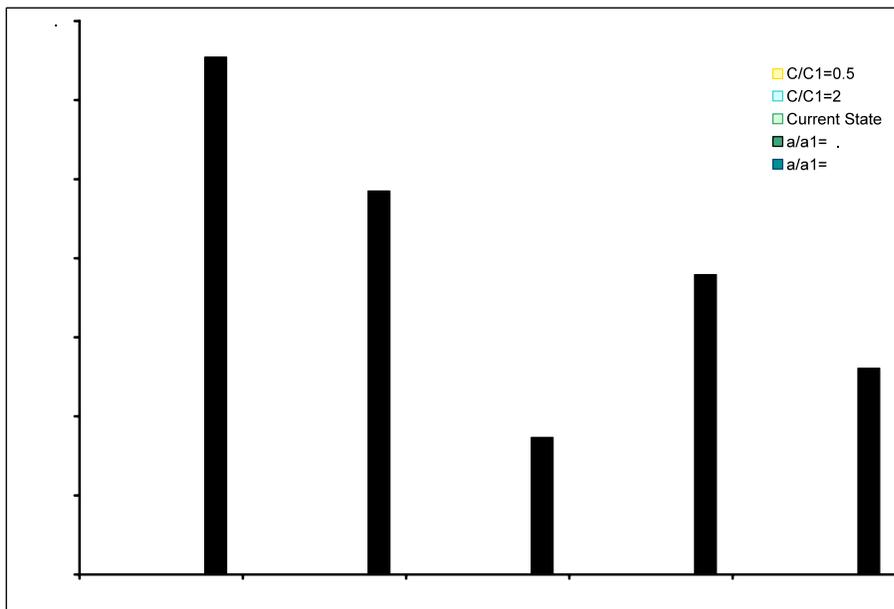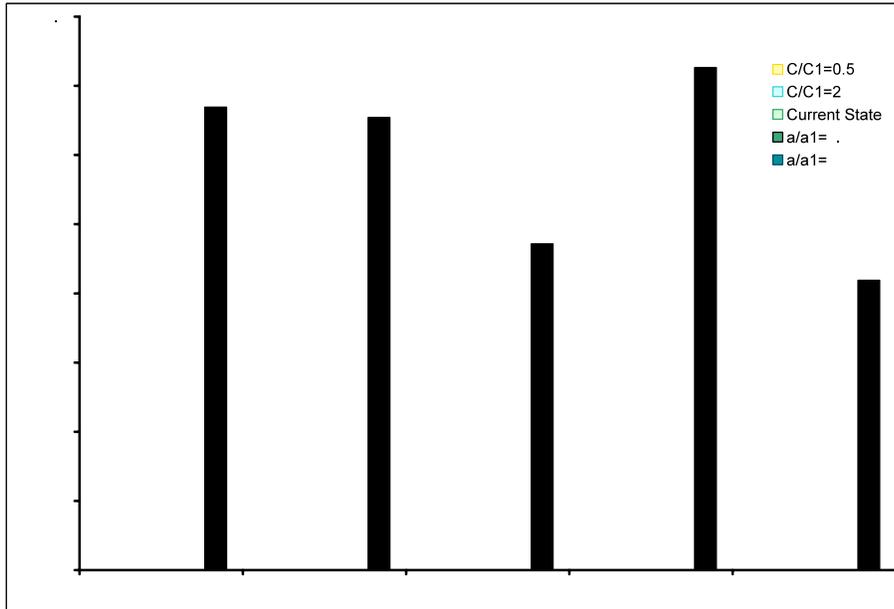
Figure 12. Peak transverse deck displacements for the two earthquakes

3) CHARACTERIZATION OF DAMPER PERFORMANCE IN DAMAGED CONDITIONS

One of the main objectives of this research program is the characterization of the performance of viscous dampers under different conditions of possible degradation of their basic response characteristics (Task 2). As described in the previous paragraph, the F.E. model allows to introduce changes in the two main damper performance parameters C and α. However, no information are available in literature about the experimental response of viscous dampers in damaged/degraded configurations that can provide physical significance to the artificial variations of the two parameters C and α. For this reason an experimental phase was completed to study the response of one viscous damper in conditions that can be realistically representing damaged stages of increasing severity. It is clear that the experimental program, limited to a single device unit, cannot be considered inclusive of the subject but it represents an important set of data for several reasons. It allows, in fact, the validation of a numerical model of the damper performance that can be used in F.E. simulations to analyze the impact of damper defects to the overall structural performance. In these terms the data are critical for this research because they allow to create realistic variations of damper behavior that are targets of the health monitoring procedure. In addition, these experimental results represent a first data sample for the process of definition of maps of deterioration at the device level. The use of deterioration maps (schematically shown in Figure 13) in concert with time maps (shown on the right) are of paramount importance for a predictive approach using which estimates can be made of remaining life of the structure affected by device performance degradation, as well as of an optimized schedule for inspection of the device conditions.
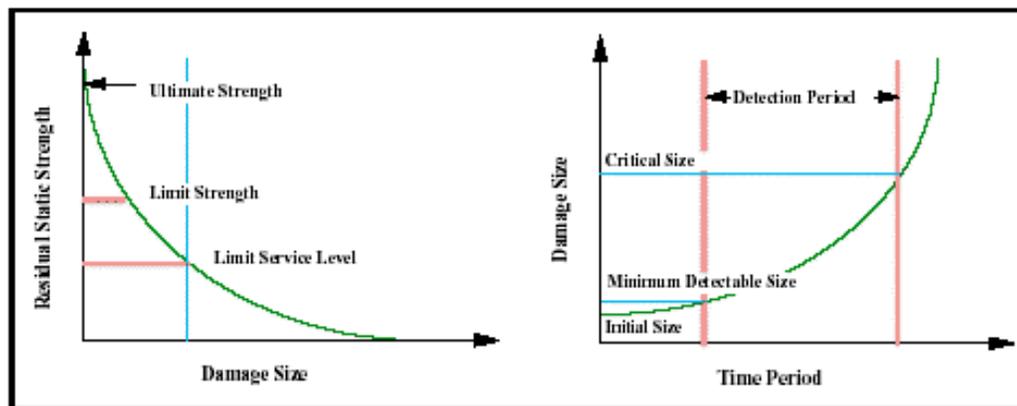
Figure 13. Example of 2D maps of deterioration

A viscous damper unit (Figure 14) was made available by F.I.P. Industriale (Italy) to complete this preliminary program. The different levels of degradation were artificially created to simulate leakage of damper, for instance associated to a damage of the damper seals. The experimental tests have been carried out for different level of Leakage (0.4, 0.8, 1.2, 1.6 liters) and at different frequencies (0.01, 0.28, 0.56 0.84, 1.11 Hz) of the imposed

sinusoidal motion. Tests were completed at the Caltrans SRMD Testing Laboratory of the University of California San Diego. The damper basic characteristics are:

Stroke: +/- 275 mm
Design capacity: 670 kN
Damping Exponent: 0.15

Tests were performed imposing a sinusoidal motion of constant peak amplitude equal to 100 mm. Three main cycles are completed for each test. In order to minimize the inertia effects at the beginning and end of the test, entrance and exit ramps were introduced resulting in a total number of four cycles. In the data analysis process only the central three cycles are considered. In Table 5 peak forces and displacements are reported for the tests at different frequency and for different amount of oil removed.
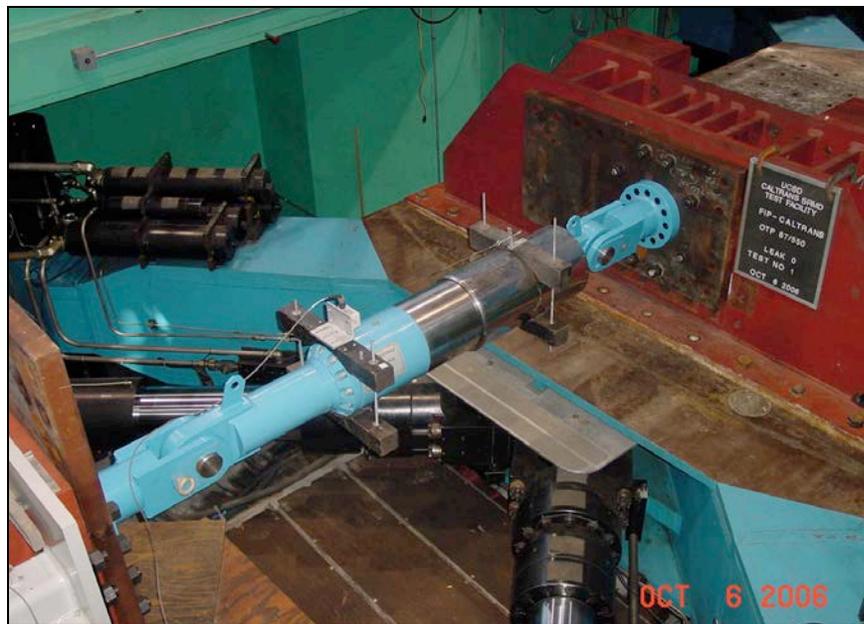
Figure 14. FIP Damper unit

TEST	Frequency (Hz)	F_{max} (kN)	F_{min} (kN)	D_{max} (mm)	D_{min} (mm)
FIP Leakage 0 Test 1	0.01	290.1413	-273.0191	99.9595	-99.5549
FIP Leakage 0 Test 2	0.28	465.4184	-443.0362	99.2253	-100.0793
FIP Leakage 0 Test 3	0.56	520.5636	-497.1634	99.4500	-100.2292
FIP Leakage 0 Test 4	0.84	556.5353	-533.1351	100.0494	-101.8475
FIP Leakage 0 Test 5	1.11	592.8463	-568.7674	101.8025	-103.4208
FIP Leakage 04 Test 1	0.01	291.8380	-269.4559	99.3601	-100.0644
FIP Leakage 04 Test 2	0.28	463.3822	-432.6859	99.4650	-99.9894
FIP Leakage 04 Test 3	0.56	511.9101	-482.7408	100.0194	-100.3191
FIP Leakage 04 Test 4	0.84	545.5062	-514.9796	100.7087	-101.7126
FIP Leakage 04 Test 5	1.11	583.3444	-557.0597	101.7426	-103.4358
FIP Leakage 08 Test 1	0.01	290.3109	-270.8133	99.2852	-100.1992
FIP Leakage 08 Test 2	0.28	461.3461	-433.5343	99.2552	-100.0794
FIP Leakage 08 Test 3	0.56	509.1952	-480.7047	100.0044	-100.1992
FIP Leakage 08 Test 4	0.84	543.4701	-514.6402	100.9035	-101.6377
FIP Leakage 08 Test 5	1.11	585.8895	-559.6048	102.0722	-103.2410
FIP Leakage 1.2 Test 11	0.01	287.5961	-265.2140	100.5738	-100.3790
FIP Leakage 1.2 Test 12	0.01	288.6142	-271.4920	99.4650	-99.7347
FIP Leakage 1.2 Test 2	0.28	460.1583	-434.8917	98.9705	-100.1243
FIP Leakage 1.2 Test 3	0.56	511.0617	-484.4376	100.409	-100.4390
FIP Leakage 1.2 Test 4	0.84	541.0946	-517.0157	100.8435	-101.6077
FIP Leakage 1.2 Test 5	1.11	580.7992	-552.9874	102.1921	-103.3759
FIP Leakage 1.6 Test 1	0.01	288.6142	-269.2862	99.5699	-99.6598
FIP Leakage 1.6 Test 2	0.28	460.1583	-432.6859	99.1803	-100.1543
FIP Leakage 1.6 Test 3	0.56	512.5888	-483.4195	100.3041	-100.6338
FIP Leakage 1.6 Test 4	0.84	542.4520	-518.0338	100.6787	-101.4579
FIP Leakage 1.6 Test 5	1.11	576.5573	-552.1390	101.6527	-103.3759

Table 5. Dampers FIP: Test Summary

A sample of performance results are shown in Figure 15, 16 and 17, for the condition of 0.8 liters of fluid removed from the damper and an excitation of 0.28 Hz.
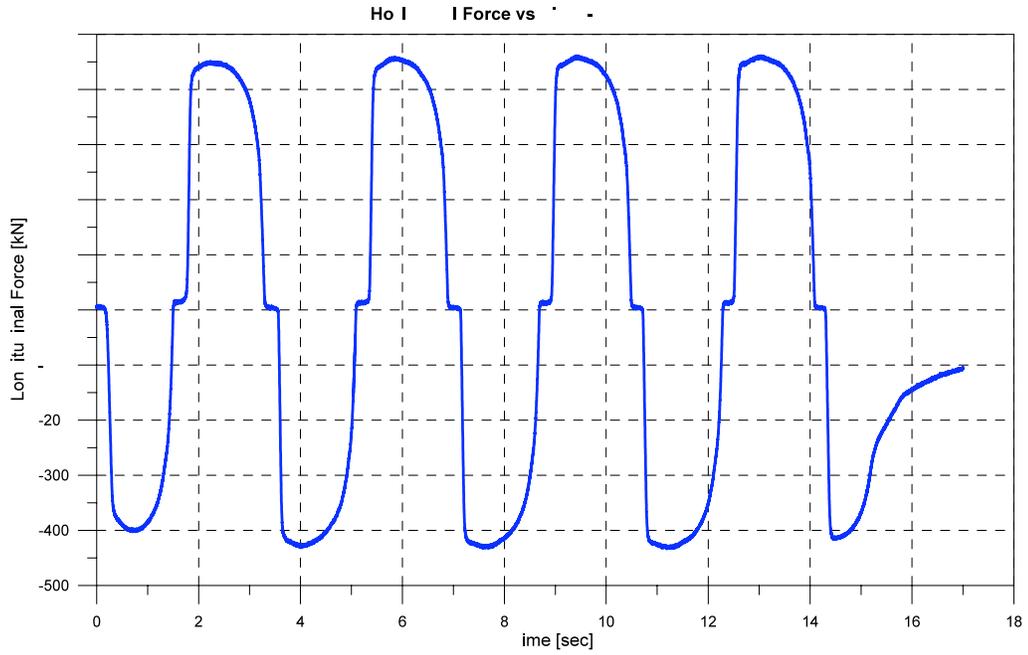
Figure 15. Test #2 Leakage = 0.8 liters: Longitudinal force
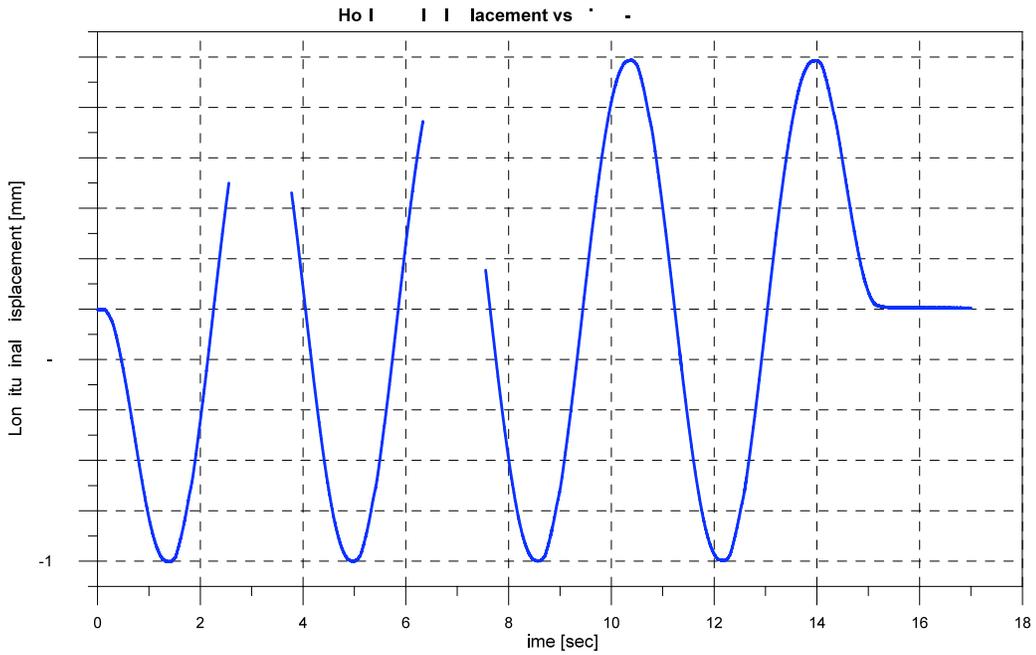
Figure 16. Test #2 Leakage = 0.8 litters: Longitudinal displacement

24
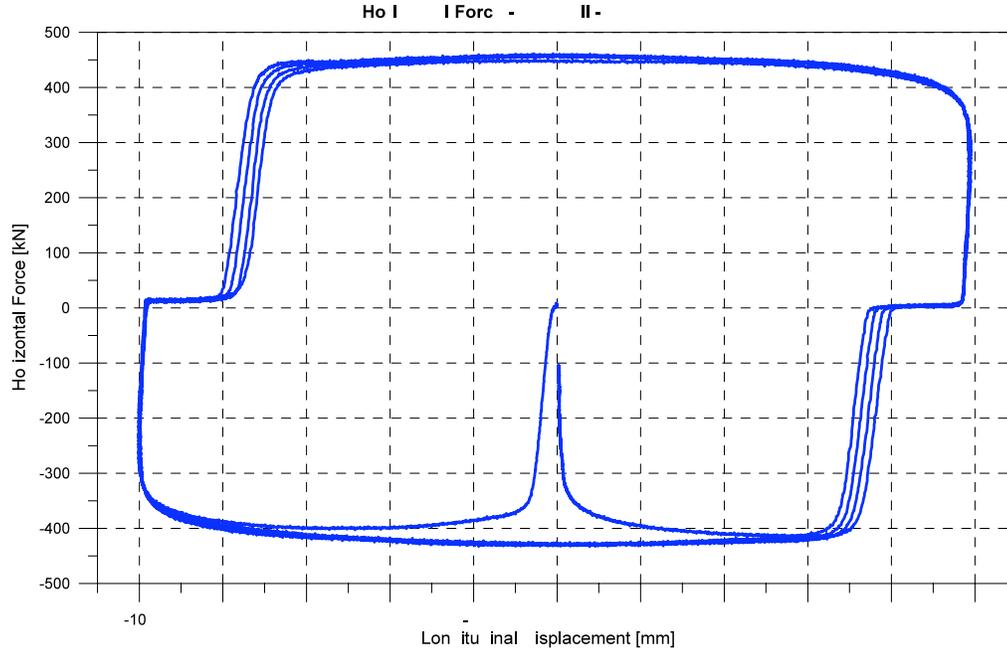
Figure 17. Test #2 Leakage = 0.8 liters: Force vs displacement

The effect of the removal of a portion of the viscous material is clearly visible in Figure 17 at displacement reversal. The damper is able to describe a portion of the assign displacement time history without developing any reaction force, describing the flat portions of the force-displacement loop. When the displacement of the internal piston is sufficient to generate again a level of pressure in the fluid, the force trend is restored. The length of the "zero force" segments depends on the amount of fluid removed.

The performance of the damper, in its original conditions, is accurately modeled by the Maxwell constitutive law, characterized by a linear spring in series to a non-linear dash-pot element (Infanti et al, 2002). The first element represents the elasticity of the system mainly due to the compressibility of the silicon fluid, while the second elements accounts for the damping properties. The constitutive equation is:

$$F = C\left(\dot{x} - \frac{\dot{F}}{K}\right)^{\alpha} \tag{1}$$

where x represent the displacement, K the elastic stiffness of the spring and α the exponent that characterize the non-linearity of the response.

In order to simulate the performance of the damper in damaged conditions, consistently with the response of Figure 17, a model was obtained with a dash-pot element in series with a gap element (Figure 18).

25
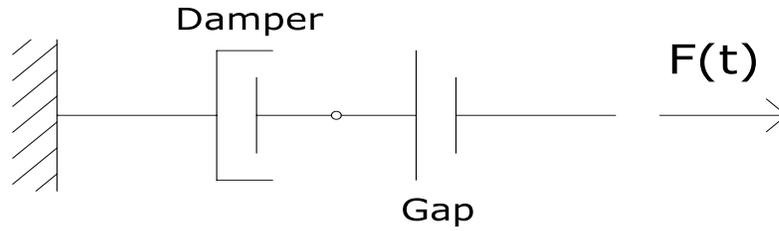
Figure 18. Model of Damper with leakage.

The force-velocity relationship can be written:

$$F = C\dot{x}^{\alpha} + K\left(x - d_g\right) \tag{2}$$

Where:
K = gap stiffness;
x = displacement;
d_g = length of gap.

The second part of the equation is equal to zero when $x<d_g$. Figure 19 shows the contribution of the two components (the dash-pot on the left and the gap element on the right) to the force-displacement response.
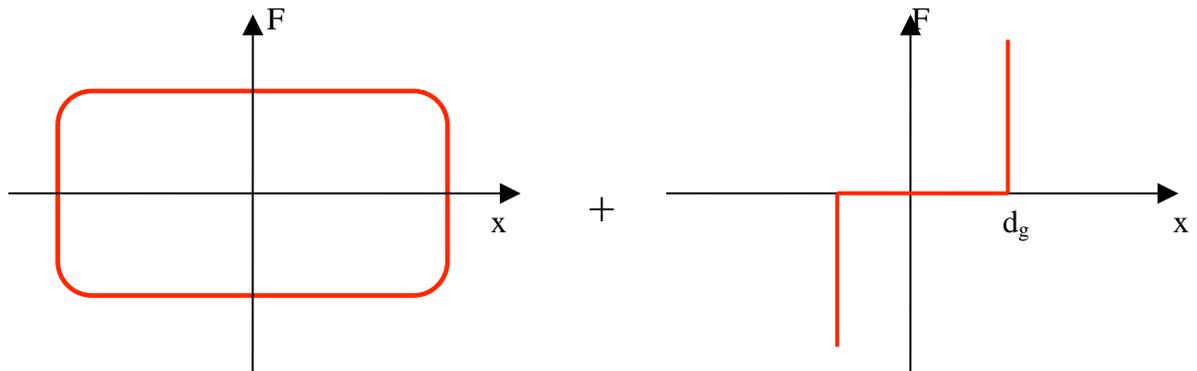
Figure 19. Model of the damaged damper.

The variation of the gap length as a function of the leakage for all the tests is reported in Figure 20. In general the lengths variation is linear with the increment of Leakage.
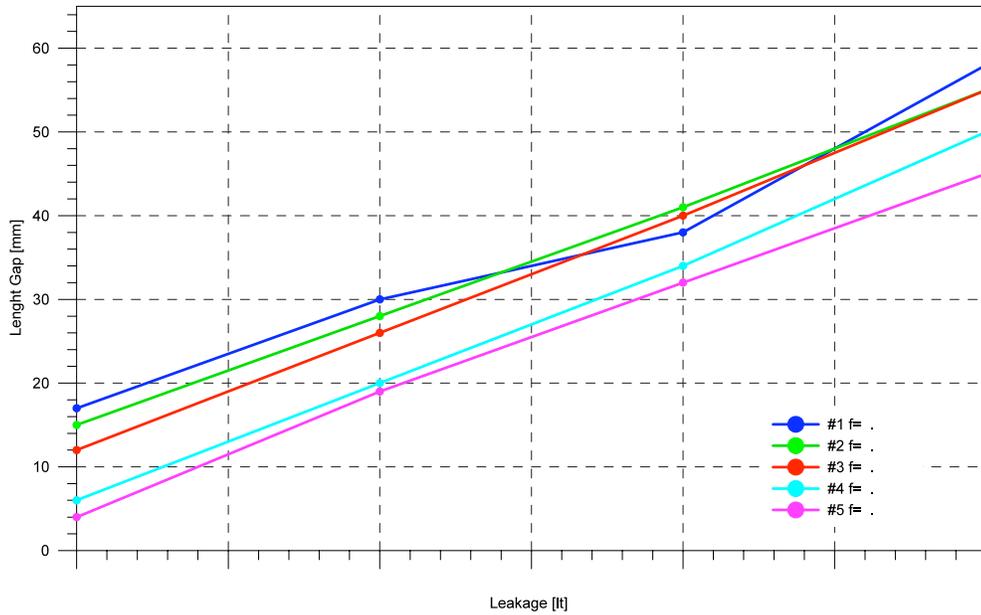
Figure 20. Variation of Length Gap with leakage for the different test

The model results are presented in Figure 21 to Figure 24. The experimental results and the model performance for Test #5, a different level of leakage are compared.
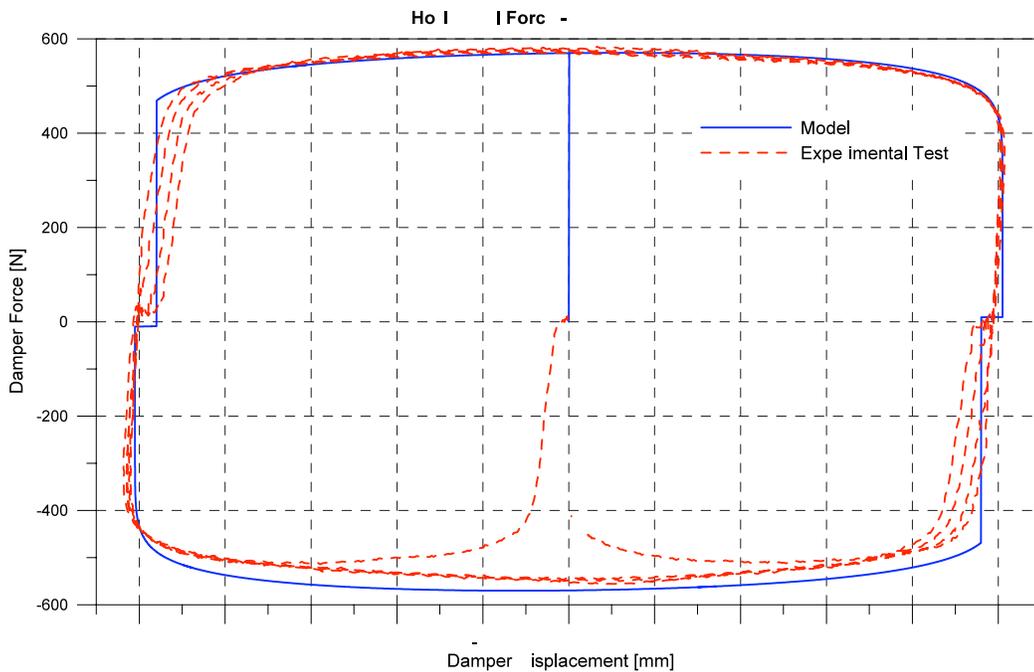
Figure 21. Test#5 Horizontal Force Leakage 0.4 liters: comparison between the model and test

27
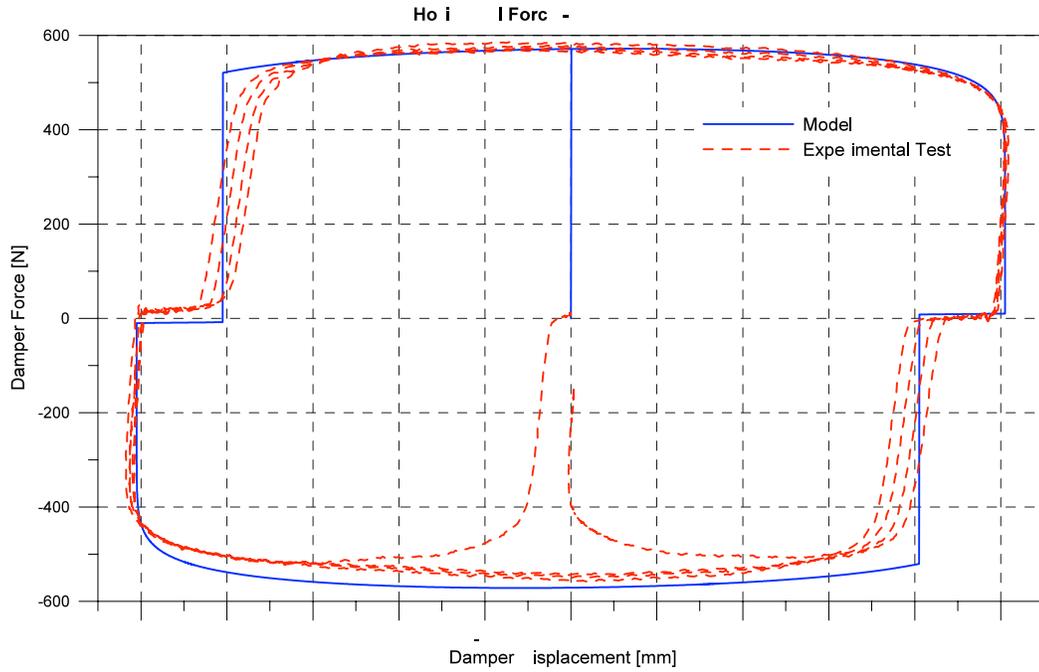
Figure 22. Test#5 Horizontal Force Leakage 0.8 liters: comparison between the model and test
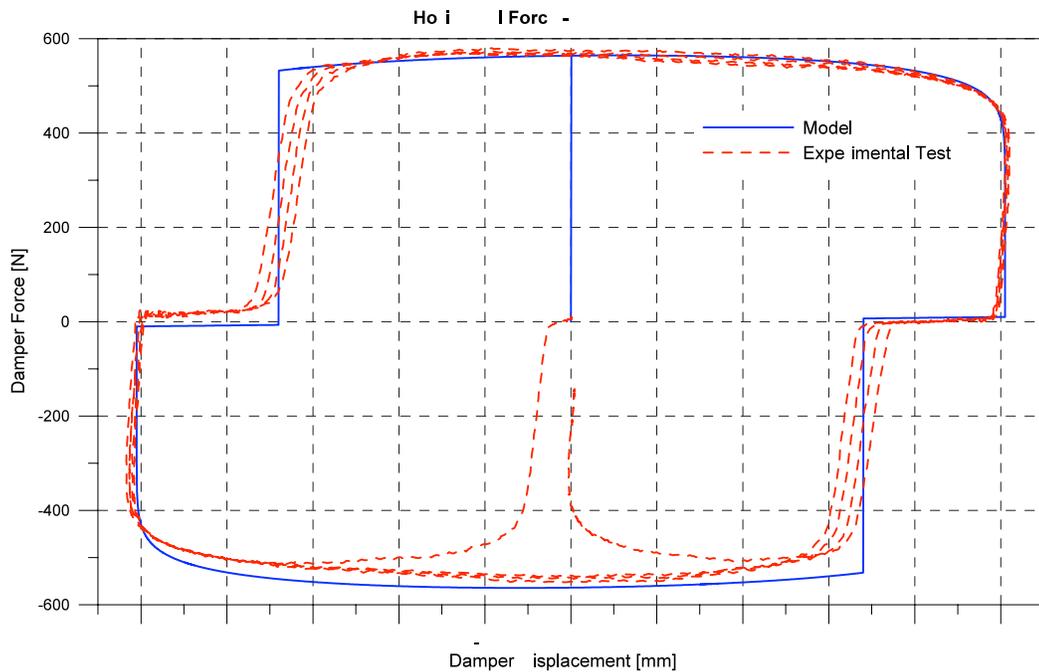
Figure 23. Test#5 Horizontal Force Leakage 1.2 liters: comparison between the model and test

28
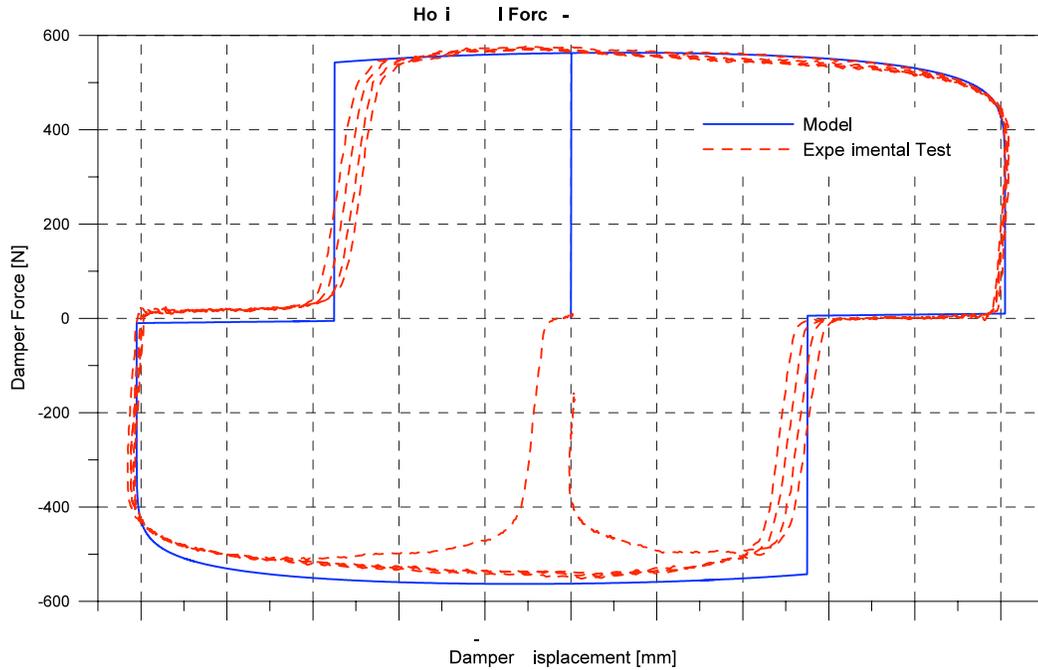
Figure 24. Test#5 Horizontal Force Leakage 1.6 liters: comparison between the model and test

In order to implement the peculiar response of the damaged damper into the F.E. model of the bridge, the attention was focused to the most representative parameter of damper response, the energy dissipated per cycle (*EDC*). The energy dissipated for every cycle was calculated for all the tests using the following equation:

$$EDC = \int F_d\big(x(t)\big)dx \tag{3}$$

The obtained *EDC* values are reported in Table 6.

TEST	EDC (kN-mm) Cycle 1	EDC (kN-mm) Cycle 2	EDC (kN-mm) Cycle 3
FIP Leakage 0 Test 1	103722	103781	103516
FIP Leakage 0 Test 2	168039	169621	170537
FIP Leakage 0 Test 3	188167	189887	190842
FIP Leakage 0 Test 4	205062	205406	206007
FIP Leakage 0 Test 5	219445	220109	219621
FIP Leakage 04 Test 1	96534	96834	97030
FIP Leakage 04 Test 2	155876	158640	160776
FIP Leakage 04 Test 3	175892	178785	180896
FIP Leakage 04 Test 4	191964	195029	197433
FIP Leakage 04 Test 5	207885	209132	210478
FIP Leakage 08 Test 1	90444	90686	90791
FIP Leakage 08 Test 2	145773	148315	150392
FIP Leakage 08 Test 3	163853	166487	168553
FIP Leakage 08 Test 4	179064	181216	183147
FIP Leakage 08 Test 5	192512	192483	193742
FIP Leakage 1.2 Test 11	86141	86483	86615
FIP Leakage 1.2 Test 12	83660	83587	83966
FIP Leakage 1.2 Test 2	134959	137098	138706
FIP Leakage 1.2 Test 3	152336	154010	155784
FIP Leakage 1.2 Test 4	165760	167487	169179
FIP Leakage 1.2 Test 5	179212	179549	180570
FIP Leakage 1.6 Test 1	75846	75966	76224
FIP Leakage 1.6 Test 2	122471	124387	125972
FIP Leakage 1.6 Test 3	138705	140478	141823
FIP Leakage 1.6 Test 4	151051	152125	153628
FIP Leakage 1.6 Test 5	162410	163131	164444

Table 6. Energy dissipated per cycle

The percentage variation of *EDC*, obtained experimentally and from the numerical model, is compared in Figure 25 for the tests at 1.11 Hz and at different levels of leakage. Details about the other tests are presented in the SRMD report No. 2007/09 (Benzoni et. al, 2007). It is visible that the effect of an increased removal of viscous fluid produces a linearly proportional effect on the damper response. The performance of the model is also sufficiently accurate to simulate the effects obtained by tests.
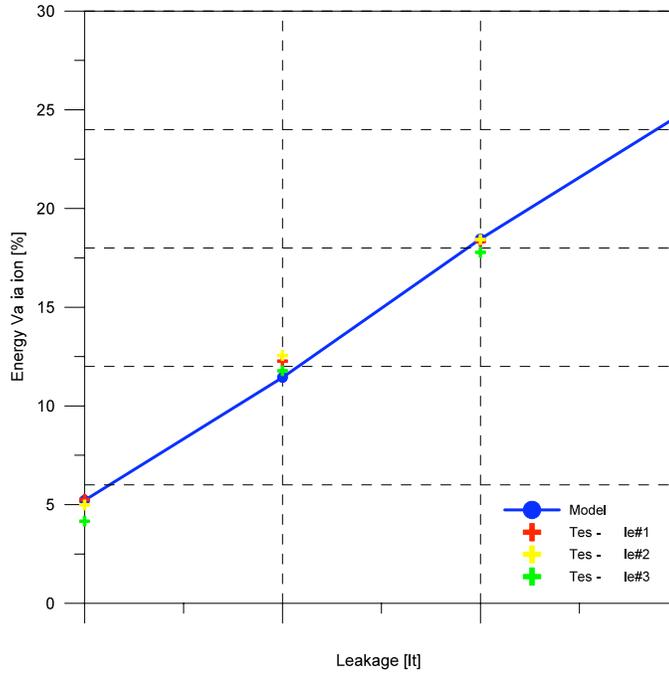
Figure 25. Test#5 (f=1.11Hz): Energy variation model and experimental data.

For the goals of this research, the most convenient approach to implement the above mentioned variation of the damper response, in case of leakage, was to convert the change in *EDC* in terms of the parameters *C* (see Figure 26). Specifically, for the dampers at the main span which have a coefficient α=1, it is possible to directly obtain the dissipated energy, in case of sinusoidal excitation, as:

$$EDC = \pi\, C x^2 \omega \tag{4}$$

Where:

C = damping coefficient;
X = maximum displacement;
ω = frequency.

31

The variation of damping coefficient ΔC is so directly related to the variation of energy:

$$\Delta C = \frac{\Delta(EDC)}{\pi x^2 \omega}$$

(5)
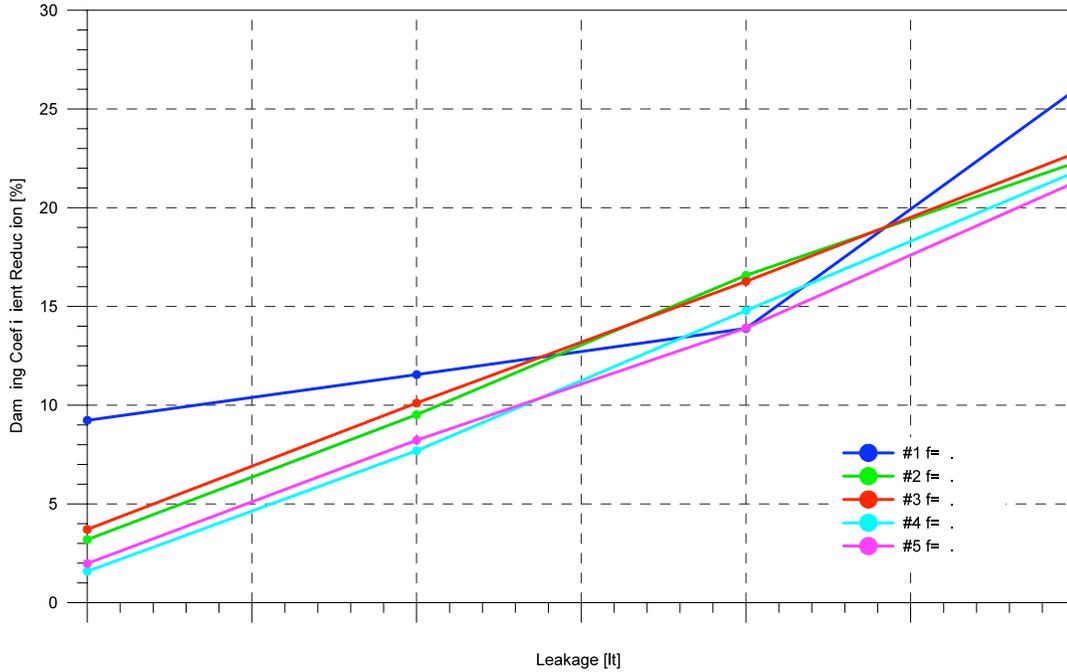
Figure 26. Damper Main Span to tower: variation of damping coefficient

The dampers at the fuses instead have a value of α equal to 0.1. In this case the energy variation cannot be directly correlated with the variation of the damping coefficient C. However, it is possible to relate the change in EDC to the equivalent damping through the following equation:

$$\xi_{eq} = \frac{EDC}{2\pi K_{eff} X^2}$$

(6)

Where:

EDC = energy dissipated;
ξ_{eq} = equivalent damping;
K_{eff} = effective stiffness;
X = maximum displacement.

Assuming a constant value of equivalent damping ξ_{eq}, the changes in *EDC* can be converted to changes in effective stiffness, as indicated in Eq. (7) and Eq. (8).

$$\Delta K_{eff} = \frac{\Delta(EDC)}{2\pi\,\xi_{eq}\,x^2} \tag{7}$$

The peak force in the device can be expressed by:

$$F_{max} = \Delta K_{eff}X = \Delta C\dot{X}^{\alpha} \qquad \Rightarrow \qquad \Delta C = \frac{\Delta K_{eff}X}{\dot{X}^{\alpha}} \tag{8}$$

Where:

F_{max} = peak force;
ΔK_{eff} = variation of effective stiffness;
X = maximum displacement;
$\dot{X}$ = peak velocity;
ΔC = variation of damping coefficient.

The change in damping coefficient as function of the amount of fluid removed in shown in Figure 27 for the dampers at fuse locations.
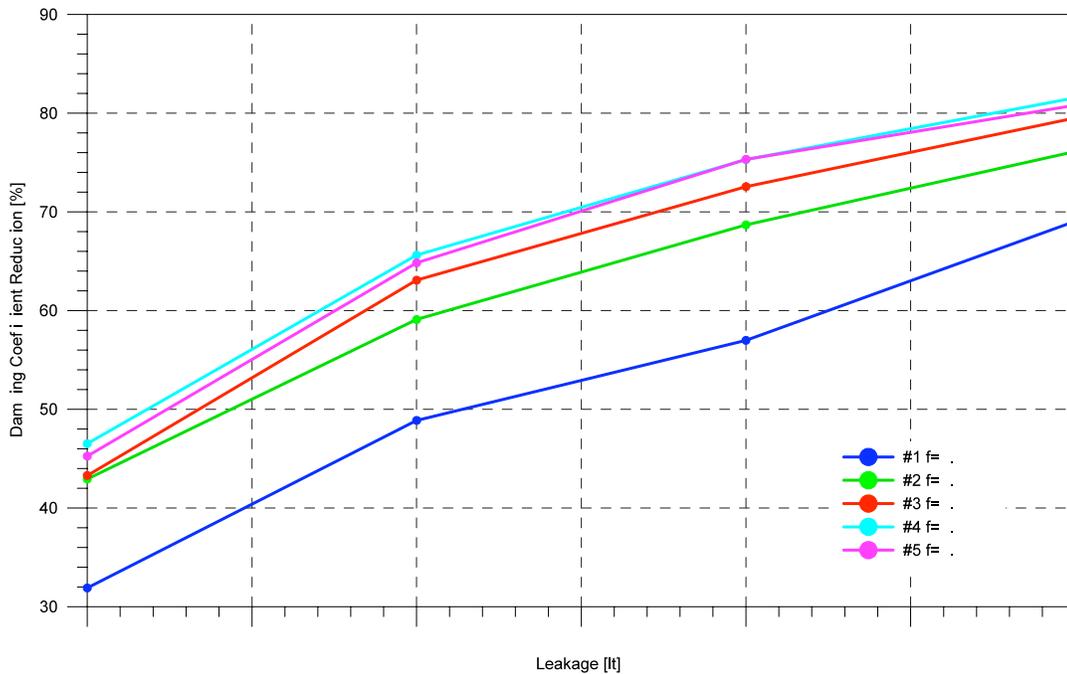
Figure 27. Dampers at Fuses: variation of damping coefficient

As presented in the following paragraphs, the experimental results from the damper in damaged conditions were used in the Adina model of the bridge to simulate degraded conditions of the devices. The above approximate conversions of the variation of the *EDC* to the damping coefficient *C* allowed to utilize the existing elements that simulate the dampers in the F.E. model. The approximation was considered sufficient for the scope of the research, where the numerical model of the bridge is only used for validation purposes. The availability of experimental results on dampers, identical to the ones installed on the bridge, but in degraded conditions, will allow the acquisition of an additional important database for the update of the F.E. model. At the time of this writing the laboratory tests on the dampers removed from the Vincent Thomas Bridge are not completed.

4) DEFINITION OF A DAMAGE DETECTION ALGORITHM ABLE TO TAKE INTO ACCOUNT THE EXISTANCE OF ENERGY DISSIPATION DEVICES

The main intent of the present research is to select an existing level III damage detection algorithm and then adapt it to the specific case of a bridge structure equipped with energy dissipators. As part of the process we will extend the level III method to a level IV method. The research approach was organized consistently with the schematic chart indicated in Figure 28.

STEP 1

| Structural model | Recorded structural response |

| Non-damaged structure | Damaged structure |

STEP 2

Extraction of mode shapes

Interpolating functions of mode shapes

STEP 3

Assessment of energy variation for structural and energy dissipation elements

Damage index assessment for each element and mode

Interpretation of the damage indicators and localization of damage

STEP 4

Assessment of the damage impact on the overall structural performance

Figure 28. Layout of analytical approach

Step 1

Different numerical models were used to validate and calibrate the damage detection algorithm. The selected existing approach required a severe level of modifications to be able to provide the desired accuracy needed for the specific task. For this reason, the approach was applied, in the early phases of development, to a very simple structure, using a Finite Element model capable of non-linear analysis. In a later stage the recorded response from the F.E model of the Vincent Thomas Bridge was also analyzed, in order to account for the level of sub-structure interaction and complexity typical of an isolated bridge. In the last stage data obtained from the sensor network available on the bridge were used. Each structural case study was initially modeled in an undamaged configuration and subsequently modified to create localized condition of structural degradation at different level of severity. For the structural elements the simulated damages were introduced through a reduction of stiffness while for the energy dissipation devices both a reduction of stiffness and of viscous dissipative properties were used to reproduce the degraded performance observed in real devices.

Step 2

The response obtained at each node of the simplified structure or at specific sensor locations of the analyzed bridge was used to extract the natural frequencies and mode shapes for the first three modes. The procedure is not limited to a specific number of modes but for the purpose of this investigation the first three modes contain the sufficient information for the damage identification process. A procedure, presented by Kim (Kim el al, 2005) for the extraction of modes shapes was adapted to the specific application and interfaced to the damage identification approach of step 3. An additional approach, the Covariance-driven Stochastic Subspace Identification method (SSI-Cov) (Peeters, 2000) was also introduced, providing better results for the bridge model.

Step 3

The non destructive damage evaluation method, originally introduced by (Stubbs et. al, 1990) was adapted to structures equipped with energy dissipation devices. Pre-damage and post-damage configurations of the structure are compared in terms of energy content obtained from flexural and axial deformations. A damage indicator, associated with arbitrary structural elements as well as the specific devices, is obtained. The procedure allows to identify the damage location after a generalized procedure of interpretation of the energy variation associated with the single elements. The selection of this approach was mainly motivated by its simplicity of application as well as by its natural reference to the energy variation of structural and anti-seismic components. Other approaches (e.g. Wolfe et al, 2002) require a local monitoring of forces and displacement directly related to the devices. In the selected approach instead, the distribution of sensors can be quite spread over the structure and the structural response can be related to the device locations through the assessment of the mode shapes. This characteristic together with the immediate connection to the energy changes makes the approach ideal also for anti-seismic devices of different nature like sliders, elastomeric bearings etc, where the forces across the device are not easy to monitor and their interaction with the rest of the structure is naturally exercised in terms of

energy change. As presented in detail in what follows, the approach also maintains the dual focus of assessing the conditions of traditional structural elements as well as of the isolation/energy dissipation devices.

Step 4

The detected structural degradation is associated to a level of severity taking into account the realistic impact on the overall structural performance in order to be able to suggest a possible plan of retrofit or replacement of damaged portions of the structure or of specific energy dissipation devices.

In the following paragraphs, the original numerical formulation of the approach is presented in two basic application cases. The first one is relative to a very simple structure without the energy dissipation devices while the second one includes dampers.

4.1 Original Approach-Structure without energy dissipators

The original procedure is founded on two main assumptions, generally confirmed by experimental results (Mazurek et. al, 1990). The first one is that the geometry of mode shapes in the vicinity of an un-damaged element of a structure changes very little when the structure is damaged elsewhere. The second one is instead related to the observation that relative modal deformations experience the greatest changes in the vicinity of the defect. Both of these assumptions converge in the general approximation that the modal strain energy (F_{ij}) in the *jth* element and the *ith* mode, remains unchanged before and after damage so that:

$$F_{ij} = F_{ij}^*$$
(9)

Where the symbol * identify the damaged condition.

If a linear elastic beam is considered, the *ith* modal stiffness is obtained as:

$$K_i = \int_0^L EI(x)\left[\psi_i^{''}(x)\right]^2 dx$$
(10)

Where L is the total length of the beam, ψ_i is the *ith* mode shape and *EI (x)* the beam's bending stiffness. Assuming the beam discretized in a number of elements and nodes, the contribution to the *ith* modal stiffness from the *jth* element can be expressed as:

$$K_{ij} = EI_j \int_a^b \left[\psi_i^{''}(x)\right] dx$$
(11)

Where EI_j is the stiffness of the *jth* element integrated along the length of the single element. *a* and *b* generically indicate the boundary of the element length. EI_j is considered as constant along the element. The term F_{ij} represents the fraction of modal energy for the *ith* mode that is concentrated in the *jth* element. Based on the definitions of Eq. (9) F_{ij} is given by:

$$F_{ij} = K_{ij} / K_j \tag{12}$$

Similarly, for the damaged structure, characterized by asterisks:

$$F_{ij}^* = K_{ij}^* / K_i^* \tag{13}$$

Where:

$$K_i^* = \int_0^L EI^*(x) \left[\psi_i''(x) \right]^2 dx \tag{14}$$

and

$$K_{ij}^* = \int_0^L EI_j^*(x) \left[\psi_i''(x) \right]^2 dx \tag{15}$$

Substituting Eqs. (12) and (13) into Eq. (9) gives:

$$1 = \frac{F_{ij}^*}{F_{ij}} = \frac{K_{ij}^* / K_i^*}{K_{ij} / K_i} \tag{16}$$

and further substituting Eqs. (10), (11), (14) and (15) into Eq. (16) yields:

$$1 = \frac{EI_j^* \int_a^b \left[\psi_i^{*''}(x) \right] dx \Big/ \int_0^L EI^*(x) \left[\psi_i^{*''}(x) \right] dx}{EI_j \int_a^b \left[\psi_i''(x) \right] dx \Big/ \int_0^L EI(x) \left[\psi_i''(x) \right] dx} \tag{17}$$

The assumption that *EI* is constant over the length of the beam, for both the undamaged and damaged structure and that $EI \cong EI^*$ allows reorganizing Eq. (17) and defining the damage localization indicator (D_{ij}) for the *jth* element and the *ith* mode as:

$$DI_{ij} = \frac{EI_j}{EI_j^*} = \frac{\int_a^b \left[\psi_i^{*"}(x)\right]dx \Big/ \int_0^L \left[\psi_i^{*"}(x)\right]dx}{\int_a^b \left[\psi_i^{"}(x)\right]dx \Big/ \int_0^L \left[\psi_i^{"}(x)\right]dx} \tag{18}$$

In general terms damage is indicated, for the *jth* element when $D_{ij} > 1$. It must be noted that the possibility of very small numbers for the denominator of Eq. (18), for instance obtained when the *jth* member is at or near a node of the *ith* mode, can result in a false prediction of damage. For this reason, in some cases, a value of unity is added to the Eq. (9) to avoid division by zero:

$$1 = \left(F_{ij}^* + 1\right) \Big/ \left(F_{ij} + 1\right) \tag{19}$$

Eq. (19) results in a new definition of the damage indicator D_{ij} as:

$$DI_{ij} \cong \frac{\left(\int_a^b [\psi_i^{*"}(x)]^2 dx + \int_0^L [\psi_i^{*"}(x)]^2 dx\right) \int_0^L [\psi_i^{"}(x)]^2 dx}{\left(\int_a^b [\psi_i^{"}(x)]^2 dx + \int_0^L [\psi_i^{"}(x)]^2 dx\right) \int_0^L [\psi_i^{*"}(x)]^2 dx} \tag{20}$$

From the damage indicator D_{ij} is possible to obtain the normalized indicator for the *jth* element and the *ith* mode as:

$$z_{ij} = \frac{DI_{ij} - \mu_{DI}^i}{\sigma_{DI}^i} \tag{21}$$

where μ_{DI}^i and σ_{DI}^i represent the mean and standard deviation of the damage index of all the elements for the *ith* mode, respectively.

With 98% of level significance the procedure indicates the existence of damage in the *jth* element and for the *ith* mode if:

$$z_{ij} \geq 2 \tag{22}$$

The combination of different modes (*NM*) results in a damage indicator, for the *jth* element, given by:

$$DI_j \cong \frac{\sum_{i=1}^{NM} \left(\int_a^b [\psi_i^{*"}(x)]^2 \, dx + \int_0^L [\psi_i^{*"}(x)]^2 \, dx \right) \int_0^L [\psi_i^{"}(x)]^2 \, dx}{\sum_{i=1}^{NM} \left(\int_a^b [\psi_i^{"}(x)]^2 \, dx + \int_0^L [\psi_i^{"}(x)]^2 \, dx \right) \int_0^L [\psi_i^{*"}(x)]^2 \, dx} \tag{23}$$

where *NM* is the number of modes taken into account. As indicated above the normalized index z_j for the *jth* element is obtained as:

$$z_j = \frac{DI_j - \mu_{DI}}{\sigma_{DI}} \tag{24}$$

where μ_{DI} and σ_{DI} represent the mean and standard deviation of the damage indicator of all the elements for all the considered modes, respectively.

The severity of damage at a given location may be estimated from the magnitude of the damage index (DI_j) at the designated location. In this formulation, the magnitude of damage, at a particular location, represents the fractional change in element stiffness. The damage severity index α_j is obtained as:

$$\alpha_j = \frac{K_j^* - K_j}{K_j} = \frac{1}{DI_j} - 1 \tag{25}$$

where K_j and K_j^* are the stiffness of the elements in the un-damaged and damaged configuration, respectively. When the calculation of the severity index is performed the single modal contributions are already be accounted for. The existence of damage is indicated by $\alpha_j \leq 0$.

4.2 Structural Model for Procedure Validation

A simple portal frame, with moment resisting joints was used as a basic case study to validate the original and the modified procedure. The portal is identical to the one proposed in Stubbs et al. (2000) in order to allow a comparison of results between the original procedure and some initial modification that was implemented. The geometry of the portal is indicated in Figure 29. The material and geometry of the elements of the frame are assumed constant with area $A=0.459\text{x}10^{-2}$ m^2, modulus of elasticity $E=0.21\text{x}10^{9}$ kN/m^2, moment of inertia $I=0.579\text{x}10^{-4}$ m^4 and density $\rho =7850$ Kg/m^3. The discretization of the frame in 31 nodes and 30 elements is shown in Figure 30.

The frame was initially analyzed using modes shapes obtained from finite element analyses using the code SAP2000 (SAP2000, 1997). In each analysis a level of structural integrity degradation was simulated by reduction of the elastic stiffness of different elements. The different case studies are reported in Table 7 with the level of damage expressed as reduction in percentage from the original elastic stiffness. The first two cases are identical to what proposed in Stubbs et al. (2000).
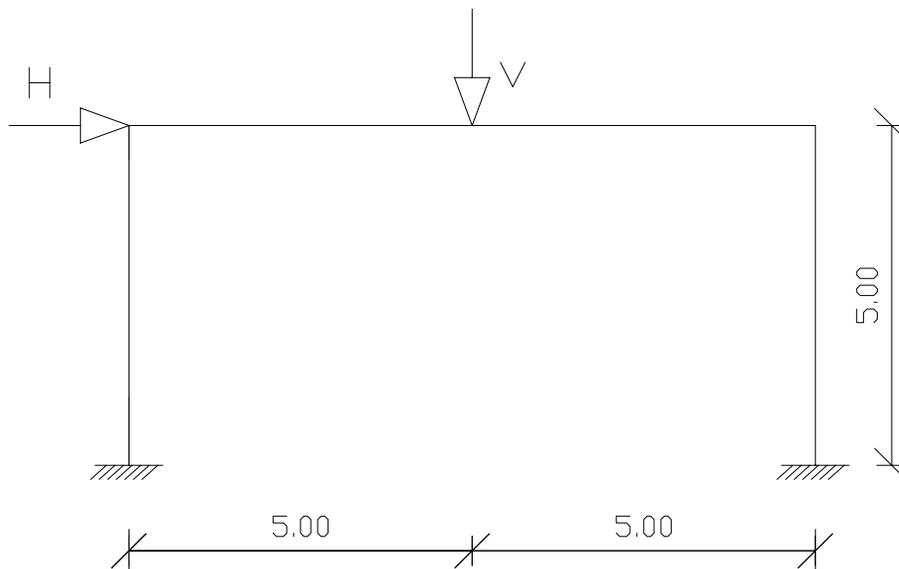
Figure 29. Portal frame
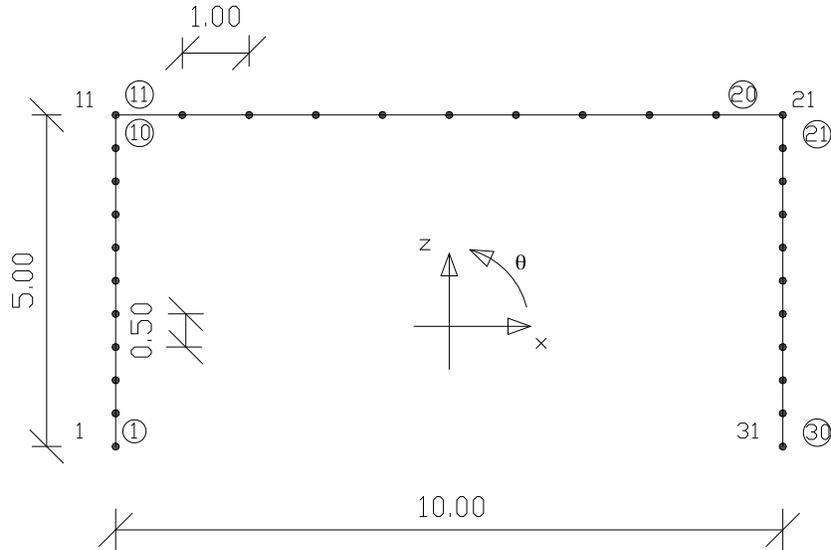
Figure 30. Finite Element Model of the frame

Case #	Damaged Element	Amount of damage	Condition of symmetry
0 Stubbs	0	0%	Sym
1 Stubbs	15, 16	10%	Sym
2	13, 18	10%	Sym
3	15,16	30%	Sym
4	9, 22	10%	Sym
5	9, 29	10%	Non Sym
6	All	10%	Sym
7	18, 20	20%	Non Sym

Table 7. Case studies for sample frame without energy dissipation system

Case #0 represents the reference structure with no level of damage. Cases #1 and #3 include 2 damaged elements at mid-span of the beam, with a level of damage equal to 10% and 30%, respectively. Case #2 still considers the damage only located in the beam but the locations were selected to simulation the damage in the elements most affected by a higher mode (third mode). Case #4 simulates symmetric damage at the top of the columns, when instead case #5 presents a damage at the top of the left column and at the bottom of the right column. Case #6 was introduced to investigate the performance of the procedure in case of largely distributed level of damage and finally case #7 considers a non symmetric damage at the right edge of the beam.

4.3 Procedure Implementation and Improvement

The numerical code for the damage detection algorithm described above was implemented in Matlab. The code receives as inputs the absolute displacements of each node of the structure, in X and Z direction and the rotations at the corners of the frame. Both displacement and rotations are normalized to the maximum value of the mode shape.

In details the procedure is implemented through the following steps:

1   Receive as input the first three modal shapes obtained from the Finite Element analysis (Sap2000);

2   For each sub-component of the frame (two columns and one beam) the best-fit curve of the mode shapes is obtained with a polynomial function of a degree appropriate to the specific mode shape;

3   Curvatures and strain energies associated to each element are calculated;

4   The damage is introduced and steps 1 to 3 are repeated for the damaged structure;

5   The variation of strain energy is calculated between un-damaged and damaged configuration;

6   Eqs (20) and (23) are used to calculate the damage index for each mode and for the first three modes combined;

7   Eq. (24) is used to estimate the normalized index for each element;

8   Eq. (25) is used to estimate the damage severity;

9   The damage location and the severity of damage are visualized.

Few critical issues were solved in order to perform the above listed steps of the procedure. First of all the concept of the algorithm requires to subdivide the structure in sub components like the columns and the beam. This allows, for instance, the identification of the best degree of the polynomial function able to accurately represent the modes shapes for each structural component. A simple mathematical curve fitting procedure was not able to take into account the internal and external boundary conditions of the structure. For this reason the rotation at nodes are used as additional information to "force" the polynomial function to be consistent with the boundary conditions.

The subdivision of the overall structure in three sub-components (two columns and one beam) allows to replace the energy terms of the overall structure (see Eq. 23)

$$\int_0^L [\psi_i^{''}(x)]^2\, dx$$

$$(26)$$

with a sum extended to the *n* sub-components:

$$\sum_{n=1}^{3} \int_0^L [\psi_i^{''}(x)]^2\, dx$$

$$(27)$$

As indicated in Eq. (23) in the original approach the contribution of the different modes is combined as a simple sum in the definition of the Damage Indicator for each structural element. The combination of modal contribution, in the original format, provided several numerical problems particularly when extended to modes as the third one or higher. Several attempts were completed in order to associate the energy variation of each sub-element with the "importance" of the specific element for the mode shape under consideration. For instance, let's consider the energy contributions of the beam elements of the sample frame for the third mode. It is clear that the elements at mid-span should be practically un-affected by the beam deformation that is supposed to be negligible at mid-span. Series of coefficients were introduced to transfer into the algorithm this type of information. This attempt however failed in the implementation phase due to the complexity of its formulation that systematically attributed excessive importance to the elements at the column-beam joints. An alternative approach instead provided a significant improvement in the numerical accuracy. It was noted that in the comparison between un-damaged and damaged response, the variation of the natural frequencies of the significant modes can represent a reliable indicator of the importance of the modal contribution. For this reason, a "weight" coefficient was introduced, taking into account the variation of the natural frequency from un-damaged to damaged configuration. This coefficient (c_i) it obtained as:

$$c_i = \frac{v_i}{\max(v_i)}$$

$$(28)$$

where:

$v_i = abs\left(f_i^D - f_i^U\right)$, in which f_i^U and f_i^D are the natural frequency of the *ith* mode for the undamaged and damaged case, respectively. The coefficient c_i is multiplied by the damage indicator DI_{ij} and allows the definition of the Normalized Damage Indicator Z_{ij} and Z_j calculated as:

$$Z_{ij} = \frac{c_i DI_{ij} - \mu\left(c_i DI_{ij}\right)}{\sigma\left(c_i DI_{ij}\right)}$$

$$(29)$$

$$Z_j = \frac{\sum_{i=1}^{NM} c_i DI_{ij} - \mu\left(\sum_{i=1}^{NM} c_i DI_{ij}\right)}{\sigma\left(\sum_{i=1}^{NM} c_i DI_{ij}\right)}$$

(30)

4.4 Application of the damage identification procedure to the structure without dampers

In this section the results for some of the most representative case studies are presented.
In Table 8 are reported the modal results of all the cases. The modal coefficients of importance c_i (Eq. 28) are reported in Table 9.

CASE #	Frequencies (Hz)		
	Mode 1	Mode 2	Mode 3
0 Stubbs	8.44	15.13	42.10
0	8.41	15.02	41.49
1 Stubbs	8.43	14.92	42.02
1	8.40	14.38	41.22
2	8.26	14.77	39.02
3	8.40	14.31	41.15
4	8.30	14.57	40.90
5	8.13	14.76	41.32
6	6.33	11.30	31.30
7	8.38	14.98	41.42

Table 8. Modal frequencies for each case

CASE #	Coefficient c_i		
	Mode 1	Mode 2	Mode 3
1	0.02	1.00	0.42
2	0.06	0.15	1.00
3	0.01	1.00	0.48
4	0.19	0.76	1.00
5	1.00	0.93	0.61
6	0.20	0.37	1.00
7	0.43	0.57	1.00

Table 9. Coefficient of mode importance for each case

Case 1

For this example the damage is identical for the two elements 15 and 16 of the beam. To simulate the damage a reduction of the modulus of elasticity E equal to 10% of the original value was introduced. Figure 31 indicates the configuration under consideration.
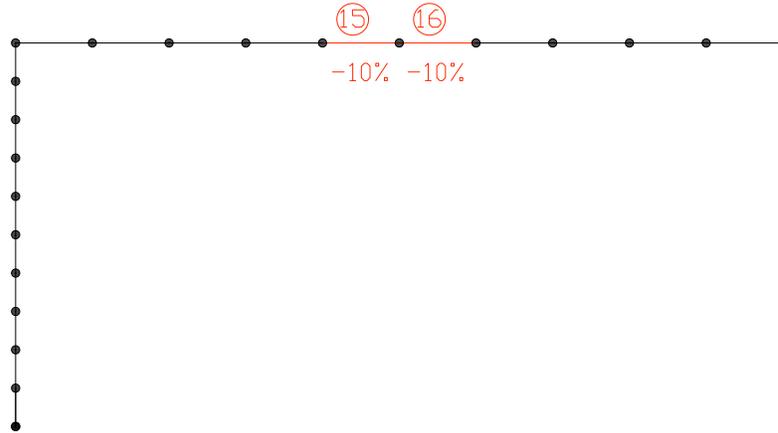
Figure 31. F.E. model for Case #1

The Normalized Damage Indicator Z_{ij} and Z_j, defined by Eq. (29) and (30), are presented in Figure 32 and 33. In both figures the element of the frame sub-components (columns and beam) are aligned on the x axis. Elements from 1 to 10 correspond to the left column, from 11 to 20 are elements of the beam and from 21 to 30 are parts of the right column. From Figure 32 the peaks of the normalized index Z_{ij} are visibly associated with elements 15 and 16 for the second mode shape. Additional peaks are detected at locations 14 and 17 for the first and third mode.

The effect of the coefficient c_i, defined in Eq. (28), in order to provide an efficient combination of the modal contributions is visible in Figure 33. The importance of the degradation detected for the elements at mid-span of the beam (elements 14 and 17) are reduced in importance due to their association only to the first and second mode. The consistency of the prevalent damage obtained for the element 15 and 16 at the second mode is confirmed by the coefficient $c_i = 1$ for the second mode.
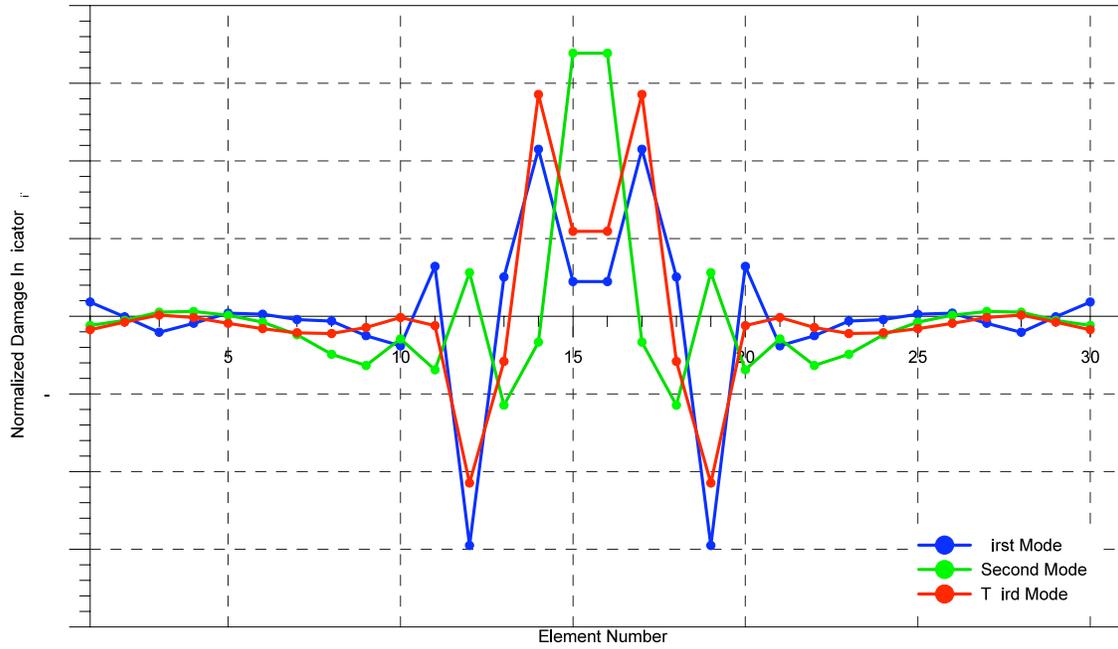
Figure 32. Case #1: Normalized Damage Index Z_{ij} mode by mode
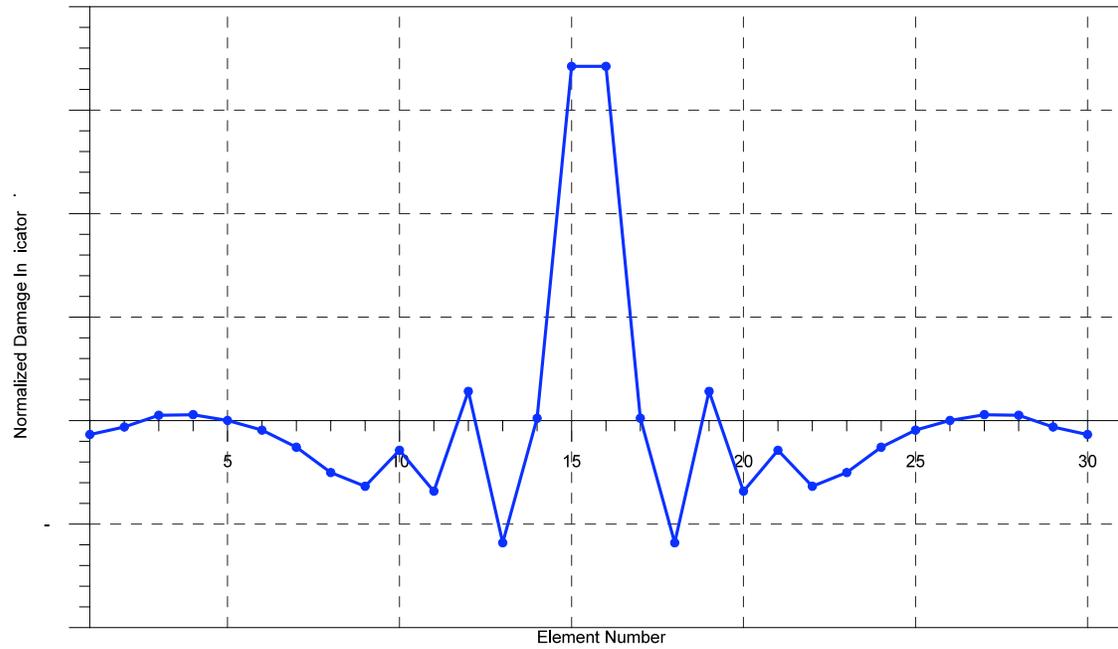
Figure 33. Case #1: Normalized Damage Index Z_j total
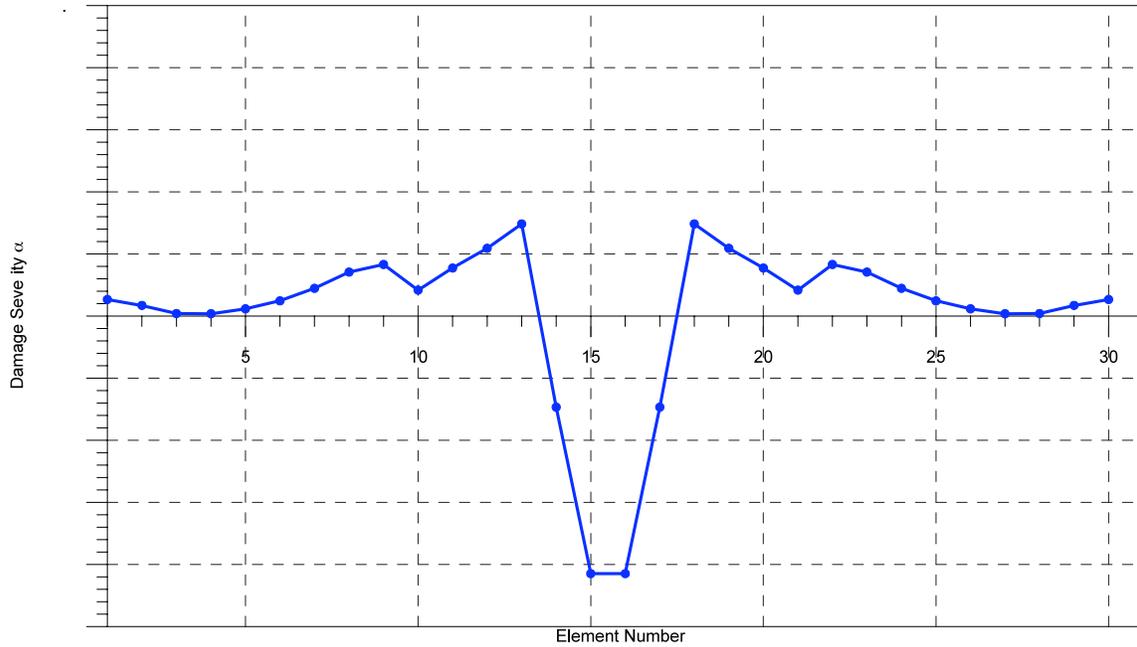
Figure 34. Case #1: Damage Severity Indicator α_j

In Figure 34 is presented the Damage Severity Indicator α_j that indicates the entity of the damage in each sub-element. For the beams element, with a theoretical damage value of 10%, the level of damage detected is 8.5%. The additional variation of characteristics associated with elements 14 and 17 appears to be responsible for the difference.

Case 3

In this case the damage location is the same of Case#1, but damage intensity is increased to 30%. To simulate the damage a reduction of the modulus of elasticity E equal to 30% of the original value was introduced. The model utilized is shown in Figure 35.
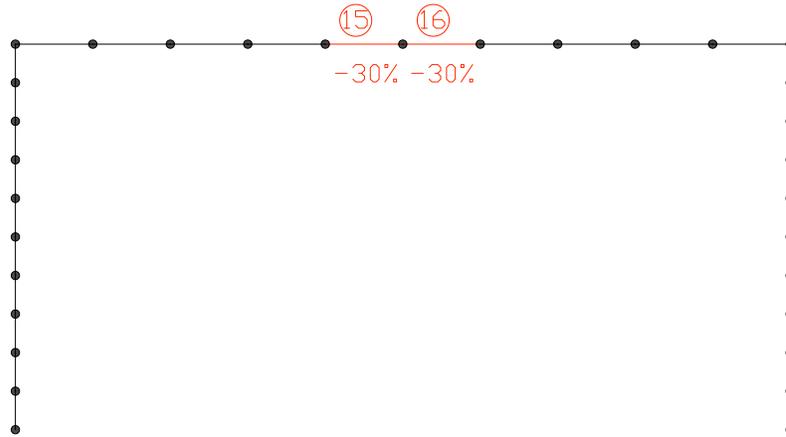
Figure 35. F.E. model for Case #3

The Damage Indicator Z_{ij} and Z_j, normalized with the coefficient of mode importance, are reported in Figure 36 and Figure 37.
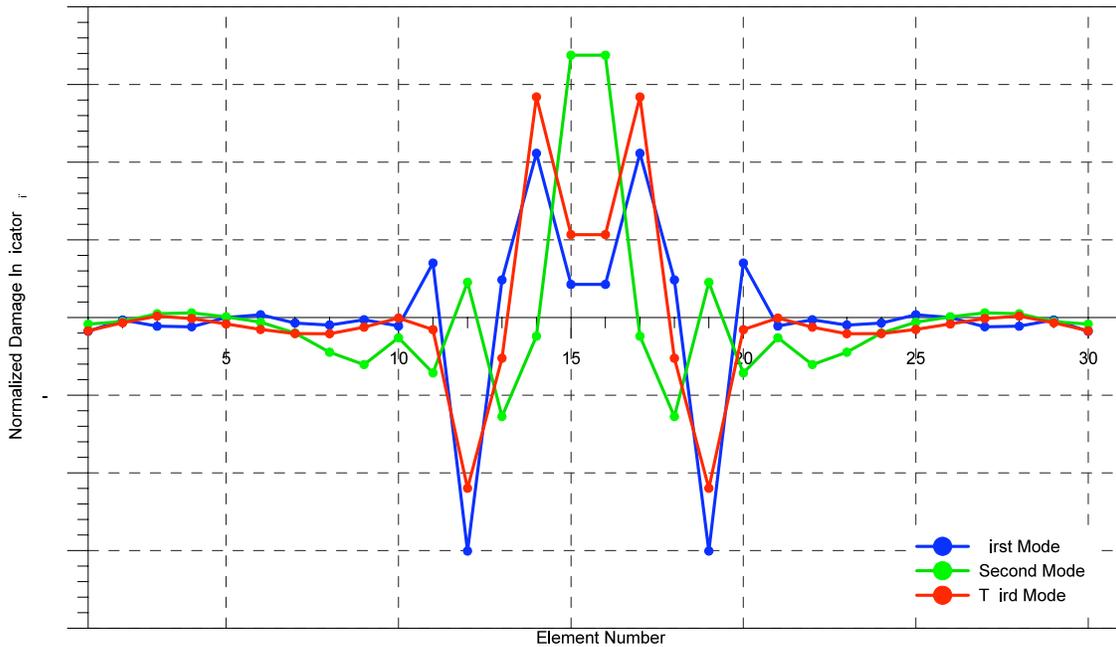
Figure 36. Case #3: Normalized Damage Index Z_{ij} mode by mode
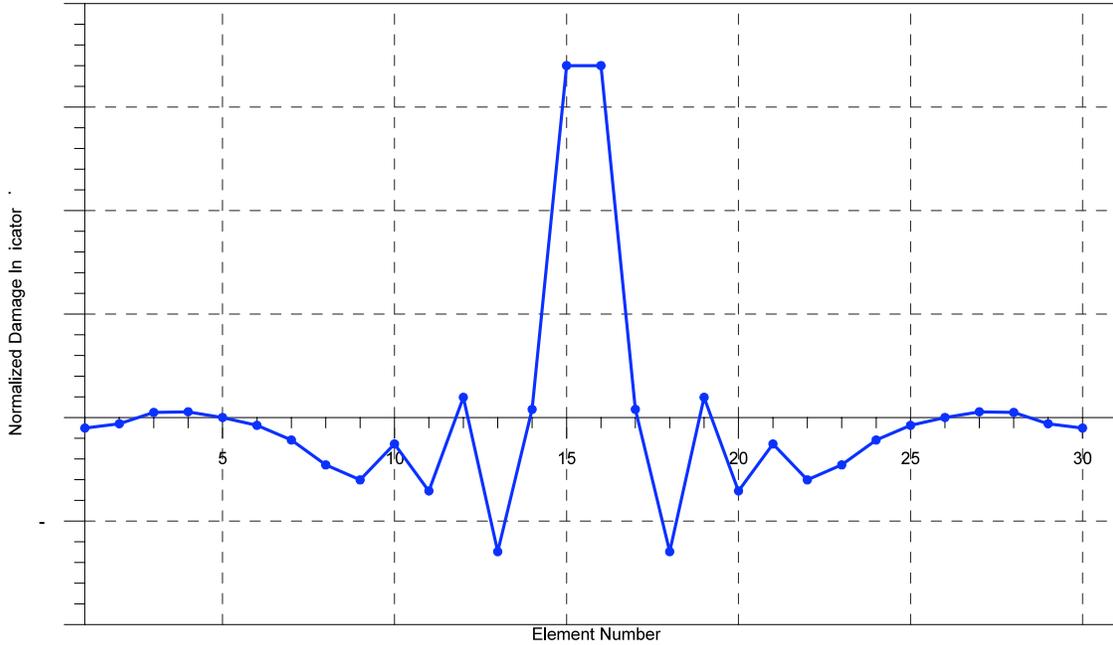
Figure 37. Case #3: Normalized Damage Index Z_j total

In Figure 38 is presented the Damage Severity Indicator α_j that indicates the entity of the damage in each sub-element. For the beams element, with a theoretical damage value of 30%, the level of damage detected is 27%. The additional degradation associated with elements 14 and 17 appears to be responsible for the difference.
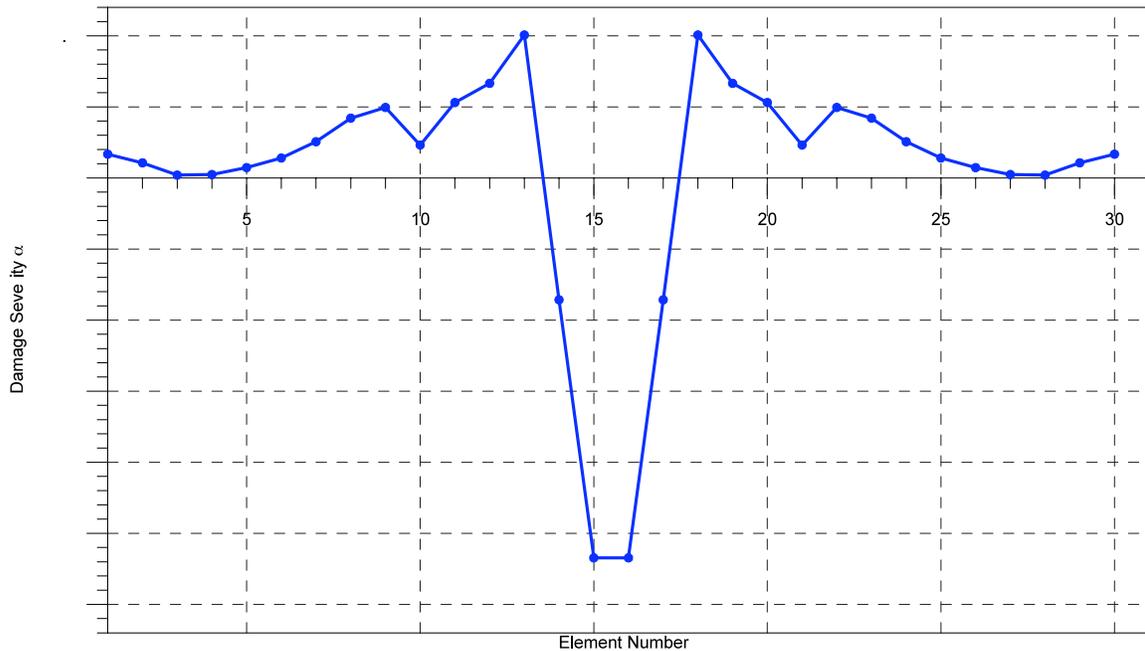
Figure 38. Case #3: Damage Severity Indicator α_j

Case 5

The damage, in this case, is artificially introduced in the two column elements 9 and 29. This is a no-symmetric case. To simulate the damage a reduction of the modulus of elasticity *E* equal to 10% of the original value was introduced.
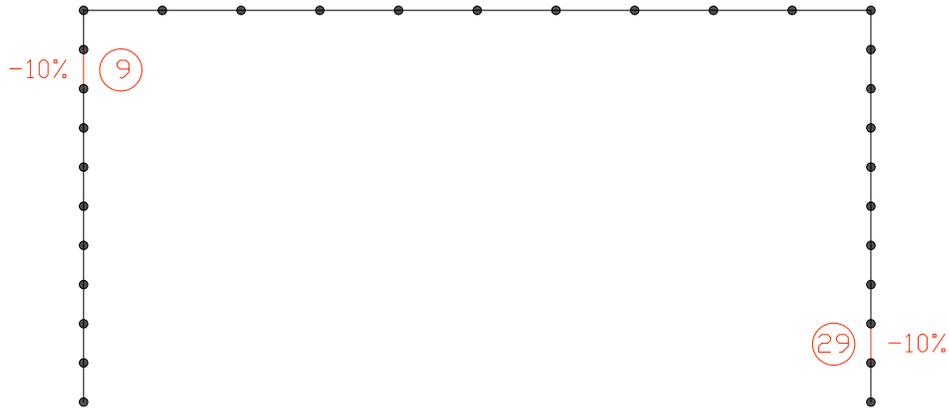
Figure 39. F.E. model for Case #5

The Normalized Damage Indicator Z_{ij} and Z_j, with the coefficient of mode importance, are shown in Figure 40 and Figure 41.
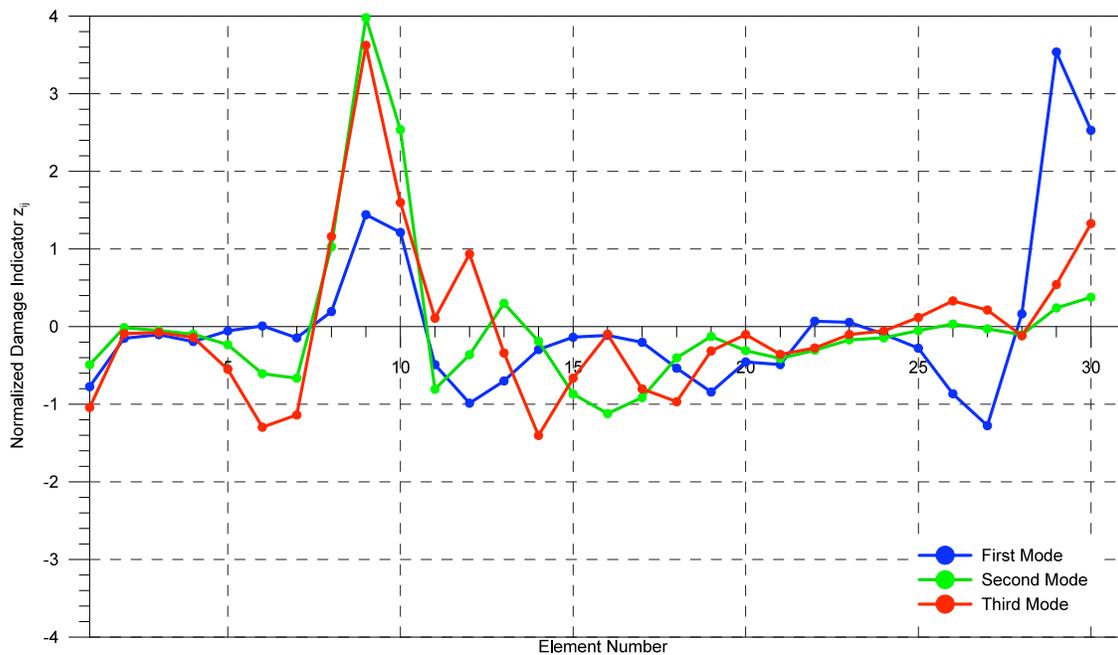
Figure 40. Case #5: Normalized Damage Index Z_{ij} mode by mode

51
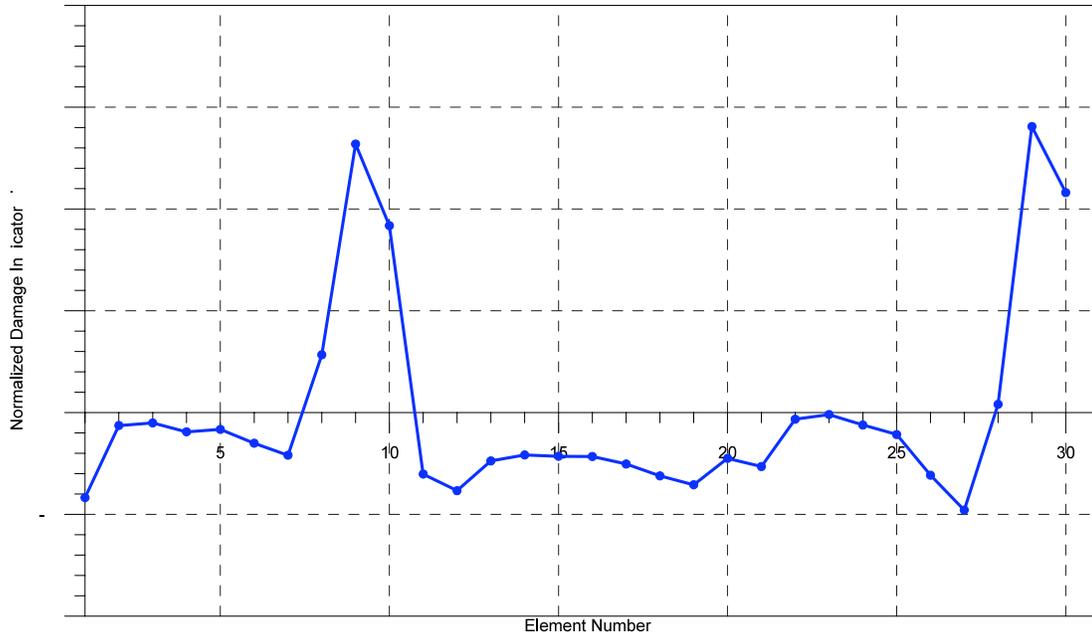
Figure 41. Case #5: Normalized Damage Index Z_j total

In Figure 42 is presented the Damage Severity Indicator α_j that indicates the entity of the damage in each sub-element. For the columns element, with a theoretical damage value of 10%, the level of damage detected is 8% for the element 9 and 6% for the element 29. The additional degradation associated with elements 8 and 10 appears to be responsible for the difference.
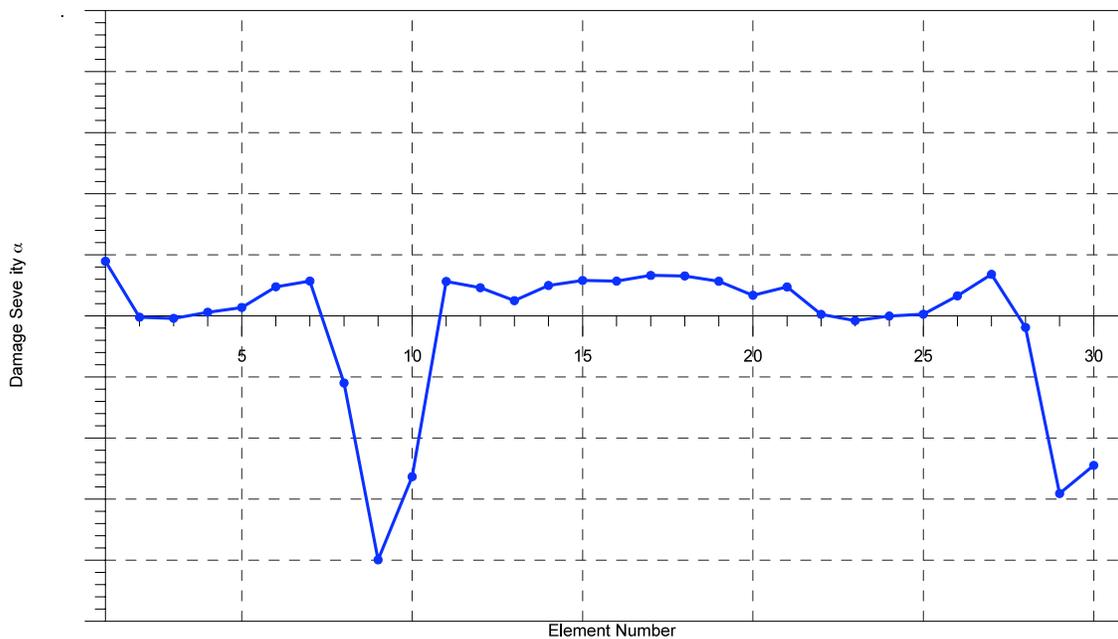
Figure 42. Case #5: Damage Severity Indicator α_j

Case 7

The damage, in this case, is in the beams element 18 and 20. This is a no-symmetric case. To simulate the damage a reduction of the modulus of elasticity E equal to 20% of the original value was introduced.
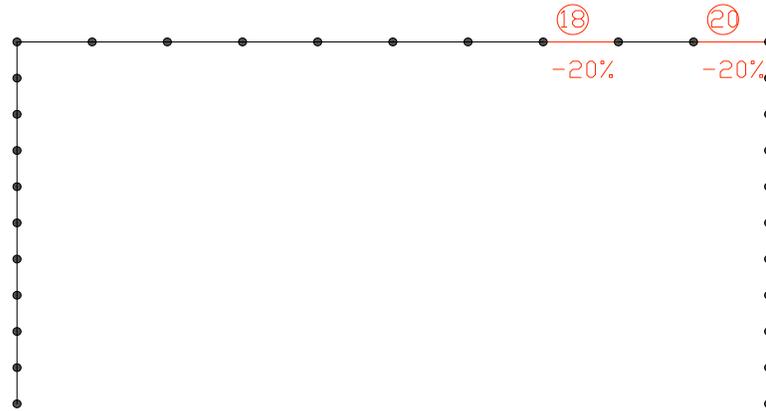
Figure 43. F.E. model for Case #7

The Normalized Damage Indicator Z_{ij} and Z_j, with the coefficient of mode importance, are shown in Figure 44 and Figure 45.
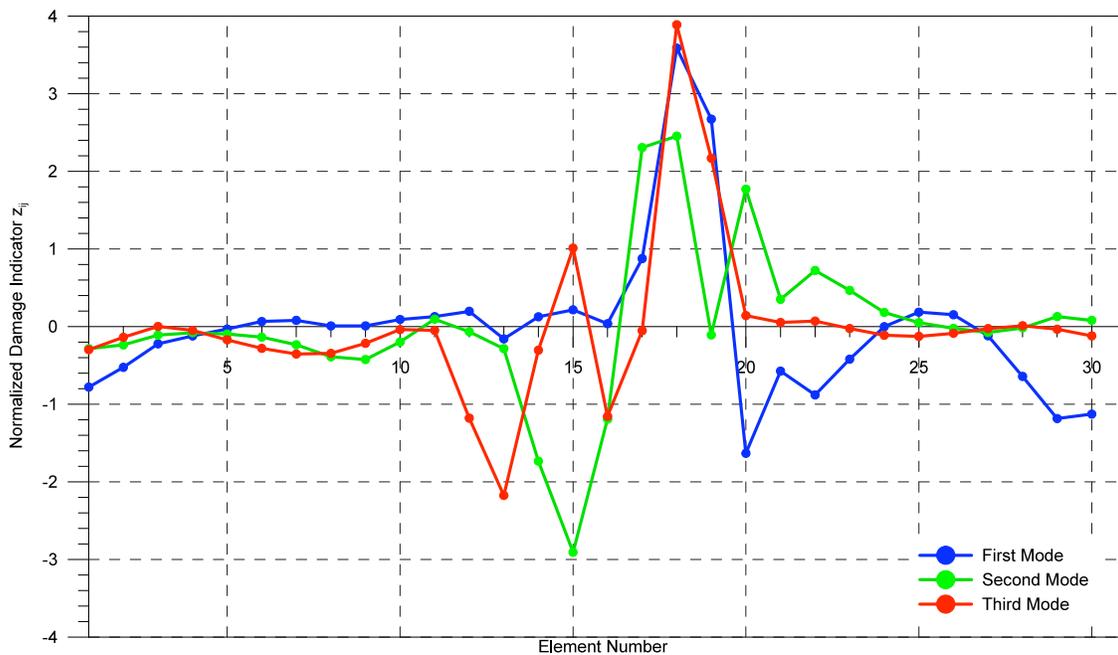
Figure 44. Case #7: Normalized Damage Index Z_{ij} mode by mode
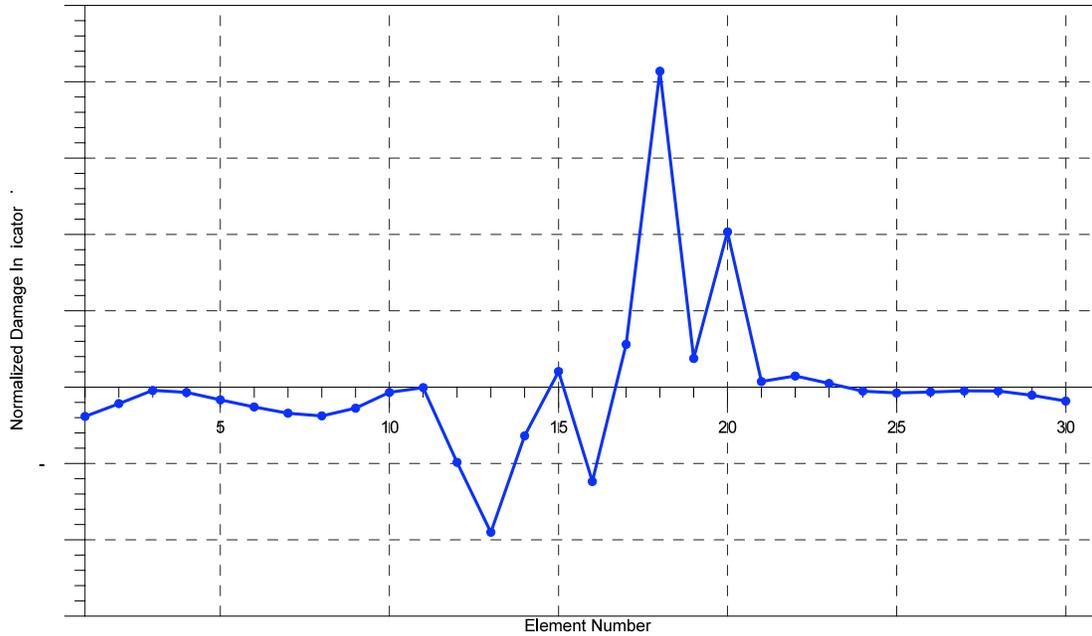
Figure 45. Case #7: Normalized Damage Index Z_j total

In Figure 46 is presented the Damage Severity Indicator α_j. The severity of the damage is quite accurate, in this case, for the element 18 (~ 18%) but underestimated for the element 20 (~13%).
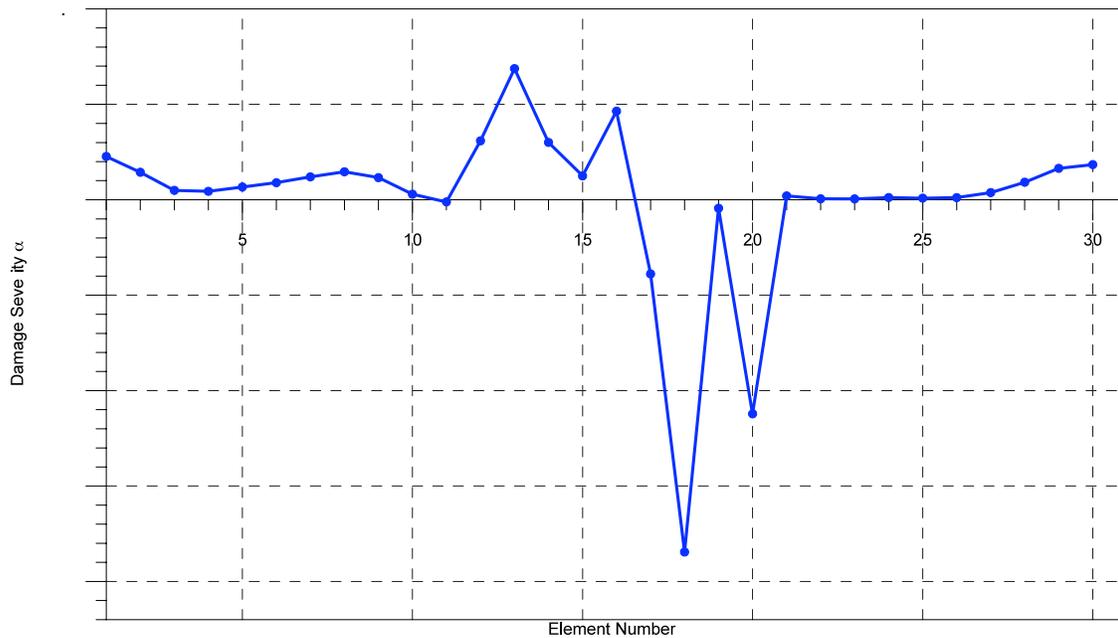
Figure 46. Case #7: Damage Severity Indicator α_j

4.5 Modified Approach-Structure with energy dissipators

The numerical code for the modal identification and damage detection algorithm was implemented in Matlab. A level of complexity was introduced in this phase when compared with the sample case studies without dampers. A dynamic non-linear analysis of the validation structure is required and mode shapes and frequencies cannot be obtained by a modal analysis performed by the F.E. program. The goal is in fact to simulate the reality of the existing structure where records from a sensor network are provided in form of acceleration signals. For this reason the numerical code of the damage detection algorithm is used with the acceleration time history of each node of the structure, in X and Z direction. A preliminary assessment of the mode shapes and fundamental frequencies, obtained from the nodal accelerations was introduced.

In details the procedure is implemented through the following steps:

1 Implementation of the portal frame model with the inelastic frame analysis program RUAUMOKO (A.J. Carr, 2004) to obtain the acceleration response of each node of the structure;

2 Assessment of the modal parameters using the Time Domain Decomposition (TDD) method (par. 4.6)

3 For each sub-component of the frame (two columns and one beam) the best-fit curve is obtained with a polynomial function of a degree appropriate to the specific mode shape;

4 Curvatures and strain energies associated to each structural and damping element are calculated;

5 The damage is introduced and steps 1 to 4 are repeated for the damaged structure;

6 The variation of strain energy between un-damaged and damaged configuration is calculated;

7 Estimate of damage index for each separate mode and for the first three modes combined;

8 Estimate of the normalized index for each element;

9 Estimate of damage severity;

10 The damage location and severity are visualized.

The procedure required initially a new formulation in order to take into account the existence of the energy dissipators. The energy contribution provided by the dampers is expressed as function of the equivalent stiffness of the damper (k_{eq}):

$$E_{damp} = k_{eq}s^2 \tag{31}$$

Where s is the length variation of the damper in relation to the modal displacements.

The equivalent stiffness is obtained as:

$$k_{eq} = \frac{F_{max}}{x(F_{max})} \qquad (32)$$

Where F_{max} is the peak force and $x(F_{max})$ is the damper stroke corresponding to the peak force value.

In the Damage Indicator definition the energy contributions for the structural elements and for the dampers need to be combined as homogeneous quantities. For this reason the stiffness associated to the dampers is normalized to the bending stiffness of the other structural elements:

$$k_m = \frac{k_{eq}}{EI} \qquad (33)$$

Where the index m refers to the damper. This level of simplification, however can, in practice, be removed accounting the energy variation of each element with its pertinent level of stiffness.

From the numerical point of view an additional requirement of normalization is needed, in order to maintain a level of homogenous contribution to the total energy for both the structural elements and the energy dissipators. For the sample cases considered here, for instance, the amplitude of the energy dissipated by the dampers is much larger than the portion related to the structural elements. Numerically this effect tends to reduce the sensitivity of the approach to the changes experienced in the structural elements when the dampers are mobilized with a significant level of stroke involved. For this reason an additional coefficient (t_{im}) is introduced. With this coefficient it is possible to normalize the maximum contribution of energy in the structural element to the maximum value of energy in the dampers.

$$t_{im} = \frac{\max_{j=1..N_{el}} \left(\int_a^b [\psi_i^{''}(x)]^2 \, dx \right)}{\max(k_m s_{im}^2)} \qquad (34)$$

Where the index i indicates the mode under consideration, index m refers to the damper, k_m is the normalized dampers stiffness, and s_{im} is the mth damper length variation for the ith mode. The numerator represents the maximum modal stiffness of each jth element for the ith mode shapes. The denominator is the maximum modal stiffness for each mth damper for the ith mode shape. The index m is needed to take into account configurations with

dampers of different length, connecting non-symmetric elements and/or with different performance characteristics.

For the Damage Indicator the two components, for structural elements and dampers, are obtained as:

- For the structural elements:

$$DI_{ij} = \frac{\left\{\int_a^b [\psi_i^{*"}(x)]^2\, dx + \left[\sum_{n=1}^{N_{el}} \int_0^{L_n} [\psi_i^{*"}(x)]^2\, dx + \sum_{m=1}^{N_d} t_{im}(s_{im}^*)^2\right]\right\} \left[\sum_{n=1}^{N_{el}} \int_0^{L_n} [\psi_i^{"}(x)]^2\, dx + \sum_{m=1}^{N_d} t_{im}(s_{im})^2\right]}{\left\{\int_a^b [\psi_i^{"}(x)]^2\, dx + \left[\sum_{n=1}^{N_{el}} \int_0^{L_n} [\psi_i^{"}(x)]^2\, dx + \sum_{m=1}^{N_d} t_{im}(s_{im})^2\right]\right\} \left[\sum_{n=1}^{N_{el}} \int_0^{L_n} [\psi_i^{*"}(x)]^2\, dx + \sum_{m=1}^{N_d} t_{im}(s_{im}^*)^2\right]} \qquad (35)$$

- For the dampers:

$$DI_{im} = \frac{\left\{t_{im} \cdot (s_{im}^*)^2 + \left[\sum_{n=1}^{N_{el}} \int_0^{L_n} [\psi_i^{*"}(x)]^2\, dx + \sum_{m=1}^{N_d} t_{im} \cdot (s_{im}^*)^2\right]\right\} \left[\sum_{n=1}^{N_{el}} \int_0^{L_n} [\psi_i^{"}(x)]^2\, dx + \sum_{m=1}^{N_d} t_{im} \cdot (s_{im})^2\right]}{\left\{t_{im} \cdot (s_{im})^2 + \left[\sum_{n=1}^{N_{el}} \int_0^{L_n} [\psi_i^{"}(x)]^2\, dx + \sum_{m=1}^{N_d} t_{im} \cdot (s_{im})^2\right]\right\} \left[\sum_{n=1}^{N_{el}} \int_0^{L_n} [\psi_i^{*"}(x)]^2\, dx + \sum_{m=1}^{N_d} t_{im} \cdot (s_{im}^*)^2\right]} \qquad (36)$$

Where:

- N_{el} is the number of sub-components of the structure. Sub-components are intended as assembly of single portions of the structure, with physical significance, as columns, beams etc:

- N_d is the total number of dampers.

The normalized Damage Indicator is obtained as:

$$z_{ij} = \frac{DI_{ij} - \mu_{DI}^i}{\sigma_{DI}^i} \qquad (37)$$

Where μ_{DI}^i and σ_{DI}^i represent the mean and standard deviation of the damage index of all the elements for the *ith* mode, respectively. With 98% of level significance the procedure indicates the existence of damage in the *jth* element and for the *ith* mode if:

$$z_{ij} \geq 2 \qquad (38)$$

The combination of different modes (*NM*) results in a damage indicator, for the *jth* structural element, defined as:

$$DI_j = \frac{\sum_{i=1}^{NM}\left\{\int_a^b [\psi_i^{*"}(x)]^2\,dx+\left[\sum_{n=1}^{N_{el}}\int_0^{L_n}[\psi_i^{*"}(x)]^2\,dx+\sum_{m=1}^{N_d}t_{im}(s_{im}^*)^2\right]\right\}\;\sum_{i=1}^{NM}\left[\sum_{n=1}^{N_{el}}\int_0^{L_n}[\psi_i^{"}(x)]^2\,dx+\sum_{m=1}^{N_d}t_{im}(s_{im})^2\right]}{\sum_{i=1}^{NM}\left\{\int_a^b [\psi_i^{"}(x)]^2\,dx+\left[\sum_{n=1}^{N_{el}}\int_0^{L_n}[\psi_i^{"}(x)]^2\,dx+\sum_{m=1}^{N_d}t_{im}(s_{im})^2\right]\right\}\;\sum_{i=1}^{NM}\left[\sum_{n=1}^{N_{el}}\int_0^{L_n}[\psi_i^{*"}(x)]^2\,dx+\sum_{m=1}^{N_d}t_{im}(s_{im}^*)^2\right]} \quad (39)$$

and for the dampers:

$$DI_m = \frac{\sum_{i=1}^{NM}\left\{t_{im}\cdot(s_{im}^*)^2+\left[\sum_{n=1}^{N_{el}}\int_0^{L_n}[\psi_i^{*"}(x)]^2\,dx+\sum_{m=1}^{N_d}t_{im}\cdot(s_{im}^*)^2\right]\right\}\;\sum_{i=1}^{NM}\left[\sum_{n=1}^{N_{el}}\int_0^{L_n}[\psi_i^{"}(x)]^2\,dx+\sum_{m=1}^{N_d}t_{im}(s_{im})^2\right]}{\sum_{i=1}^{NM}\left\{t_{im}\cdot(s_{im})^2+\left[\sum_{n=1}^{N_{el}}\int_0^{L_n}[\psi_i^{"}(x)]^2\,dx+\sum_{m=1}^{N_d}t_{im}\cdot(s_{im})^2\right]\right\}\;\sum_{i=1}^{NM}\left[\sum_{n=1}^{N_{el}}\int_0^{L_n}[\psi_i^{*"}(x)]^2\,dx+\sum_{m=1}^{N_d}t_{im}(s_{im}^*)^2\right]} \quad (40)$$

Where *NM* is the number of modes taken into account. As indicated above the normalized index z_j for the *j*th element is obtained as:

$$z_j = \frac{DI_j - \mu_{DI}}{\sigma_{DI}} \quad (41)$$

Where μ_{DI} and σ_{DI} represent the mean and standard deviation of the damage indicator of all the elements for all the considered modes, respectively.

When the coefficient c_i is applied (Eq. 28) the Normalized Damage Indicator Z_{ij} and Z_j can be written as:

$$Z_{ij} = \frac{c_i DI_{ij} - \mu(c_i DI_{ij})}{\sigma(c_i DI_{ij})} \quad (42)$$

$$Z_j = \frac{\sum_{i=1}^{NM} c_i DI_{ij} - \mu\left(\sum_{i=1}^{NM} c_i DI_{ij}\right)}{\sigma\left(\sum_{i=1}^{NM} c_i DI_{ij}\right)} \quad (43)$$

Similarly to the original formulation of the procedure the damage severity index α_j is obtained as:

$$\alpha_j = \frac{\sum_{i=1}^{NM}\left(K_{ij} + \sum_{j=1}^{n_{el}} K_{ij}\right)\sum_{j=1}^{n_{el}} K_{ij}^*}{\sum_{i=1}^{NM}\left(K_{ij}^* + \sum_{j=1}^{n_{el}} K_{ij}^*\right)\sum_{j=1}^{n_{el}} K_{ij}} - 1 = \frac{1}{DI_j} - 1 \tag{44}$$

Where K_{ij} and K_{ij}^* are the modal stiffness of the elements in the un-damaged and damaged configuration, respectively. The existence of damage is indicated by $\alpha_j \leq 0$.

4.6 Assessment of Mode Shapes using the Time Domain Decomposition (TDD) method

To estimate the mode shapes from the nodal acceleration responses of the sample frame, separate components of the input signal were used. Specifically, for the first and third mode, mainly influenced by the column response, an acceleration time history in x direction was applied. Instead, for the second mode of the frame, mainly controlled by the behavior of the beam, an input in vertical (z) direction was applied. The input signal is obtained as a random white noise with frequencies in the range of 0 Hz to 60 Hz.

The TDD (Time Domain Decomposition) method presented by Kim. (Kim et al., 2005) is implemented through the following steps:

1 Identification of the natural frequencies from the Power Spectral Density (PSD) of the response signal at each node of the frame;

2 Compute the Transfer Function (FTT) between the response at an arbitrary reference point and the response at each node. In the sample frame cases used for procedure validation, the reference points were selected accordingly to the structural component and the direction of the response. For instance, the vertical accelerations at the nodes of the beam were referred to the response at the column beam joint. The response signals of the column nodes were instead referred to the first unrestrained node at the base of the column. It must be noted that this selection is theoretically not necessary even though it simplifies the interpretation of the results;

3 For each Transfer Function the frequency components above the maximum expected value (e.g. 50 Hz for the sample frames analyzed) are substituted with zeroes;

4 Compute the scaled time history by taking the inverse discrete Fourier transformation of the filtered FTT;

5 Third-order digital Butterworth band-pass filters are applied to isolate each mode. The limits of the bands are determined by inspecting the spectrum and coherence functions of the acceleration signals;

6   Compute the output energy correlation matrix E_i, using the filtered time histories, obtained as:

$$E_i = Y_i Y_i^T$$

(45)

where Y is the filtered output acceleration time history that contains only the *ith* mode. The matrix can be interpreted as the energy correlation of the *ith* mode with respect to the location of the sensors.

7   The Singular Value Decomposition (SVD) of E_i is performed using the following equation:

$$E_i = U\Omega U^T$$

(46)

Where U is a matrix containing singular vectors of Y_i and Ω is a diagonal matrix containing the singular values of Y_i. The first column of the singular vector matrix U is the mode shape for each isolated mode.

For the application of the procedure, the mode shape needs to be reproduced by a continuous function. This is to allow the computation of the curvature values for the definition of the energy terms. The degree of the interpolating polynomial function is established by minimization of the approximation error. The total error is obtained as sum of two distinct terms: Ep_k (Eq. 47) and Ea_k, (Eq. 50) defines as:

$$Ep_k = \frac{e_k - e_m}{e_M - e_m}$$

(47)

Where:

$$e_k = \sum_{j=1}^{Nel} \left(Y_j - y_j^k \right)^2$$

(48)

$$e_M = \max\left(e_k\right) \text{ and } e_m = \min\left(e_k\right)$$

(49)

The term Y_j represents the modal displacement of the *jth* node obtained with the TDD method. The displacement at the same *jth* node, obtained with a polynomial function of degree *k,* is indicated as y_j^k

In order to improve the accuracy of the minimization process an additional error component is introduced, based on the area described by the mode shape between two contiguous nodes:

$$Ea_k = \frac{g_k - g_m}{g_M - g_m}$$

(50)

Where:

$$g_k = \sum_{j=1}^{Nel} \left(A_j - a_j^k \right)^2$$

(51)

$$g_M = \max(g_k) \text{ and } g_m = \min(g_k)$$

(52)

In Eq. (51) the terms A_j and a_j^k represent the areas under the mode shape and the interpolation function of degree k, respectively. Each error term Ep_k and Ea_k is bounded between the values of 0 and 1. The total error is obtained as sum of the two previous normalized terms. The error minimization process is repeated for each mode and for each sub component, defined as assembly of single elements (e.g. columns, deck etc.).

The polynomial function degree is obtained as the degree corresponding to the minimum of the total error. An example of the degree selection is shown in Figure 47 with a minimum at k=14.
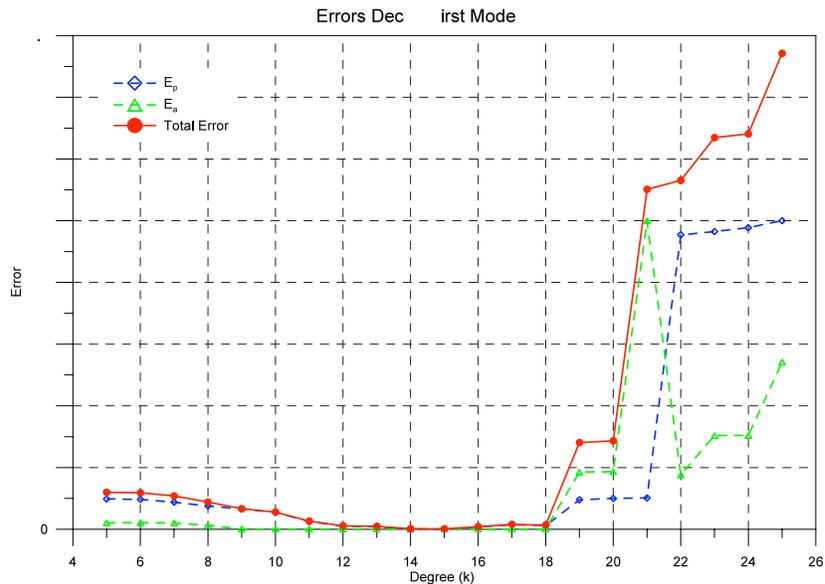
Figure 47. Error variation with the variation of the degree (k) of the polynomial function

4.7 Structural Model with Dampers for Procedure Validation

A simple portal frame with moment resisting joints and braced dampers was used as a basic case study to validate the modified procedure. Three different configurations were analyzed (Table 10):

- **Configuration A**: dampers in symmetric positions with identical performance characteristics (Figure 48);

- **Configuration B**: dampers in symmetric positions with different characteristics. Damper #2 (element 32) has stiffness equal to 50% of the stiffness of damper #1 (element 31) (Figure 49);

- **Configuration C**: dampers are located in non symmetric positions but they have the same performance characteristics (Figure 50).

The material and geometry of the elements of the frame are assumed constant with area $A=0.459 \times 10^{-2} \text{m}^2$, modulus of elasticity $E=0.21 \times 10^9 \text{kN/m}^2$, moment of inertia $I=0.579 \times 10^{-4} \text{m}^4$ and density $\rho =7850 \text{ Kg/m}^3$.

The dampers performance is modeled by a force-velocity relationship of the type given below:

$$F = C\dot{x}^{\alpha}$$

(53)

Where:
− F is the damper force;
− C is the damping coefficient, in this case equal to 7 kNsec/m;
− α is the damping exponent, equal to 1;
− $\dot{x}$ is the velocity component.

Conf	Stiffness [kN/m]		Joint Connection		Condition of Sym
	31	32	31	32	
A	$K_1=379$	$K_1=379$	2-13	19-29	Sym
B	$K_1=379$	$K_2= K_1/2 = 190$	2-13	19-29	No-Sym
C	$K_1=379$	$K_1=379$	2-13	18-25	No-Sym

Table 10. Configurations for the portal frame with dampers
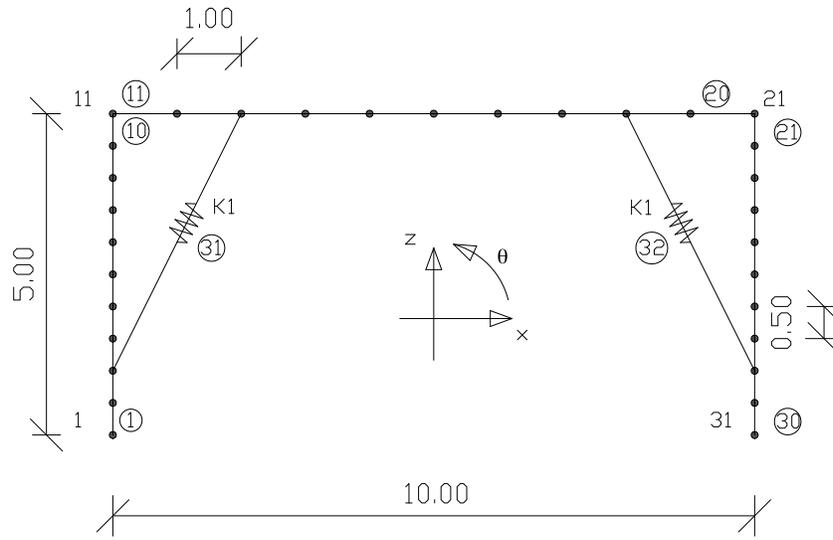
Figure 48. Finite element model for structure with damper -Configuration A
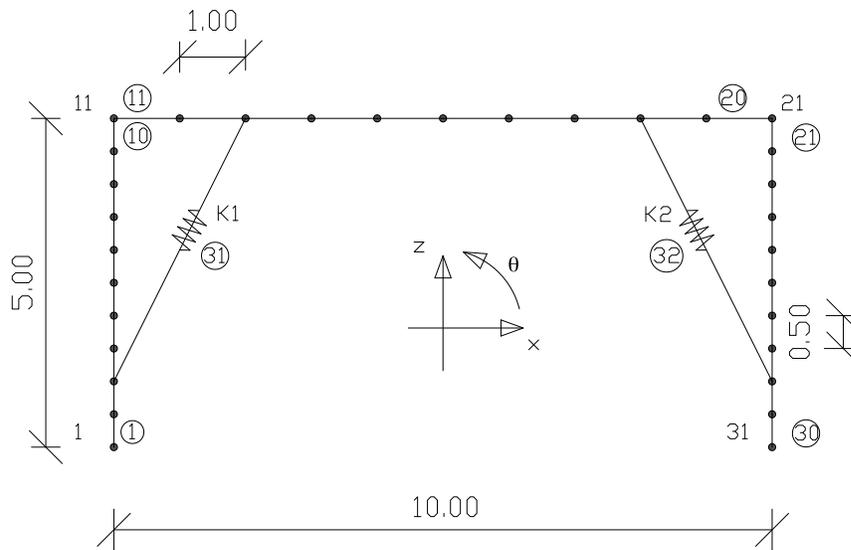
Figure 49. Finite element model for structure with damper -Configuration B
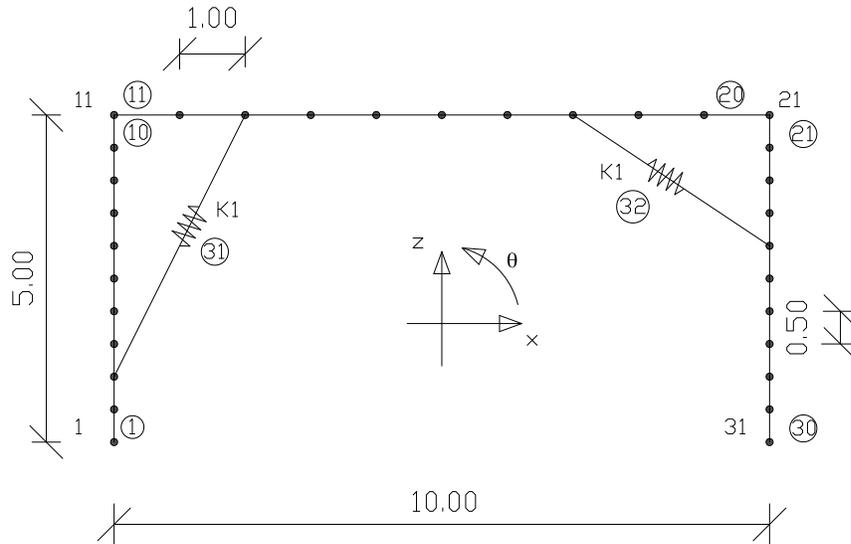
Figure 50. Finite element model for structure with damper -Configuration C

The input signal selected was a white noise with frequency between 0 and 60Hz (Figure 51). The same signal is utilized for the portal frame in the un-damaged and damaged configuration.
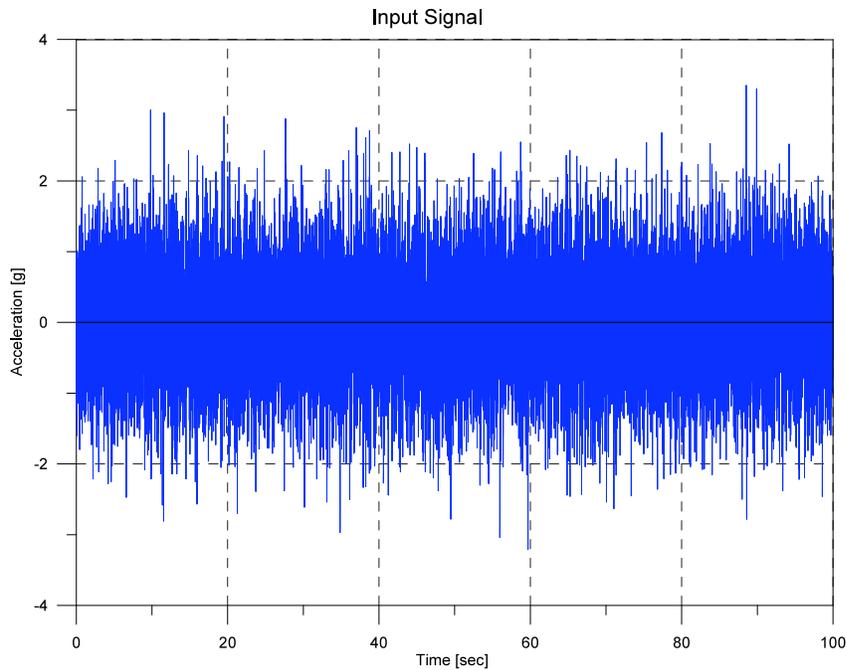
Figure 51. Input signal for the portal frame

For every configuration (A to C) different case studies were analyzed (see Table 11). In each analysis a level of structural degradation was simulated in the structural elements and/or in the energy dissipators. In order to simulate a degraded configuration the elastic stiffness was reduced for the structural elements while for the dampers a reduction of the damping coefficient was operated. In Table 11 the different case studies are listed with the level of degradation expressed as percentage of the original value of stiffness (and/or damping). In some case dampers are maintained at their original performance in order to verify if the modified procedure is able to isolate deficiencies localized only in structural elements.

Case #	Damaged Element	Amount of damage	Condition of symmetry
0	Undamaged	0%	Sym
1	31, 32	10%	Sym
1bis	31, 32	30%	Sym
2	31	10%	No Sym
3	31, 15, 16	10%	No Sym
4	15, 29	10%	No Sym
5	15, 16	10%	Sym
6	14, 24	10%	No Sym
7	7, 10	10%	No Sym
8	1, 10, 21,30	10%	Sym
9	11, 12, 13, 14, 15	10%	No Sym
10	20, 21, 32	10%	No Sym
11	15, 16, 31, 32	10%	Sym

Table 11 Case studies for frames with energy dissipation system

Case #0 represents the reference structure with no level of damage. Cases #1 and #1bis include the damage in the two dampers (elements 31 and 32) but with different level of damage, 10% and 30% respectively. Case #2 includes the damage only in one damper (element 31) while case #3 includes damaged elements at mid-span of the beam and in the dampers. Case #4 considers the damage in the beam and in one column to create a non-symmetric condition. Case #5 considers the damage located only at mid span of the beam in the elements with maximum curvature for the second mode shape. Case #6 is a non-symmetric case with damaged elements in the beam and in one of the columns close to the restrain. Case #7 considers the damage in two elements of one column affected by different variation of curvature. In case #8 the damage is located at the top and bottom of the columns. This case is intended to validate the procedure for damage at the structure restrains. Configurations #9 and #10 include the damage in contiguous elements in the column (case #9) and in the beam (case #10). These two examples are intended to verify the capability of the algorithm to assess the entity of the damage in addition to its location.

4.8 Application of the damage identification procedure to the structure with dampers

In this section the results for some of the most representative case studies are presented.
In Table 12 are reported the modal results of all the cases of configuration A (identical dampers). The modal coefficients of importance c_i (Eq. 28) are reported in Table 13.

Case #	Frequencies (Hz)		
	Mode 1	Mode 2	Mode 3
no damper	8.410	15.020	41.590
A0	8.575	15.733	42.242
A1	8.570	15.730	42.240
A1-bis	8.570	15.730	42.240
A2	8.570	15.700	42.200
A3	8.560	14.536	41.408
A4	8.351	15.057	41.731
A5	8.563	14.569	41.439
A6	8.535	15.234	40.489
A7	8.571	15.640	41.899
A8	7.769	15.067	41.076
A9	8.216	14.292	38.600
A10	8.308	15.178	41.693
A11	8.560	14.536	41.408

Table 12. Natural frequencies for configuration A cases

Case #	Coefficient c_i		
	Mode 1	Mode 2	Mode 3
A1	1.00	0.60	0.46
A1-bis	1.00	0.60	0.46
A2	0.12	0.78	1.00
A3	0.01	1.00	0.70
A4	0.33	1.00	0.76
A5	0.01	1.00	0.69
A6	0.02	0.28	1.00
A7	0.02	0.27	1.00
A8	0.69	0.57	1.00
A9	0.10	0.40	1.00
A10	0.48	1.00	0.99
A11	0.01	1.00	0.70

Table 13. Coefficient of mode importance for each case

Case A1

For this example the damage is identical for the two dampers. The degradation is introduced as a 10% reduction of the original damping coefficient *C*. The new value is *C*=6.3kNsec/m. A schematic of the F.E. model is shown in Figure 52.

Figure 52. F.E. model for Case #A1

The Normalized Damage Indicator Z_{ij} and Z_j, defined by Eq. (42) and (43), are presented in Figure 53 and Figure 54. In both figures the elements of the frame sub-components (columns and beam) are aligned on the x axis. Elements from 1 to 10 correspond to the left column, from 11 to 20 are elements of the beam and from 21 to 30 are parts of the right column. Elements 31 and 32 represent the dampers. From Figure 53 the peaks of the normalized index Z_{ij} are visibly associated with elements 31 and 32 (the dampers) for all the three modes. Additional peaks, not reaching the threshold that classify a damage (Z_j =2), are detected at locations 13 and 18 for the first and third mode and at elements 12, 15, 16 and 19 for the second mode. The existence of additional elements experiencing a visible damage index indicates the sensitivity of the approach to take into account the interaction between dampers and structural elements. In fact elements 12, 13, 18 and 19 are the elements of the beam directly affected by the damper performance (Figure 54).
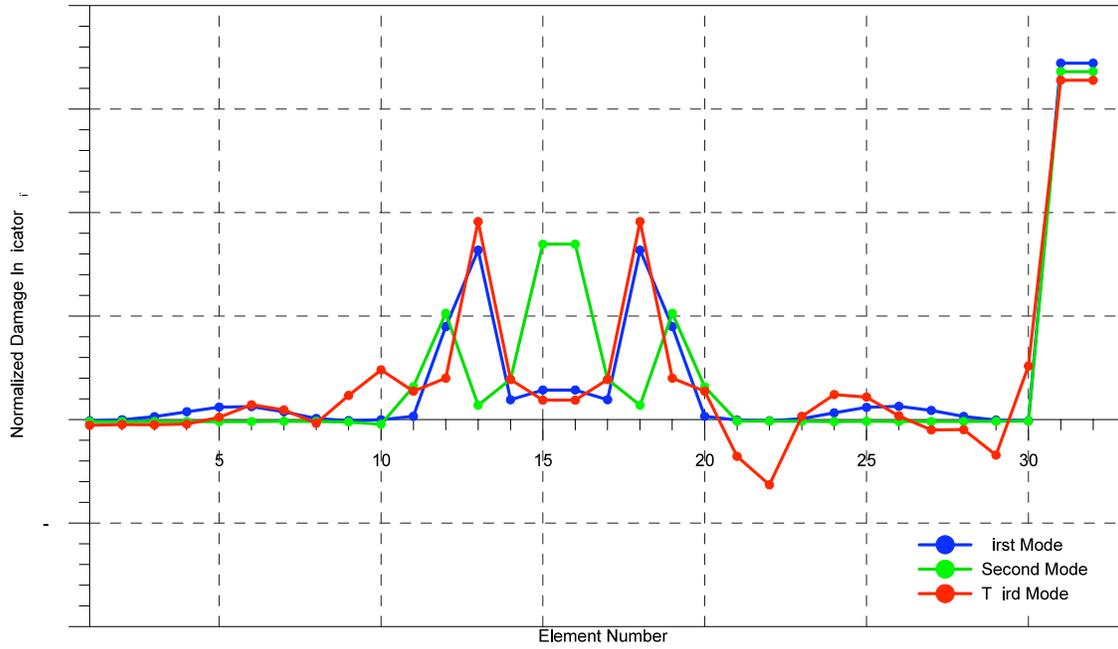
Figure 53. Case #A1: Normalized Damage Index Z_{ij} for each mode
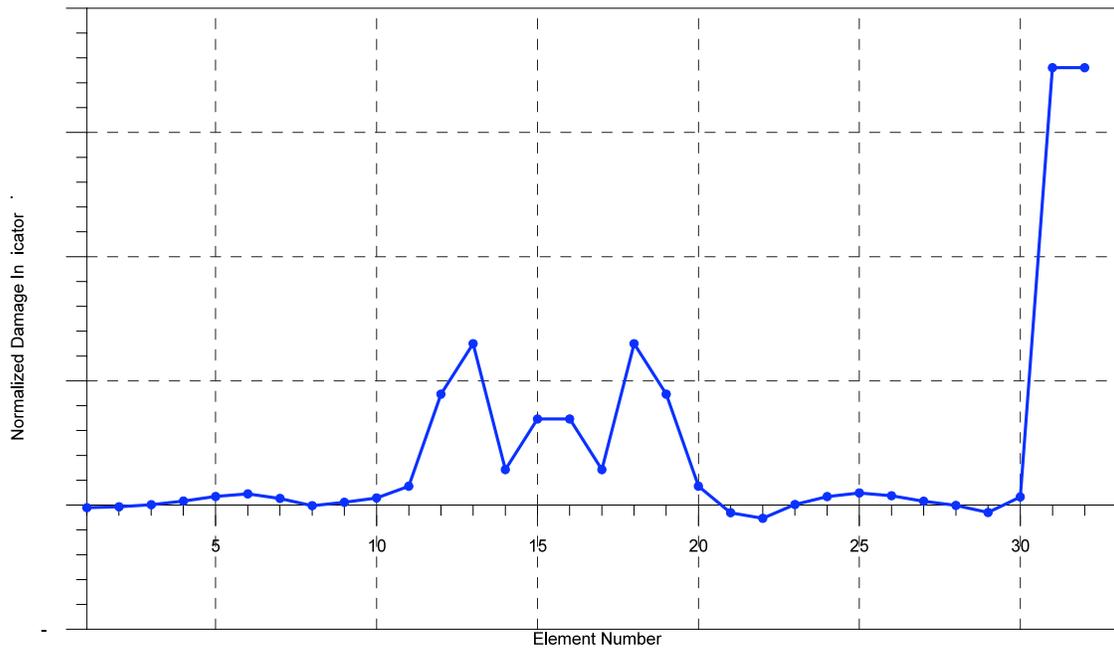
Figure 54. Case #A1: Normalized Damage Index Z_j total
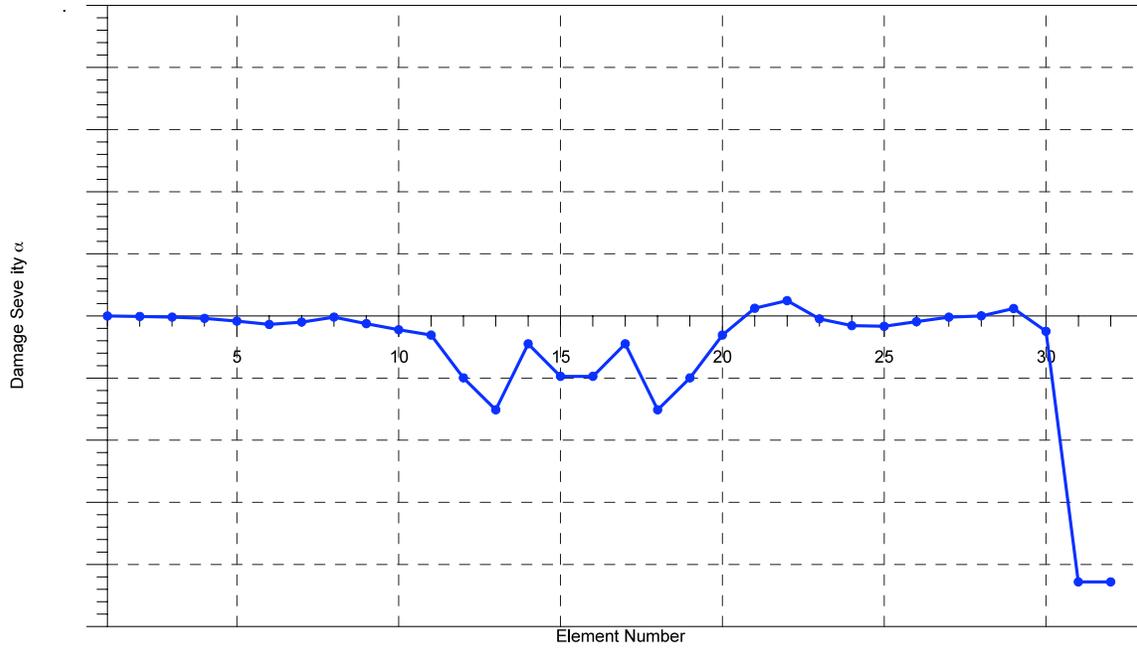
Figure 55. Case #A1: Damage Severity Indicator α_j

Case A2

The damage is introduced only in one of the two dampers to validate the accuracy of the approach in a not-symmetric configuration. To simulate the damage a reduction of the damping coefficient for the damper #31 equal to 10% (C=6.3 kNsec/m) was introduced. The frame model is shown in Figure 56.

Figure 56. Model utilized for Case #A2

The Damage Indicator Z_{ij} and Z_j as well as the Severity Indicator α_j are presented in Figure 57, Figure 58 and Figure 59, respectively.
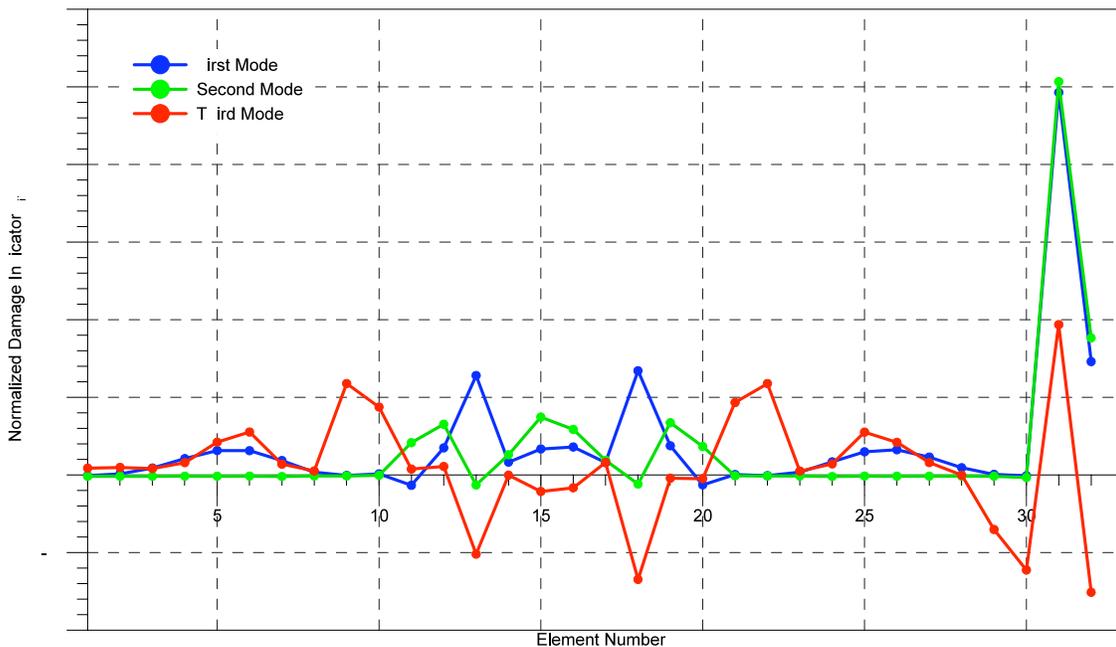
Figure 57. Case #A2: Normalized Damage Index Z_{ij} for the first three modes

The damage is quite accurately assessed for element 31 that correspond to the damper on the left side of the frame. The detected severity is ~11%.
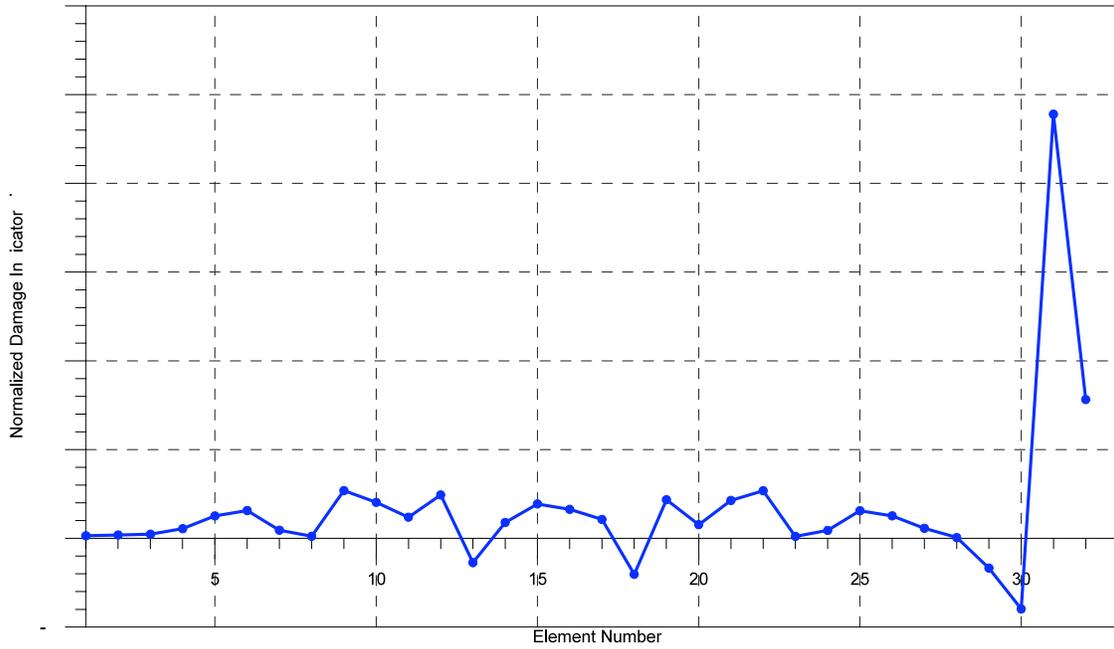
Figure 58. Case #A2: Normalized Damage Index Z_j total
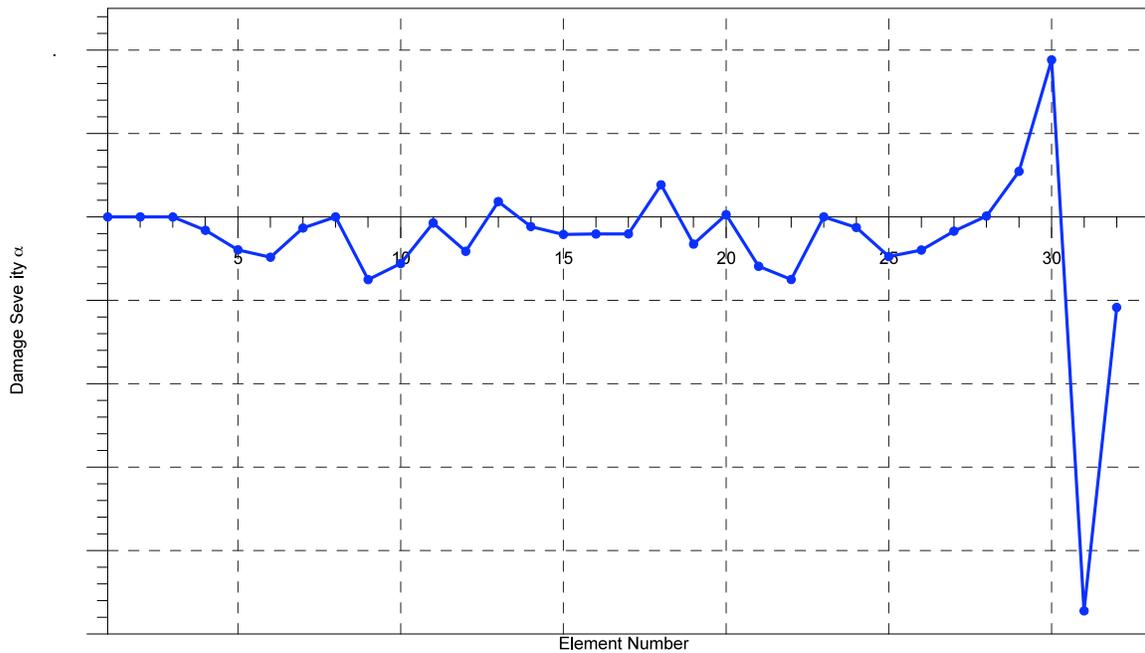
Figure 59. Case #A2: Damage Severity Indicator α_j

Case A5

For this scenario only structural elements are damaged. The goal of this analysis was to verify the accuracy of the algorithm to correctly process, in the energy calculations, the contribution of the structural elements, even with the presence of dampers in the un-damaged conditions. The damage (10%) is only in elements 15 and 16 of the beam. Figure 60 indicates the configuration under consideration.
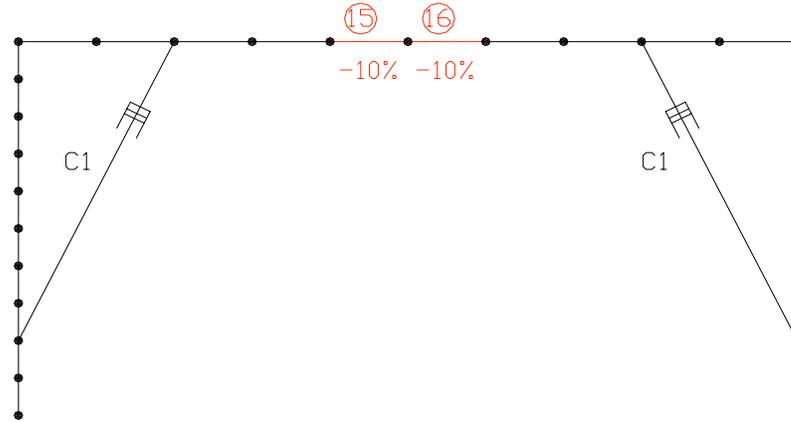
Figure 60. Model utilized for Case #A5

The Normalized Damage Indicator Z_{ij} and Z_j are plotted in Figure 61 and Figure 62, while Figure 63 presents the Damage Severity Indicator α_j.
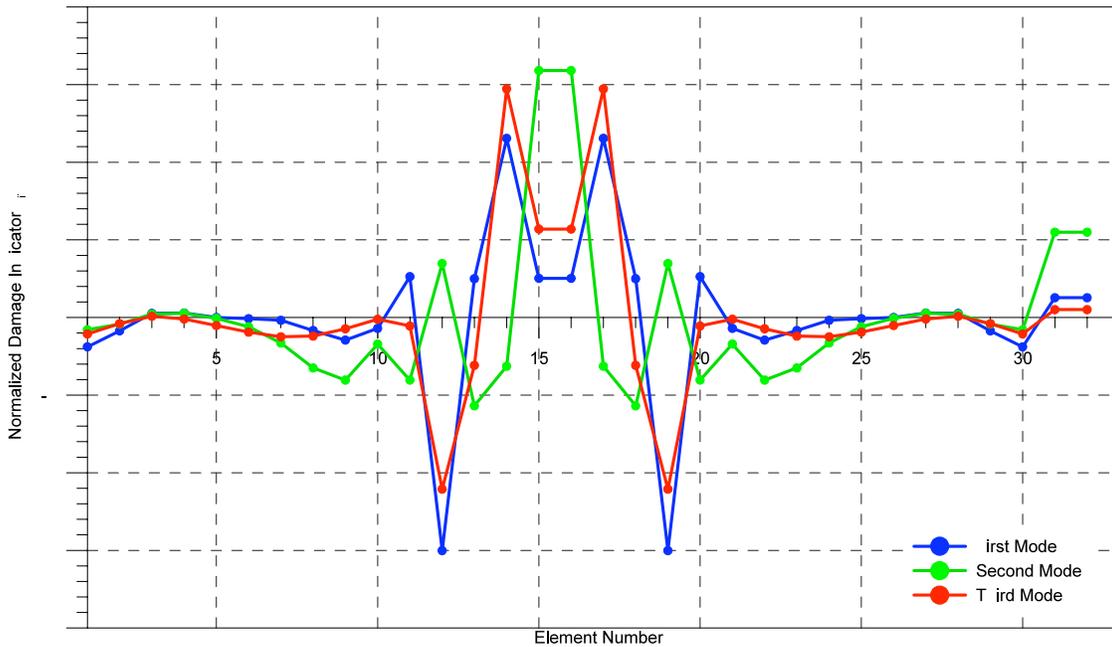
Figure 61. Case #A5: Normalized Damage Index Z_{ij} for each mode

Figure 61 indicates that elements 14 and 17 could be affected by a significant degradation, due to the high values of Damage Indicator Z_{ij} for mode 1 and 3. The analysis of Table 13 however indicates, through the coefficient c_i, that the contribution of mode three and particularly of mode 1 are not largely significant. The application of the normalization coefficient c_i to the damage indicator (Figure 62) removes the contribution of element 14 and 17 and concentrate the degradation to the right elements. The level of severity assessed for this case is 8%.
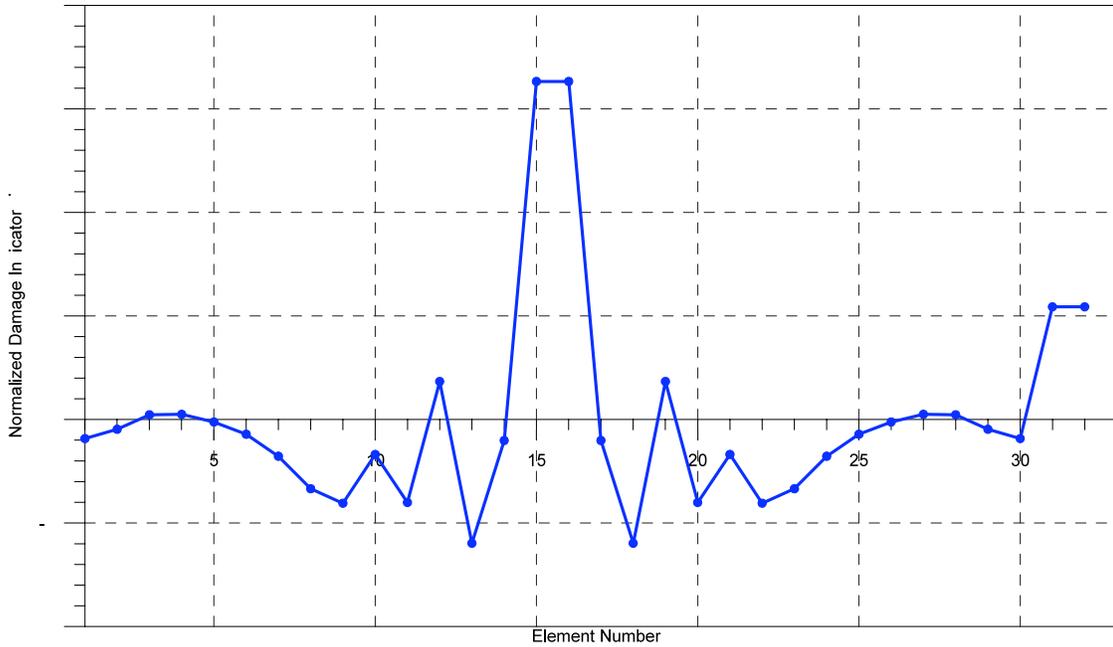
Figure 62. Case #A5: Normalized Damage Index Z_j total
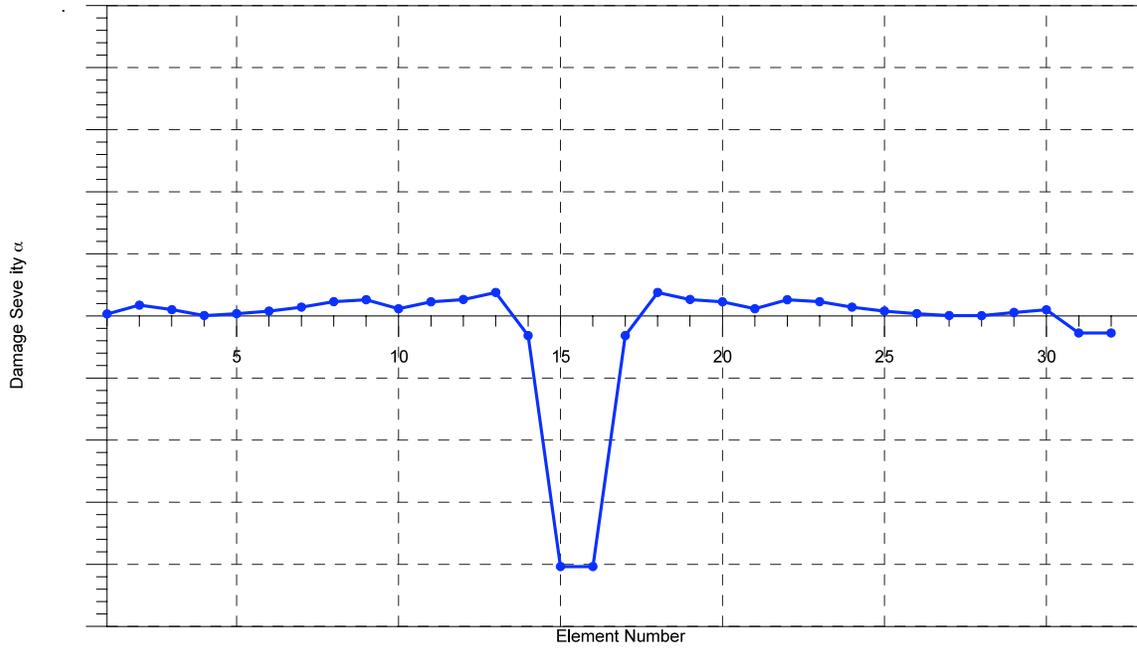
Figure 63. Case #A5: Damage Severity Indicator α_j

Case A11

In this case the damage is concentrated again in elements 15 and 16 of the beam but also in both the dampers (Figure 64). The reduction of the damping coefficient for the damper #31 and #32 is equal to 10% of the original value (C=6.3 kNsec/m). The same amplitude of reduction is applied to the modulus of elasticity of elements 15 and 16.
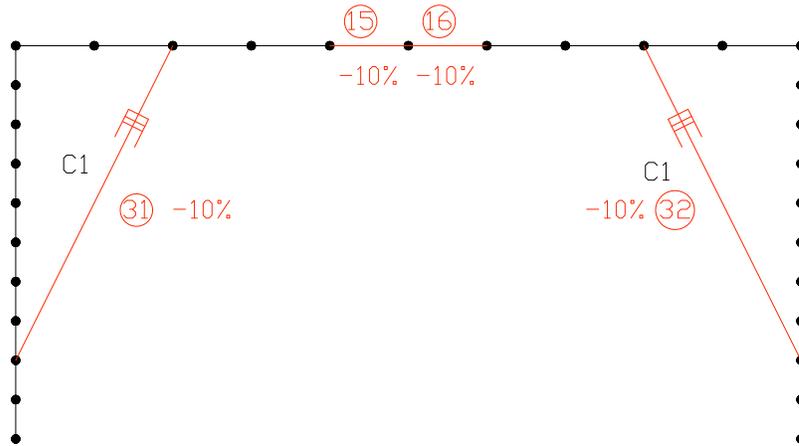
Figure 64. Model for Case #A11

The Normalized Damage Indicator Z_{ij} and Z_j and the Severity index α_j are presented in Figure 65, 66 and 67, respectively. The severity of the damage is accurate, in this case, for the damper elements (~ 11%) but underestimated for the structural elements (~7%).
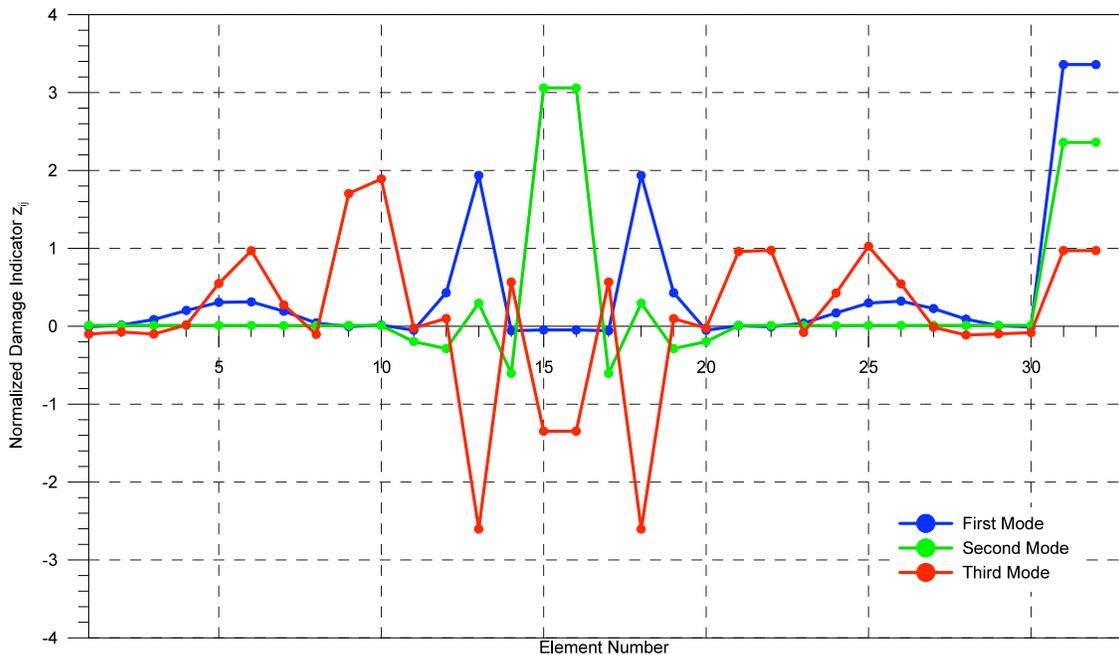
Figure 65. Case #A11: Normalized Damage Index Z_{ij} mode by mode
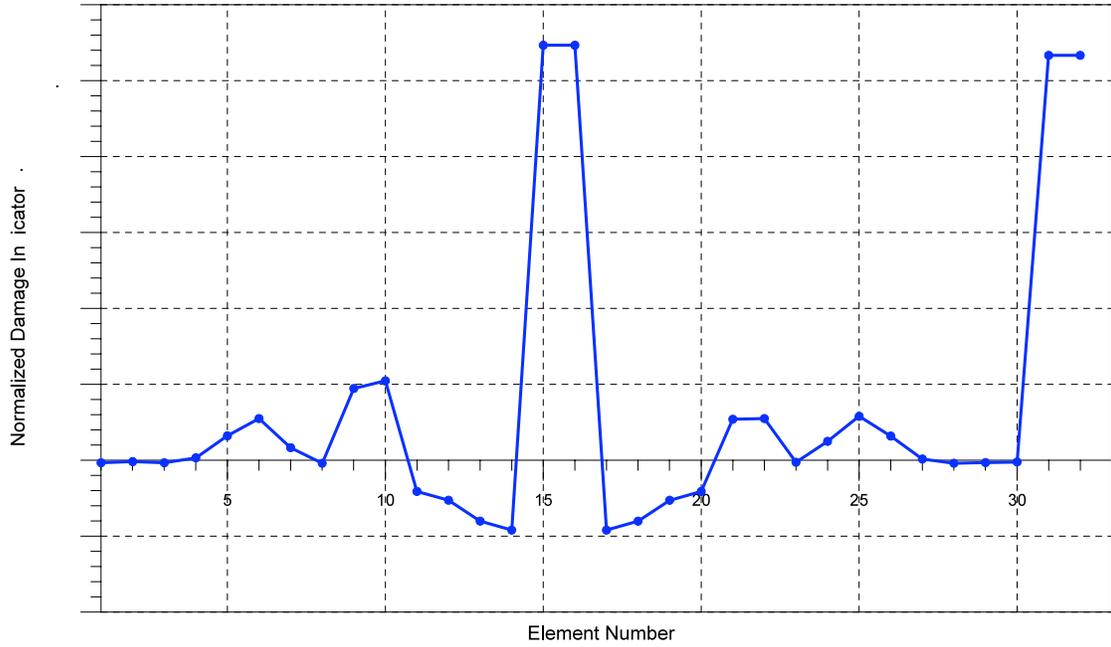
Figure 66. Case #A11: Normalized Damage Index Z_j total
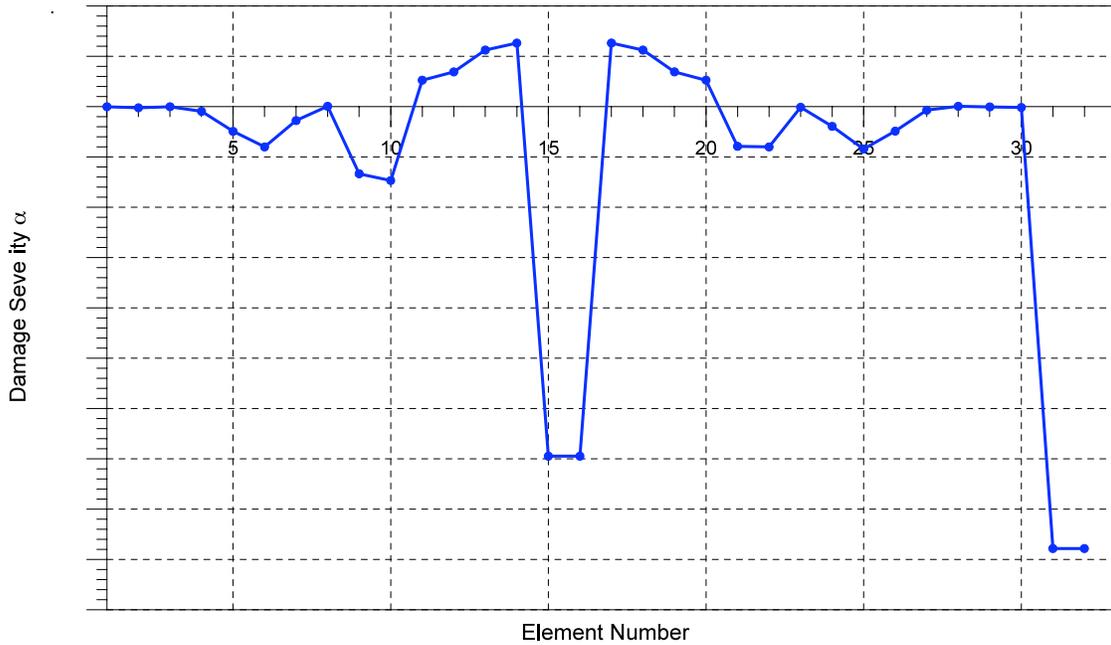
Figure 67. Case #A11: Damage Severity Indicator α_j

The first three natural frequencies for configuration B (dampers with different characteristics) are reported in Table 14. The coefficient of importance for each mode c_i is shown in Table 15 for each case study of this configuration.

Case #	Frequencies (Hz)		
	Mode 1	Mode 2	Mode 3
no damper	8.41	15.020	41.590
B0	8.530	15.560	42.080
B1	8.522	15.508	42.031
B2	8.527	15.527	42.049
B3	8.515	14.365	41.249
B4	8.304	14.892	41.566
B5	8.522	14.398	41.280
B6	8.492	15.069	40.319
B7	8.530	15.466	41.743
B8	7.719	14.881	40.922
B9	8.179	14.134	38.432
B10	8.251	15.003	41.537

Table 14. Modal frequencies for configuration B cases

Case #	Coefficient ci		
	Mode 1	Mode 2	Mode 3
B1	0.24	1.00	0.94
B2	0.23	1.00	0.94
B3	0.04	1.00	0.73
B4	0.32	1.00	0.80
B5	0.04	1.00	0.72
B6	0.04	0.35	1.00
B7	0.09	0.53	1.00
B8	0.65	0.65	1.00
B9	0.10	0.42	1.00
B10	0.44	1.00	0.97

Table 15. Coefficient of mode importance for each case

Case B2

Only one damper has a reduction of damping coefficient (10%) with respect to its original value (Figure 68). No structural elements are degraded but the dampers have different characteristics (see Table 10). The damper on the right side of the frame has a value of elastic stiffness 50% lower than damper #31.

Figure 68. Model for Case #B2

The coefficient Z_{ij}, reported in Figure 69, indicates mode by mode the variation of energy content for each element. Clearly damper #31 shows a peak of variation associated to the second mode. Some change is also detected at element 13, for the second and third mode. In the normalized index Z_j the situation appears more evident with respect to the degradation assessed for damper #31. Some residual contribution is still visible for element 13, where damper #31 is connected to the beam. This second effect however is not considered as a damage if the threshold of Z_j =2 is assumed. The severity of damage identified for the damper element is ~8%.
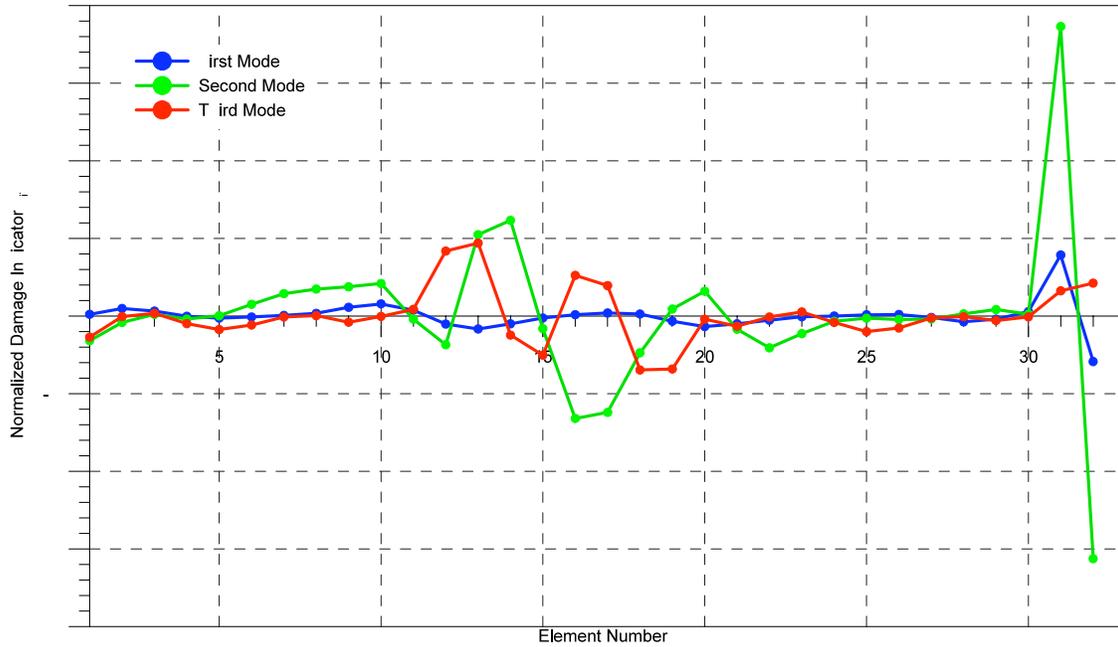
Figure 69. Case #B2: Normalized Damage Index Z_{ij} mode by mode
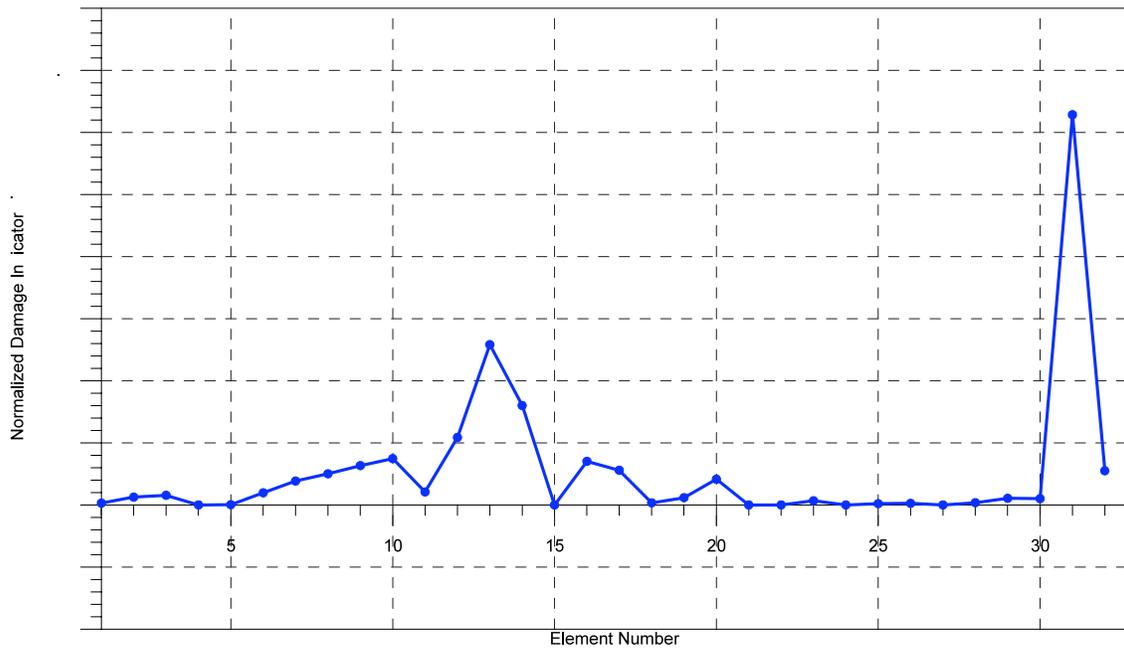
Figure 70. Case #B2: Normalized Damage Index Z_j total
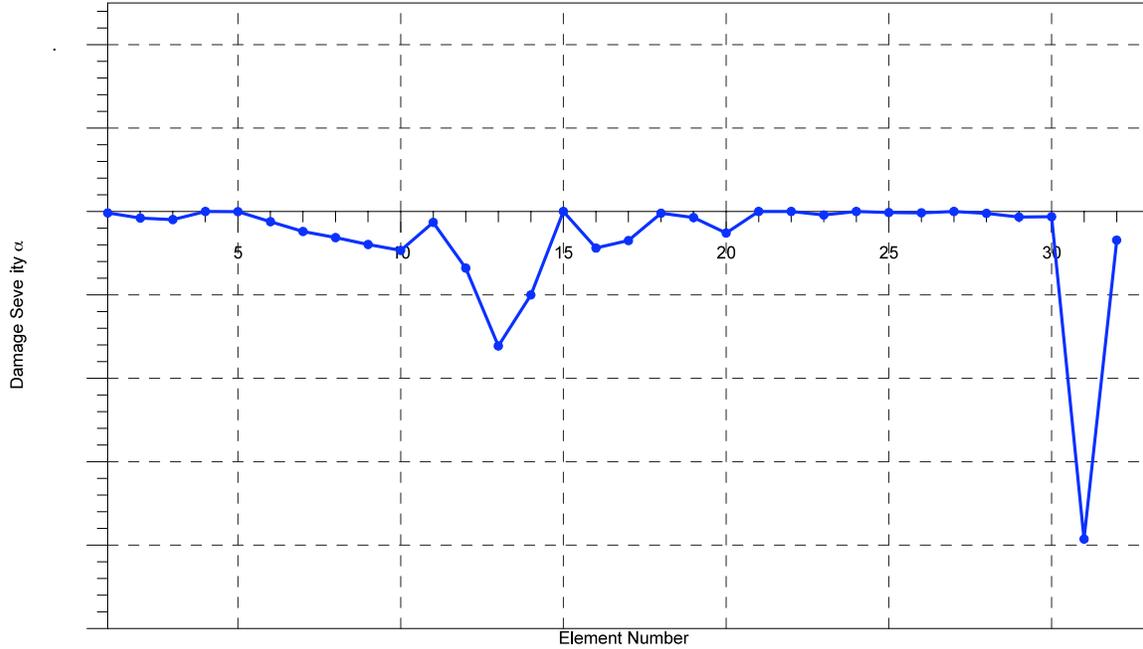
Figure 71. Case #B2: Damage Severity Indicator α_j

An example of configuration type C is also reported.

In Table 16 and 15 the natural frequencies and coefficient c_i, for the configuration type C cases are presented, respectively.

Case #	Frequencies (Hz)		
	Mode 1	**Mode 2**	**Mode 3**
no damper	8.410	15.02	41.590
C0	8.600	15.560	41.930
C1	8.585	15.512	41.901
C2	8.596	15.530	41.901
C3	8.584	14.383	41.105
C4	8.370	14.896	41.411
C5	8.592	14.416	41.135
C6	8.563	15.060	40.159
C7	8.599	15.470	41.599
C8	7.509	14.409	40.358
C9	8.248	14.151	38.291
C10	8.340	15.020	41.401

Table 16. Modal frequencies for each case

Case #	Coefficient c_i		
	Mode 1	**Mode 2**	**Mode 3**
C1	0.31	1.00	0.60
C2	0.13	1.00	0.97
C3	0.01	1.00	0.70
C4	0.35	1.00	0.78
C5	0.01	1.00	0.69
C6	0.02	0.28	1.00
C7	0.01	0.27	1.00
C8	0.69	0.73	1.00
C9	0.10	0.39	1.00
C10	0.48	1.00	0.98

Table 17. Coefficient of mode importance for each case

Case C1

As an example, case #C1 results are presented in terms of Z coefficients and severity indicator α_j. The damage indicators are able to show the existence of degradation in both dampers. The severity of the damage, however, is acceptable for element #31 (8%) but is too low for element 32 (~7%). This scenario, with different dampers of different characteristics, suggests the need of a better tuning of the severity index.
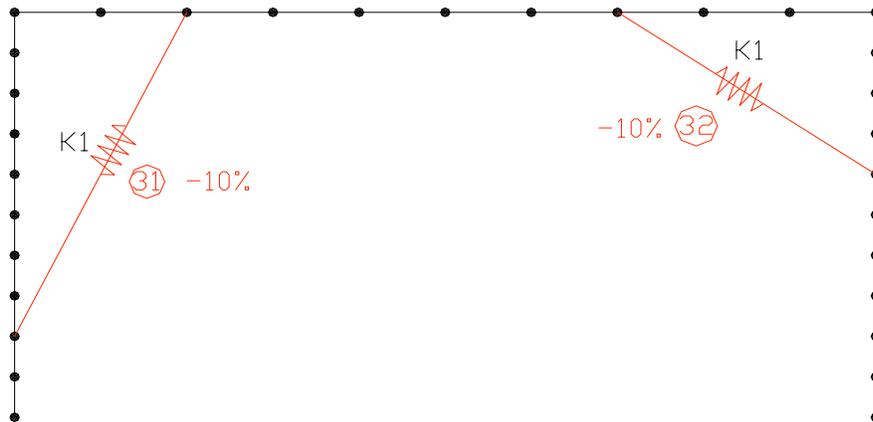
Figure 72. Model utilized for Case #C1
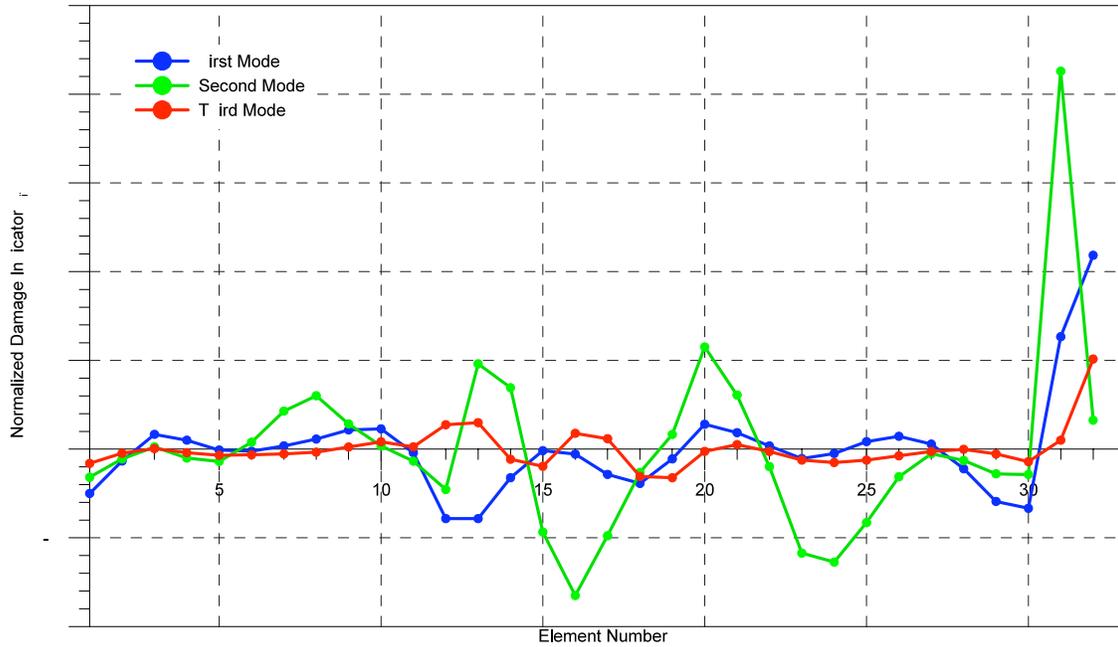
Figure 73. Case #C1: Normalized Damage Index Z_{ij} for each mode
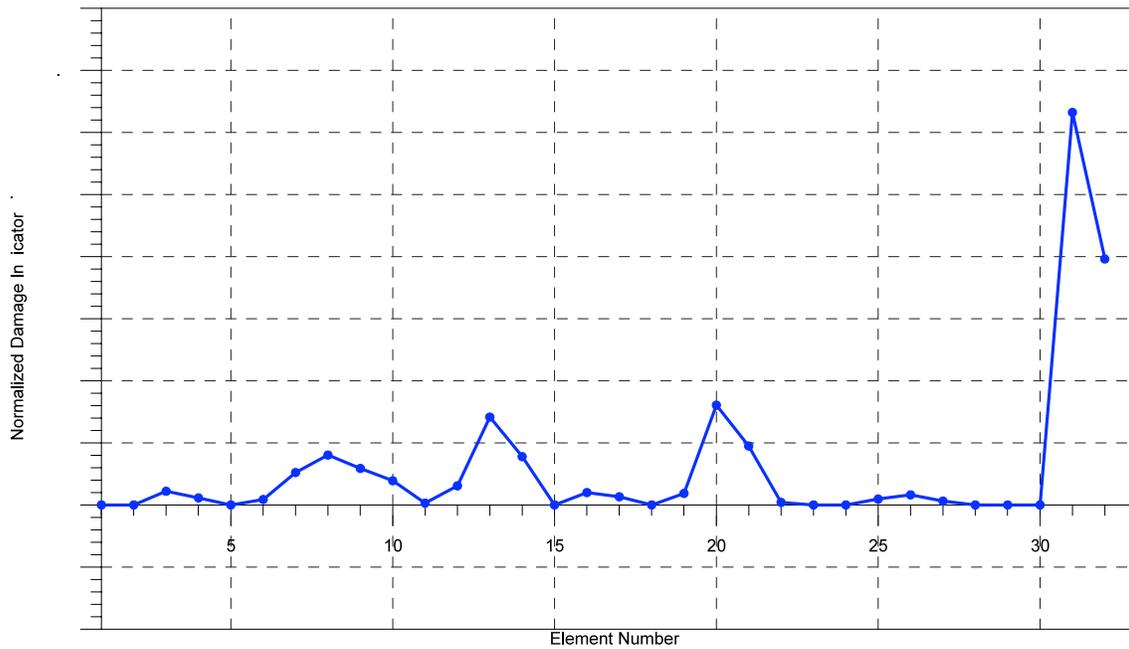
Figure 74. Case #C1: Normalized Damage Index Z_j total
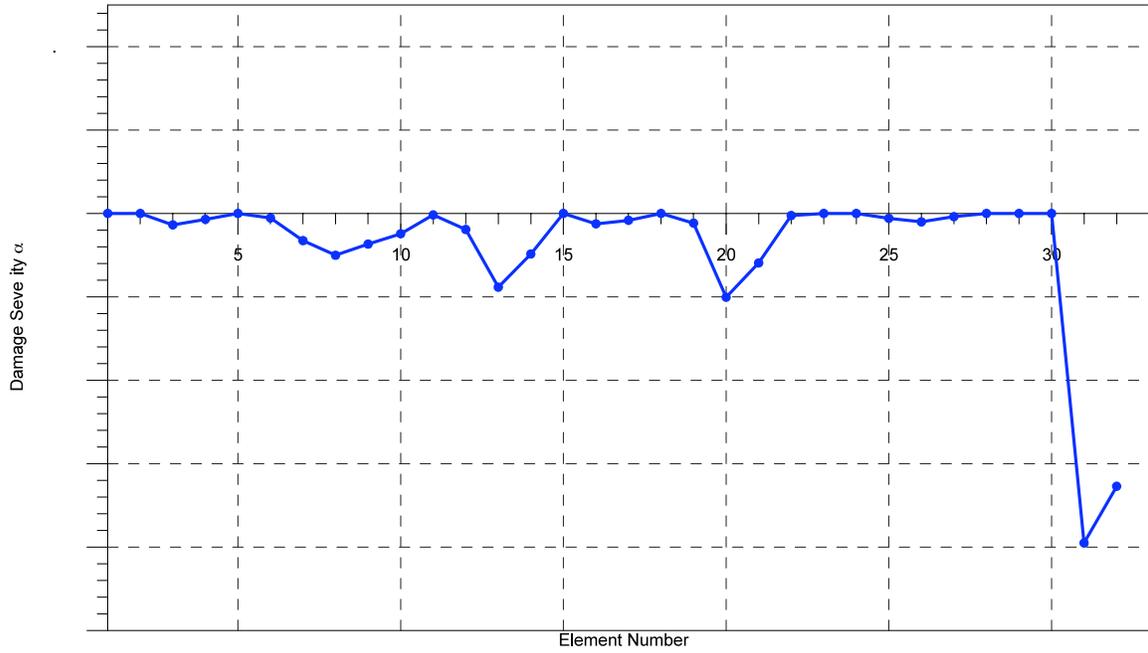
Figure 75. Case #C1: Damage Severity Indicator α_j

5) VINCENT THOMAS BRIDGE APPLICATION – THEORETICAL DATA

The procedure for the damage identification was applied to the responses provided by a numerical model of a real bridge structure. In particular the Vincent Thomas Bridge (San Pedro, CA) was considered, due to a quite recent installation of energy dissipators (viscous dampers), as part of a seismic retrofit program. The numerical model of the bridge was validated, as briefly described in paragraph 1, for a preliminary phase of parametric study of the effects of the dampers on the structural response. Detail of this phase can be found in report SRMD 2005/12 (Benzoni et. al, 2005). As a first approach to the damage identification procedure, applied to the bridge, responses were obtained from the numerical model of the bridge in three different configurations: bridge un-damaged and bridge with reduction of the performance characteristic of the dampers by 30% and 50%. In particular, the damping coefficient of the dampers was reduced by the above mentioned percentage with respect to the nominal values.

The input signal selected was a white noise with frequency between 0 and 60Hz (Figure 76). The same signal is utilized for the bridge in the un-damaged and damaged configuration.
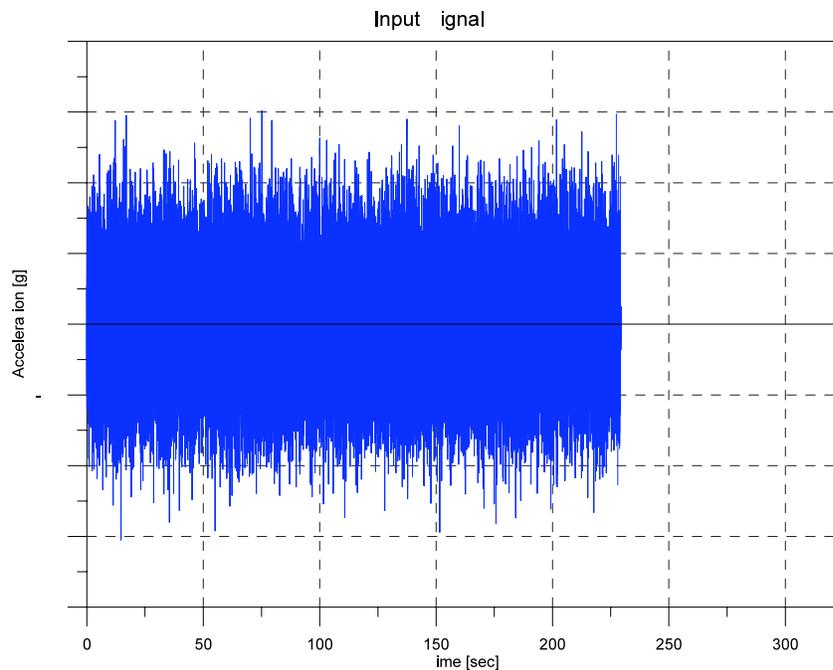
Figure 76. Input signal for the Vincent Thomas Bridge Model

The numerical model is utilized here only to produce responses for the bridge conditions at different levels of degradation. It is important to note that the application of the damage identification procedure does not require the existence of a F.E. model. An example of application, from recorded data, will be presented in the next chapter. What is required is instead a simplified interpretative scheme. The scheme is used for the discretization of the real structure in elements and sub-components (e.g. column, deck etc.), in order to be able to

assemble the normalized Damage Indicator Z_j for all the *jth* elements. The number and length of the elements that constitute the interpretative scheme is arbitrary. The procedure is in fact unaltered by the number and length of the elements. It is of course suggested that a preliminary analysis be conducted with a reduced number of elements and eventually detailed in regions where a structural deficiency is suspected. A reasonable balance between number of elements and data signals available should also be maintained. For instance, for the F.E. model of the Vincent Thomas Bridge, the response is available in every node. For this reason it is theoretically possible to describe the mode shapes with a very extensive number of points. However, it was experienced that the higher the number of points utilized, the higher will be the noise level in the assessed mode shapes. For the interpretative scheme of the bridge application, configurations with different number of elements (12, 25 and 64) were tested. The application reported here is limited to 12 elements, to show the capacity of the approach to function also in case of high simplification level. It must be noted also that the interpretative scheme does not have to include all portions of the existing structure. The interaction between all the structural components is in fact accounted for in the response signals, but the energy approach can be used to inspect only a limited portion of the real structure. The interpretative scheme assumed for this specific application is reported in Figure 77.
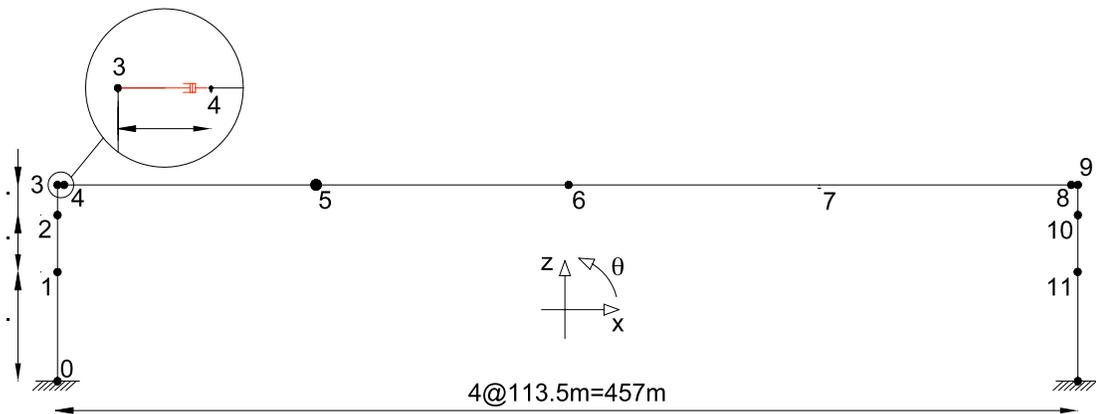
Figure 77. Bridge Interpretative Scheme with 12 elements (units: meters)

For the specific interest of this research, only the portion of the structure directly interested by the dampers (the piles and the deck of the main span), was considered. As indicated above, additional portions can be added, like the complete height of the towers and the structure from the towers to the abutments, but the considered part of the bridge seemed appropriate for the goal to validate the performance of the procedure. The dampers connecting the bridge towers and the deck are also grouped, in the scheme of Figure 77, in two elements (element between node 3 and 4 and element between node 8 and 9). Each element represents a set of 4 dampers in the real structure. This is just a simplification in the interpretative scheme that could be removed introducing additional elements in the

calculation of the damage indicators. This aspect will be discussed in the chapter relative to the field implementation of the procedure (chapter 7).

Displacement read-outs were extracted from the 3D Finite Element model described in Chapter 2, at locations corresponding to the nodes indicated in Figure 77. Based on these signals the mode shapes needed to be assessed. Two approaches were followed, as described in the following paragraph.

5.1 Covariance-driven Stochastic Subspace Identification method (SSI-Cov)

The assessment of the mode shapes from the F.E. model responses was initially attempted by using the output-only response method proposed by Kim (Kim et al., 2005). The accuracy of the mode shapes was found not satisfactory, for the use in the proposed procedure. For this reason a different approach, based on the Covariance-driven Stochastic Subspace Identification method (SSI-Cov) was implemented (Peeters, 2000).

The SSI-Cov method is as well an output-only response approach. This characteristic is considered of paramount importance for the proposed application because the structure is treated as excited by an unknown input and only output measurements (e.g. accelerations) are available. This condition closely represents the reality of a complex structure under a program of monitoring for structural health assessment purposes. For the SSI-Cov method the deterministic knowledge of the input is replaced by the assumption that the input is a realization of a stochastic process (white noise).

Measurements for modal analysis applications typically contain some redundancy. Since the spatial resolution of the experimental mode shapes is determined by the position and the number of the sensors, usually many sensors (mostly accelerometers) are used in a modal analysis experiment. Theoretically, if none of the sensors is placed at a node of a mode, all signals carry the same information on eigen-frequencies and damping ratios. To decrease this redundancy, some signals are *partially* omitted in the identification process, leading to algorithms that are faster and require less computer memory without losing a significant amount of accuracy. In the end, the omitted sensors are again included to yield the "full" mode shapes. With the SSI-Cov method it is possible to separate the uncertain variables (input and noise) from periodic variable such as vibrations frequencies of structure.

For large, real structures, in order to obtain a good model for modal analysis applications the construction of a stabilization diagram appears very practical. In case of the SSI-Cov method, an efficient construction of the stabilization diagram is achieved by computing the SVD of the covariance Toeplitz matrix only once. This is an iterative procedure where the system order n is fixed, step by step, and the modal parameters for the order (frequency of vibration 'ω', damping ratio 'ξ' and modal vector 'v') are determined.
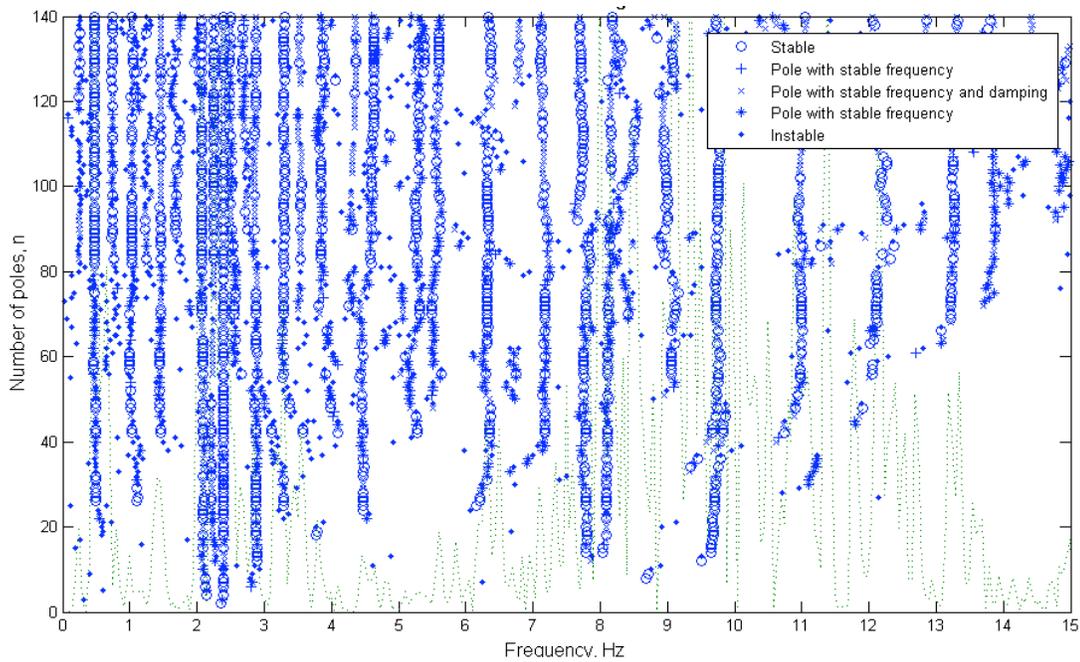
Figure 78. Example of Stabilization diagram obtained with the SSI-COV method for the undamaged case. The criteria are 1% for frequencies, 5% for damping ratios and 1% for the mode shape correlations

The repetition of blue dots (stable poles) corresponding to peaks of the green dashed curve (the PSD of the signal) isolates the natural frequencies. A band-pass filter is then applied in order to separate the single modal components. For the bridge application the natural frequencies for the first three modes and the ranges of frequency used to extract each modal contribution are reported in Table 18 and Table 19, respectively.

	Frequency [Hz]		
		Damaged 30%	
	Undamaged		Damaged 50%
I mode	0.260	0.274	0.276
II mode	0.480	0.477	0.477
III mode	0.739	0.746	0.750

Table 18. Modal frequencies

	Filter Ranges		
	Undamaged	Damaged 30%	Damaged 50%
I mode	0.2 - 0.3 Hz	0.2 - 0.3 Hz	0.2 - 0.4 Hz
II mode	0.4 - 0.5 Hz	0.4 - 0.5 Hz	0.4 - 0.6 Hz
III mode	0.7 - 0.8 Hz	0.7 - 0.8 Hz	0.6 - 0.8 Hz

Table 19. Filter ranges

The Modal coefficient of importance c_i are reported in Table 20.

	Coefficient c_i	
	Damaged 30%	**Damaged 50%**
I mode	1.00	0.64
II mode	0.21	0.27
III mode	0.50	1.00

Table 20. Coefficient of mode importance for each case

In Figure 79 to Figure 87 the modes shapes identified by the Kim approach and by the SSI-Cov method are compared with the mode shape identified by the Adina F.E. Model (FEM). It is visible the improvement of the SSI-Cov method in terms of symmetry of the mode shapes.
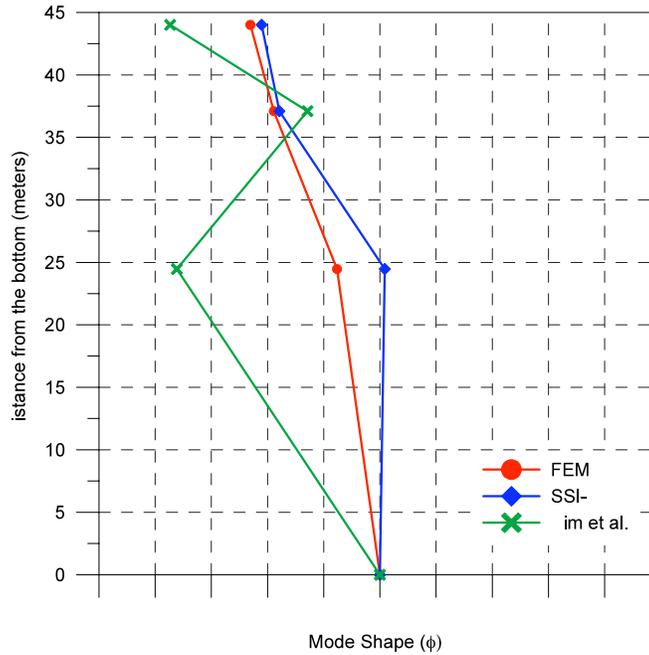
Figure 79. Undamaged Structure: first mode for the East Pylon
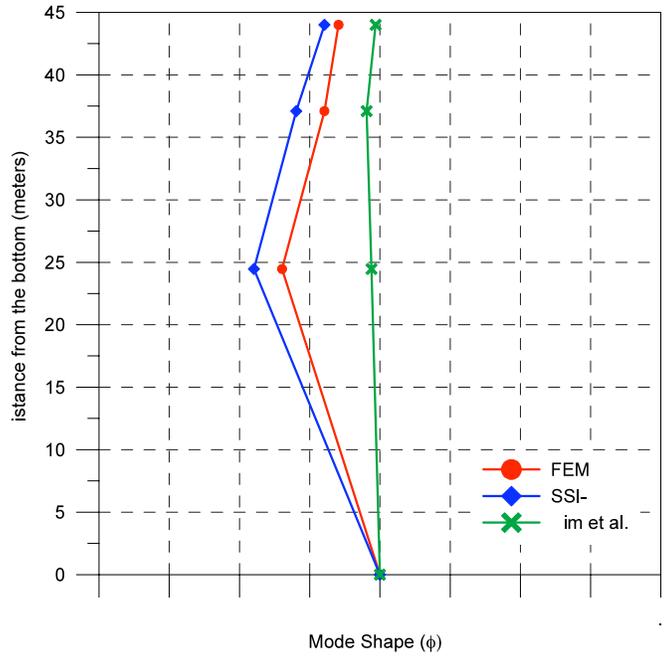
Figure 80. Undamaged Structure: second mode for the East Pylon
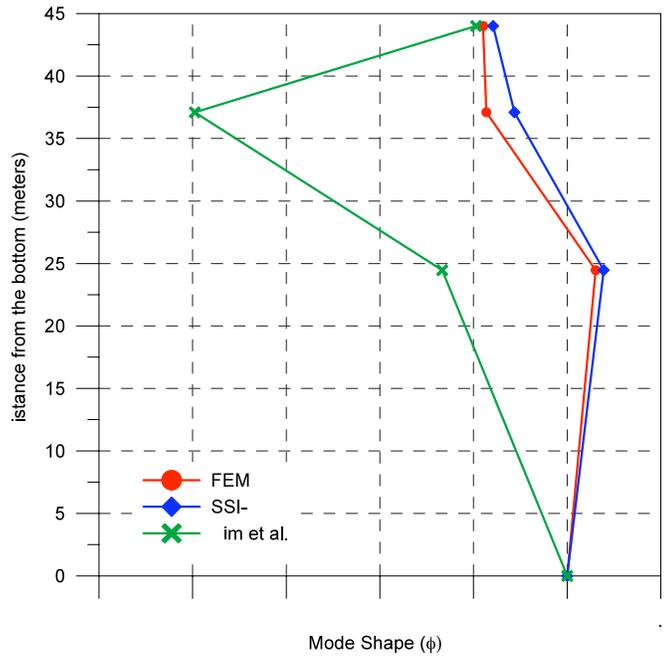
Figure 81. Undamaged Structure: third mode for the East Pylon
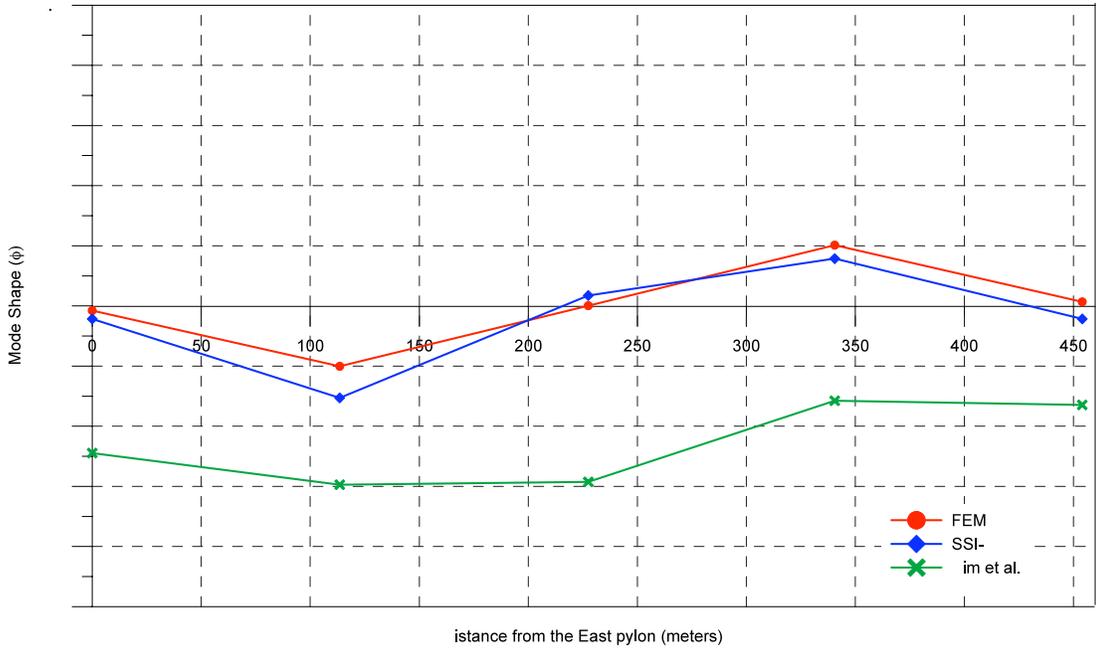
Figure 82. Undamaged Structure: first mode for the deck
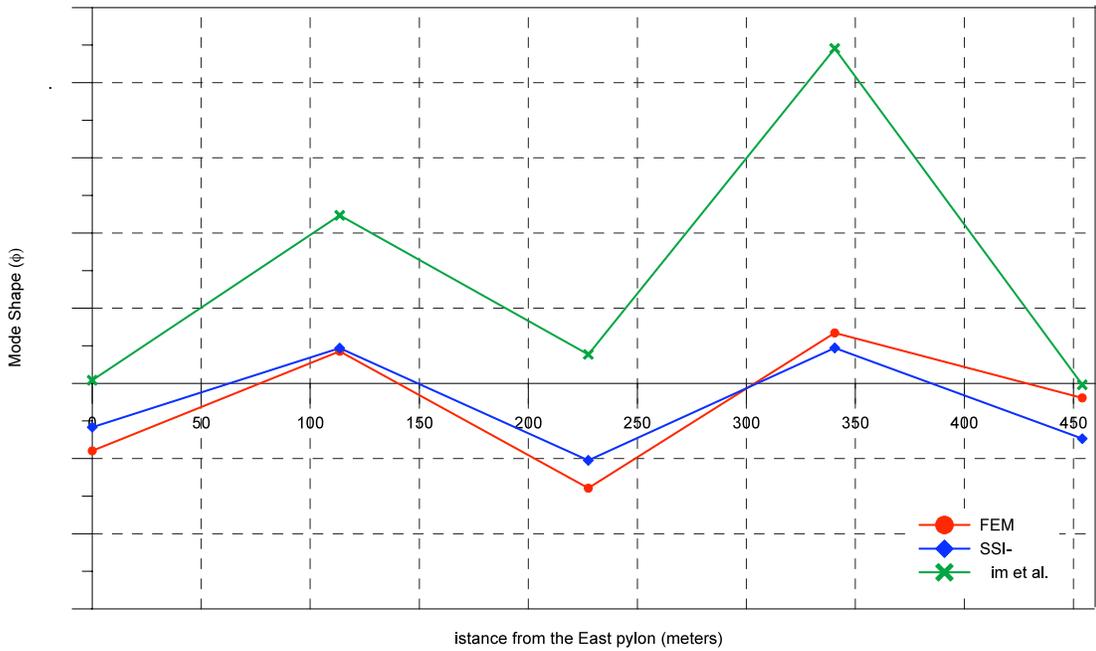
Figure 83. Undamaged Structure: second mode for the deck
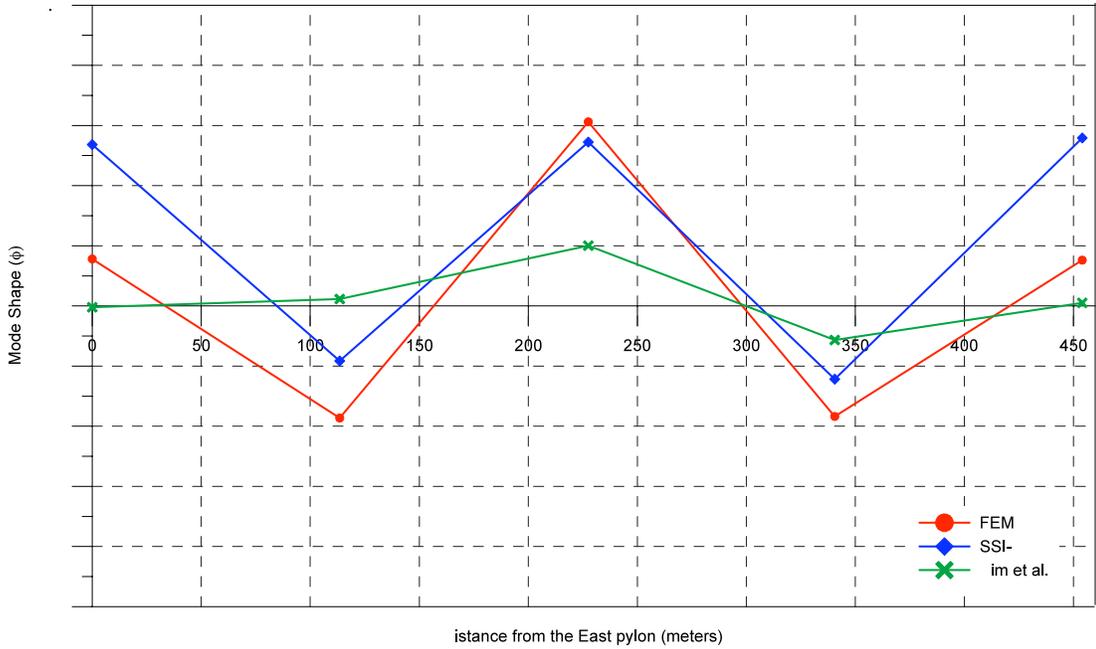
Figure 84. Undamaged Structure: third mode for the deck
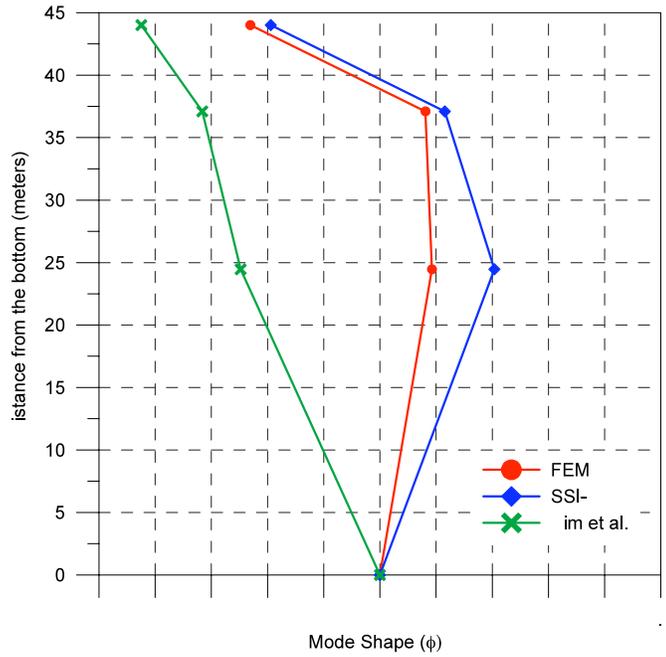
Figure 85. Undamaged Structure: first mode for the West Pylon
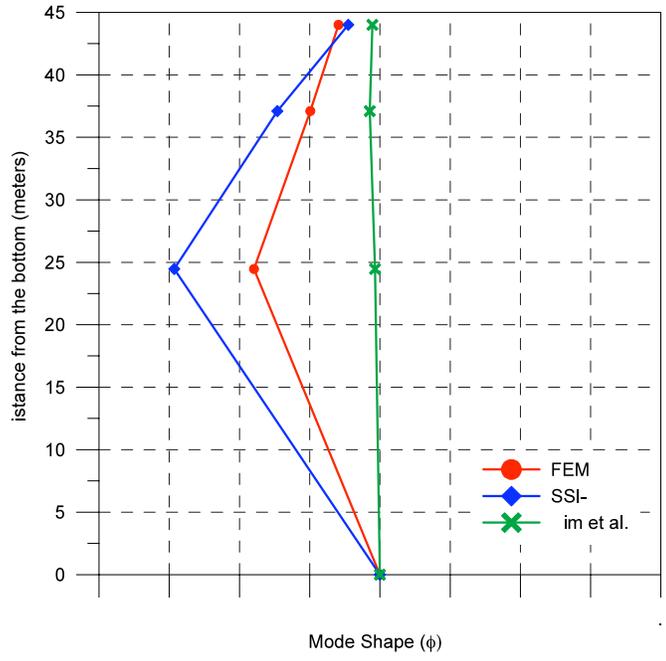
Figure 86. Undamaged Structure: second mode for the West Pylon
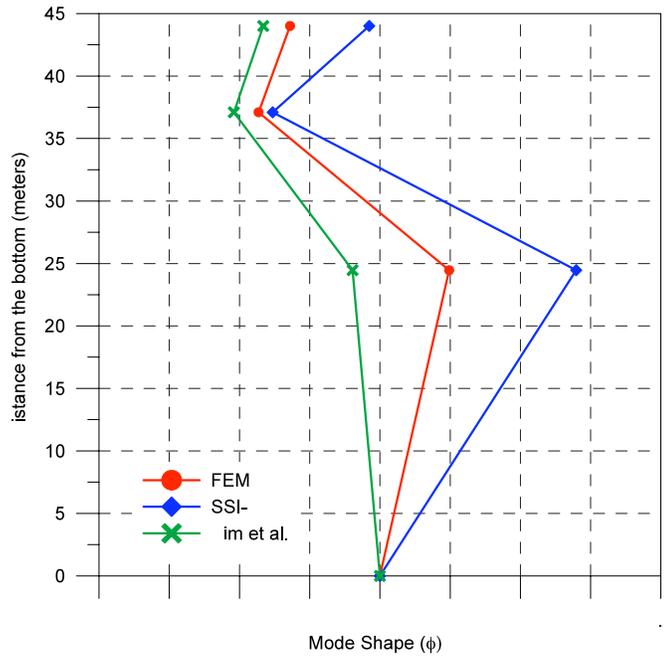
Figure 87. Undamaged Structure: third mode for the West Pylon

92

5.2 Application of the damage identification procedure to the bridge model

Case 1: 30% damage in dampers

The mode shapes for the bridge pylons and deck are shown in Figure 88 to Figure 96. Three modes shapes were considered. The dashed lines indicate the shapes obtained from the displacement records, while the solid lines correspond to the polynomial interpolation. The first three dominant mode shapes of the damaged structure occur at 0.274, 0.477 and 0.746Hz compared to 0.260, 0.480 and 0.739 Hz for the un-damaged structure.
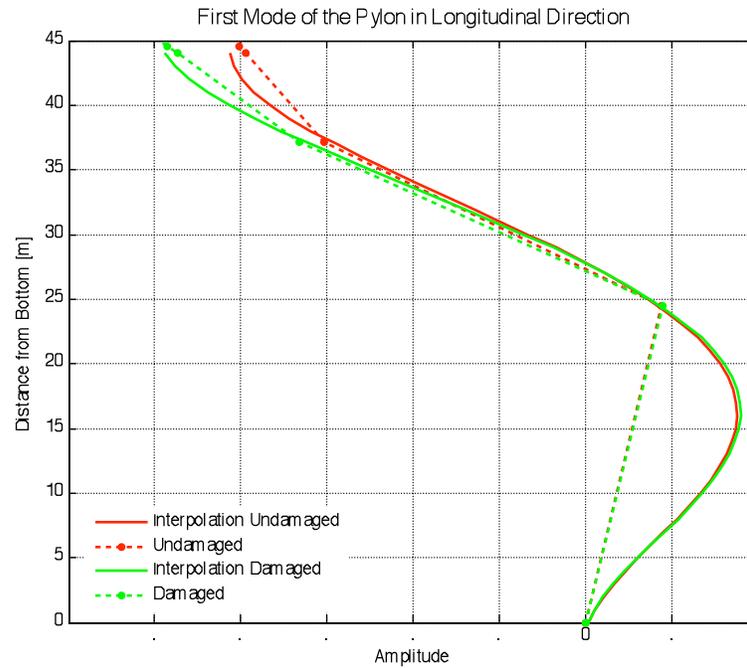
Figure 88. Damage 30%:First mode of the East pylon
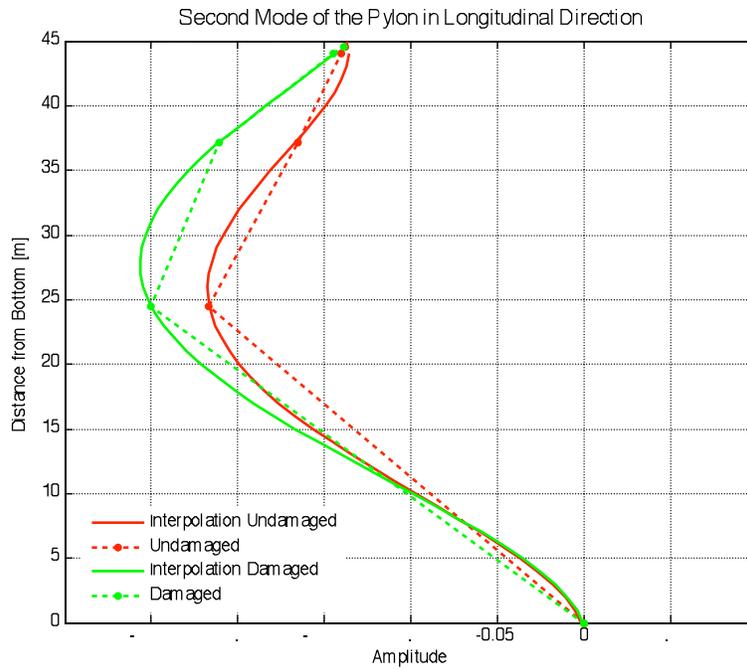
Figure 89. Damage 30%: Second mode of the east pylon
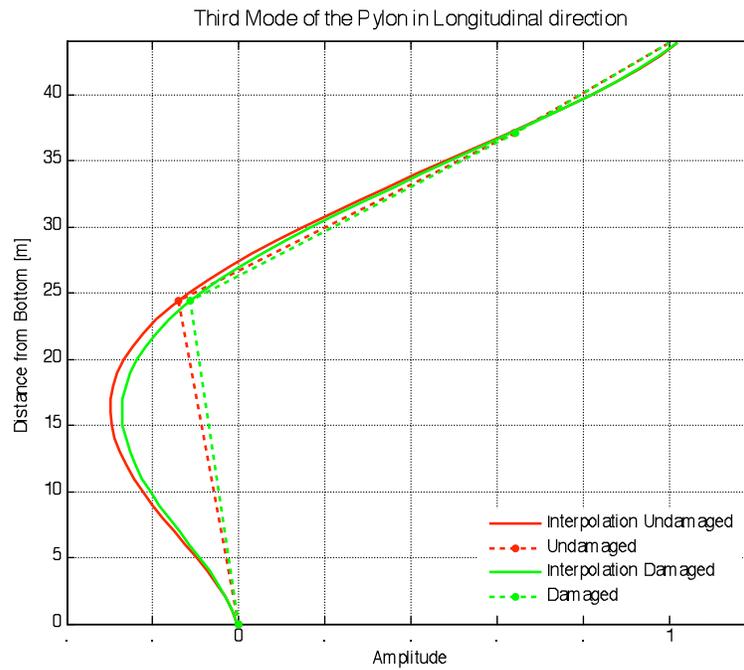
Figure 90. Damage 30%: Third mode of the East pylon
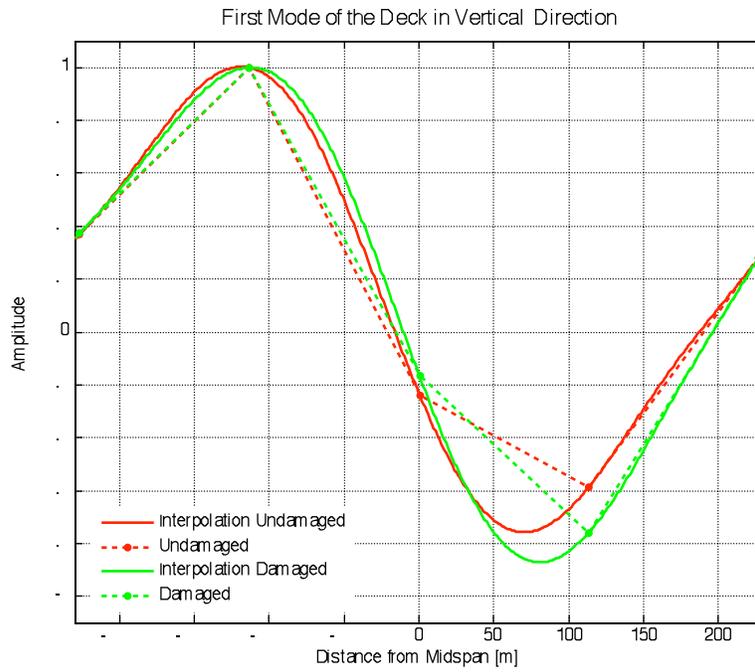
Figure 91. Damage 30%: First mode of the deck
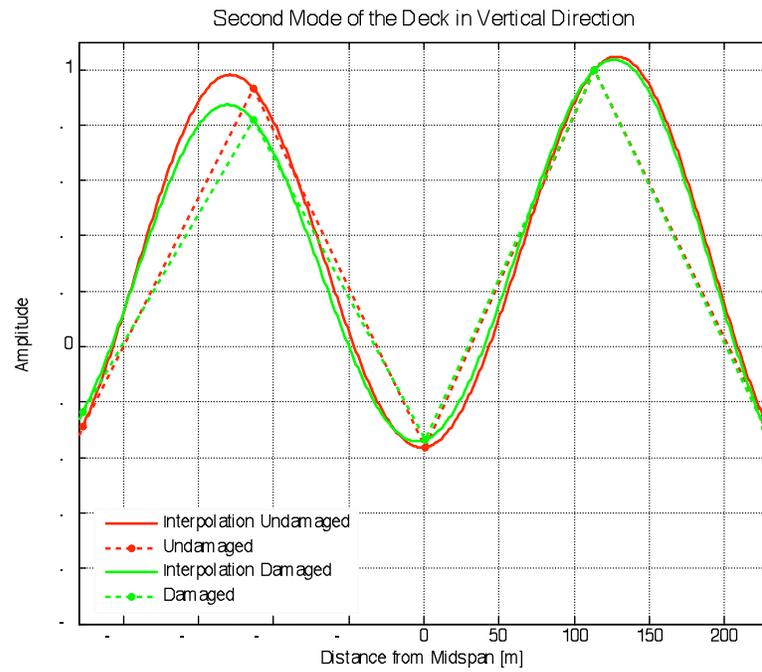
Figure 92. Damage 30%: Second mode of the deck
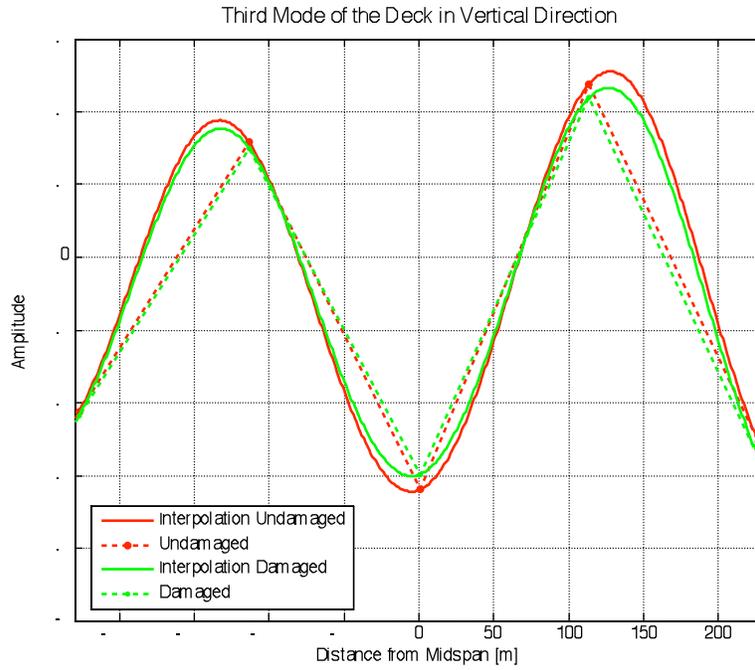
Figure 93. Damage 30%: Third mode of the deck
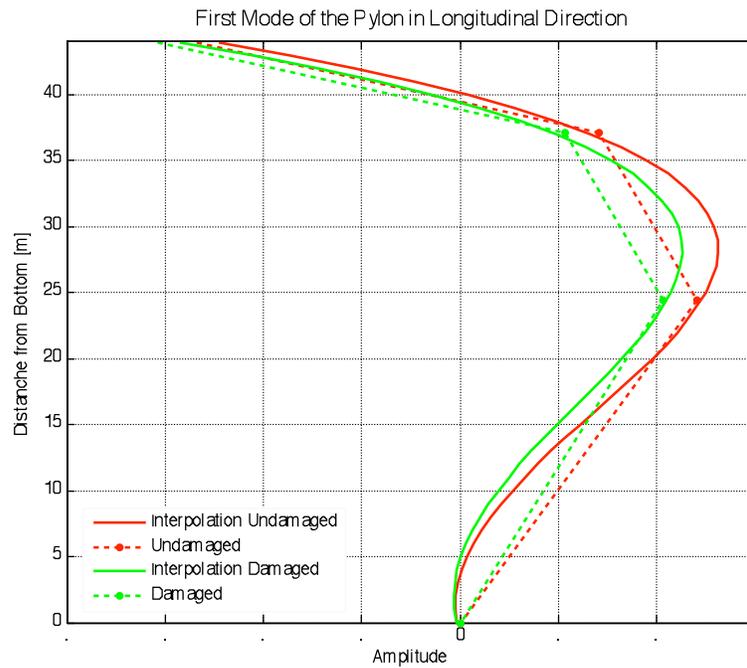
Figure 94. Damage 30%: First mode of the West pylon
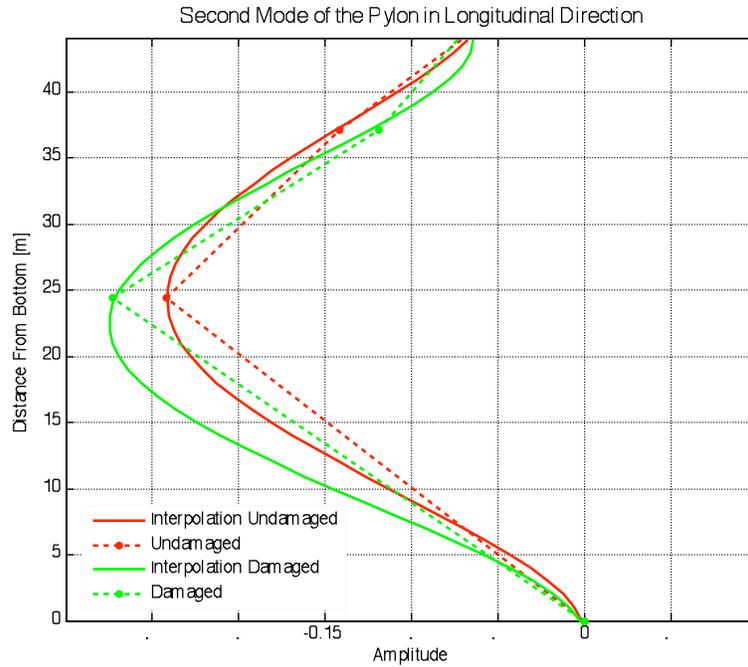
Figure 95. Damage 30%: Second mode of the West pylon
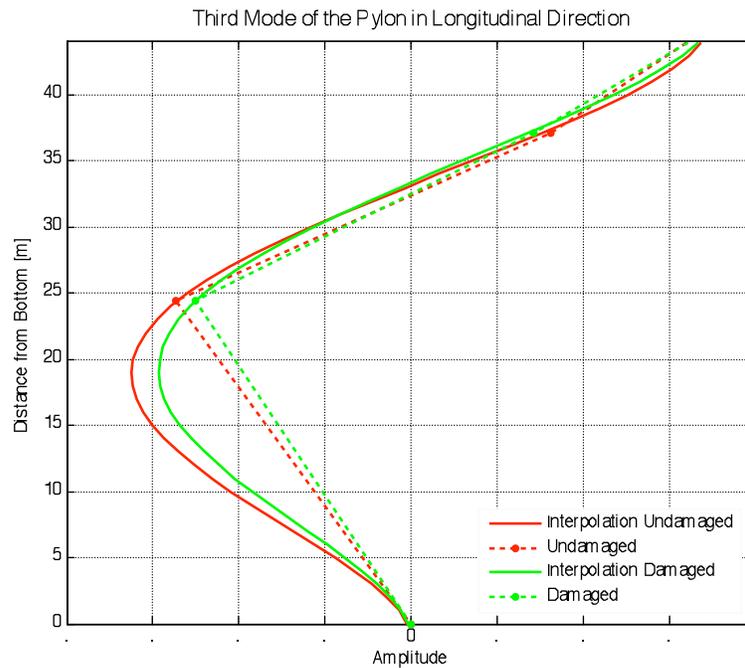
Figure 96. Damage 30%: Third mode of the West pylon

After the assessment of the best polynomial functions reproducing the mode shapes, the interpretative scheme of the structure was sub-divided in 1 m long elements. The availability

of a continuous polynomial functions allow to estimate the curvature of each single element and so the damage indicators.

The damage indices are presented in Figure 97 to Figure 99 for the 30% damage case. The East pylon, the deck and the West pylon are projected on the same x axis. The last two elements correspond to the energy dissipators. The Figures indicate that the damage exists in the dampers. Peaks of the parameter Z_{ij} are visible also for elements at the top of the West pylon. However Figure 99 indicates for these elements a positive coefficient of severity. Based on Eq. (44), a positive coefficient of severity α_j does not represent damage.
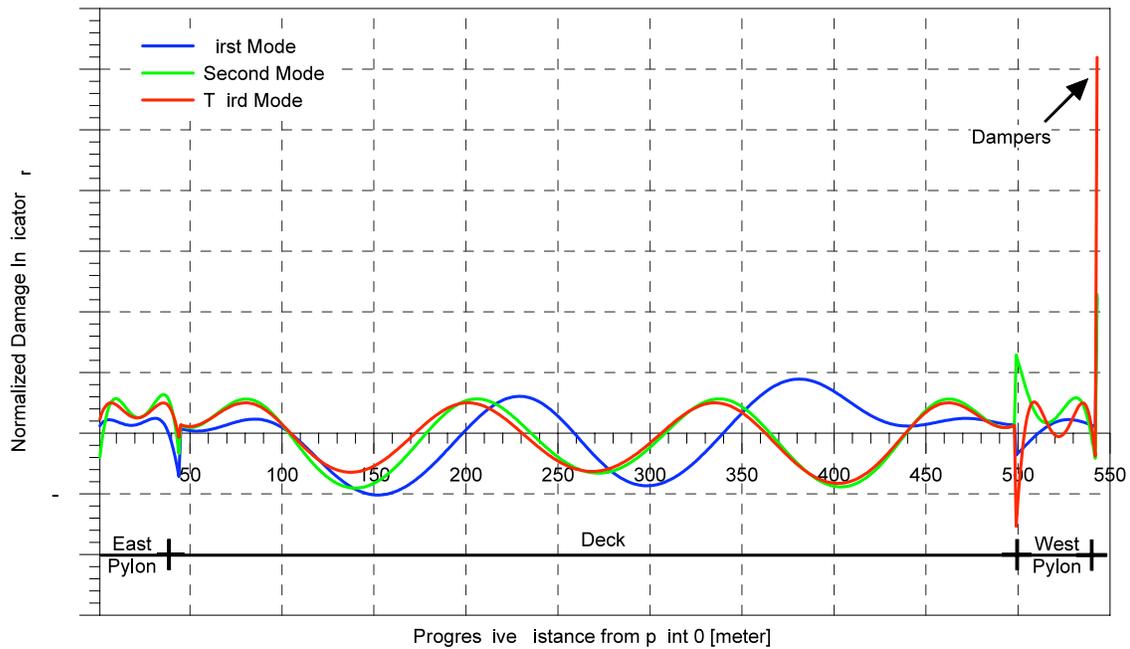
Figure 97. Damage 30%: Normalized Damage Index Z_{ij} for each mode
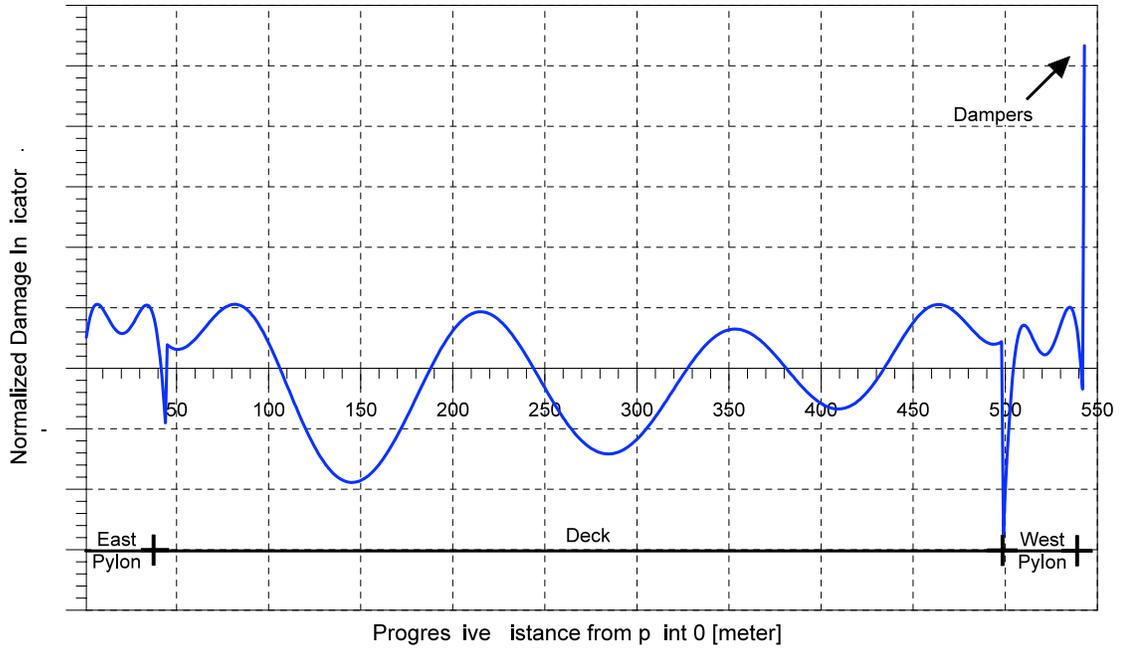
Figure 98. Damage 30%: Normalized Damage Index Z_j total
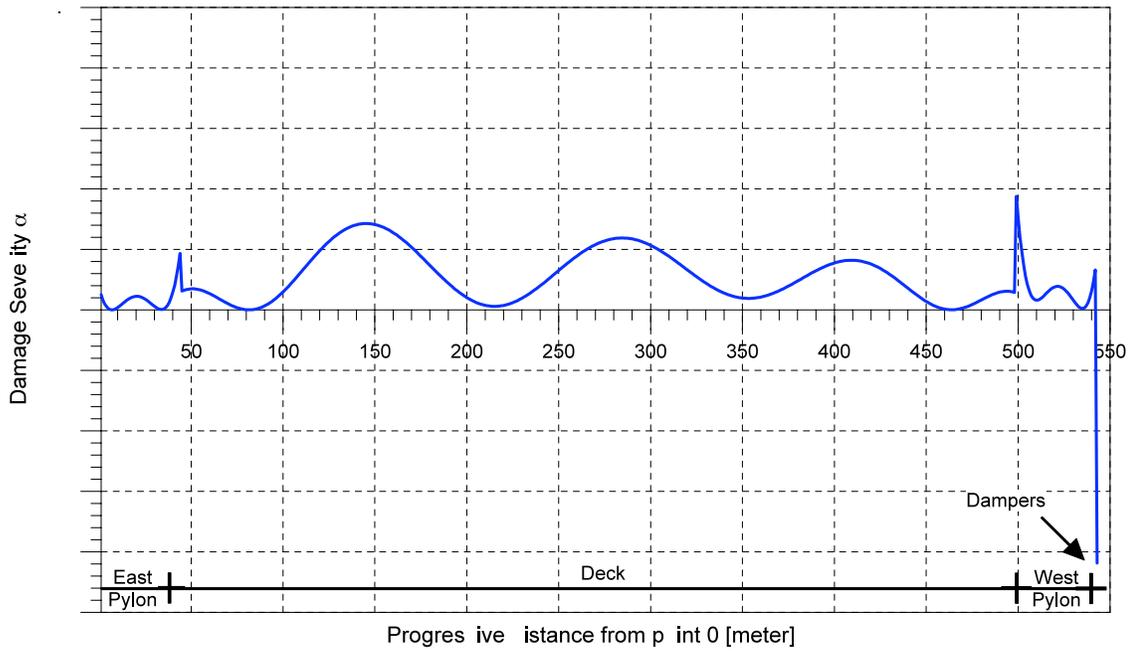
Figure 99. Damage 30%: Damage Severity Indicator α_j

Case 2: 50% damage in dampers

As presented before, the following figures report mode shapes and damage indices for the configuration of damaged dampers, in the amount of 50% reduction of their original damping coefficient. The first three dominant mode shapes of the damaged structure occur at 0.274, 0.477 and 0.750Hz compared to 0.260, 0.480 and 0.739Hz for the un-damaged structure. From the severity indicator α_j (Figure 111) it is detected a degradation of ~55% for the dampers on the East side of the main span and of ~65% for the dampers on the West side.
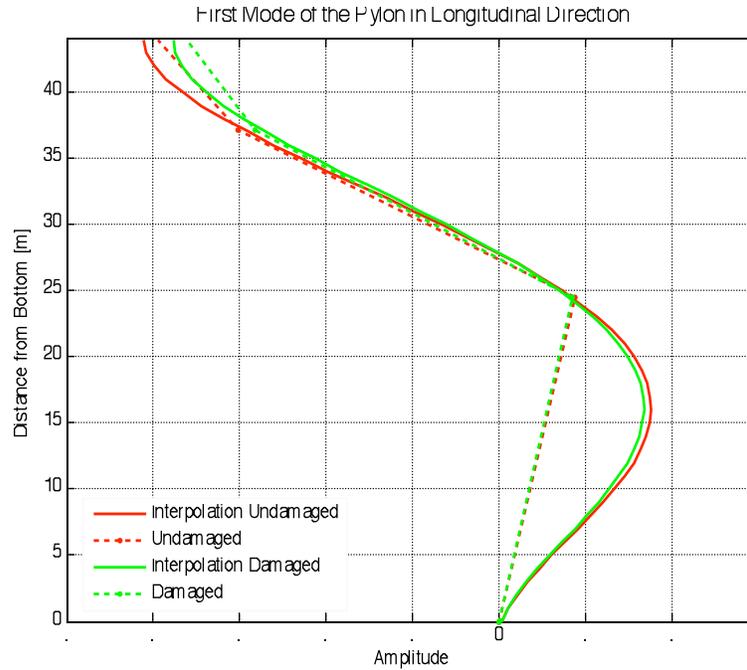
Figure 100: Damage 50%: First mode of the East pylon
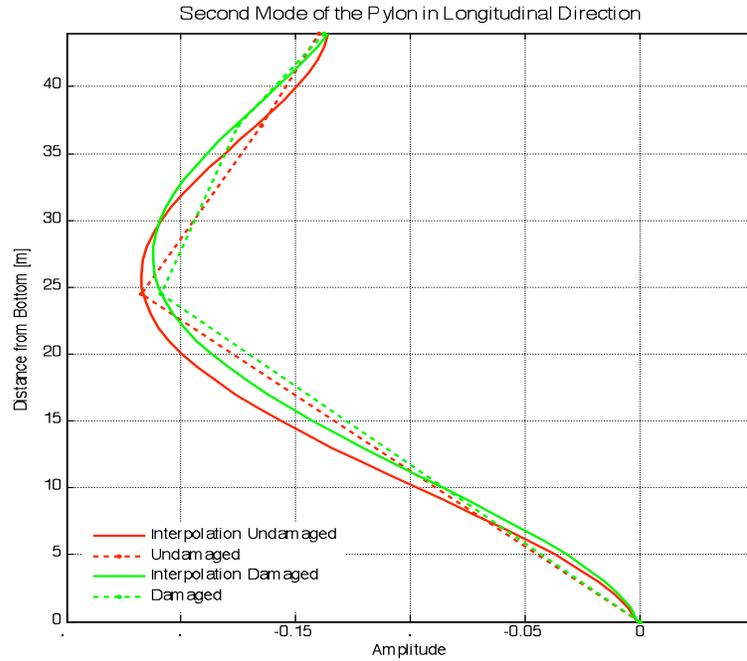
Figure 101. Damage 50%: Second mode of the East pylon
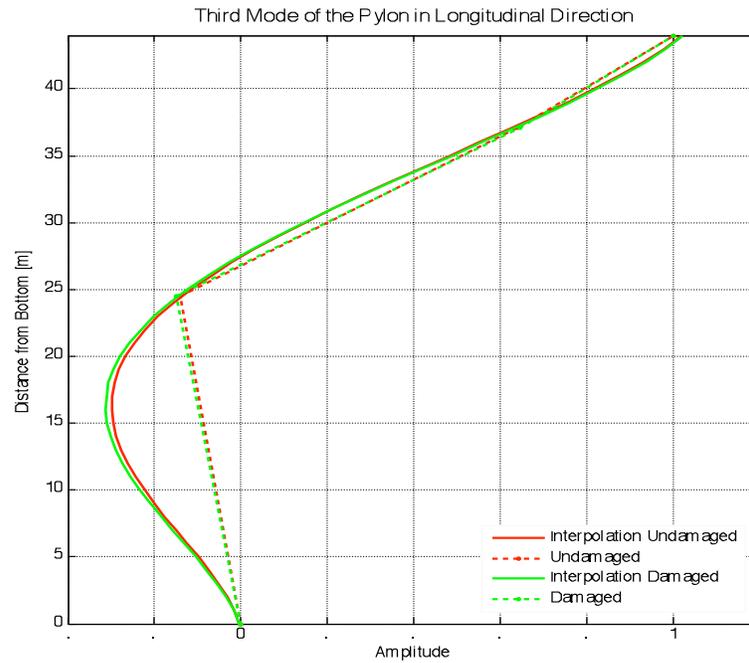
Figure 102. Damage 50%: Third mode of the East pylon
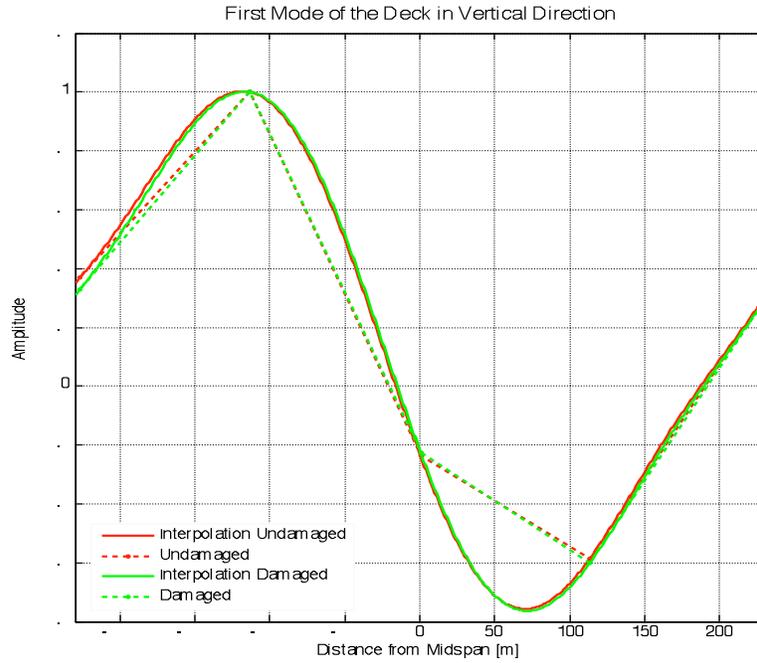
Figure 103. Damage 50%: First mode of the deck
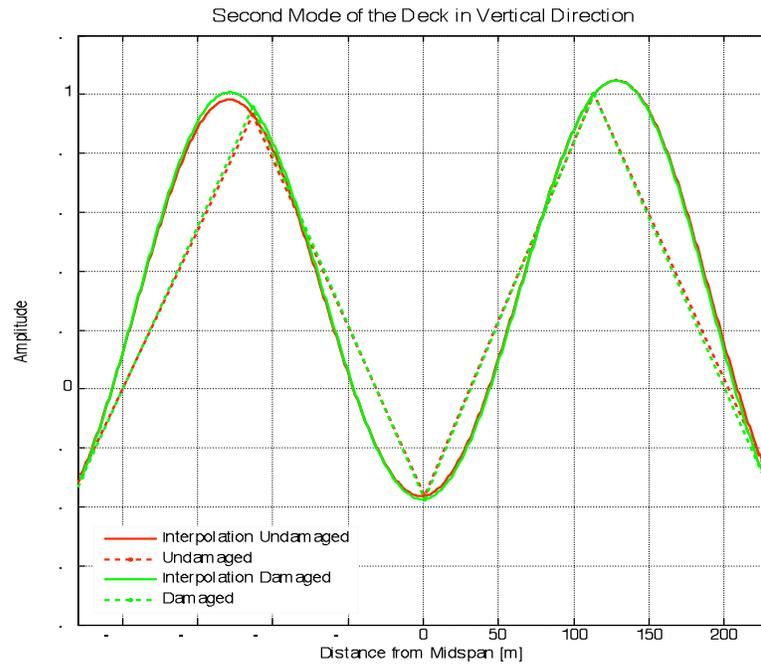
Figure 104. Damage 50%: Second mode of the deck
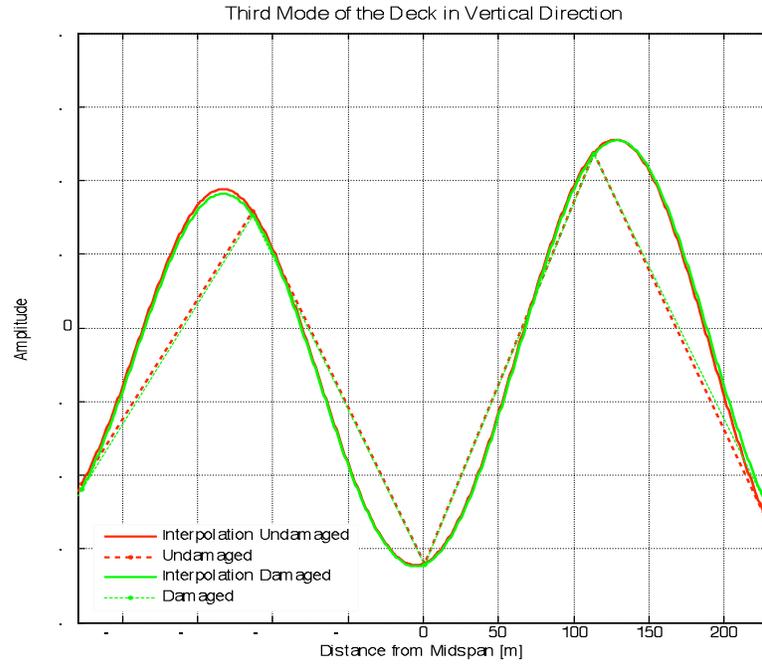
Figure 105. Damage 50%: Third mode of the deck
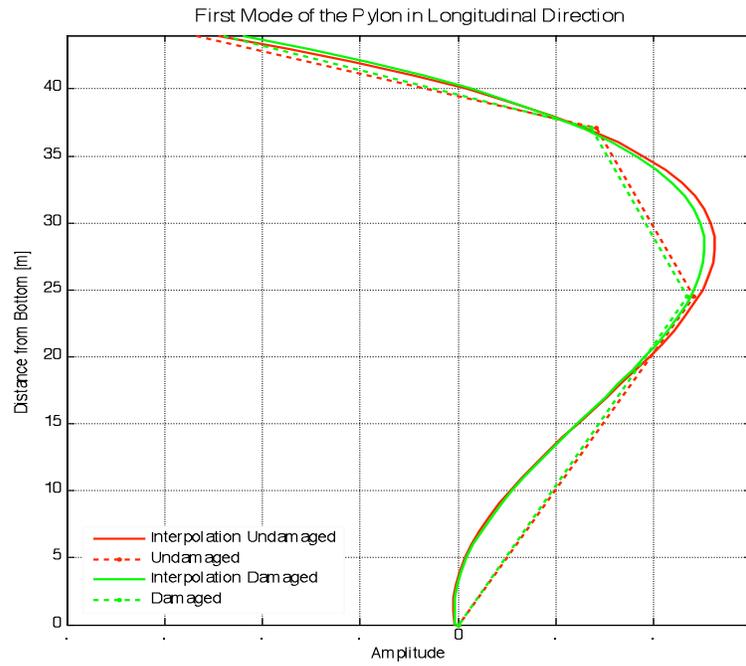
Figure 106. Damage 50%: First mode of the West pylon

103
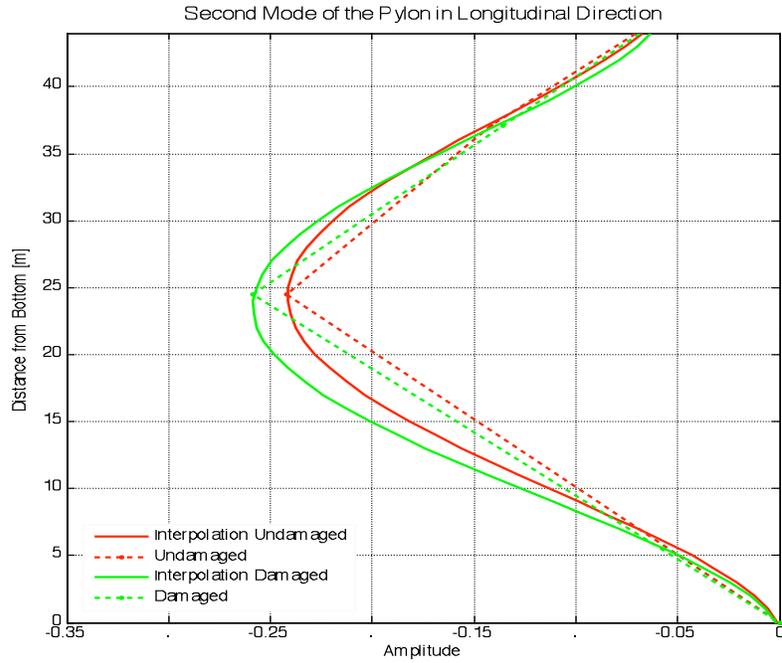
Figure 107. Damage 50%: Second mode of the West pylon
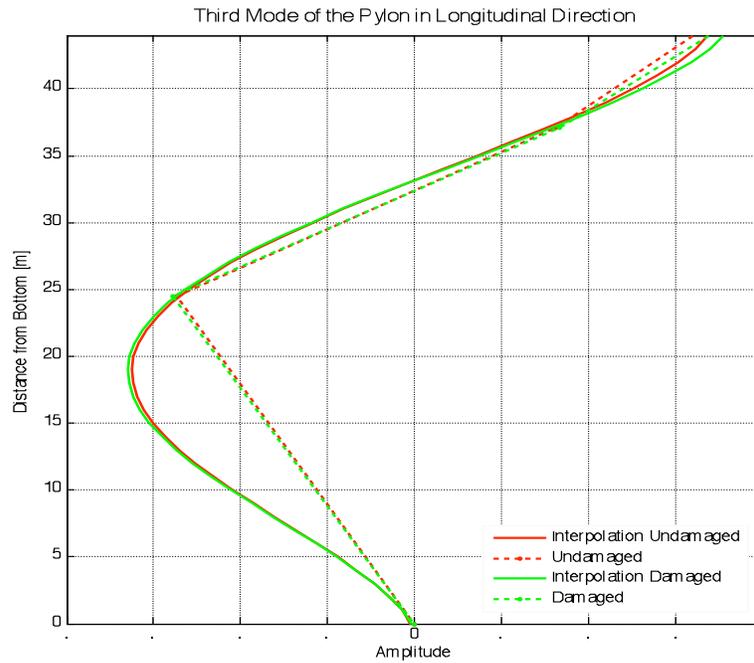
Figure 108. Damage 50%: Third mode of the West pylon
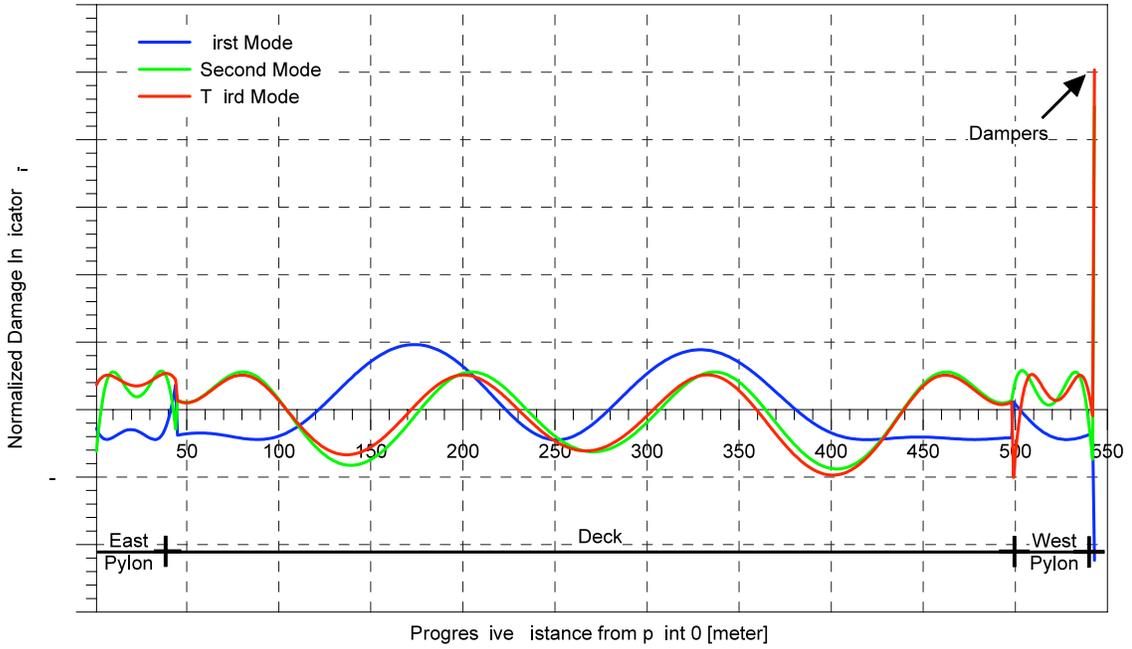
Figure 109. Damage 50%: Normalized Damage Index Z_{ij} for each mode
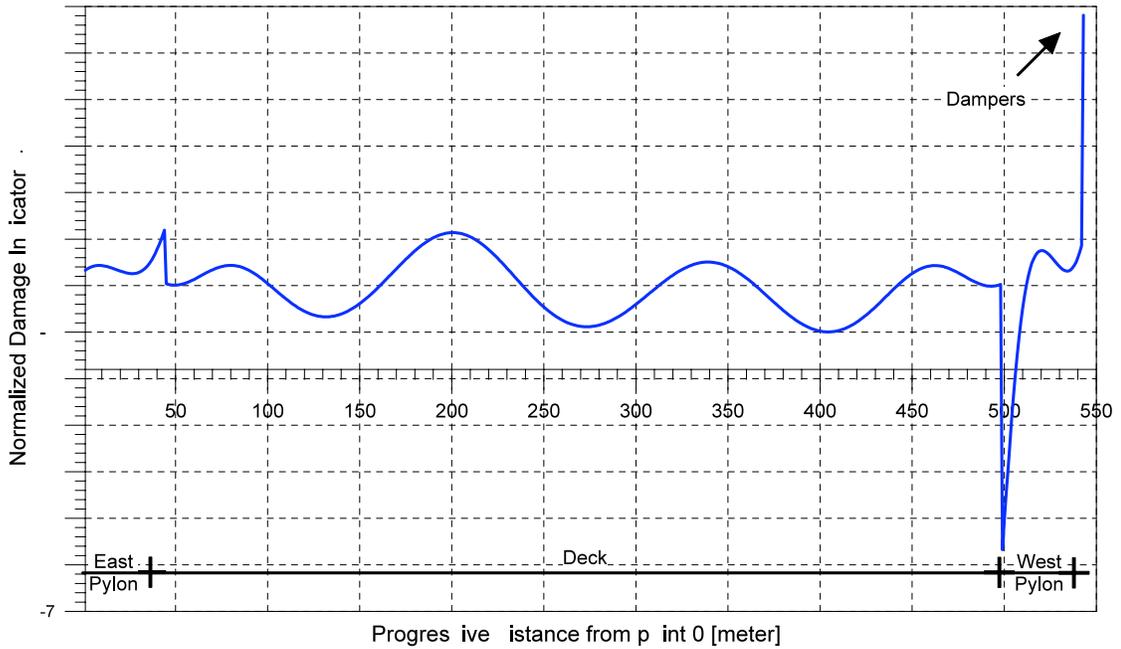
Figure 110. Damage 50%: Normalized Damage Index with mode coefficient Z_j total
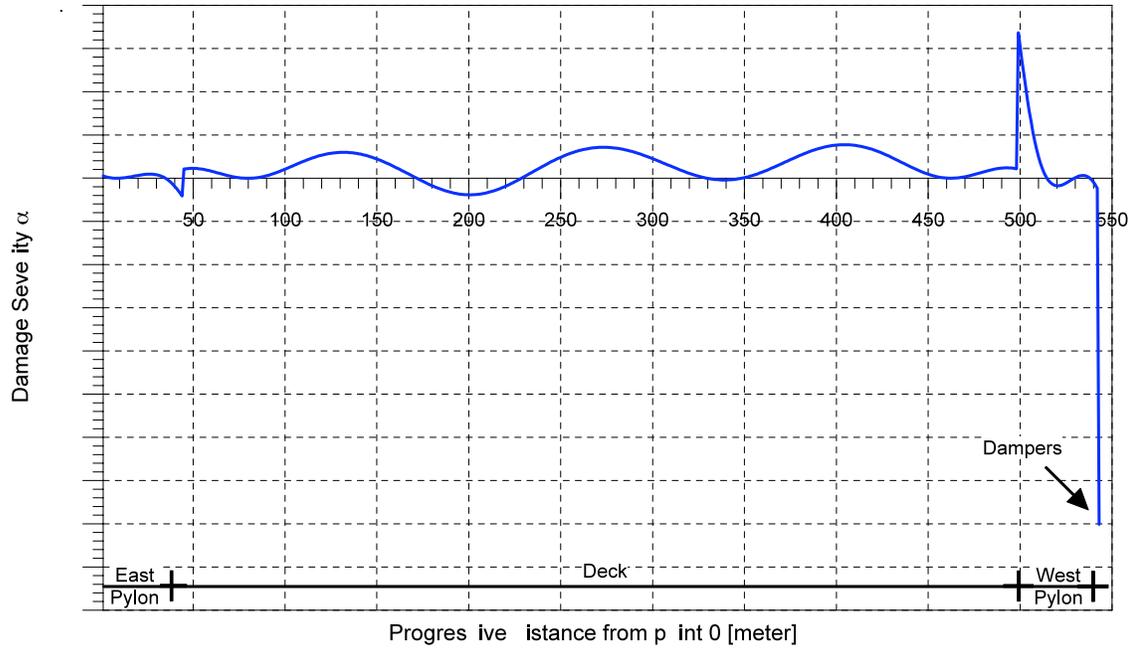
Figure 111. Damage 50%: Damage Severity Indicator α_j

6) VINCENT THOMAS BRIDGE APPLICATION – EXPERIMENTAL DATA

The modal system identification and the damage evaluation of the bridge, using acceleration data recorded in April 2003, June 2006 and December 2006 was completed in this phase. The time domain decomposition method described above was utilized to extract the modal parameters of the bridge from the 2003 and 2006 data. To locate and estimate the severity of the damage in the structure the damage identification algorithm, with the appropriate modifications to take into account the existence of dampers, was applied.

Sensor localizations and characteristics are reported in Table 1 and Figure 5. Because of the location of the sensors is not possible to consider the entire bridge structure but only the East side from mid-span to the abutment. Data samples were collected on April 18, 2003, June 12, 2006, June 13, 2006 and December 2006. For the 2003 data the record length is 380 seconds and sampling frequency was 100Hz. Acceleration units are cm/sec^2. For the June 2006 data the record length is 64 seconds (June 12) and 65 seconds (June 13) and sampling frequency is 200Hz. Accelerations are in g units. For the December 2006 data the record length is 68 seconds with sampling frequency equal to 200Hz. Accelerations were reported in cm/sec^2. The all sets of records are ambient data sets under wind and traffic excitation.

The December 2006 data are used as representative of the un-damaged configuration of the structure. This is because the structure, at the time of this event, was equipped with a new series of dampers. Disregarding the time sequence of events allows to compare a bridge configuration with certainly un-damaged dampers with a condition of dampers very likely degraded in their performance (April 2003).

To estimate the mode shapes from the real data the following records were considered:

- The vertical component of motion of the deck was used for the damage detection procedure applied to the deck structure between mid-span and the east pier;

- The motion in the bridge longitudinal direction to detect possible degradation in the elements of the East Pylon;

- The vertical motion of the deck and the motion in longitudinal direction to estimate possible degradation in the dampers between main span and east tower and between east side span and east tower.

The position and the number of the sensors used for the extraction of the mode shape are indicated in Figure 112 and Figure 113. Three sensors (16, 18 and 22) are used for the deck's mode shape and other three sensors (13, 12 and 10) are used for the pylon's mode shape.
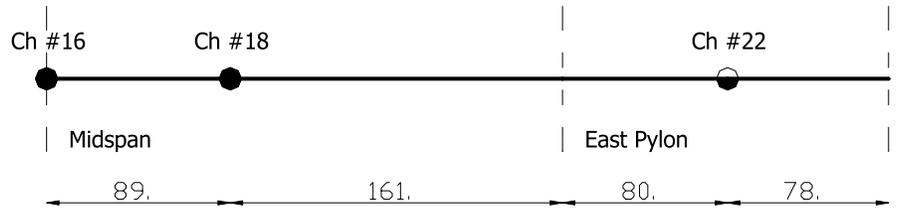
Figure 112. Location of the Vertical Channels on the deck
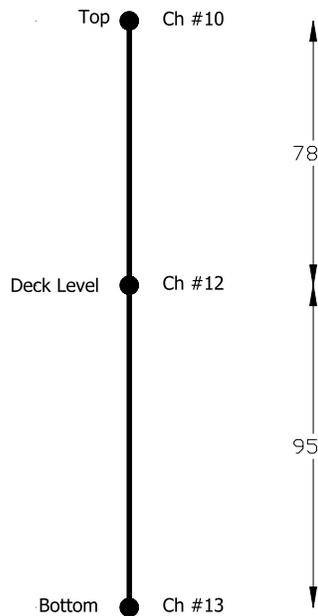
Figure 113. Location of Channels used to assess the mode shapes of the East pylon

The interpretative scheme needed for the damage assessment procedure is reported in Figure 114. The nodes indicated in Figure 114 represent positions where actual data are available (#1, #2, #5 for the deck, #7, #9 and #10 for the pylon), as well as additional nodes used for the placement of the dampers (node #3, #4, #8) and for restraining conditions (#6). As described above, this interpretative scheme is used for the assessment of the mode shapes. After the mode shapes are obtained a further discretization in a large number of elements is usually completed for the computation of the damage indicators.

108
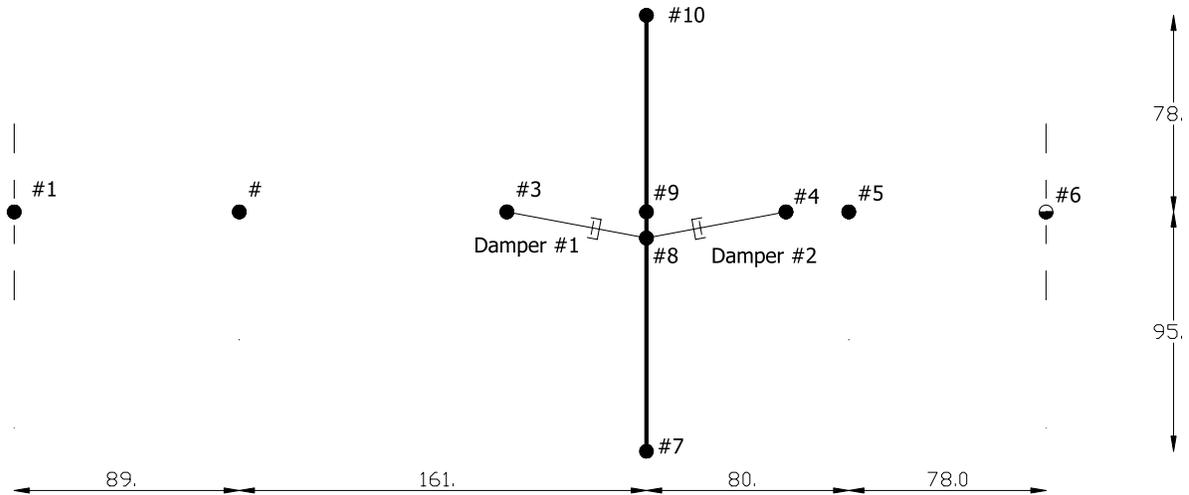
Figure 114. Interpretative scheme of the VTB

6.1 Modal system identification from acceleration data

Even though the SSI-Cov approach for assessment of the mode shapes was found particularly reliable and practical for this specific application, the TDD approach proposed by Kim (Kim et. al, 2005) was initially used in this phase. The reason was to attempt a comparison between findings with a parallel work, performed on the same set of data, by Prof. Stubbs (Stubbs et al, 2006). An additional analysis performed with the use of the SSI-Cov approach is presented in Chapter 6.3.

The TDD procedure for mode shapes estimate was carried out through the following steps:

- Identification of the natural frequencies from the PSD of the available signals;

- Transfer Functions are computer between the records and a reference signal. Channel #13, at the bottom of the pylon was chosen as reference signal;

- For each Transfer Function the frequency components are replaced with zeros except for the frequencies between 0.05Hz and 10Hz. The first three natural frequencies are in fact included in this range;

- The scaled time histories are computed by inverse discrete Fourier transformation of the frequency filtered FTTs;

- Digital Butterworth band-pass filters are applied to isolate each mode. The filters are determined by inspection of the PSDs;

- The output energy correlation Matrix, E_i, is computed using the filtered time histories:

$$E_i = Y_i Y_i^T \qquad (54)$$

where *Y* is the filtered output acceleration time history that contains only the *ith* mode.

- A singular value decomposition (SVD) of E_i is performed:

$$E_i = U \Omega U^T \qquad (55)$$

where *U* is a unitary matrix holding the singular vectors u_{ij}, and Ω is a diagonal matrix holding the scalar singular values. The first column of the singular vector, u_i, is the desired mode shape for each filtered mode.

The PSD for all channels are shown in Figure 115 and Figure 116 for the set of data recorded on December 2006.
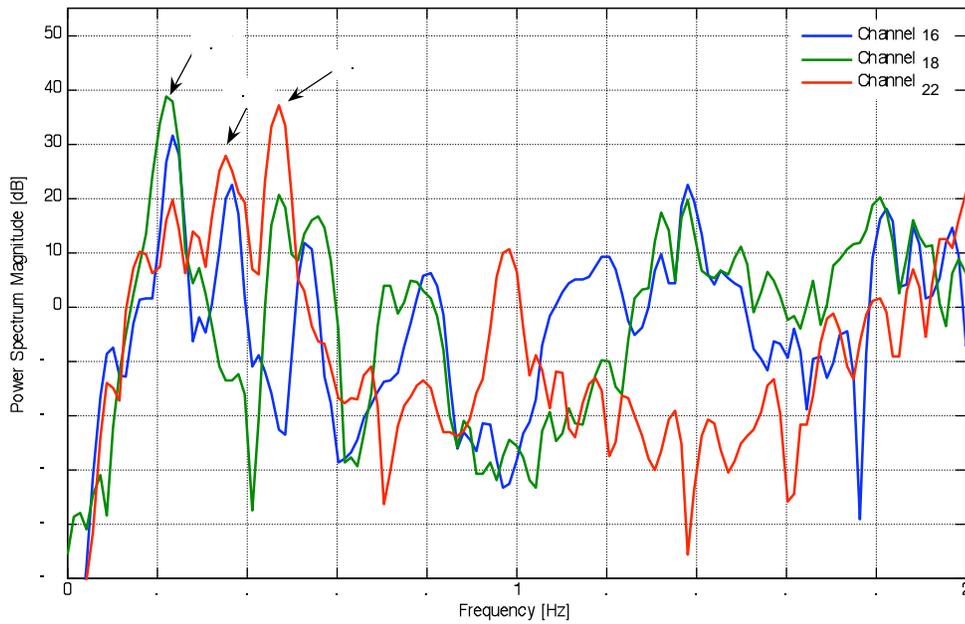
Figure 115. Power Spectral Density of the deck response (December 2006)
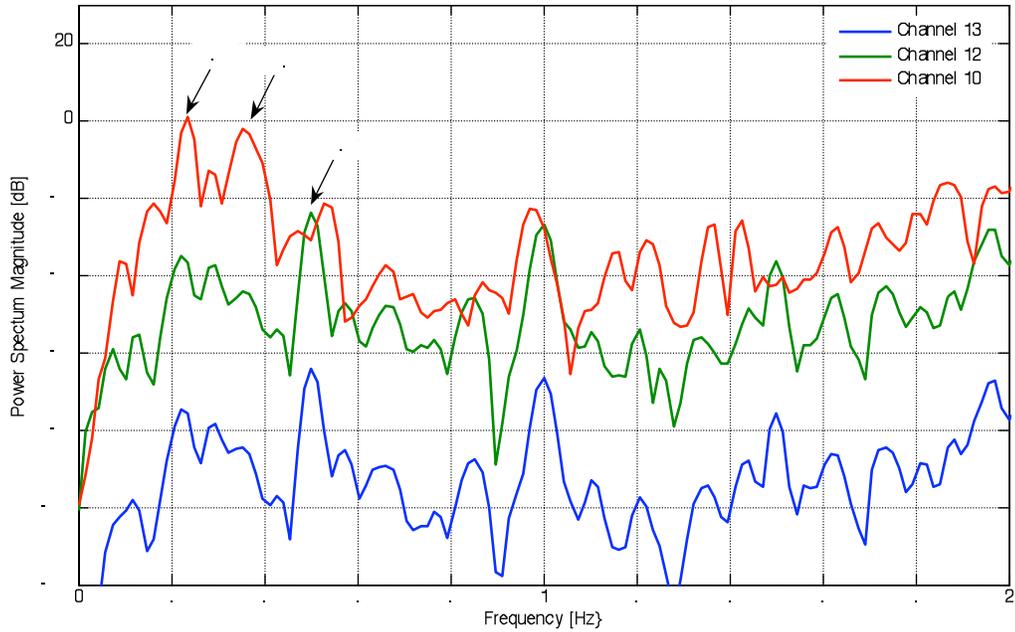
Figure 116. Power Spectral Density of the pylon response (December 2006)

The first three dominant modes for the deck and for the pylon and the frequency ranges used to isolate the single modes are listed in Table 21 and Table 22.

Frequencies [Hz]		
	Deck	**Column**
I mode	0.25	0.22
II mode	0.39	0.39
III mode	0.46	0.47

Table 21. Data December 2006: Modal frequencies

Filter Ranges		
	Deck	**Column**
I mode	0.20 – 0.26 Hz	0.19 - 0.26 Hz
II mode	0.30 – 0.40 Hz	0.30 - 0.40 Hz
III mode	0.44 – 0.51 Hz	0.47 - 0.51 Hz

Table 22. Data December 2006: Filter ranges

The first three modal shapes for the deck and for the pylon are shown in Figure 117 and Figure 118.
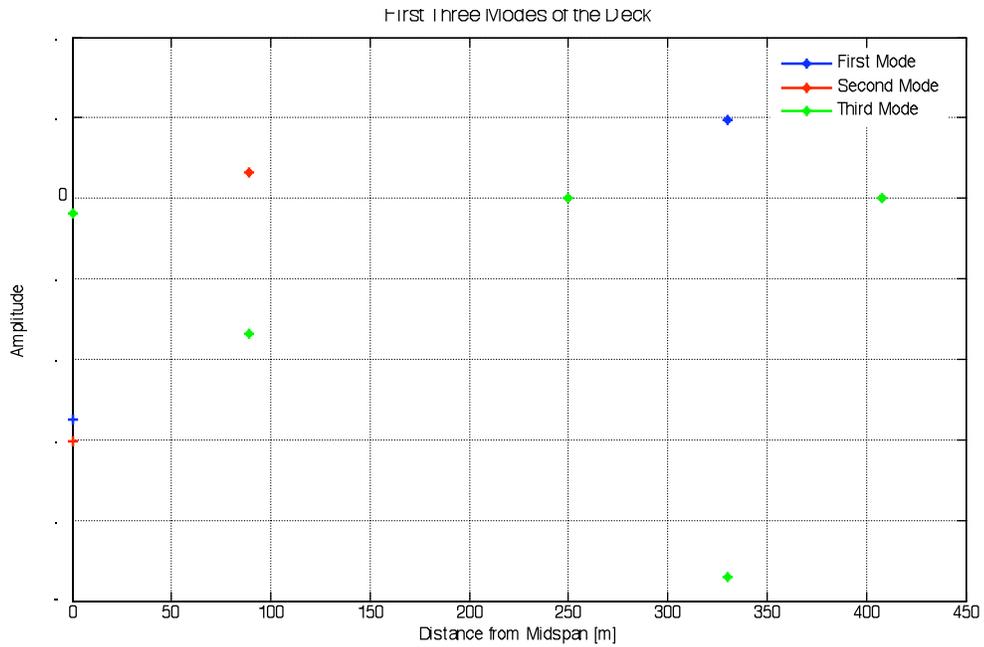
Figure 117. First three mode shapes of the deck in vertical direction (December 2006)
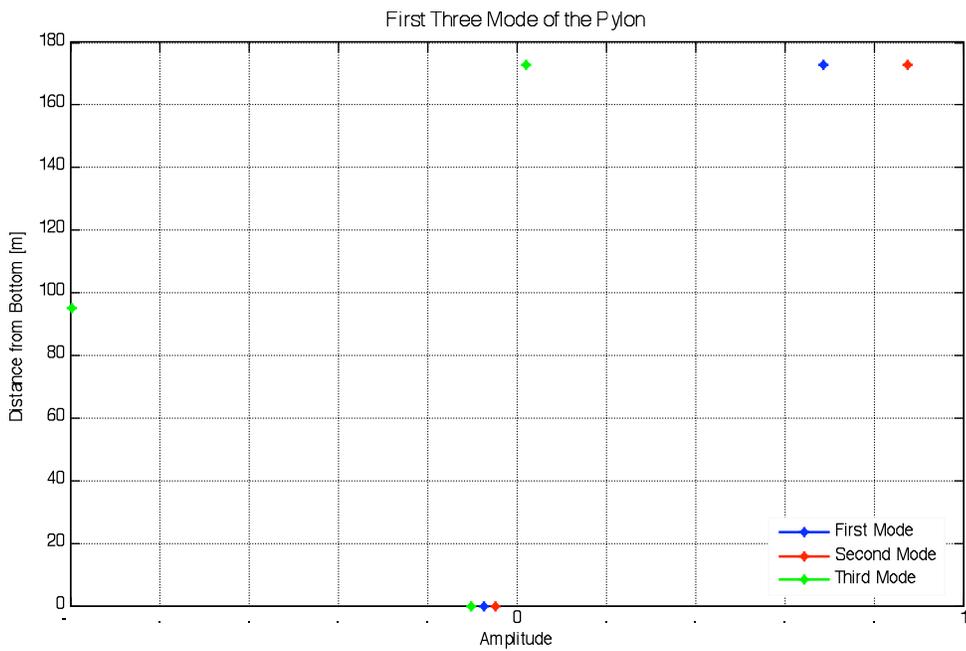
Figure 118. First three mode shapes of the East pylon in longitudinal direction (December 2006)

The same set of sensor was used to extract the mode shapes from the June 2006 data. The procedure described above was repeated for these records. The PSD functions for all channels are shown in Figure 119 and Figure 120.
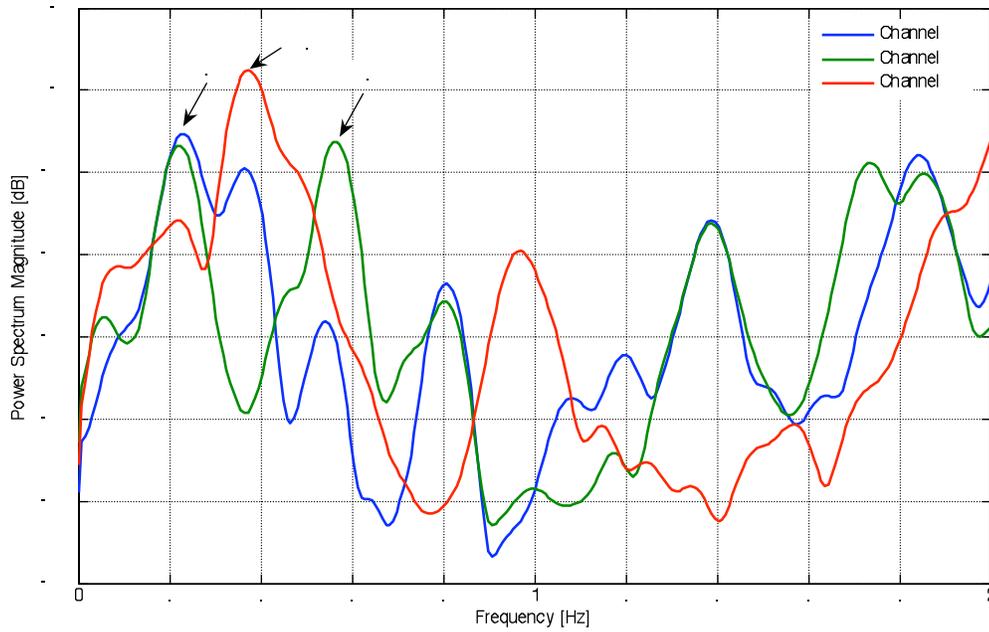
Figure 119. Power Spectral Density of the deck response (June 2006)
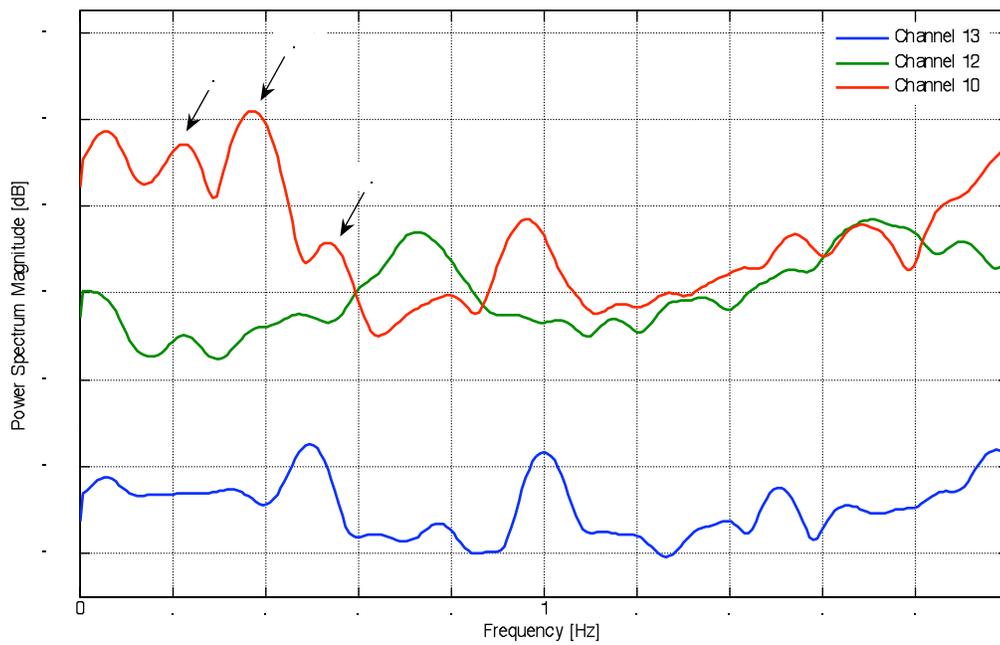
Figure 120. Power Spectral Density of the pylon response (June 2006)

The first three dominant frequencies and frequency bands for the deck and for the pylon are listed in Table 23 and Table 24.

Frequencies [Hz]		
	Deck	**Column**
I mode	0.24	0.20
II mode	0.34	0.34
III mode	0.54	0.58

Table 23. Data June 2006: Modal Frequencies

Filter Ranges		
	Deck	**Column**
I mode	0.16 – 0.26 Hz	0.16 - 0.27 Hz
II mode	0.30 – 0.41 Hz	0.28 - 0.36 Hz
III mode	0.50 – 0.60 Hz	0.46 - 0.59 Hz

Table 24. Data June 2006: Filter ranges

The first three modal shapes for the deck and for the pylon are shown in Figure 121 and Figure 122.
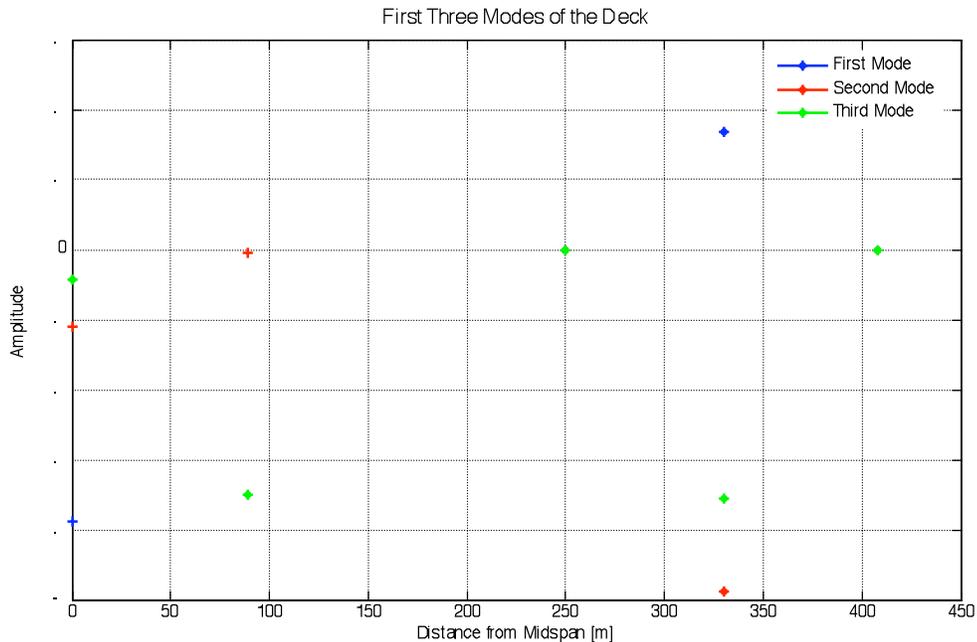
Figure 121. First three mode shapes of the deck in vertical direction (June 2006)
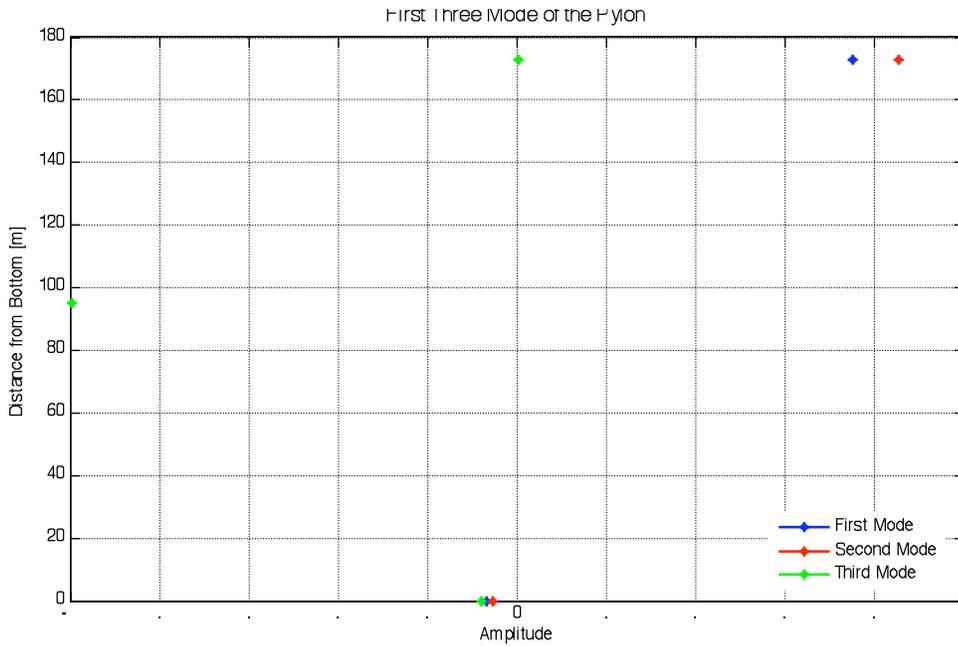
Figure 122. First three mode shapes of the East pylon in longitudinal direction (June 2006)

The same plots presented above are repeated here for the modal analysis based on the bridge response recorded April 2003.
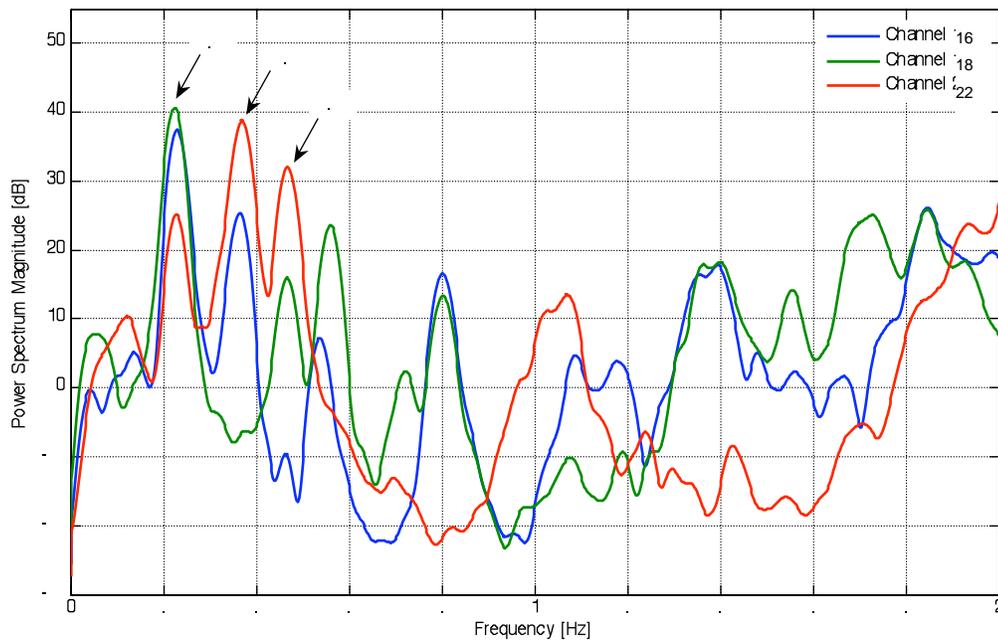
Figure 123. Power Spectral Density of the deck response (April 2003)
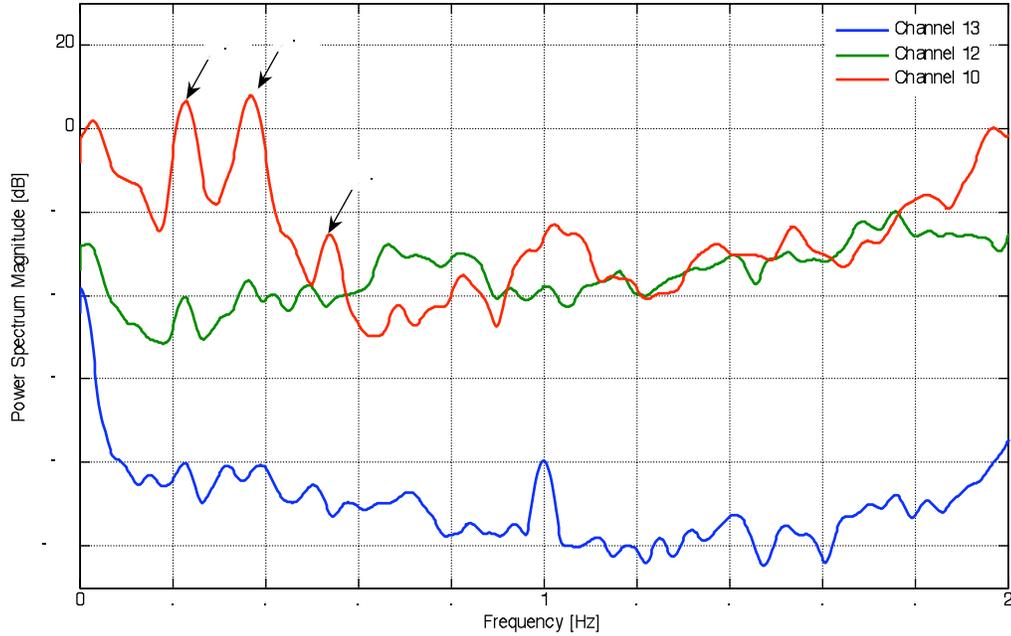
Figure 124. Power Spectral Density of the pylon response (April 2003)

The first three dominant frequencies and frequency bands for the deck and for the pylon are listed in Table 25 and Table 26.

	Frequencies [Hz]	
	Deck	**Column**
I mode	0.22	0.22
II mode	0.37	0.37
III mode	0.46	0.54

Table 25. Data April 2003: Modal Frequencies

	Filter Ranges	
	Deck	**Column**
I mode	0.20 – 0.30 Hz	0.19 - 0.26 Hz
II mode	0.32 – 0.40 Hz	0.30 - 0.40 Hz
III mode	0.41 – 0.50 Hz	0.47 - 0.57 Hz

Table 26. Data April 2003: Filter ranges
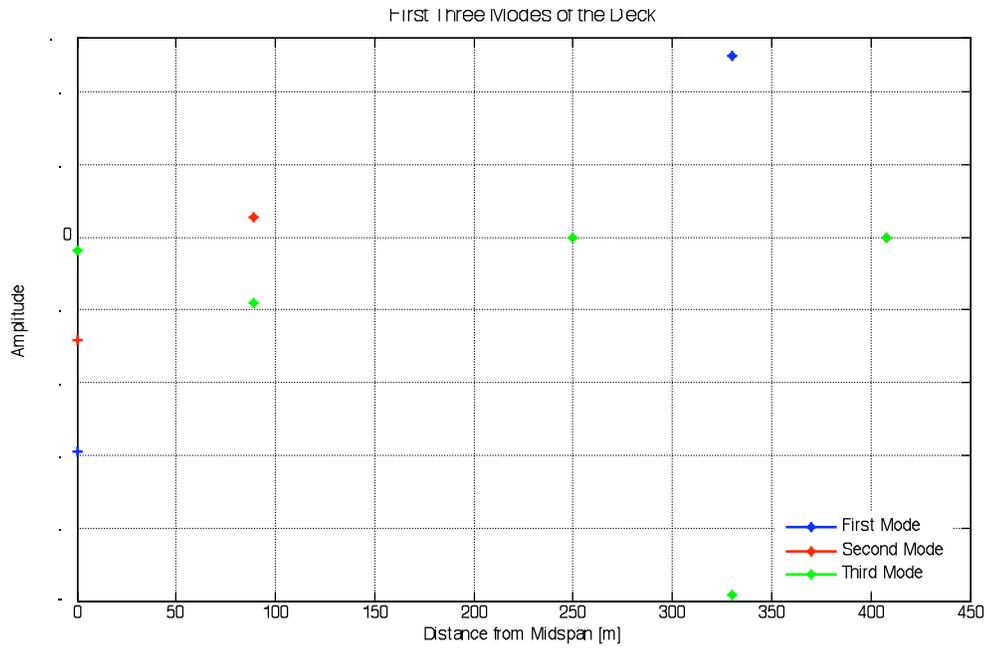
Figure 125. First three mode shapes of the deck in vertical direction (April 2003)
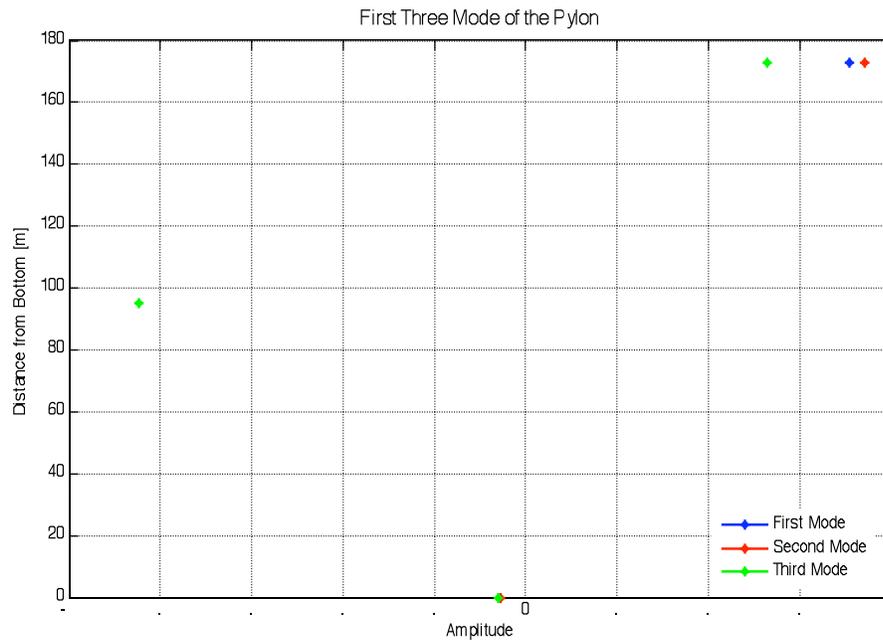
Figure 126. First three mode shapes of the East pylon in longitudinal direction (April 2003)

6.2 Application of the damage identification procedure to the bridge response

The set of data recorded on April 2003 and December 2006 were used to estimate the location and the associate severity of the possible degradation that occurred in structural elements and/or energy dissipators. As mentioned above the data are used in a time reverse order because the December 2006 data represents the configuration of bridge with devices in un-damaged configuration, when instead the April 2003 data set corresponds to a bridge configuration with degraded dampers.

For the damage detection the signals recoded by the sensors positioned on the north edge of the deck and pylon were used (See Figure 5). This line of sensors in fact is the most complete, providing the largest number of consistent signals. The damper devices are separated in two different groups of four dampers (see Table 27). The first group includes the dampers between the side span and the tower and the second group gathers the devices located between main span and the tower.

Dampers		**C**	**α**
Group #1	side span to tower	2.5	1
Group #2	main span to tower	4.0	1

Table 27. Location and characteristics of the dampers in the model

The interpretative scheme of the bridge under consideration (Figure 114) was subdivided, after the assessment of the mode shape functions, in a large number of elements, used for the computation of the damage indicators. The number of records available from the two considered data sets, for the pylon, is insufficient for a detailed application of the damage detection algorithm. For this reason the available signals of the pylon response were used for the assessment of their mode shapes only, in order to be able to calculate the relative stroke of the dampers connecting the pylon to the deck. However, in terms of damage identification, the pylons were not analyzed. The deck and the dampers were instead investigated through the specific damage identification algorithm. Due to the specific goal of monitoring the damper's state of performance the focus on this reduced portion of the structure appeared appropriate.

To evaluate the Damage Index for each *jth* element and *ith* mode shape, the following equation was used for the structural elements:

$$DI_{ij} = \frac{\int_a^b [\psi_i^{*"}(x)]^2\,dx \left/ \left[\sum_{n=1}^{N_{el}} \int_0^{L_n} [\psi_i^{*"}(x)]^2\,dx + \sum_{m=1}^{N_d} t_{im}(s_{im}^*)^2 \right] \right.}{\int_a^b [\psi_i^{"}(x)]^2\,dx \left/ \left[\sum_{n=1}^{N_{el}} \int_0^{L_n} [\psi_i^{"}(x)]^2\,dx + \sum_{m=1}^{N_d} t_{im}(s_{im})^2 \right] \right.} \tag{56}$$

where the symbol * identifies the damaged condition.

For the dampers the Damage Indicator was calculated as:

$$DI_{im} = \frac{t_{im}(s^*_{im})^2 \Big/ \left[\sum_{n=1}^{N_{el}} \int_0^{L_n} [\psi_i^{*''}(x)]^2 \, dx + \sum_{m=1}^{N_d} t_{im}(s^*_{im})^2 \right]}{t_{im}(s_{im})^2 \Big/ \left[\sum_{n=1}^{N_{el}} \int_0^{L_n} [\psi_i^{''}(x)]^2 \, dx + t_{im}(s_{im})^2 \right]} \tag{57}$$

Where:

- $t_{im} = \dfrac{\max_{j=1..N_{el}} \left(\int_a^b [\psi_i^{''}(x)]^2 \, dx \right)}{\max(s_{im}^{\ 2})}$ is the normalization factor for the dampers stiffness;

- s_{mj} is the dampers deformation for each damper and mode;
- $\psi(x)$ is the mode shape and x is the spatial dimension;
- N_d is the total number of dampers (2 groups);
- N_{el} is the total number of elements.

It must be noted that Eqs. (56) and (57) are different from Eqs. (35) and (36) presented in the general description of the algorithm. In fact in Eqs. (35) and (36) the total energy term is added to the energy of each element. This was due to the addition of a unity to both side of Eq. (9) as indicated in Eq. (19). The reason of this addition was to prevent possible false prediction of damage due to very small numbers at the denominator of Eq. (18). For the present set of data and structural configuration this technique was not required.

A damaged condition is considered occurring if $DI_{ij} \geq 1$. If $DI_{ij} < 1$, damage does not exist. For each possible damage location there are as many DI_{ij} s available as there are mode shapes taken into account. The following expression was used to combine the contribution of the NM modes into the damage index DI_j for a single location:

$$DI_j = \frac{\sum_{i=1}^{NM} \left(\int_a^b [\psi_i^{*''}(x)]^2 \, dx \Big/ \left[\sum_{n=1}^{N_{el}} \int_0^{L_n} [\psi_i^{*''}(x)]^2 \, dx + \sum_{m=1}^{N_d} t_{im}(s^*_{im})^2 \right] \right)}{\sum_{i=1}^{NM} \left(\int_a^b [\psi_i^{''}(x)]^2 \, dx \Big/ \left[\sum_{n=1}^{N_{el}} \int_0^{L_n} [\psi_i^{''}(x)]^2 \, dx + \sum_{m=1}^{N_d} t_{im}(s_{im})^2 \right] \right)} \tag{58}$$

and similarly for the dampers:

$$DI_m = \frac{\sum_{i=1}^{NM} \left(t_{im} \cdot (s^*_{im})^2 \Big/ \left[\sum_{n=1}^{N_{el}} \int_0^{L_n} [\psi_i^{*''}(x)]^2 \, dx + \sum_{m=1}^{N_d} t_{im}(s^*_{im})^2 \right] \right)}{\sum_{i=1}^{NM} \left(t_{im} \cdot (s_{im})^2 \Big/ \left[\sum_{n=1}^{N_{el}} \int_0^{L_n} [\psi_i^{''}(x)]^2 \, dx + \sum_{m=1}^{N_d} t_{im}(s_{im})^2 \right] \right)} \tag{59}$$

The Normalized values of the Damage Index (Z_{ij} end Z_j) for each mode for the *jth* location can be calculated as indicated in Eqs (42) and (43).

For a confidence level of 84%, there is the damage if $Z_i \geq 1$. The severity of damage at a given location may be estimated from the magnitude of the damage index at the designated location. In this formulation, the magnitude of damage at a particular location is expressed as the fractional change in stiffness $\left(\alpha_j \right)$ for the element:

$$\alpha_j = \frac{K_j^* - K_j}{K_j} = \frac{1}{DI_j} - 1$$

(60)

If there isn't damage in the elements $\alpha_j = 0$, if the damage exists $\alpha_j \leq 0$.

The first three mode shapes for the deck and for the pylon are presented in the following figures. The modal amplitude for the locations were sensors are not available is assessed by polynomial interpolation. The degree of the polynomial is established as function of the number of locations where data are available. The boundary conditions for node #9 (Figure 108) are also imposed. Figure 127 to Figure 132 show the mode shapes (dashed lines) together with the polynomial fit (solid line).
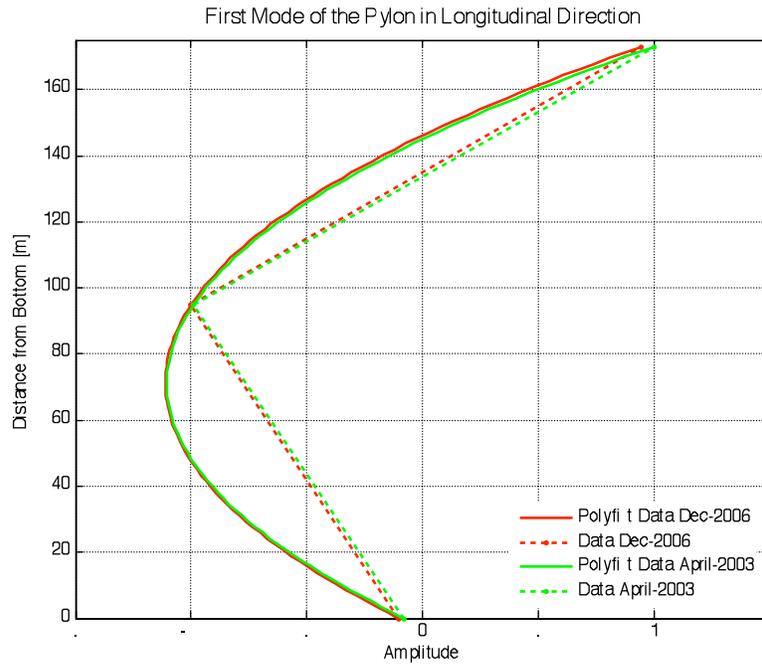
Figure 127. Data December 2006 and April 2003: First mode of the East pylon
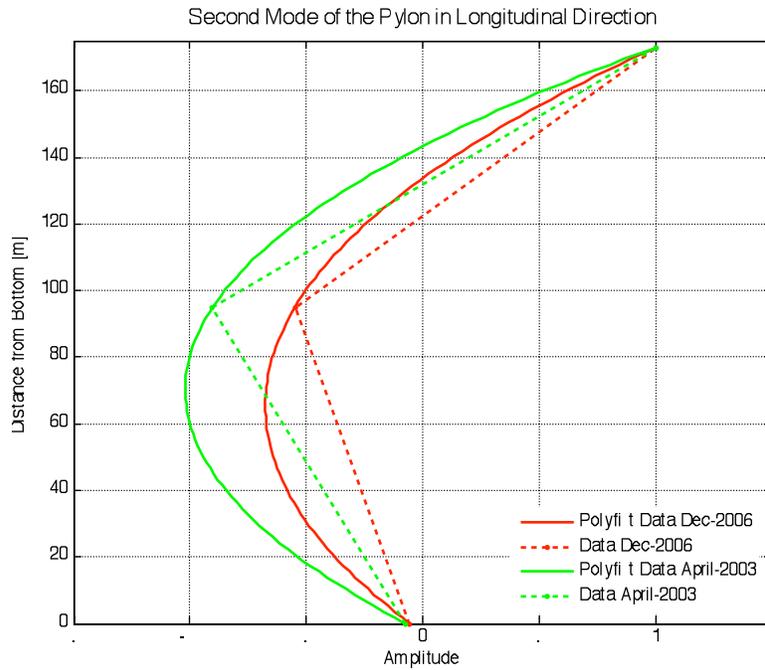
Figure 128. Data December 2006 and April 2003: Second mode of the East pylon
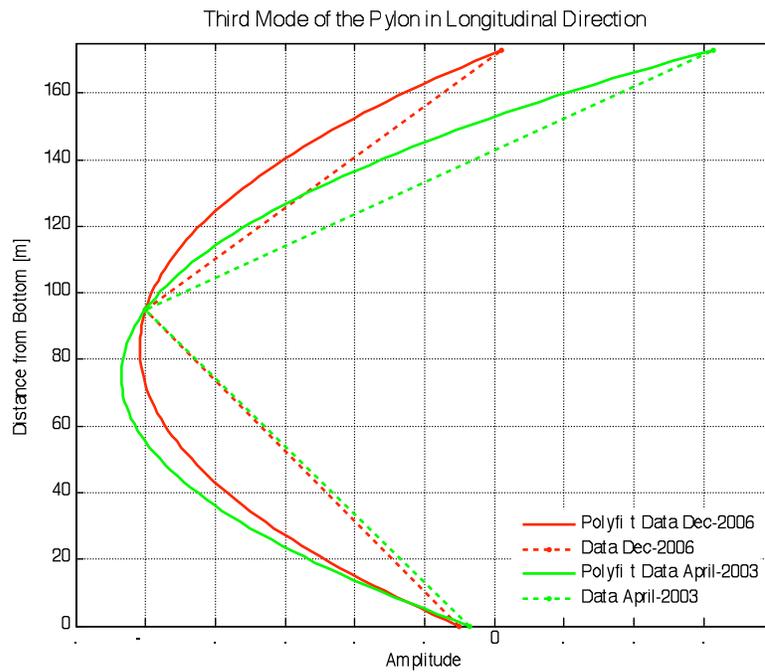
Figure 129. Data December 2006 and April 2003: Third mode of the East pylon
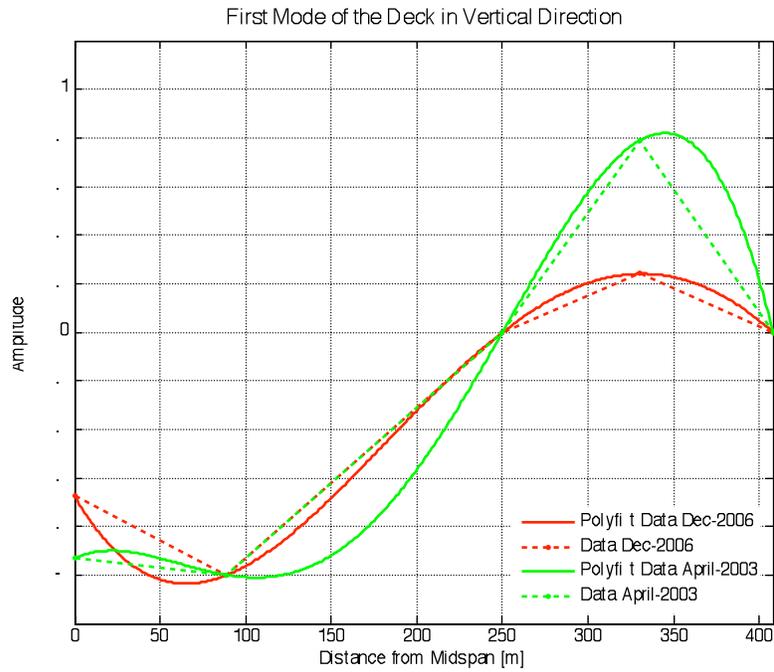
Figure 130. Data December 2006 and April 2003: First mode of the deck
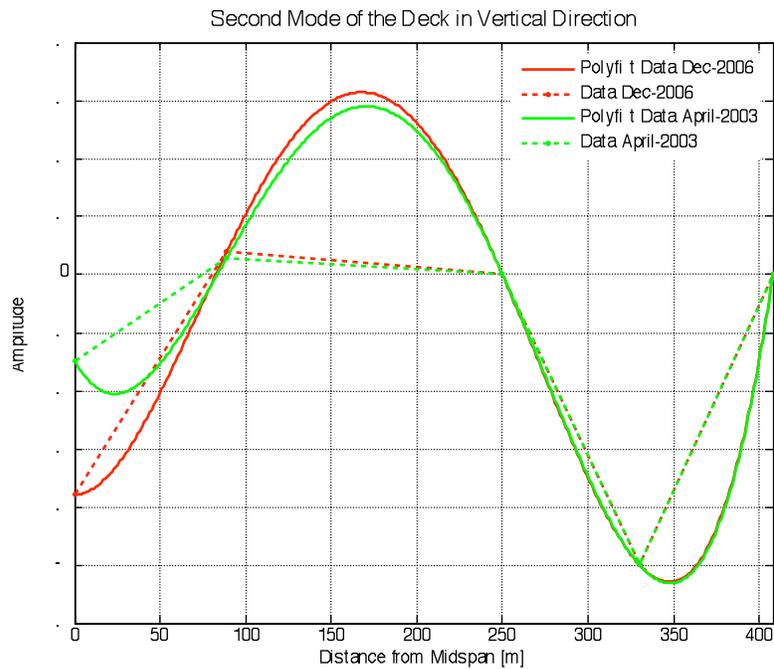
Figure 131. Data December 2006 and April 2003: Second mode of the deck
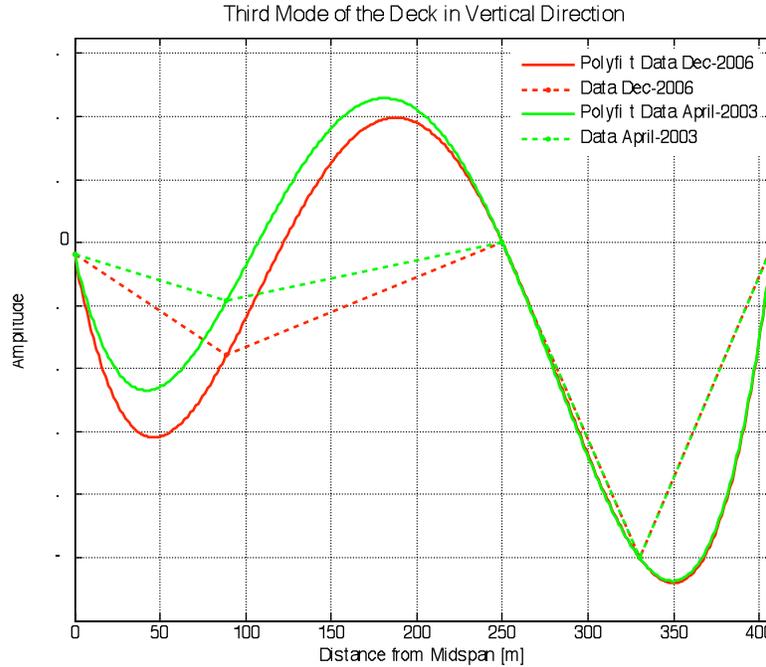
Figure 132. Data December 2006 and April 2003: Third mode of the deck

Figure 133 and Figure 134 shows the damage indices for each mode and total, respectively, with applied coefficient of importance for the mode shapes, c_i. The length of the single element of the interpretative scheme is 1 m so the x axis indicates the location of the damage from deck mid-span (element 1). The dampers D#1 and D#2 are reported as elements 409 and 410 respectively. In Figure 134, 135 are reported, in red, the positions of the sensor locations (see Figure 114) to provide a reference with the real structure. Figure 135 shows the existence of damage in the first set of dampers, presented as element 409 (D#1).The severity of the damage is approximately 65% when compared with the undamaged configuration of the dampers. Two additional areas of possible damage are detected. The first one at 150-200 meters from the mid-span and the second one at 330-408 m from mid-span. The results are in excellent agreement with the result obtained by Stubbs (Stubbs et al., 2006).

The Modal coefficients of importance c_i for the two cases considered are reported in Table 28.

	December2006 April 2003	December2006 June 2006
Coefficient c_i		
I mode	0.94	1.00
II mode	1.00	1.00
III mode	0.58	0.33

Table 28. Coefficient of mode importance for each case
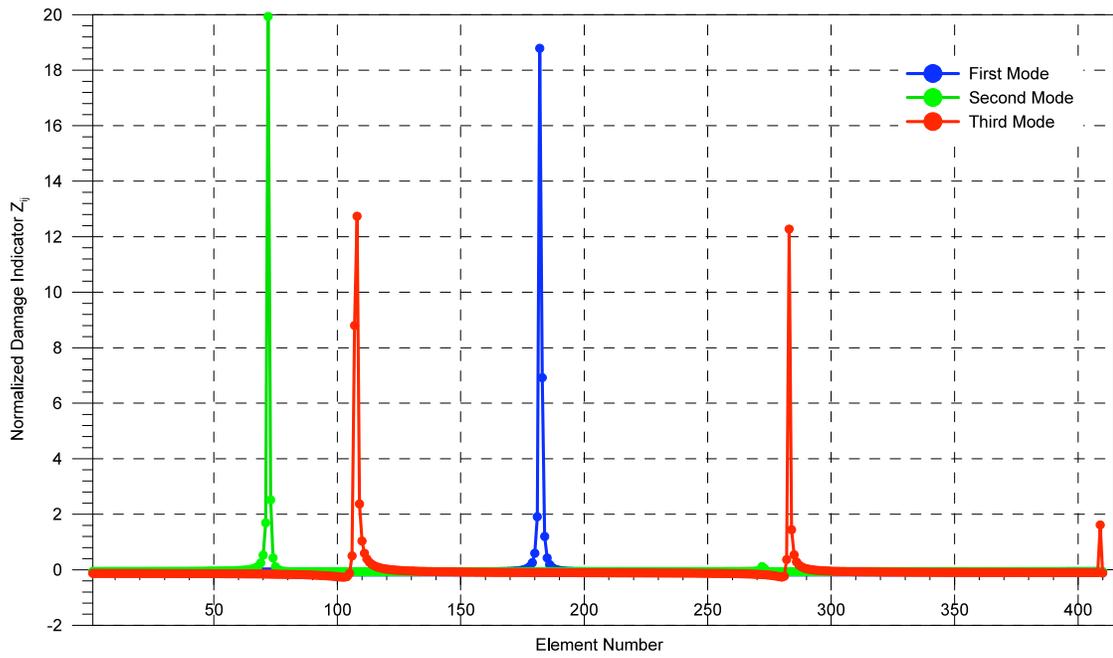
Figure 133. Data December 2006-April 2003: Normalized Damage Index Z_{ij}
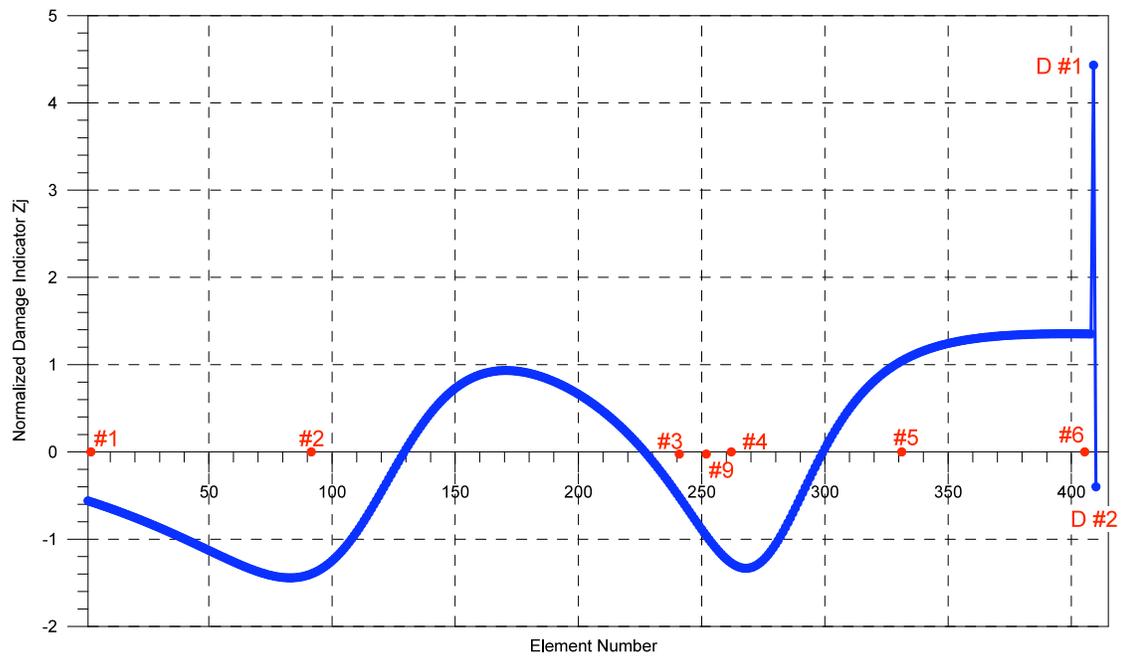
Figure 134. Data December 2006-April 2003: Normalized Damage Index Z_j total

124
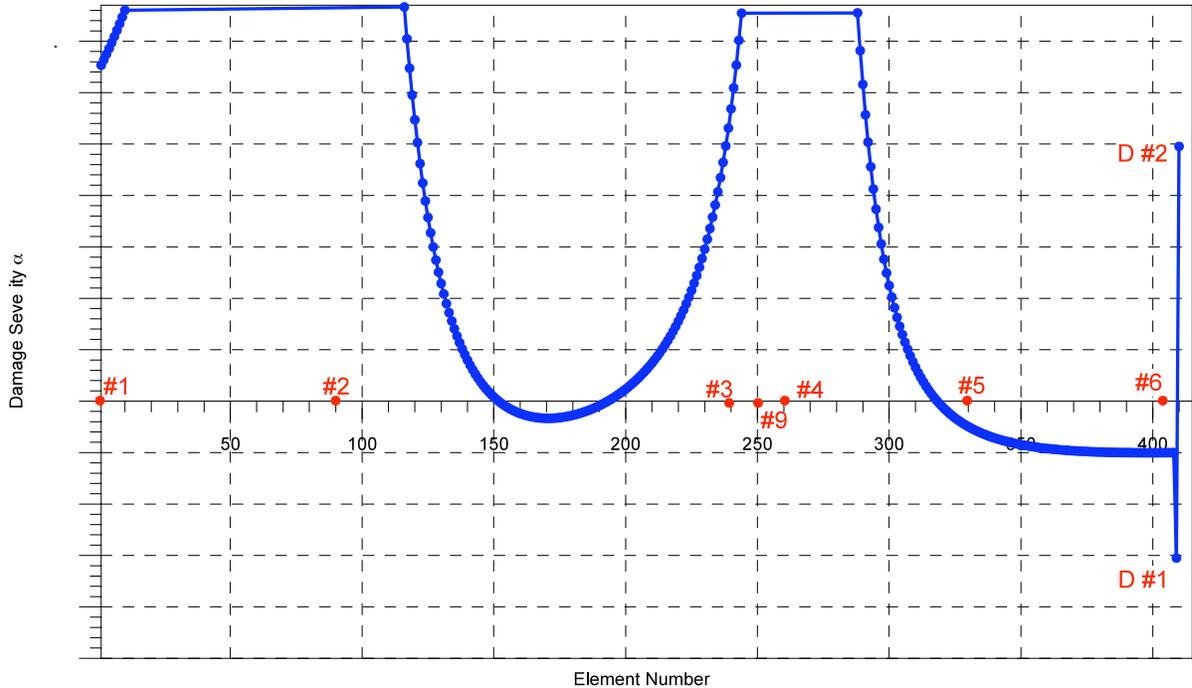
Figure 135. Data December 2006-April 2003: Damage Severity α_j

An additional analysis was performed using the data sets obtained June 2006 and December 2006. As before, in order to verify the condition of dampers, the data of December 2006 were used as a reference (un-damaged dampers). The status of the damper devices in June 2006 is unknown. The analysis, documented by Figure 142 to Figure 144 indicates that the dampers were not suffering any level of degradation at the time of data recording in June 2006. In Figure 143 and Figure 144 are reported, in red, the positions of the sensor locations (see Figure 114) and the two last elements representing the two set of dampers (D#1, D#2).
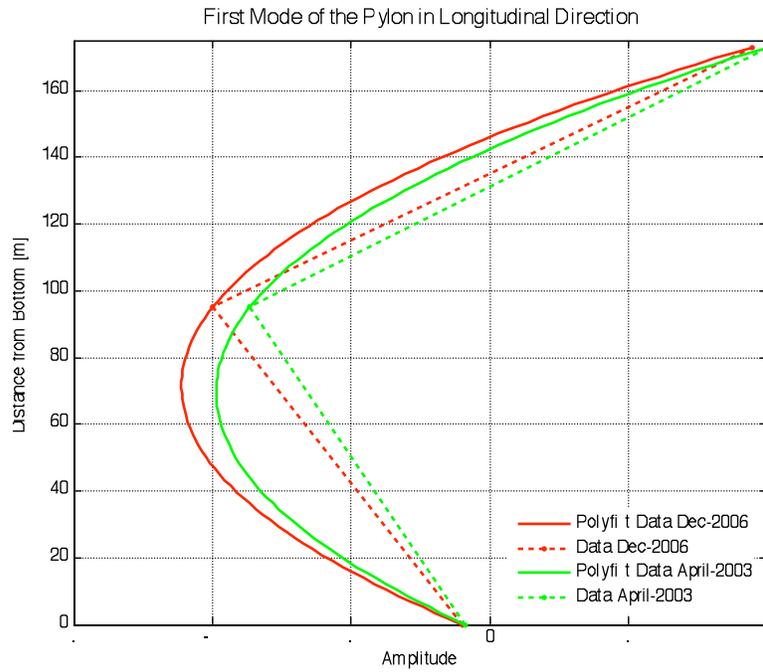
Figure 136. Data December 2006 and June 2006: First mode of the East pylon
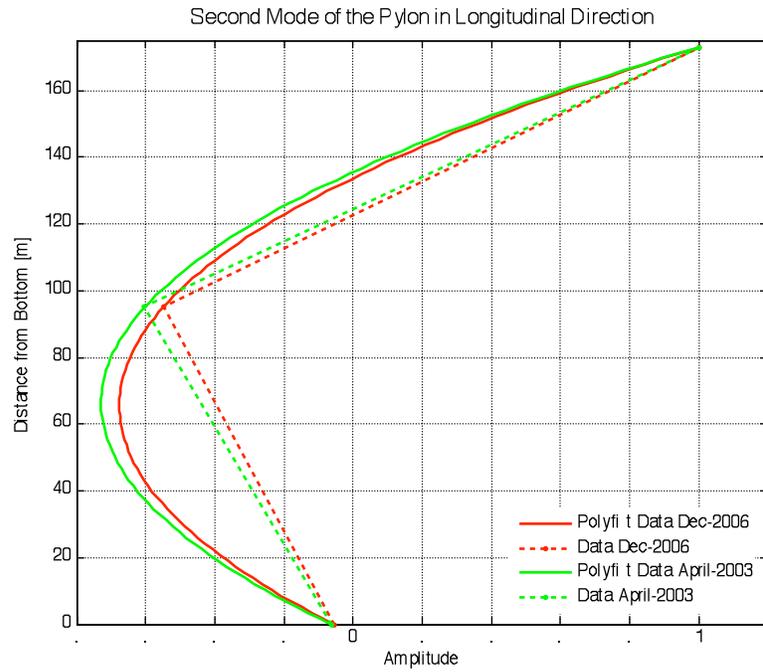
Figure 137. Data December 2006 and June 2006: Second mode of the East pylon
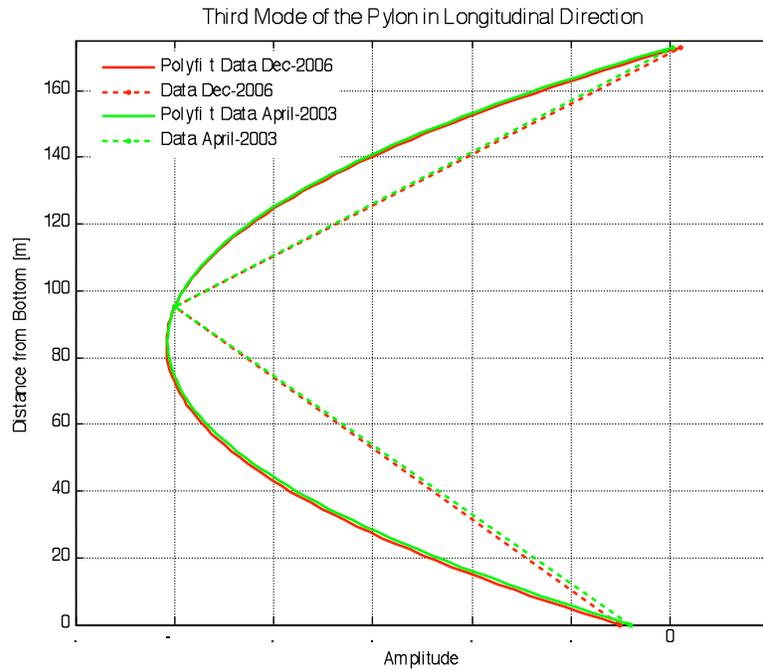
Figure 138. Data December 2006 and June 2006: Third mode of the East pylon
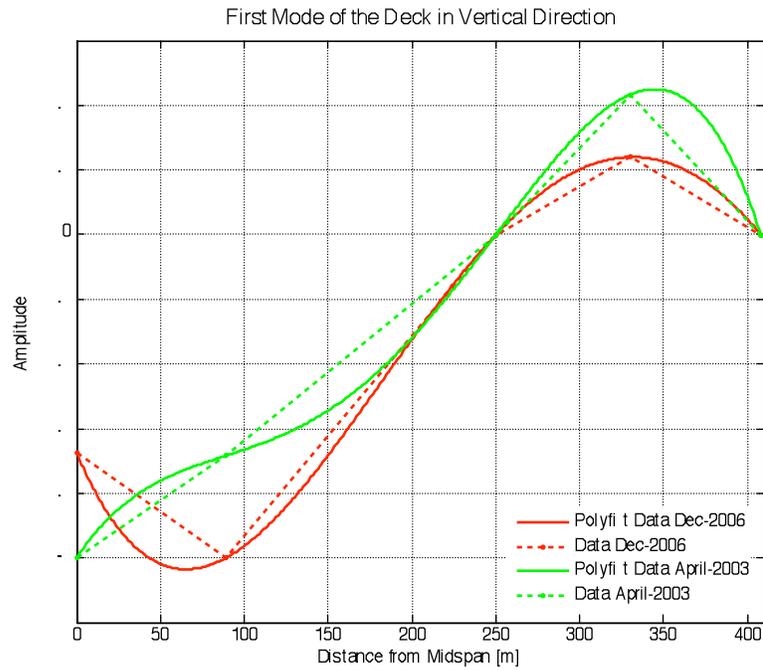
Figure 139. Data December 2006 and June 2006: First mode of the deck
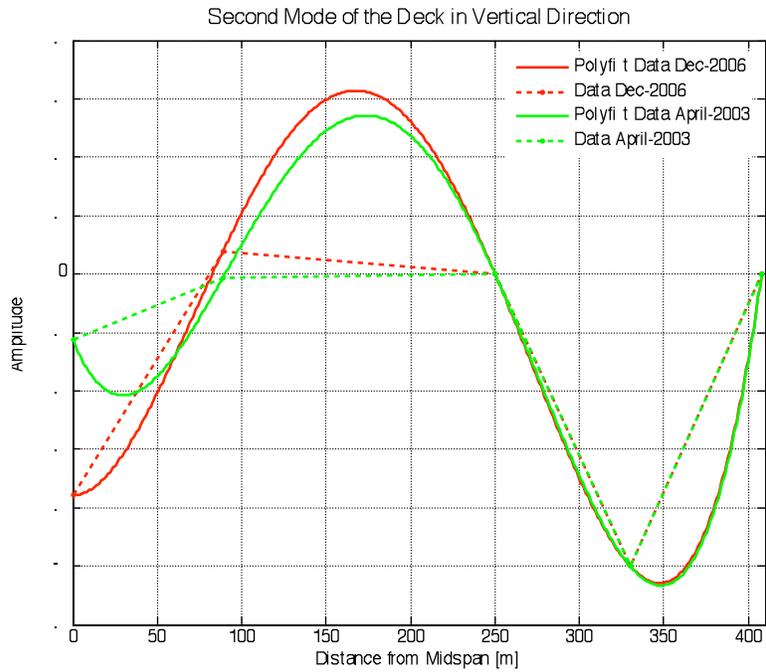
Figure 140. Data December 2006 and June 2006: Second mode of the deck
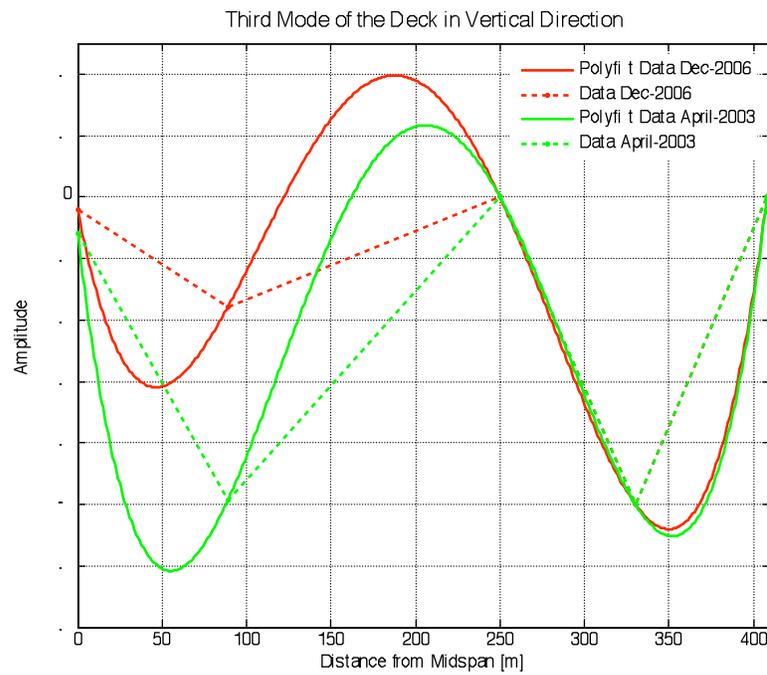
Figure 141. Data December 2006 and June 2006: Third mode of the deck
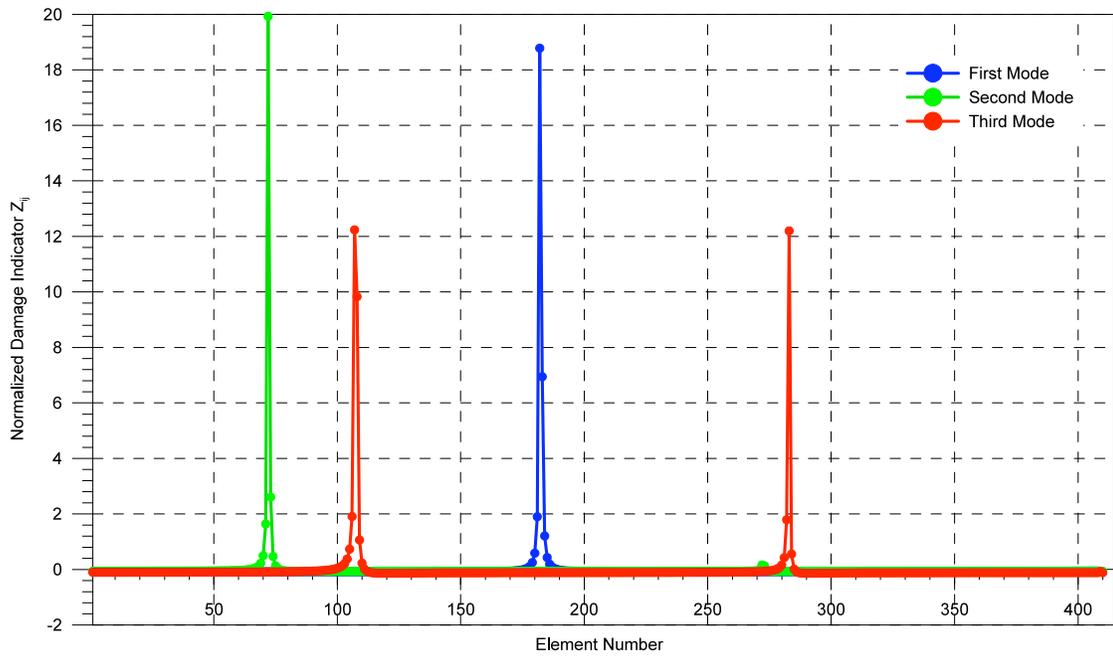
Figure 142. Data December 2006- June 2006: Normalized Damage Index Z_{ij}
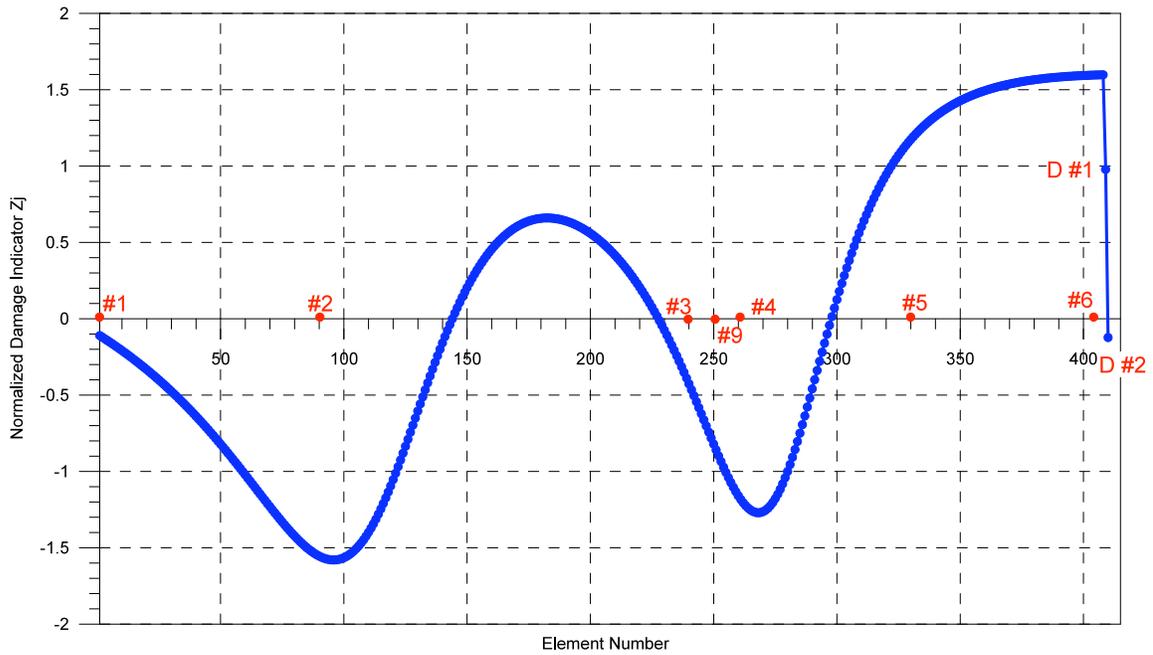
Figure 143. Data December 2006- June 2006: Normalized Damage Index Z_j total
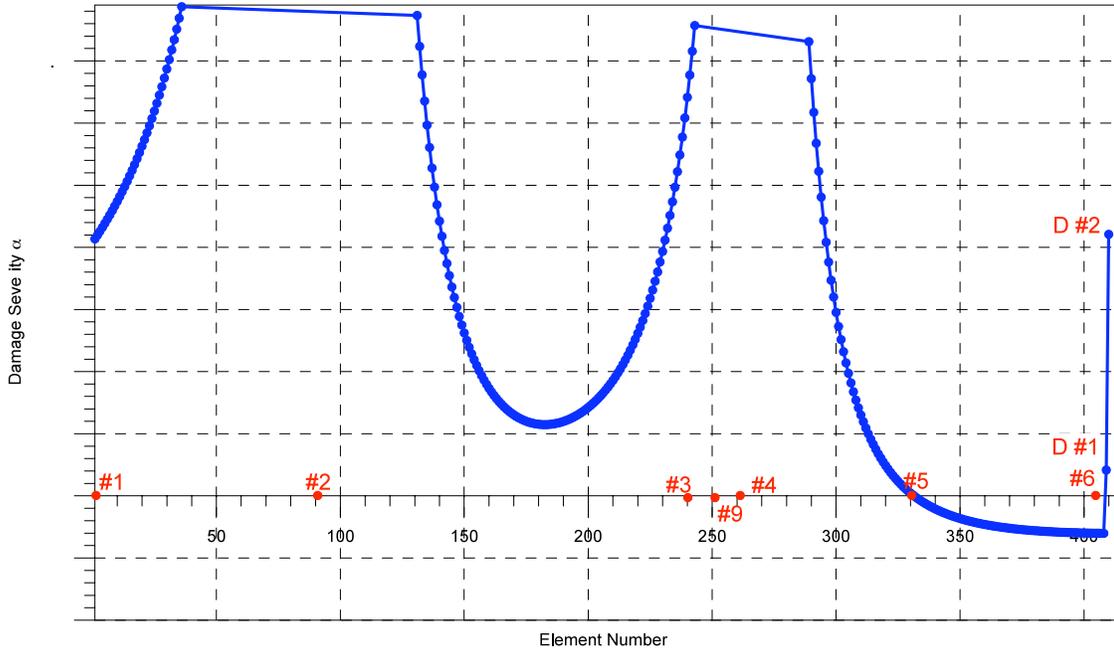
Figure 144. Data December 2006- June 2006: Damage Severity α_j

6.3 Covariance-driven Stochastic Subspace Identification method (SSI-Cov)

The assessment of the mode shapes from the acceleration data recorded in April 2003, June 2006 and December 2006 was initially attempted by using the output-only response method proposed by Kim (Kim et al., 2005). In addition, an analysis of the same data sets was carried out using, for the mode shape assessment, the Covariance-driven Stochastic Subspace Identification method (SSI-Cov).

In order to obtain a good model for modal analysis applications it is necessary to obtain a stabilization diagram (see Figure 145). An efficient stabilization diagram is achieved by computing the SVD of the covariance Toeplitz matrix only once. This is an iterative procedure where the system order n is fixed, step by step, and the modal parameters for the order (frequency of vibration 'ω', damping ratio 'ζ' and modal vector 'v') are determined.
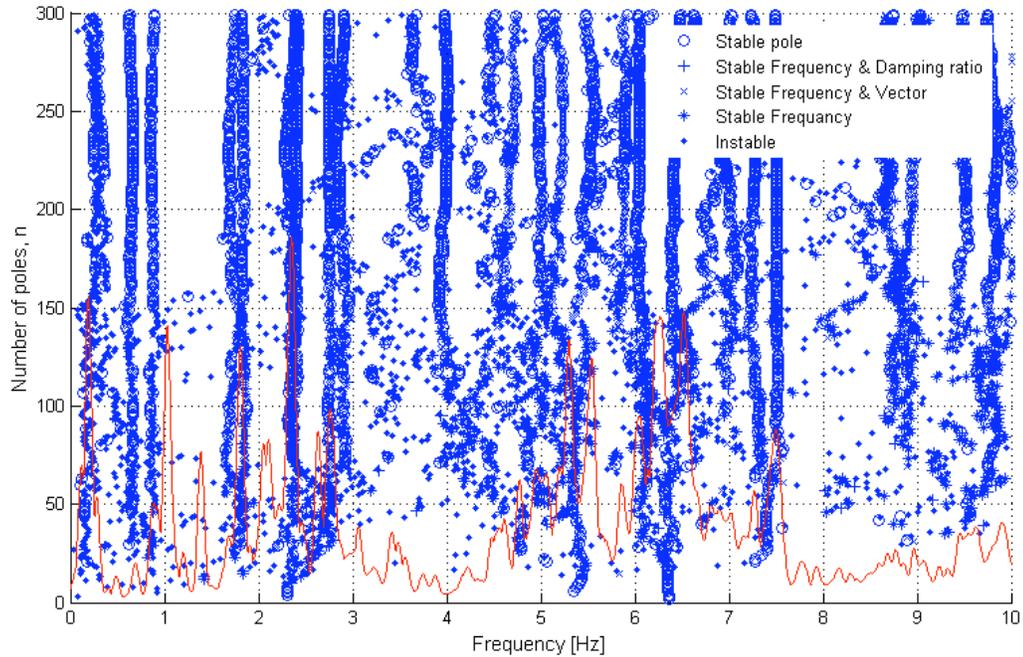
Figure 145. Example of Stabilization diagram obtained with the SSI-COV method for the undamaged case. The criteria are 1% for frequencies, 5% for damping ratios and 2% for the mode shape correlations

The repetition of blue dots (stable poles) corresponding to peaks of the red curve (the PSD of the signal) indicates the natural frequencies. A band-pass filter is then applied in order to separate the single modal components. For the bridge application, the natural frequencies for the first three modes and the ranges of frequency used to extract each modal contribution are reported in Table 29 and Table 30, respectively.

Frequency [Hz]			
	December 2006	**June 2006**	**April 2003**
I mode	0.293	0.263	0.238
II mode	0.446	0.344	0.411
III mode	0.748	0.648	0.627

Table 29. Modal frequencies

Filter Ranges			
	December 2006	**June 2006**	**April 2003**
I mode	0.2 - 0.4 Hz	0.2 - 0.3 Hz	0.2 - 0.3 Hz
II mode	0.4 - 0.6 Hz	0.3 - 0.4 Hz	0.3 - 0.5 Hz
III mode	0.6 - 0.8 Hz	0.6 - 0.7 Hz	0.5 - 0.7 Hz

Table 30. Filter ranges

The Modal coefficient of importance c_i are reported in Table 31.

	Coefficient c_i	
	December2006 April 2003	December2006 June 2006
I mode	0.71	0.27
II mode	0.57	1.00
III mode	1.00	1.00

Table 31. Coefficient of mode importance for each case

In Figure 146 to Figure 151 the modes shapes identified by the Kim approach are compared with the mode shape identified by the SSI-Cov.
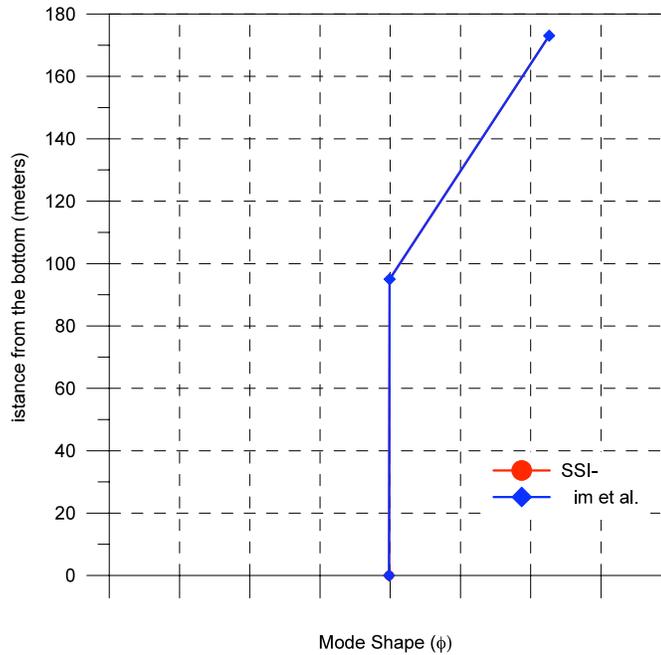
Figure 146. December 2006: first mode for the East Pylon
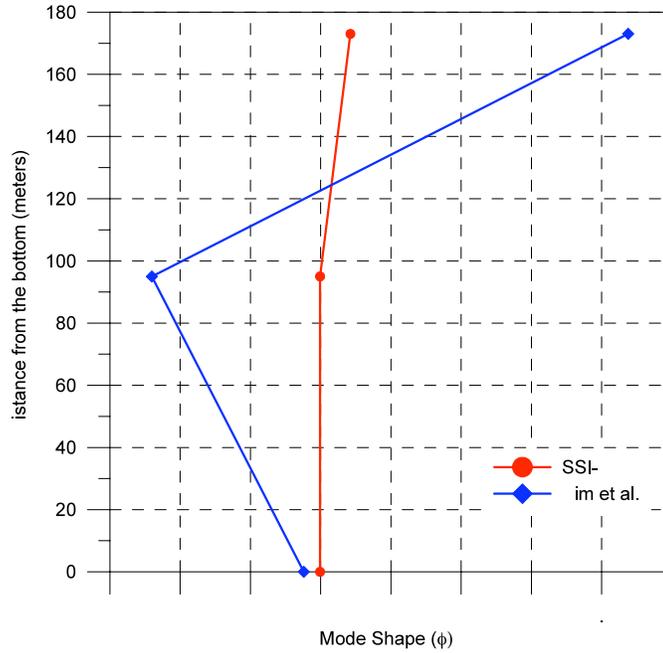
Figure 147. December 2006: second mode for the East Pylon
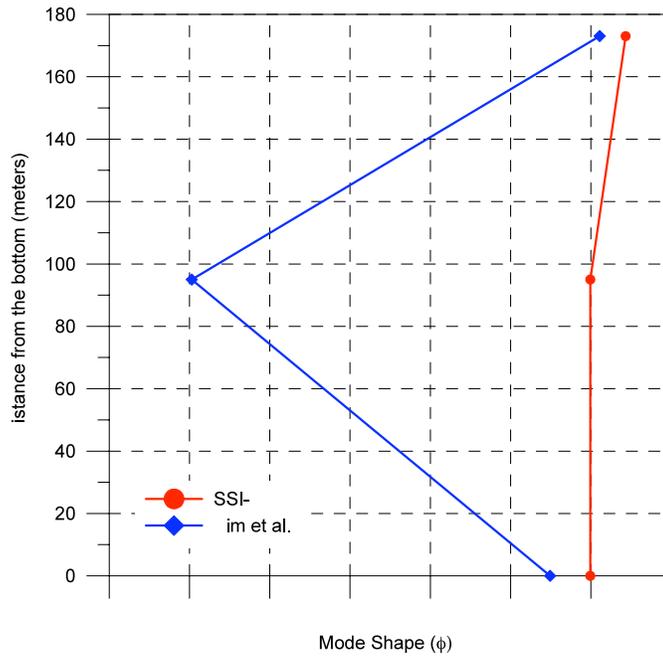
Figure 148. December 2006: third mode for the East Pylon
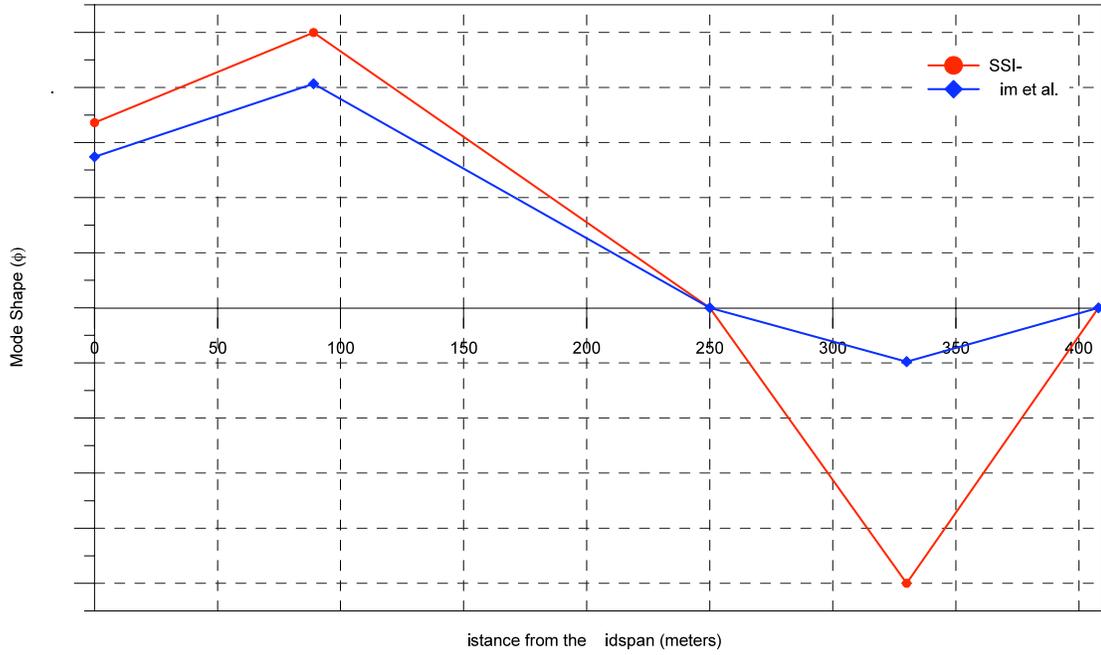
Figure 149. December 2006: first mode for the deck
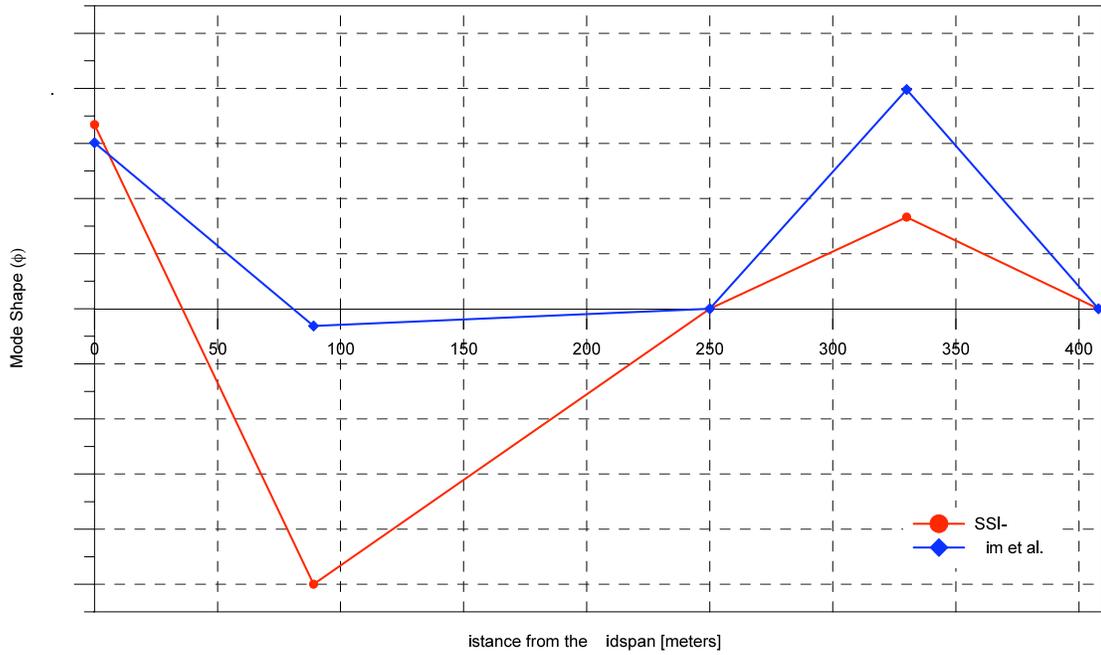
Figure 150. December 2006: second mode for the deck
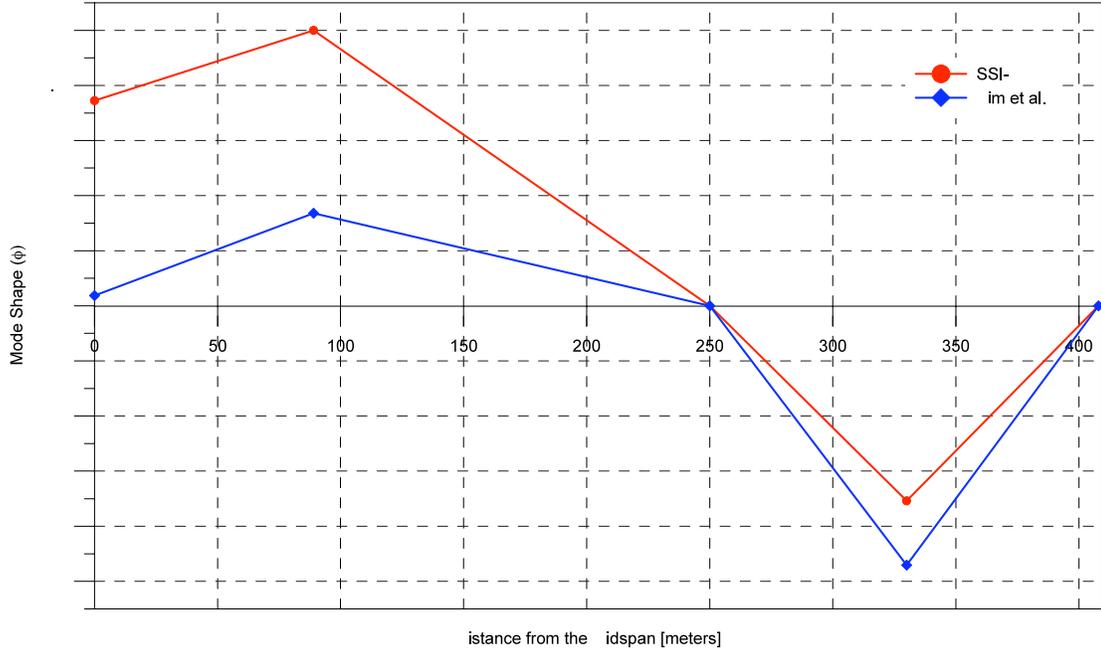
Figure 151. December 2006: third mode for the deck

6.4 Application of the damage identification procedure to the bridge response

The mode shape obtained with the SSI-Cov method from the set of data recorded on December 2006, June 2006 and April 2003 were used to estimate the location and the associate severity of the possible degradation that occurred in structural elements and/or energy dissipators.

To evaluate the Damage Index for each *jth* element and *ith* mode shape Eq. (56) and Eq. (57) was used for the structural elements and the dampers, respectively. A damaged condition is considered occurring if $DI_{ij} \geq 1$. If $DI_{ij} < 1$, the damage does not exist. For each possible damage location there are as many DI_{ij} s available as there are mode shapes taken into account. The contribution of the NM modes is combined into the damage index DI_j by use of Eq. (58) for the structural elements and Eq. (59) for the dampers. The Normalized values of the Damage Index (Z_{ij} end Z_j) for each mode and for the *jth* location can be calculated as indicated in Eqs (42) and (43). For a confidence level of 84%, the damage is considered present if $Z_i \geq 1$. The severity of damage, at a given location, may be estimated from the magnitude of the damage index at the designated location. In this formulation, the magnitude of damage at a particular location is expressed as the fractional change in stiffness $\left(\alpha_j\right)$ for each element:

$$\alpha_j = \frac{K_j^* - K_j}{K_j} = \frac{1}{DI_j} - 1 \tag{61}$$

The condition of $\alpha_j = 0$ represents an undamaged configuration. If the damage exists $\alpha_j \leq 0$.

Figure 152 and Figure 153 show the damage indices separated by modes and combined, respectively, with applied the coefficient of importance for the mode shapes, c_i. The length of the single element of the interpretative scheme is 1 m so that the x axis indicates the location of the damage from deck mid-span (element 1). The dampers D#1 and D#2 are reported as elements 409 and 410, respectively and graphically reported at the right end of the diagram.

Results are presented in Figure 153 and Figure 154. Figure 154 shows the existence of damage in the first set of dampers, indicated as element 409 (D#1). The severity of the damage is approximately 60% when compared with the undamaged configuration of the dampers. One additional area of possible damage is detected at 180-250 meters from the mid-span. Both damage conditions are confirmed by the previous analysis completed with the alternative mode shape estimate.

The third damage location, identified at 330-408 m from mid-span, with the mode shape obtained from the Kim approach (see Figure 134 and Figure 135) is not visible anymore.

The Modal coefficients of importance ci for the two cases considered are reported in Table 31.
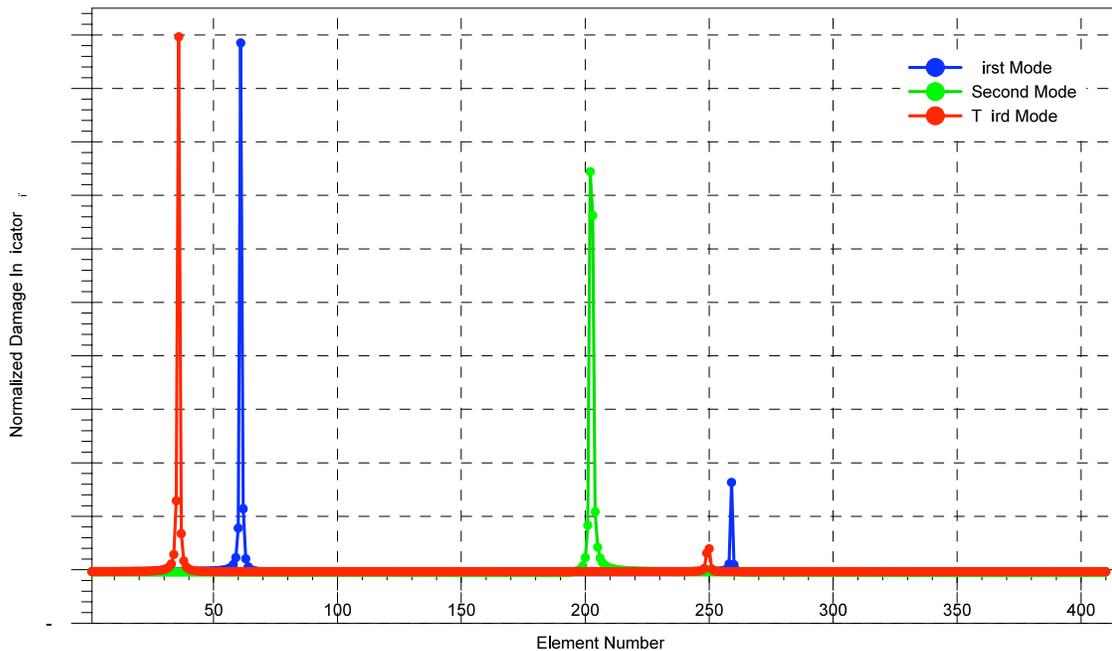
Figure 152. Data December 2006-April 2003: Normalized Damage Index Z_{ij}
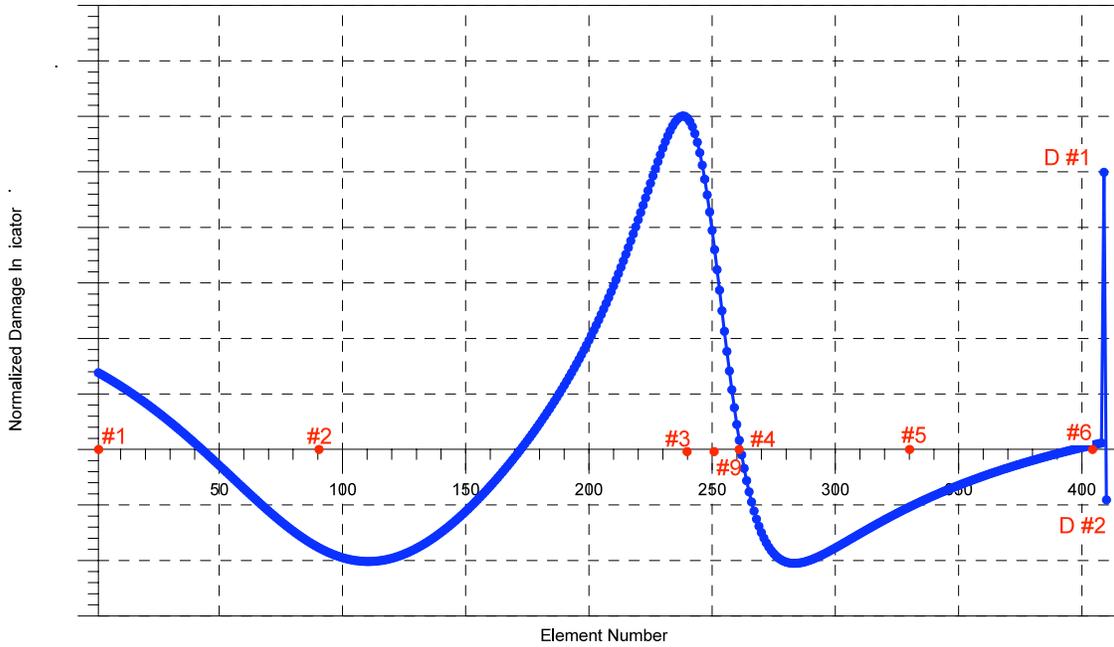
Figure 153. Data December 2006-April 2003: Normalized Damage Index Z_j total
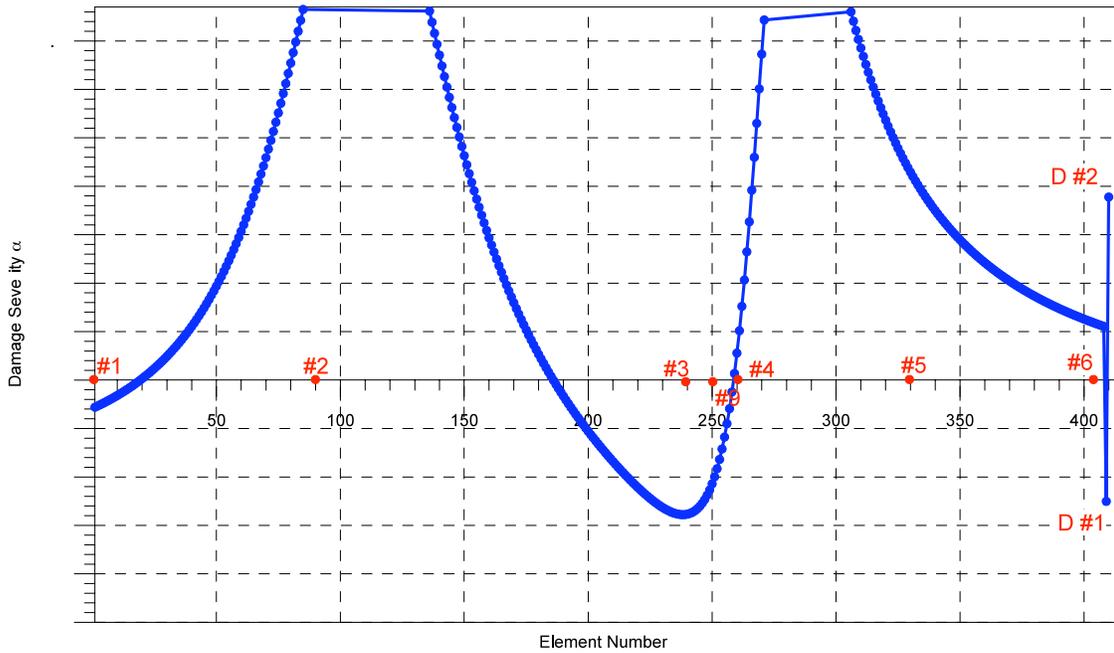
Figure 154. Data December 2006-April 2003: Damage Severity α_j

In order to verify the condition of dampers in June 2006, the data set of December 2006 was used as a reference (un-damaged dampers). The analysis, documented by Figure 155 to Figure 157, indicates that the dampers were suffering a level of degradation at the

time of data recording in June 2006 in contrast with the results obtained with the use of the modal shape extraction by the Kim method (see Figure 143 and Figure 144). This new analysis appears to be able to represent more accurately the realistic scenario of degradation. In fact, in June 2006 the dampers were still damaged. They were replaced during the month of October 2006.

Figure 156 shows the existence of damage in the first set of dampers, presented as element 409 (D#1). One area of possible damage is detected on the deck structure at 180-250 meters from the mid-span and a second one at 0-50 m from mid-span. This additional location wasn't identified from the April 2003 data.
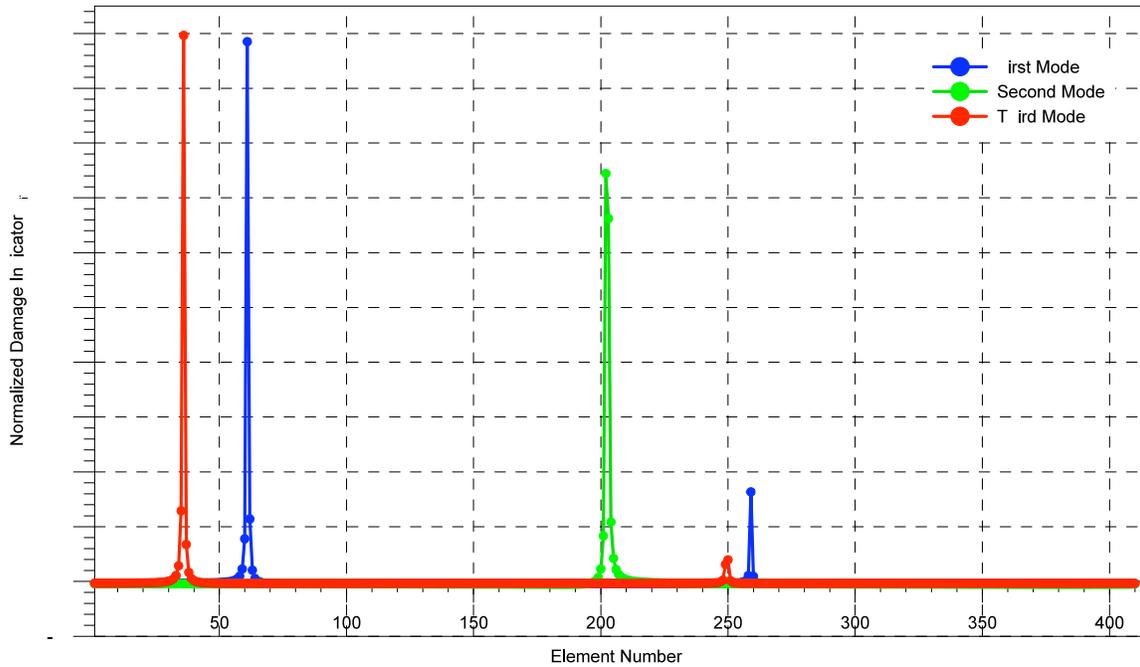
Figure 155. Data December 2006- June 2006: Normalized Damage Index Z$_{ij}$
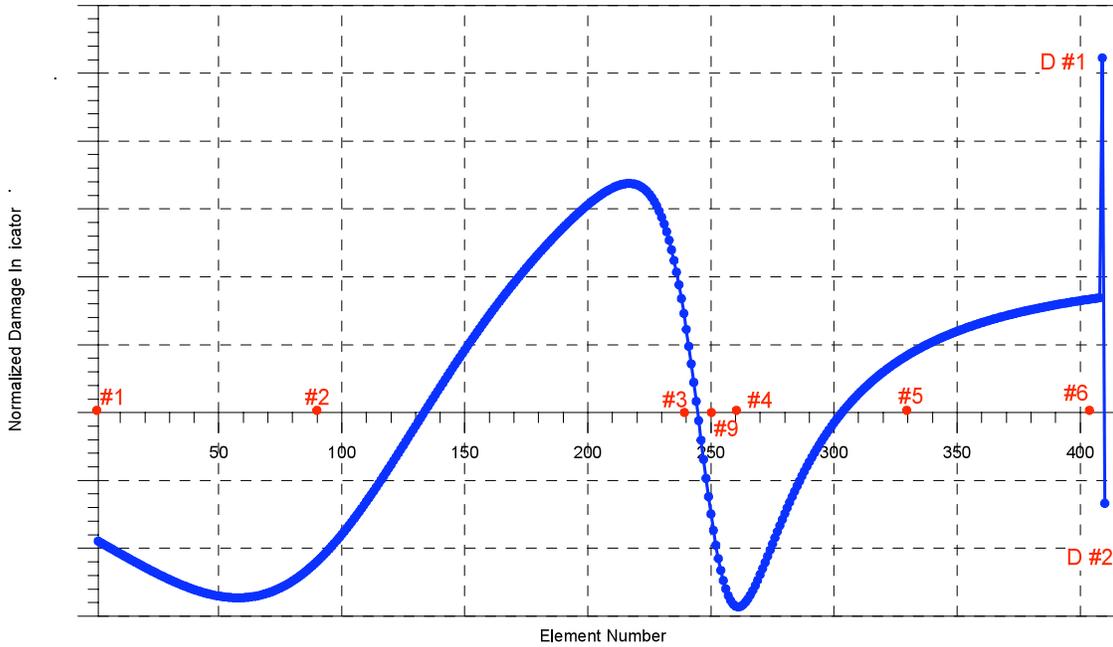
Figure 156. Data December 2006- June 2006: Normalized Damage Index Z_j total
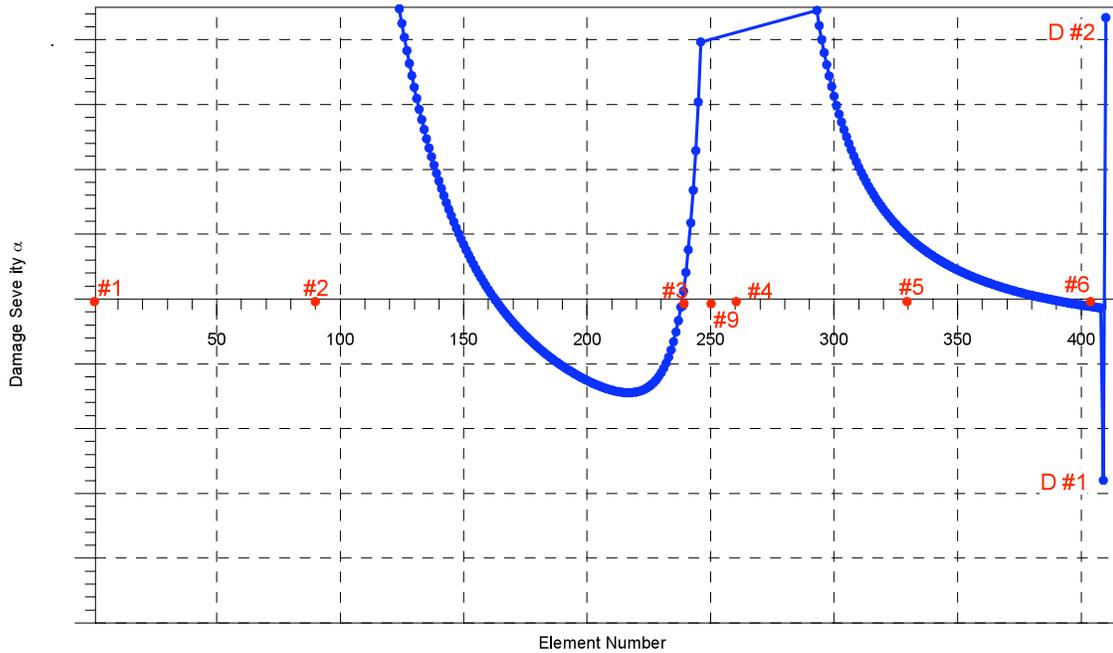
Figure 157. Data December 2006- June 2006: Damage Severity α_j

7) IMPLEMENTATION OF THE PROCEDURE FOR HEALTH MONITORING PROGRAMS AND FURTHER DEVELOPMENT

One of the main features of the presented procedure is the possibility to be implemented with a minimum set of data that allows the assessment of mode shapes. As indicated above the procedure does not necessarily require the support of a F.E. model. Only a simplified interpretative scheme is assembled to correlate results with specific physical locations on the real structure. The portions of the structure analyzed by the algorithm also can be subjectively selected to isolate a specific area of the structure or to allow a damage identification in case a non-complete set of data. The requirement of availability of data only for the estimate of mode shapes significantly reduces the extension of the needed sensor network. In this sense the procedure is particularly robust because is founded on the comparison of two data sets, indicated above as un-damaged and damaged. This characteristic permits to relax the requirement of great accuracy in the definition of the dynamic response of the bridge (number of sensors for the assessment of mode shapes). In fact, if a reasonable assessment of the mode shapes is obtained, the analysis of the energy variations, in a comparative mechanism, proved to be able to detect the possible structural damages even when the amount of available data is not large.

For field implementation the assumption used in this research program of multiple dampers lumped in one equivalent element should be removed. This requires to diversify the structural response, for instance, between the north and south line of sensors of the bridge of Figure 5. The availability of data recorded at the edges of the damper devices would increase significantly the accuracy of the damage detection algorithm.

Due to the minimum manual intervention needed to execute the damage identification algorithm, the procedure is ready to be implemented in an automatic way. Assuming a set of data recording is available at a given time (reference configuration), the streaming of further data can be temporary stored and can activate a trigger of the algorithm execution. The new set of data can be compared, through a defined interpretative scheme, with the reference signals. The analysis is performed in Matlab in few seconds and could be linked to a mechanism that activates the option to save the new data or discharge them in case no significant variation is detected. In this sense the procedure respects the title of the present research as "continuous monitoring of seismic isolated bridges". The continuous condition does not require a constant streaming of data but a systematic and period activation of the procedure.

In order to respect all the characteristics of a level IV approach to structural health monitoring, the procedure should be able to indicate the impact of damage on the structure. From the presented example it is visible that the accuracy of the algorithm is such that when a level of degradation is detected in a set of dampers, the structural elements connected to the devices are generally showing sign of deterioration as well. If the interpretative scheme of the structure is supported by a reasonable number of sensor locations, the algorithm is capable of automatically detect the impact of the damage on the structure. However, further analyses, in this sense can be completed with the support of F.E. models. In Chapter 2 an

example was presented of this approach, where the simulated damage of dampers is evaluated in terms of overall structural performance variation.

The subject of interaction between "local" damage at the device level and structural performance underlines a very important topic for further development of the procedure. The availability of 2D maps of deterioration, results of a complete durability analysis of the devices, is expected to allow the assessment of possible evolutions of the detected degradation and of further interaction with the structural properties of the bridge. The damage detection procedure will also be used to update the above mentioned deterioration maps, monitoring the evolution of critical parameters of the device response with time. The use of the identification procedure can thus be seen as a tool for an early detection of characteristic variations of the device performance, not necessarily impacting immediately the structural response. However, when a first warning is triggered, an higher level of inspections and focus on the device performance, supported by maps of deterioration, can allow an estimate of the remaining life of the structure and/or of the devices. In order to formalize this comprehensive program further research effort is needed.

8) CONCLUSIONS AND FURTHER DEVELOPMENT

The modified damage identification procedure was validated against results of F.E. models of simplified structures and of an existing bridge structure (Vincent Thomas Bridge). The procedure proved to be accurate in detecting early degradations of the device characteristics as well as of the structural elements directly connected to the devices. Using acceleration records from the Vincent Thomas Bridge sensor network, the procedure was validated for configurations with dampers in excellent and damaged conditions (data December 2006 and April 2003). The results also indicates the existence of possible structural deficiencies at a location on the bridge deck ~ 200 m east of mid-span and at the connection between deck and east pier.

The procedure is presently implemented in a software package ready for use with the data from the Vincent Thomas Bridge network. The configuration of the bridge and the location of sensors is pre-loaded in the software module such that new accelerometric records could be immediately processed and could provide information's in terms of damage and severity index for the structural elements as well as the viscous dampers. For the transfer to the Caltrans Engineers of the current tool, result of this research effort, two critical steps should be completed:
1) Training of Caltrans Personnel in use of the procedure and interpretation of results.
2) Interface with maintenance personnel to ensure that the developed software package is providing the result of the damage identification procedure in a convenient format.

The nature of the presented procedure allows also the implementation of different type of anti-seismic devices (friction devices, rubber bearings etc.). A research effort is in progress to extend the existing procedure to different type of isolators and energy dissipators, common to Caltrans bridge structures, as well as to different bridges equipped with anti-seismic devices.

REFERENCES

Abe, M., Fujino, Y., Yoshida, J., (1997), "Examination of Performance of Menshin Elevated Highway Bridges During Kobe Earthquake", *Proc. NCEER-INCEDE Workshop on Earthquake Engineering Frontiers in Transp. Fac., Report NCEER-97-0005, National Center for Earthquake Eng. Research, Buffalo, 183-194.*

Adams, R. D., Caweley, P., Pye, C. J., and Stone, B. J., (1978), "A vibration technique for non-destructively assessing the integrity of structures". *Journal of Mechanical Engineering Science, 20, pp 93-100.*

Adina R. & D Inc., (2001), "ADINA (Automatic Dynamic Incremental Nonlinear Analysis)", *Report ARD 01-9, Watertown, MA, US.*

Agbabian, M.S., Masri, S.F., Miller, R. K., Caughey, T. K., (1991) "System Identification Approach to detection of Structural Changes". *ASCE Journal of Engineering Mechanics, 117 (2), 370-390*

Benveniste A. and Fuchs J.-J, (1985), "Single sample modal identification of a non stationary stochastic process", *IEEE Transactions on Automatic Control, 30(1), 66-74, Jan.*

Benzoni, G. & Seible, F., (1998), "Design of the Caltrans seismic response modification device test System". *In Proc. US-Italy Workshop on Seismic Protective System for Bridges (ed. I.M. Friedland & M.C. Costantinou), pp 173-187.*

Benzoni, G. & Seible, F., (2000), "Benicia-Martinez Friction Pendulum bearings-prototype Test Results". *Caltrans SRMD Testing Facility Report, SRMD 2000/4-17, La Jolla, CA.*

Benzoni, G., Kyler, M. R., Seible, F., (2003), "Richmond-San Rafael, Taylor Dampers Types 1-2 Proof Tests", *Caltrans SRMD Testing Facility Report, SRMD 2003/05, La Jolla, Ca, November*

Benzoni, G., Innamorato, D., (2003), "Prototype tests of Sumitomo Co. Dampers Type RDT80 and RDT200". *Caltrans SRMD Testing Facility Report SRMD 2003/01, La Jolla, CA, February.*

Benzoni G., Casarotti C., (2005), "Continuous Monitoring of Isolated Bridges: Parametric Analysis of the Effects of Damper Characteristics". *Repotr SRMD 2005/12, La Jolla, CA, November.*

Benzon,i G., Amaddeo, C., Infanti,S, "Experimental evaluation of damper performance under simulated damage condition", *Report SRMD 2007/09, La Jolla, CA, September.*

Biswas, M., Pandey, A. K., Samman, M. M., (1994), "Modified Chain-Code Computer Vision Techniques for Interrogation of Vibration Signatures for Structural Fault Detection", *Journal of Sound and Vibration, 175 (1), pp. 89-104.*

Carr, A. J., (2004), *"Ruaumoko: 3-dimensional version", Univ. of Canterbury, Canterbury, New Zealand.*

Chaundhary, M. T. A., Abe, M., Fujino, Y., Yoshida, J., (2000), "System Identification of Two Base-Isolated Bridges Using Seismic Records", *ASCE Journal of Structural Engineering, 126 (10),1187-1195.*

Conte, J., Elgamal, A., El Zarki, M., Fountain, T., Masri, S., Trivedi, M., (2003), "ITR: Collaborative Research: An Integrated Framework for Health Monitoring of Highway Bridges and Civil Infrastructure*". NSF Annual Report - Activities and Findings 10/02 to 6/03.*

Doebling, S.W., Farrar, C. R., Prime, M. B., Shevitz, D. W., (1996), "Damage Identification and Health Monitoring of Structural and Mechanical Systems From Changes in Their Vibration Characteristics: A Literature Review", *Los Alamos National Laboratory, Los Alamos, New Mexico, Report LA-13070-MS, May.*

Ewins D. J., (2000), "Modal Testing: Theory, Practice and Application (2nd edition)", Research Studies Pr.

Farrar, C.R., James III, G.H., (1997), "System identification from ambient vibration measurements on a bridge". *Journal of Sound and Vibration 205(1), pp 1-8.*

Farrar, C.R., and Jauregui, D., (1996), "Damage detection algorithms applied to experimental and numerical modal data from the I-40 Bridge". *Technical Rep. No. LA-13074-MS, Los Alamos National Laboratory, Los Alamos, New Mexico, January.*

HITEC, (1999), "Summary of Evaluation Findings for the Testing of Seismic Isolation and Energy Dissipating Devices". *CERF Report #40404.*

Haung, N.E., Long, S.R., Sheng, Z., (1996), "The Mechanism for Frequency Downshift in Nonlinear Wave Evolution", *Advance Applied Mechanics, 32, 59-111.*

Housner, G.W., Bergman, L.A., Caughey, T.K., Chassiakos, A.G., Claus, R.O., Masri, S.F., Skelton, R.E., Soong, T.T.,Spencer, B. F., Yao, J.T.P., (1997), "Structural control: past, present and future", *Journal of Engineering Mechanics (ASCE), 123 (9), 897-971.*

Infanti, S., Castellano, M.G., Benzoni, G., (2002), "Non-Linear Viscous Dampers: Testings and Recent Applications", *ATC-17-2 Seminar on Response Modification Technologies for Performance-Based Seismic Design, Los Angeles, Ca, May 30-31.*

Ingham, T.J., Rodriguez, S., Nader, M., (1997), "Nonlinear analysis of the Vincent Thomas Bridge for seismic retrofit". *Computer & Structures, Vol. 64, No. 5/6, pp. 1221-1238.*

Kelly, J. M., (2001), "The seismic protection of Large Public Buildings: Main Requirements and Benefits of Using Innovative Anti Seismic Techniques", *7th International Seminar on Seismic Isolation, Passive Energy Dissipation and Active Control of Vibrations Structures, Assisi, Italy, October 2-5.*

Kim, J.T., (1993), "Assessment of relative impact of model uncertainty on the accuracy of nondestructive damage detection in structures". *Ph.D. dissertation, Texas A&M University, College Station, Texas.*

Kim, J.T., Ryu, Y.S., Cho, H.M, Stubbs, N., (2002), "Damage identification in beam-type structures: frequency-based method vs mode-shape-based method". *Engineering and Structures, 25, pp. 57-67.*

Kim, J.T., Stubbs, N., (2002), "Improved damage identification method based on modal information". *Journal of Sound and Vibration, 252(2), pp 223-238.*

Kim B.H., Stubbs N., Park T., (2005), "A new method to extract modal parameters using output-only responses". *Journal of Sound and Vibration 282, pp. 215-230.*

Lee, Y.Y., Liew, K.M., (2001), "Detection of damage locations in a beam using the Wavelet Analysis". *International Journal of Structural Stability and Dynamics, 1(3): 455-50.*

Lee, Z-K, Wu, T-H, Loh, C-H., (2003), "System identification on the Seismic Behavior of an Isolated Bridge", *Earthquake Engineering and Structural Dynamics, 32, 1797-1812.*

Maia, N.M.M., Silva, J.M.M., (1997), "Theoretical and Experimental Modal Analysis", *Research Studies Press Ltd, Tauton, U.K.*

Mazurek, D.F. and DeWolf, J.T., (1990), "Experimental Study of Bridge Monitoring Technique". *Journal of Structural Engineering, ASCE, v. 116, No. 9, pp. 2532-2549.*

Mellon, D.E., (1997), "Caltrans proposed testing of the seismic response modification devices for the Toll Bridge Retrofit Program". *In Proc. National Seismic Conf. on Bridges and Highways, Sacramento, CA, USA, July 1997.*

Naaseh, Simin, SE., (2001), "Practical Solutions for Seismic Isolation Lessons Learned". *5th World Congress on Joints, Bearings, and Seismic Systems for Concrete Structures.*

Pandey, A. K., Biswas, M., and Samman, M. M., (1991), "Damage detection from changes in curvature mode shapes". *Journal of Sound and Vibration, 145, pp. 321- 332.*

Pandey, A. K., Biswas, M., (1994), "Damage Detection in Structures Using Changes in Flexibility", *Journal of Sound and Vibration, 169(1), pp. 3-17*

Park, S., Bolton, R.W., Stubbs, N, (2006), "Blind Test results for nondestructive damage detection in a steel frame". *Journal of Structural Engineering, 132 (5), pp.800-809.*

Peeters B., (2000), "System identification and damage detection in civil engineering". *Ph.D. thesis, Department of Civil Engineering, K.U. Leuven, Belgium,*

Rytter A,. (1993), "Vibrational based inspection of civil engineering structure". *PhD dissertation, University of Aalborg, Denmark.*

Salane, H. J., Baldwin, J. W., Duffield, R. C., (1981), "Dynamics Approach for Monitoring Bridge Deterioration", *Transportation Research Record, 832, 21-28.*

SAP: 2000 analysis reference, (1997), *Comput. Struct.*

Sikorsky, C., Stubbs, N., Karbhari, V., (2003), "Automation of Damage Index Method to Evaluate Structural Safety". *Proceedings of the 13th International Offshore and Polar Engineering Conference, Honolulu, Hawaii, May 25-30, pp. 289-296.*

Smyth, A.W., Pei, J.S., Masri, S.F., (2003), "System Identification of the Vincent Thomas suspension bridge using earthquake records". *Earthquake Engineering and Structural Dynamics, 32, pp. 339-367*

Stubbs, N., Broome, T.H., and Osegueda, R., (1990), "Non destructive construction error detection in large space structures". *AIAA Journal, 28, pp. 146-152.*

Stubbs, N., Kim, J.T., Topole, K., (1992), "An efficient and robust Algorithm for damage localization in Offshore Platforms". *Proc.,ASCE 10th Structures Congress '92, San Antonio, pp. 543-546..*

Stubbs N., Park S., Sikorsky C., Choi S., (2000), "A global non-destructive damage assessment methodology for civil engineering structures". *International Journal of System Science, volume 31, number 11, pp 1361-1373.*

Stubbs, N., Selcuk, D., (2006), "System Identification and Damage Detection of the Vincent Thomas Bridge Using Data Between 2003 and 2006", *Report to Caltrans, October 2006.*

Topole, K.G., Stubbs, N., (1995), "Non-Destructive damage evaluation of a structure from limited modal parameters". *Earthquake Engineering and Structural Dynamics, 24, pp. 1427-1436.*

Vandiver, J. K., (1975), "Detection of structural failure on fixed platforms by measurement of dynamic response". *Proceedings of the 7th Annual Offshore Technology Conference, Houston, Texas, Paper 2267.*

Van Overschee, P., De Moor, B., (1996), "Subspace identification for linear system: theory, implementation and application". *Kluwer Academic Publisher: Dordrecht, Netherlands.*

Wolfe R.W., Masri S. F., and Caffrey, J., (2002), "Some structural health monitoring approaches for nonlinear hydraulic dampers". *Journal of Structural Control, 9, pp. 5-18.*

Wu, X., Ghaboissi, J., and Garrett, J. H., (1992), "Use of neural networks in detection of structural damage". *Computers and Structures, 42, pp. 49-59.*